STUDIES ON STRUCTURE ACTIVITY CORRELATION IN CATALYTIC HYDROGENOLYSIS OF RENEWABLE GLYCEROL

A THESIS SUBMITTED TO THE

UNIVERSITY OF PUNE

FOR THE DEGREE OF DOCTOR OF PHILOSOPHY

IN

CHEMISTRY

BY

RASIKA B. MANE

RESEARCH GUIDE

DR. CHANDRASHEKHAR V. RODE

CHEMICAL ENGINEERING AND PROCESS DEVELOPMENT DIVISION

CSIR-NATIONAL CHEMICAL LABORATORY

PUNE- 411 008, INDIA

OCTOBER 2013

Dedicated to my beloved Family and Guide….

सीएसआयआर–राष्ट्रीय रासायनिक प्रयोगशाला
(वैज्ञानिक तथा औद्योगिक अनुसंधान परिषद)
डॉ. होमी भाभा मार्ग, पुणे – 411 008. भारत
CSIR-NATIONAL CHEMICAL LABORATORY
(Council of Scientific & Industrial Research)
Dr. Homi Bhabha Road, Pune - 411008. India

Certificate of the Guide

Certified that the work incorporated in the thesis entitled **"Studies on Structure Activity Correlation in Catalytic Hydrogenolysis of Renewable Glycerol"** submitted by **Ms. Rasika B. Mane** was carried out by the candidate under my supervision/guidance. Such material as has been obtained from other sources has been duly acknowledged in the thesis.

Date: 08-10- 2013

Dr. Chandrashekhar V. Rode

(Supervisor/Research Guide)

डॉ. चं. व. रोडे/Dr. C. V. RODE
वैज्ञानिक/Scientist
राष्ट्रीय रासायनिक प्रयोगशाला
National Chemical Laboratory
पुणे/ PUNE-411 008.

Communication Channels
NCL Level DID : 2590
NCL Board No. : +91-20-25902000
EPABX : +91-20-25893300
: +91-20-25893400
FAX
Director's Office : +91-20-25902601
COA's Office : +91-20-25902660
COS&P's Office : +91-20-25902664
WEBSITE
www.ncl-india.org

Declaration by the Candidate

I declare that the thesis entitled **"Studies on Structure Activity Correlation in Catalytic Hydrogenolysis of Renewable Glycerol"** submitted by me for the degree of Doctor of Philosophy is the record of work carried out by me during the period from 30-11-2010 to 08-10-2013 under the guidance of **Dr. C. V. Rode** and has not formed the basis for the award of any degree, diploma, associateship, fellowship, titles in this or any other University or other institution of Higher learning.

I further declare that the material obtained from other sources has been duly acknowledged in the thesis.

Date: 08-10-2013

Rasika B. Mane

CSIR-National Chemical Laboratory,

Pune-411 008

Acknowledgement

I wish to express my sincere gratitude to my research guide, ***Dr. C. V. Rode****, Chief Scientist, Chemical Engineering and Process Development Division, CSIR-National Chemical Laboratory (NCL), Pune, for inducting me in the fascinating world of catalysis, his constant support, invaluable guidance, numerous discussions, constructive suggestions and encouragement during the course of this work. He has been a constant source of inspiration to me during my stay at NCL. His enthusiastic attitude, innovative ideas, and scientific knowledge have inspired me profoundly. I will be remaining ever grateful to him for his teaching and guidance in a cordial manner, and wonderful personality. It has been an intellectually stimulating and rewarding experience to work with him.*

I would like to thank former head of the Chemical Engineering and Process Development Division, Dr. B. D. Kulkarni, and Dr. V. V. Ranade, the present Chair of CEPD Division, for providing me all the divisional facilities required for my research work.

I would like to thank Dr. S. Sivaram (former Director) and Dr. S. Pal, Director, NCL, Pune, for allowing me to carry out research and providing all infrastructural facilities at NCL. I am grateful to Council of Scientific and Industrial Research (CSIR, New Delhi), for awarding me the research fellowship.

I would like to thank Dr. M. Shirai, Dr. A. Yamaguchi, AIST, Sendai, Japan, Dr. H. S. Roh, Yonsei University, South Korea, Dr. R. C. Chikate of Abasaheb Garware College, Pune, and Prof. A. K. Nikumbh, Chemistry Dept. University of Pune, for very useful scientific discussions during the period of my research.

I take this opportunity to express my deepest sense of gratitude towards Dr. K. R. Patil, Dr. C. S. Gopinath, Dr. A. S. Kumbhar, Dr. P. N. Joshi, Dr. P. P. Wadgaonkar, Mr. A. S. Patil for their timely help, constant support, and valuable guidance.

I owe my special thanks to all scientific and non-scientific staff of NCL. I would like to thank Mr. H. M. Raheja, Mr. David Soloman, Mr. R. K. Jha, Mr. A. B. Gaikwad, Mr. R. R. Patane, Mr. G. M. Kamble, Mr. S. Chinnadurai, Mr. Dure, Mr. Wanjale, Mr.

Shinde, Mr. Nalavade, for their help and cooperation in completing my research work successfully.

I also wish to thank my seniors and friends, Dr.s V. Kshirsagar, J. Nadageri, A. Garade, I. Kumar, Mr. V. Mate, A. Hengane, A. Jha, N. Biradar, R. Patil, S. Kamble, D. Mhmane, S. Sakate, Atul, Rameshwar, Virendra, Tejansh, Rajan, Ms. Sharada, Ms. Mandakini, Mrs. Aparna, Ms. Shobha, Mrs. Chetana, Mr.s A. Ghalwadkar, S. Nagane, P. Lasonkar, P. Mohite, M. Patil, S. Jadkar, N. Kore, Yogesh, Ms. Pratibha, and all other research scholars and friends in NCL who are not named in person, for their valuable suggestions and helping hand.

Words are not enough to express my love and gratitude to my family members. It gives me great pleasure to thanks my parents, my sisters for always providing unconditional support and helping me over the years.

Rasika Bharat Mane

List of contents

List of tables

List of schemes

List of figures

Abbreviations

1,2-PDO	1,2-propanediol
NREL	National renewable energy laboratory
BD	Biodiesel
FAME	Fatty acid methyl esters
RMC	Raw material consumption
MONG	Matter organic non-glycerol
EDI	Electrodeionization
TEMPO	2,2,6,6-tetramethylpiperidin-1-oxyl
PLA	Polylactic acid or polylactide
1,3-PDO	1,3-propanediol
EG	Ethylene glycol
PU	Polyurethane
PG	Precipitation gel
IM	Impregnation
OG	Oxalate gel
CP	Co-preciptation
HLT	Hydrotalcite
SOMC	Surface organometallic chemistry on metals route
EISA	Evaporation-induced self assembly
IW	Incipient wetness
ASA	Amorphous silica alumina
Cu-Cr	Copper chromite
NMT	Copper chromite catalysts
NMT-P	Copper chromite catalyst prepared by literature patented procedure
CAP (K_2CO_3)	Cu-Al catalysts prepared by using K_2CO_3 as a precipitating agent
CAP (Na_2CO_3)	Cu-Al catalysts prepared by using Na_2CO_3 as a precipitating agent

CAP (NaOH)	Cu-Al catalysts prepared by using NaOH as a precipitating agent
CAP (KOH)	Cu-Al catalysts prepared by using KOH as a precipitating agent
CAF (NaOH)	Solid state fusion followed by precipitation using NaOH flakes
CAF (KOH)	Solid state fusion followed by precipitation using KOH flakes
CAF (KNO_3)	Solid state fusion using KNO_3
Cu-Al-1	10% Cu and 90% Al
Cu-Al-3	30% Cu and 70% Al
Cu-Al-5	50% Cu and 50% Al
Cu-Al-7	70% Cu and 30% Al
Cu-Al-8	80% Cu and 20% Al
20% Cu–Al_2O_3	20% Cu impregnated on Al_2O_3
S–ZrO_2	Sulfated zirconia
FA-1	Cu impregnated on parent fly ash
FA-2	Cu on fused fly ash by precipitation
FA-3	Cu impregnated on acid treated fly ash
FA-4	Cu on acid treated fly ash by precipitation
BET	Brunauer, Emmett and Teller
XRD	X-ray diffraction
TEM	Transmission electron microscopy
HR-TEM	High-resolution transmission electron microscopy
SAED	Selected area electron diffraction
EDS	Energy-dispersive X-ray spectroscopy
SEM	Scanning electron microscope
ICP-AES	Inductively coupled plasma atomic emission spectroscopy
XPS	X-ray photoelectron spectroscopy
ESCA	Electron Spectroscopy for Chemical Analysis

RSF	Relative sensitivity factor
EXAFS	Extended X-ray absorption fine structure
XANES	X-ray absorption near edge structure
FT-IR	Fourier transform infrared spectroscopy
TG and DTA	Thermogravimetric and differential thermal analysis
NH_3-TPD	Temperature programmed desorption of ammonia
Py-IR	Pyridine infrared
CO_2-TPD	Temperature programmed desorption of carbon dioxide
TPR	Temperature programmed reduction
N_2O chemisorption	Nitrous oxide chemisorption
WGSR	Water gas shift reaction
GHSV	Gas hourly space velocity
LHSV	Liquid hourly space velocity
WHSV	Weight hourly space velocity
GC	Gas ghromatography
HPLC	High performance liquid chromatography
FID	Flame ionization detector
TCD	Thermal conductivity detector
FFAP	Free fatty acid phase
TOF	Turnover frequency
NL	Normal liter
CAP (Na_2CO_3R)	Cu-Al catalyst prepared by direct addition of 0.05 M of each of copper and aluminium nitrates to the solution of Na_2CO_3 taken in the round bottom flask
CAP (K_2CO_3F)	Cu-Al prepared by using K_2CO_3 as a precipitating agent and thoroughly washed with water during filtrarion till free from potassium
APR	Aqueous phase reforming
TOS	Time on stram

PEFCs	Polymer electrolyte fuel cell
CN	Co-ordination number
OSC	Oxygen storage capacity

ABSTRACT

Studies on Structure Activity Correlation in Catalytic Hydrogenolysis of Renewable Glycerol

Glycerol is one of the renewable and top-12 building block chemicals that can be obtained as a byproduct from various processes such as soap manufacturing, fatty-acid production, fatty-ester production and microbial fermentation of carbohydrates. [1,2] The surplus glycerol in the market available today is a co-product of biodiesel production which has resulted in the significant drop in its market price from 1.5-2 \$ kg^{-1} to 0.4 \$ kg^{-1}. Hence, value addition of glycerol is through catalytic conversion to commodity and fine chemicals is highly desirable for improving the process economics of biodiesel production and also to develop sustainable processes. Selective hydrogenolysis of glycerol to 1,2-propanediol (1,2-PDO) is of much interest due to its commercial importance as well as from catalysis point of view which proceeds through two distinct pathways, (i) consecutive glycerol dehydration to acetol (on acid sites) followed by its hydrogenation to 1,2-PDO (on metal sites), which is a preferred route (ii) and through dehydrogenation-dehydration-hydrogenation mechanism to form glyceraldehyde and acetol respectively, in presence of a base. Both noble metals and Cu-Cr catalyst systems have been reported for glycerol hydrogenolysis however, they suffer from serious drawbacks of lower 1,2-PDO selectivity and toxic nature of Cr respectively.

In this work, we aimed at designing highly active and selective, inexpensive, non-hazardous and more stable catalyst for glycerol hydrogenolysis to 1,2-PDO. A novel, non-noble and non-chromium Cu-Al catalyst developed in this work was reported for the first time for *in situ* glycerol hydrogenolysis to 1,2-PDO under inert atmosphere without using an external hydrogen. Use of waste fly ash was also successfully attempted for catalyzing glycerol hydrogenolysis to 1,2-PDO for the first time in this work. The selected catalysts were tested for time on stream activity (TOS) in a continuous fixed bed reactor. The structure activity correlation enabled us to propose the plausible reaction

pathways for glycerol dehydration and hydrogenolysis under different reaction conditions. This thesis includes total 10 chapters out of which **Chapter 1** gives the general introduction including the concept of sustainability and the detailed literature survey on glycerol hydrogenolysis reaction highlighting the copper based catalysts as the best choice for glycerol hydrogenolysis. The objectives and scope of the work are given at the end of the chapter. **Chapter 2** includes experimental procedures followed for the preparation of various catalysts, their characterization and activity testing for glycerol hydrogenolysis, dehydration and water gas shift reactions in both batch and continuous operations.

Chapter 3 elaborates the characterization and activity testing of Cu-Cr catalysts with and without promoters. Among various promoters (Ba, Zn, Al) studied, Ba showed the highest activity and selectivity in hydrogenolysis of glycerol due to its highest acidity and the stabilization of Cu^0 phase with a particle size of ~69 nm.[3] TOS achieved with this catalyst was > 800 h without any deactivation-activation cycle with a selectivity of >90% to 1,2- PDO.[4,5]

The detailed characterization and performance of a non-chromium and non-noble metal Cu-Al catalyst is discussed in **Chapter 4.** Cu-Al nano catalyst prepared by simultaneous co-precipitation digestion technique, showed a stable particle size of 7–11 nm which was lower than that of Cu–Cr catalyst. The inhibition of the sintering of the active phase (Cu^0) due to presence of Cu_2O, as evidenced by XRD and the higher acidity (1.567 mmol NH_3 g^{-1}) of Cu-Al catalyst were responsible for its higher activity for glycerol hydrogenolysis.[6] TOS activity and stability of this catalyst was also established for continuous dehydration and hydrogenolysis of glycerol to acetol and 1,2-PDO, separately.[7,8]

Chapter 5 reports the effect of preparation parameters and pretreatment conditions for Cu-Al catalyst. The catalyst prepared by co-precipitation using Na_2CO_3 showed the predominant presence of metallic Cu phase with a crystallite size of 5 nm, well segregated spherical morphology and highest acidity in the activated sample. These

intrinsic properties contributed to achieve the highest glycerol conversion of 62% and 1,2-PDO selectivity of 88% in glycerol hydrogenolysis.[9]

Chapter 6 reports a very interesting study on utilization of waste fly ash as a catalyst for glycerol hydrogenolysis. The waste fly ash was modified with Cu by various methods among which, alkali pretreated fused fly ash with Cu (FA-2, Al:Cu=1:1) showed the highest activity and 1,2-PDO selectivity (>85%) in glycerol hydrogenolysis.[10]

Chapter 7 discusses the glycerol aqueous phase reforming (APR) over Cu-Al catalyst for H_2 generation followed by *in situ* hydrogenolysis of glycerol to 1,2-PDO under inert atmosphere. This is a first report of Cu-Al catalyst showing excellent TOS activity of 450 h for continuous autogeneous hydrogenolysis of aqueous glycerol under N_2 pressure with 1,2-PDO selectivity of 36 % at 180 ^{o}C. The multifunctional role of Cu-Al catalysts was responsible for C-C cleavage, glycerol dehydration to acetol followed by its hydrogenation to 1,2-PDO while completely suppressing the alkane formation.[11]

Chapter 8 describes the extent of different copper species formed and alteration in acid sites in various copper catalysts modified with Ba, Mg, Zr, Zn, Al, and Cr and their role in glycerol dehydration reaction.[12]

Due to its multifunctional role, Cu-Al catalyst was also studied for water gas shift reaction (WGSR) and these results are discussed in **Chapter 9**. From our results, Cu –Al catalyst with a composition of 70:30 was found to be the most efficient catalyst for WGSR. The observed activity results were explained based on catalyst characterization by XRD, TPR, BET, SEM and HR-TEM.

Chapter 10 summarizes the salient features of my research work and specific conclusions derived from these findings.

References

1. C.-H. Zhou, J. N. Beltramini, Y. –X. Fan, G. Q. Lu, *Chem. Soc. Rev.* **2008**, 37, 527-549.

2. T. Werpy, G. Petersen, *Top value-added chemicals from biomass*, Vol. 1, Results of screening for Potential Candidates from Sugars and Synthesis Gas, **2004**, US Department of Energy (US DOE).
3. **R. B. Mane,** A. A. Ghalwadkar, A. M. Hengne, Y. R. Suryawanshi, C.V. Rode, *Catal. Today* **2011**,164, 447-450.
4. C. V. Rode, A. A. Ghalwadkar, **R. B. Mane,** A. M. Hengne, S. T. Jadkar, N. S. Biradar, *Org. Process Res. Dev.* **2010**, 14, 1385-1392.
5. **R. B. Mane**, C. V. Rode, Recycling and Reuse of Materials and Their Products, *Advances in Materials Science book series* (Edi.s: S. Thomas), Vol. 3, Chapter 2, Apple Academic Press, Inc., **2013**, pp. 9-26.
6. **R. B. Mane,** A. M. Hengne, A. A. Ghalwadkar, S. Vijayanand , P. H. Mohite, H. S. Potdar, C. V. Rode, *Catal. Lett.* **2010,** 135, 141-147.
7. C. V. Rode, **R. B. Mane**, A. M. Hengne, A. A. Ghalwadkar, P. H. Mohite, H . S. Potdar, WO Patent 2011/138643 A2.
8. **R. B. Mane**, C.V. Rode, *Org. Process Res. Dev.* **2012**, 16, 1043-1052.
9. **R. B. Mane,** S. E. Kondawar, P. S. Niphadkar, P. N. Joshi , K. R. Patil, C.V. Rode, *Catal. Today* **2012**, 198, 321-329.
10. C.V. Rode, **R. B. Mane,** A. S. Potdar, P. B. Patil, P. S. Niphadkar, P. N. Joshi, *Catal. Today* **2012**, 190, 31-37.
11. **R. B. Mane**, C. V. Rode, *Green Chem.* **2012**, 14, 2780-2789.
12. **R. B. Mane**, A. Yamaguchi, A. Malawadkar, M. Shirai, C. V. Rode, *RSC Adv.* **2013,** 37, 16499-16508.

Chapter 1

Introduction and literature survey

This chapter gives the general introduction of biorefinery and the concept of sustainability by using renewable bio-feedstock. In particular, the realization of this concept is demonstrated by an example of glycerol as it is a co-product of biodiesel production. A conventional multistep process using petroleum based propylene for a very important commodity chemical, 1,2-propanediol (1,2-PDO) can be turned into a sustainable process by direct hydrogenolysis of glycerol. This chapter also includes detailed literature survey on glycerol dehydration and hydrogenolysis reactions highlighting the copper based catalysts as the best choice for both the reactions. The objectives and scope of the work are given at the end of the chapter.

1.1. BIOREFINERY CONCEPT

During the 20th century, petroleum and/or fossil fuels, a non-regenerative source was an important feedstock of modern society for its requirement of power, housing, clothing, agriculture and a host of synthetic materials and chemicals. Over the past 70 years or so, the crude oil price increased more than five times and presently is > USD 100 per barrel and the experts predict the era of this expensive fossil resource (crude oil) will diminish in 2040. In addition, the CO_2 emission by intensive use of fossil resources is seriously threatening the climate of the earth.[1] While entering into 21st century, the world wide main challenge is to provide a growing population with adequate food, energy and raw materials, without burdening the natural environment. Therefore, the researchers and/or chemical and **petroleum companies** are oriented towards the development of alternative renewable resources for sustainable production of fuels, chemicals and materials. This has led to the concept of **Biorefinery** which is at the centre of bio-based economy involving various pathways for the biomass conversion into energy and materials. Biorefinery concept is typically based on two different "platforms" (**Figure 1.1**) forming a wide range of different energy and material product streams.[2]

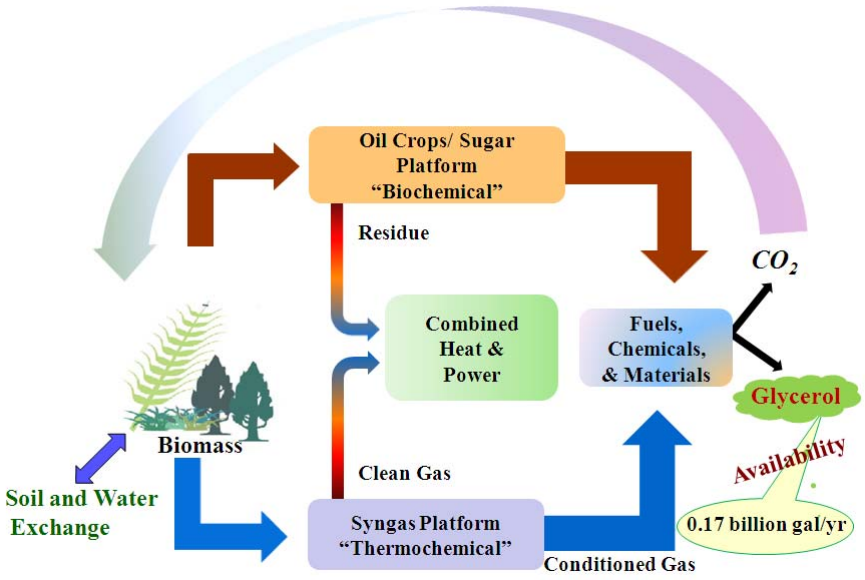

Figure 1.1. Biorefinery close loop in the biomass and bio-energy chain. (National Renewable Energy Laboratory (NREL)) [2]

The "sugar platform" is realized through biochemical processes with a focus on fermentation of sugars extracted from biomass feedstock. On the other hand, "syngas platform" is based on thermochemical conversion of biomass feedstock and by-products obtained from gasification process. The biorefinery concept is analogous to today's petroleum refineries, which produce multiple fuels and products in an integrated complex. The bio-economy will be more attractive in future by lowering the overall energy intensive unit operations of a biorefinery, that can be achieved by maximizing the use of all feedstock components, byproducts and waste streams, as well as using economic operation scales, common processing operations, materials, and equipment.

Biodiesel (BD) is one of the best examples of the biorefinery concept in which BD is produced as a fuel along with glycerol as a co-product.[3-6] Now-a-days biodiesel production is increasing globally at the average annual growth rate of 42%, which provides around 4 billion gallons of glycerol.[7] Thus, glycerol being a renewable feedstock and one of the primary top 12 building blocks of biorefinery, its downstream processing to value-added chemicals is one of the most important current topic of research. The chemistry of BD production along with glycerol co-generation is discussed in the following section.

1.1.1. Biodiesel production and co-generation of glycerol

In a short span of time, biodiesel technology has made the transition from a research endeavor to worldwide commercial production due to its several advantages such as (i) it can be used in all conventional diesel engines without any modifications, (ii) offers same performance and engine durability as petroleum diesel fuel, (iii) non-flammable, nontoxic, (iv) reduces tailpipe emission, visible smoke, and noxious fumes and odors.

Biodiesel is produced from transesterification of fatty acid containing materials *viz.* vegetable oils or animal fats, waste greases, and edible oil-processing wastes. In the production of biodiesel, the triglycerides in the fats and oils are reacted with methanol in presence of acid or base catalysts to make fatty acid methyl esters (FAME) or in other words, biodiesel and glycerol (**Scheme 1.1**). As a rule of thumb, about 10 kg of glycerol is produced for every 100 kg of FAME as per the raw material consumption (RMC)

norms shown in **Scheme 1.2.**

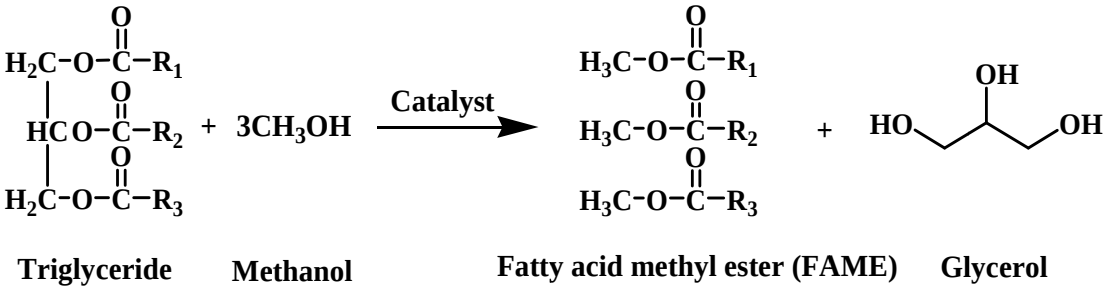

R_1 / R_2 / R_3 = long chain alkyl groups

Scheme 1.1. Transesterification of fats and oils with methanol to give BD and glycerol.

100 kg oil +

21.7 kg methanol

1.5 kg NaOH (or KOH) ⟶ **100 kg BD**

+ 10.4 kg glycerol

+ 11.3 kg methanol

Scheme 1.2. Raw material consumption norms of BD production.

However, crude glycerol obtained from biodiesel production, contains some most common impurities like methanol, water, inorganic salts (catalyst residues), free fatty acids, unreacted mono-, di-, and triglycerides, methyl esters, and a variety of other "matter organic nonglycerol" (MONG) in varying amounts.[8,9] Several steps of treatments are necessary to improve the quality of bio-glycerol, which involve neutralization, removal of (i) excess methanol, (ii) catalyst and (iii) soap using a vacuum flash process.[10] Depending on the type of separation process used, the final glycerol

purity is about 80–95%.[11] As such, the crude glycerol can be sold to glycerol refineries at a low cost. After refining, glycerol becomes a highly pure product (97% plus purity) and further refining can take the purity up to 99.5% to 99.7% using vacuum distillation or ion exchange processes.[12] However, these processes are expensive and economically prohibitive for small biodiesel plants that prefer to discard the glycerol co-product as a waste. Recently, a breakthrough in bio-glycerol purification has been made by EET Corporation (USA) and Dow using electrodeionization (EDI) technique in presence of cation/anion selective membranes for desalting glycerol.[13] This technique provides alternatives to costly and labor intensive vacuum distillation, which could further help to improve the economics of the biodiesel production. New biodiesel plants are based on the use of heterogeneous catalysts producing 99.9 % pure and limpid glycerol, free of any salt contaminants.[12,14]

The worldwide biodiesel production is rising steeply, *e.g.* in 2004 there were 22 plants having biodiesel production capacity of 157 million gallons per year while today, 148 plants are producing biodiesel at the rate of 2 billion gallons per year and it will reach 37 billion gallons by 2016, which implies that approximately 4 billion gallons of crude glycerol would enter in the market from biodiesel only.[15] This surplus availability of glycerol leads to decrease in refined glycerol market price. For example, in 2007, the refined glycerol price was painfully low, approximately $0.30 per pound (compared to $0.70 before the expansion of biodiesel production) in the United States. Accordingly, the price of crude glycerol decreased from about $0.25 per pound to $0.05 per pound.[16] Indeed, a recent model based on the production and sale of 80% glycerol by mass, predicted an inverse linear relationship between the production cost of biodiesel and variations in the market price of glycerol.[17] Considering the market scenario of crude glycerol and its purification made easy by EDI technique, developing new catalysts and routes for glycerol utilization is highly desirable.

1.2. GLYCEROL BACKGROUND

Glycerol is the simplest trihydric alcohol (IUPAC name : propane-1,2,3-triol; CAS number: 56-81-5) commercially also known as glycerin(e) (whatever grade or degree of

purity) with other names as 1,2,3-trihydroxypropane, or glycyl alcohol. It is derived from both natural and petrochemical feed stocks. The name "glycerol" is the Greek word for "sweet" (*glykys)* and is a colorless, odorless, viscous liquid having sweet taste. It is completely soluble in water and alcohols, and slightly soluble in many common solvents such as ether and dioxane and completely insoluble in hydrocarbons. Glycerol is present in large quantities in nature, in vegetable oils and animal fats, in the form of 'triglycerides.

Discovery of glycerol molecule dates back (**Figure 1.2**), to 1779 by Swedish chemist, Carl Willhelm Scheele who isolated it by boiling olive oil with litharge (PbO, used in lead glazes on ceramics).[18] After a long gap of time, in 1823 French researcher Eugune Chevereul, while studying Scheele's product isolated glycerol in the water phase coined it as glycerin (Greek : glukeros, sweet).[19] It wasn't until 1855 that Charles-Adolphe Wurtz correctly proposed the formula for glycerol showing that the natural polyol was involved in the triglyceride structure which is a main component of fats and oils. It was Alfred Nobel, who found first industrial application of glycerol, in 1860 by transforming it to nitroglycerin, which gave access later to dynamite.[20]

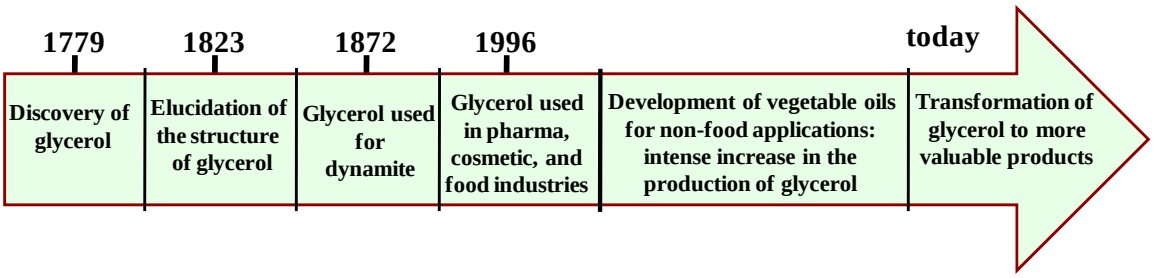

Figure 1.2. The history of glycerol.

Glycerol has some properties like specific gravity of 1.261 g L^{-1}, melting point of 18.2 ^{o}C and boiling point of 290 ^{o}C under normal atmospheric pressure, accompanied by decomposition. Due to unique combination of physical and chemical properties (**Table 1.1**),[21] chemists in 20th century, started exploring new applications of glycerol especially, in the pharmaceutical and cosmetic industries. Indeed, according to Soap and Detergent Association, there are 1500 uses of glycerol.[22]

Glycerol has been so far, mainly used in pharmaceuticals, personal care

products, polyether polyols for urethanes and food products, that adds up to 60% consumption of refined glycerol. **Figure 1.3** shows a complete breakdown of glycerol consumption according to its end uses.

Table 1.1. Physicochemical properties of glycerol at 20 ^{o}C

Chemical formula	$C_3H_5(OH)_3$
Molecular weight (g mol^{-1})	92.09382
Density (g cm^{-3})	1.261
Viscosity (Pa.s)	1.5
Melting point (^{o}C)	18.2
Boiling point (^{o}C)	290
Food energy (k cal g^{-1})	4.32
Flash point (^{o}C)	160 (closed cup)
Surface tension (m Nm^{-1})	64.0
Temperature coefficient (mN (mK)$^{-1}$)	-0.0598

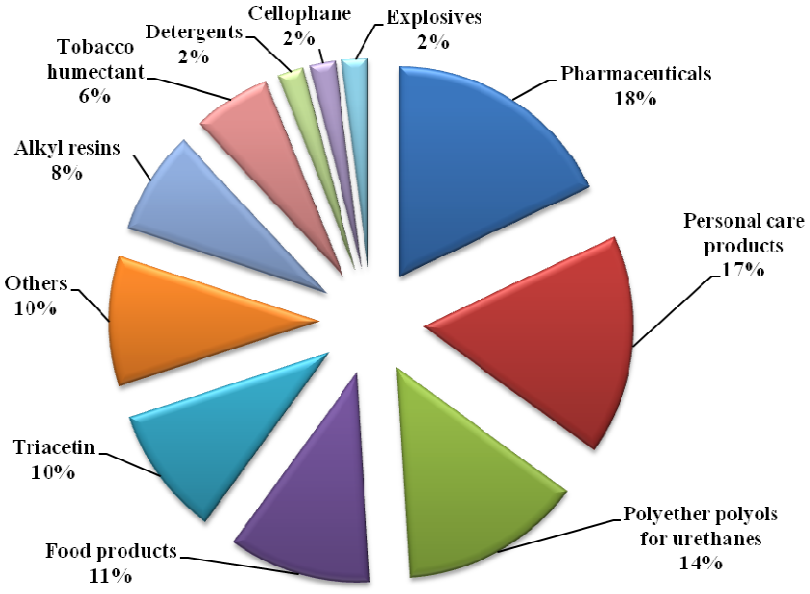

Figure 1.3. End uses of refined glycerol. [*Source: The Innovation Group Chemical Profile : Glycerin*][23]

Initially, glycerol was obtained from saponification reaction in the oleochemical industry. But during World wars I and II, increased demand of glycerol was not satisfied by the soap –making industry. Hence, synthetic glycerol production was started in Europe and USA by using epichlorohydrin as a starting material. At the end of the 20th century, deplecting petroleum oil reserves accompanied by an increase in the crude oil barrel price, researchers again focused on production of glycerol from bio-renewable sources. As discussed in the section 1.1.1. glycerol was found to be an important co-product of biodiesel production, constituting 1% of total biomass. Increased demand and the production of biodiesel in 21st century led to the surplus availability of low price pure as well as crude glycerol in the market.

Considering the reactive nature of this triol, its easy availability from bio-renewable resource, researchers world over have been intensively investigating this interesting molecule for last couple of decades. This is seen in an overwhelming increase in number of publications is from 2500 to 8000 during last 20 years.[24] A comprehensive information on glycerol including its prospects is compiled by Rossi, which is the first book on this topic published in 2008.[25] Developing new processes from glycerol in its turn will greatly increase the net sustainability and profitability of biodiesel hence, valorization of glycerol to various products of industrial importance are summarized below.

1.3. VALORIZATION OF GLYCEROL

The synthesis of high- value products from renewable glycerol is highly beneficial as it creates opportunity for better revenue and thus reducing subsidy requirement for an industry having overcapacity of BD production.[26] Glycerol being a highly functionalized molecule, it can be processed in different ways to obtain several platform chemicals as shown in **Scheme1.3.** Technology development for glycerol valorization has broad crosscutting applications in biorefinery as glycerol is structurally analogous to inexpensive sugar molecules such as glucose, xylose, *etc.* Various unit processes used to obtain numerous chemicals from glycerol include oxidation, hydrogenolysis,

dehydration, gasification, fermentation, esterification and etherification *etc.*[27-29] This has been systematically reviewed in several publications.[30-36]

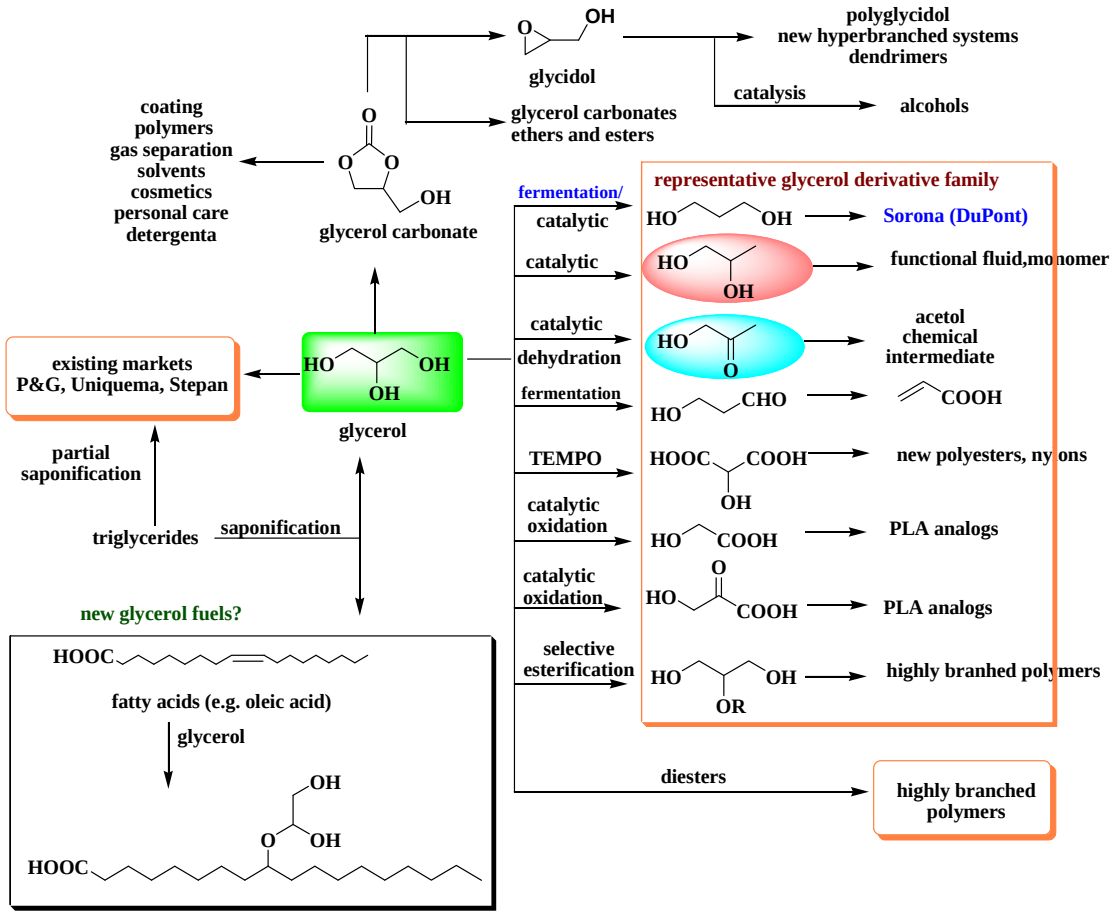

TEMPO-2,2,6,6-tetramethylpiperidin-1-oxyl

PLA –Polylactic acid or polylactide

Scheme 1.3. Commodity chemicals from glycerol.

Primary feasibility based on the economic analysis in terms of sale price/total production ratio of various products from glycerol is shown in **Figure 1.4.**[37] Among these, although hydrogen production from glycerol is considered as the clean renewable energy resource, but it has the lowest profitability because of low production rates and higher purification cost. 1,3-propanediol (1,3-PDO) shows the highest profitability while,

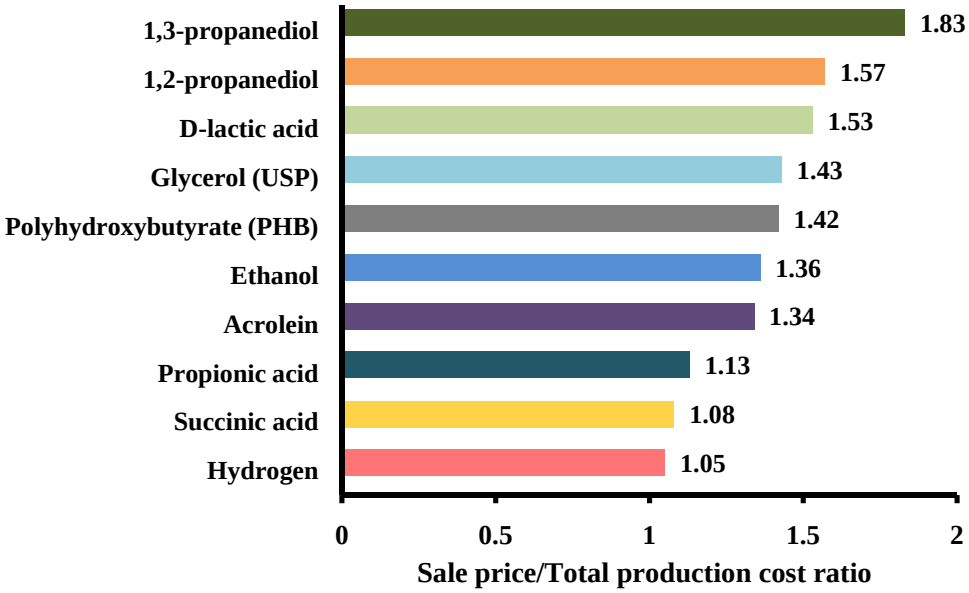

Figure 1.4. Global economic sale price/total production cost ratio. [37]

1,2-propanediol (1,2-PDO) is the second best product from economics point of view, from glycerol. **Table 1.2** shows the plans of several multinationals for commercialization of selected products from glycerol. Between the two diols, catalytic process for 1,2-PDO has become more matured than that for 1,3-PDO, as evident from majority of the commercial plants announced for 1,2-PDO production (**Table 1.2**). Therefore in this thesis, we mainly focused on development of new catalysts and their structure activity correlation for selective hydrogenolysis of glycerol to 1,2-propanediol.

1.4. HYDROGENOLYSIS OF GLYCEROL

Hydrogenolysis is a class of reduction that involves cleavage of C-C and C-O bond in an organic substrate and simultaneous addition of hydrogen to the resulting molecular fragment.[39] Hydrogenolysis for removing oxygen from the molecule, is typically referred to as hydrodeoxygenation. As glycerol is a saturated compound and has higher O/C content than most commodity chemicals, C-O hydrogenolysis is one of the most attractive routes in the conversion of glycerol. The hydrogenolysis of glycerol gives several products as shown in **Scheme 1.4** among which 1,3-PDO, 1,2-PDO, 1-propanol, 2-propanol and ethylene glycol (EG) are industrially important. Although both 1,3- and

Table 1.2. Companies utilizing glycerol as feedstock [38]

Company	Upcoming commercialization of products from glycerol
Perstorp	Glycerol derivatives.
Solvay	10 kt epichlorohydrin plant (2007) in France, 100 kt plant in Thailand (2011).
DuPont-Tate & Lyle	1,3-PDO plant (2007), no capacity indicated.
Archer Daniels Midlands (ADM)	100 kt 1,2-PDO & EG plant in the USA (2009).
Cargill	Cargill & Ashland, a joint venture for a 65 kt 1,3-PDO facility in Frankfurt (2009).
Huntsman	1,2-PDO process, customer approval trials.
Synergy Chem.	27 kt 1,2-PDO plant (2006) in USA.
Ineos	Proposed 1,2-PDO plant to complement their biofuels project in Europe.
Biomethanol Chemie	100 kt Bio-methanol plant using glycerol as feed in Holland.
Dow	150 kt Epichlorohydrin plant in China (2010). Plans to develop glycerol based polyols for polyurethane (PU) foams.
BASF	100 kt 1,2-PDO plant in Europe.
Metabolic Explorer	1,3-PDO plant in collaboration with IFP in France (2007).
Davy Process	Vapour phase technology to convert glycerol to 1,2-PDO licensed to Ashland & Cargill.

1,2-diols are hydrogenolysis products but their pathways differ in dehydration step intermediates as discussed later. Since the focus of this work is on 1,2-PDO, the hydrogenolyis of glycerol to 1,2-PDO is discussed in more details in the following sections.

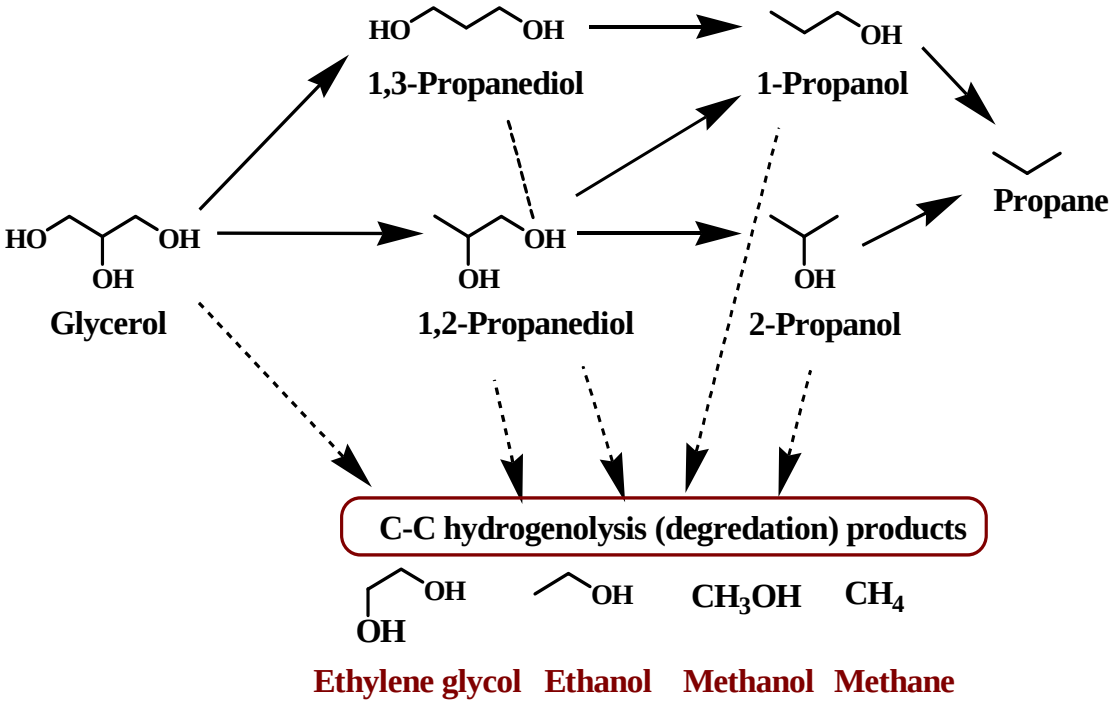

Scheme 1.4. Glycerol hydrogenolysis pathways.

1.4.1. Hydrogenolysis of glycerol to 1,2-Propanediol

1,2-Propanediol (propylene glycol) is a three-carbon diol with a stereogenic centre on the central carbon atom and is a clear, colourless, viscous, practically odorless compound with a slightly bittersweet taste and completely soluble in water. The physical properties of the 1,2-PDO are given in **Table 1.3.** Because of its physical properties and reactive nature of one or both hydroxyl groups, it finds wide spread applications as polyester resins, liquid detergents, pharmaceuticals , cosmetics, tobacco humectants, flavors and fragrances, personal care, paints and animal feed *etc.* As 1,2-PDO is non toxic to the living organisms, it is widely used in antifreeze formulations as a replacement for toxic ethylene glycol. The breakup of major industrial applications of 1,2-PDO is shown in **Figure 1.5.** The global production of the 1,2-propanediol is >1.5 million tons per year with an annual growth rate of 4% at the rate of \$1.6 Kg^{-1}. [41]

Table 1.3. Physical properties of 1,2-propanediol [40]

Chemical formula	$C_3H_6(OH)_2$
Molecular weight (g mol^{-1})	76.09
Density (g cm^{-3})	1.04
Viscosity at 20 ^oC (cps)	60.5
Melting point (^oC)	-60
Boiling point (^oC)	187.3
Freezing point (kcal g^{-1})	-60*
Flash point (^oC)	107 (Open cup)
Surface tension at 25 ºC (dynes cm^{-1})	0.37
Heat of Vaporization at 1 atm (cal g^{-1})	165
Refractive Index (nD)	20 1.4329
Specific Gravity at 20/ 4 (ºC)	1.0363
Specific Heat at 25 ºC (cal g^{-1})	0.59
Vapor Pressure at 20 ºC (mm Hg)	0.05

*Sets to glass below this temperature

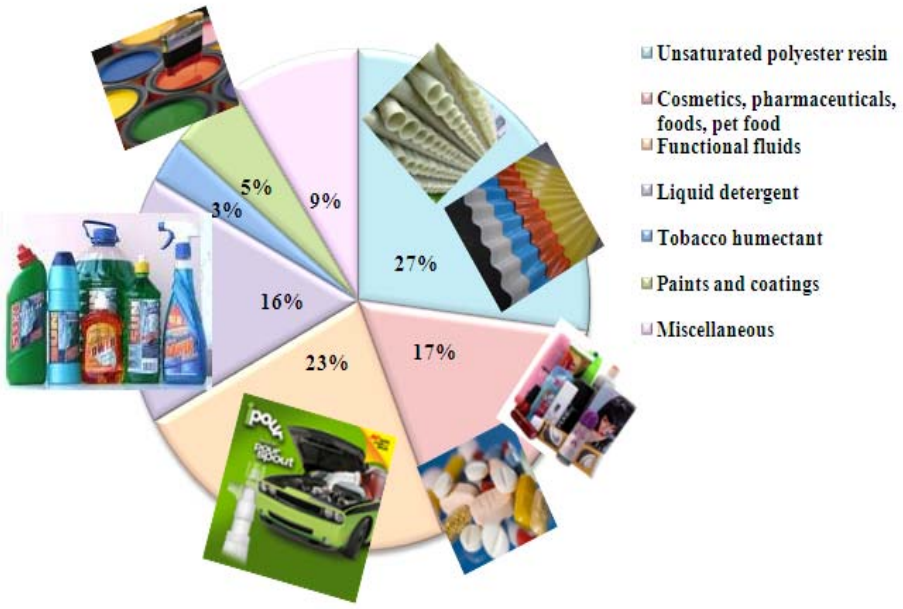

Figure 1.5. Uses of 1,2-propanediol.

The first synthesis of 1,2-PDO was reported by Wurtz [42] in 1859, by hydrolysis of propylene glycol diacetate. The first commercial production of 1,2-PDO was started in 1931 by Carbide and Carbon Chemicals Corp.[43] using the chlorohydrin route involving hydrolysis of propylene oxide (**Scheme 1.5**). In another variation, propylene oxide is

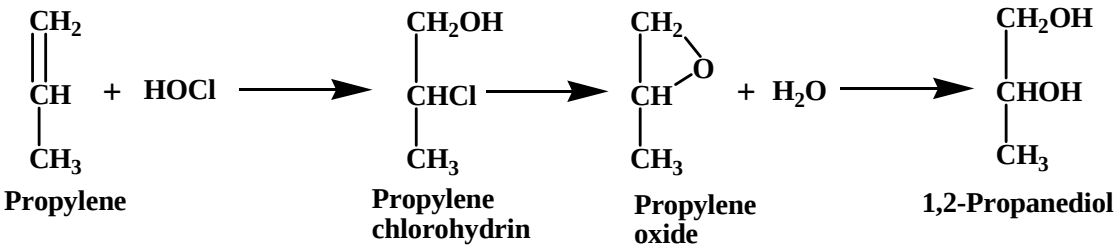

Scheme 1.5. Conventional route for glycerol hydrogenolysis to 1,2-propanediol.

made by hydroperoxide (Halcon) process in which peroxidation process converts either isobutane or ethylbenzene directly to an alkyl hydroperoxide which then reacts with propylene to make propylene oxide, and *tert*-butyl alcohol or methylbenzyl alcohol, respectively. These processes were commercially exploited by Dow Chemicals in 1942 and later by Wyandotte Chemical Corp. in 1948. Both these process are dependent on the non-renewable petroleum derived source propylene having the following drawbacks,

(i) Depleting petroleum resources,

(ii) Sensitive to price fluctuations in crude oil,

(iii) Multistep processes,

(v) Generation of hydrochloric acid.

All these drawbacks can be overcome using glycerol based process for 1,2-PDO. Glycerol being renewable resource, makes it a sustainable process and simultaneously offering economical benefits to biodiesel production.

Hydrogenolysis of glycerol to 1,2-PDO consists of removal of oxygen atom in the form of water and addition of hydrogen. Depending on whether the reaction proceeds on acid or basic catalytic sites, with and without the formation of intermediate compounds, three reaction pathways have been proposed in the literature (**Scheme 1.6**) as given below,

(i) dehydrogenation-dehydration-hydrogenation (glyceraldehyde route),

(ii) dehydration-hydrogenation,

(iii) metal-glycerol chelate mediated hydrogenolysis.

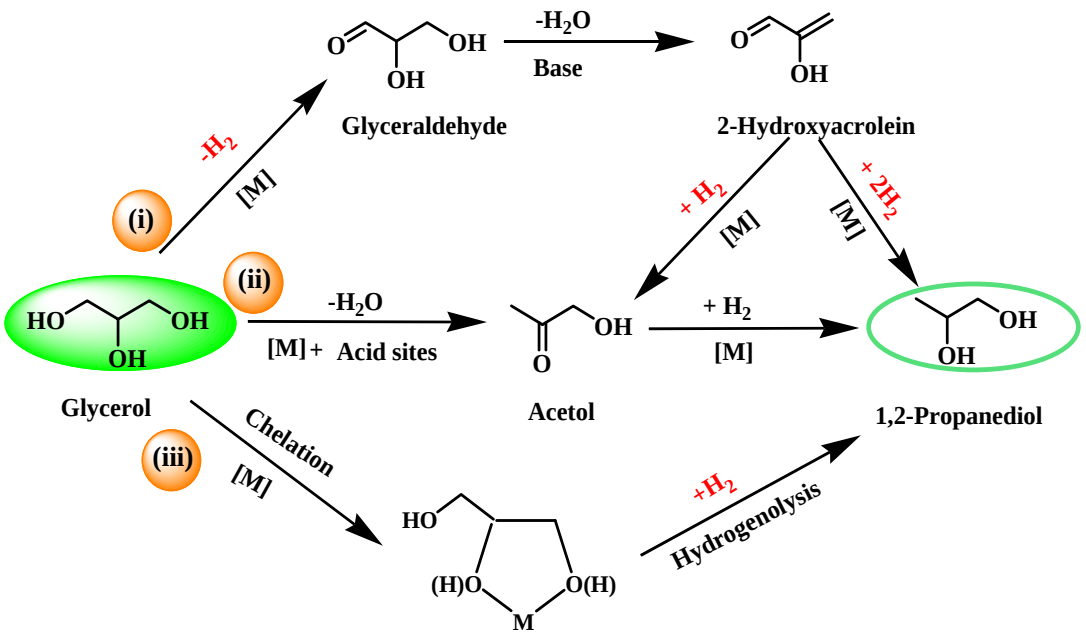

Scheme 1.6. Glycerol hydrogenolysis pathways to 1,2-propanediol.

Under hydrogenolysis conditions, apart from 1,2-PDO, formation of other hydrogenolysis, C-C cleavage and excess hydrogenolysis products such as 1,3-PDO, ethylene glycol, methanol , ethanol ,CO_2, methane and 1-propanol, 2-propanol, propane, respectively, are also observed depending on catalyst systems and reaction conditions (**Scheme 1.4**).

Glycerol hydrogenolysis to 1,2-PDO is a well studied reaction and a vast literature is published in the form of publications and patents, the survey of which is given below.

1.5. LITERATURE SURVEY

1.5.1. Hydrogenolysis of glycerol to 1, 2-PDO with external hydrogen

Several types of catalysts have been studied for glycerol hydrogenolysis to 1,2-PDO which can be broadly classified as follows.

(i) Copper based catalysts

(ii) Supported noble metals catalysts and

(iii) Combination of copper and noble metals catalysts

Most of these studies have been carried out in a batch mode particularly for catalyst screening purpose, without any solvent as well as in presence of solvents including water. Some of the reports are also on continuous glycerol hydrogenolysis in a fixed bed reactor. The foregoing discussion is organized first, giving the published literature according to the types of catalysts mentioned (**Tables 1.4 to 1.7**) above and then summarizing the patented literature (**Table 1.8**).

1.5.1.1. Copper based catalysts

The literature on Cu catalysts for glycerol hydrogenolysis published till date is summarized in **Table 1.4.** Connor and Adkins first reported Cu-Cr-Ba oxide catalysts for glycerol hydrogenolysis at 250 ^{o}C and 35 bar H_2 pressure giving 85% selectivity to 1,2-PDO.[44] Thereafter more than 50 years' gap, Montassier *et al.* studied several metals among which Raney Cu gave the best performance with glycerol conversion of 86% and 1,2-PDO selectivity of 66%.[45,46] Mechanistic pathway for glycerol hydrogenolysis to 1,2-PDO was also proposed for the first time by the same group *via* initial glycerol dehydrogenation to glyceraldehyde (in equilibrium with enolic tautomer), followed by dehydration to alpha hydroxy acrolein and hydrogenation of the later gives 1,2-PDO (**Scheme 1.6**). The same research group observed linear relationship between 1,2-PDO selectivity and hydrogen pressure, the former reaching to 84.5% at 40 bar over Cu/C catalyst.[47] Cu in combination with Zn gave complete 1,2-PDO selectivity under 80 bar H_2 pressure, but glycerol conversion was as low as 20% even after 90 h of reaction

time.[48] In 2005, the research group of Prof. Suppes of Missouri proposed a simpler route through first step acid catalyzed glycerol dehydration to acetol followed by its hydrogenation to 1,2-PDO over copper chromite catalysts.[49] This led to a two step strategy involving reactive-separation process for glycerol to 1,2-PDO for achieving complete glycerol conversion with 85 to 95% 1,2-PDO selectivity at 250 °C , 25 bar H_2. [50, 51] This pioneering work of Prof. Suppes was translated into a commercial process for 1,2-PDO licensed by Synergy. In this process, the intermediate acetol is also a starting material for hydrogen production by catalytic steam reforming, synthesis of pyruvaldehyde through oxidation and in many other organic transformations. It was found that Cu catalysts possessed an intrinsic activity towards selective cleavage of C-O bond without breaking C-C bond, desirable for the selective glycerol hydrogenolysis to 1,2-PDO. Taking this lead, several researchers focused on development of more efficient Cu catalysts as seen from **Table 1.4.**

The improved glycerol conversion of 51 % and 1,2-PDO selectivity of 96% was obtained over the carbon supported Cu-Cr catalysts having high specific surface area. [52] The co-precipitated Cu-Cr catalyst with Cu:Cr ratio of 1:2 formed an acidic $CuCr_2O_4$ spinel phase having hydrogen storage capacity, was found to increase glycerol conversion to 80% with 1,2-PDO selectivity of 84%.[53] Cu-Cr catalysts could be further modified by incorporating various promoters *viz.* Al, Zn an Ba among which, Ba as a promoter gave highest glycerol conversion (34 %) and selectivity of 85% to 1,2-PDO in 5 h reaction time. More importantly, Ba promoted Cu-Cr catalyst showed a high stability of more than 800 h in a continuous operation with increased glycerol conversion of 65%.[54,55] Cu-Cr catalysts were prepared by sol-gel and non-alkoxide sol-gel methods with different Cu to Cr molar ratios, in order to understand the reaction pathway and structure –activity relationship for glycerol hydrogenolysis to 1,2-PDO.[56-58] The above discussion indicates that although chromium is not an environmentally friendly component but still active research is in progress on Cu-Cr system since it is one of the robust and most efficient catalyst for glycerol hydrogenolysis. Such studies are also useful to understand structure activity co-relation which in turn helps to improve and/or to develop new catalysts without chromium.

Castle and Gomez first described glycerol hydrogenolysis using copper and zinc

catalyst under very high pressure and temperature conditions (150 bar; 240–272 ^{o}C) with 75– 85% selectivity to 1,2-PDO while, [59,60] for co-precipitated Cu-ZnO catalysts, pre-reduction step was found to stabilize the copper particle size, which otherwise tend to aggregate in presence of water.[61] In another report of the same authors, the increased TOF at elevated pressures indicated that the initial glycerol dehydrogenation step was not rate-limiting. Therefore, a more-alkaline support was necessary for subsequent dehydration of glyceraldehyde or more-active hydrogenation catalyst was desirable to improve the activity.[62] On the contrary, CuO-ZnO catalysts prepared by co-precipitation (CP) and oxalate gel (OG) methods showed sintering of CuO due to reaction water rather than higher reaction temperature. [63] Further, the detrimental effect of water could be counteracted by incorporation Ga in CuO-ZnO catalyst which gave stable catalyst due to a physical separation of the copper particles by Ga_2O_3 or $ZnGa_2O_4$ particles.[64]

The studies of Cu catalysts supported on various aluminium-containing acidic supports (Hβ, HY, HZSM-5, and 13X) showed that only alumina as a support gave the highest glycerol conversion and 1,2-PDO (93%) selectivity. This is because the higher acidity of zeolites increased the selectivity to acrolein as well as higher CuO-support interaction caused incomplete reduction of CuO to active metallic copper. [65] Akiyama and co-workers used commercial copper catalysts supported on Al_2O_3, Cr_2O_3, ZnO, and SiO_2 as well as Ni on SiO_2 for gas-phase hydrogenolysis of glycerol at an ambient pressure of H_2 in which quantitative glycerol conversion and high selectivity to 1,2-PDO was achieved by maintaining temperature gradients in the catalyst bed. [66,67] The pre-reduction step of Cu catalyst could be avoided by co-impregnation with silver however, the activity of the $CuAg/Al_2O_3$ was lower than the parent pre-reduced Cu/Al_2O_3.[68] In our recent work, Cu-Al mixed oxide catalyst prepared by simple co-precipitation method was found to be highly active, selective and stable giving time on stream activity (TOS) of 400 h for both glycerol dehydration as well as for hydrogenolysis. [69,70] The effect of precipitating agents for the same catalysts showed that Na_2CO_3 was the best precipitating agent due to formation of predominant metallic Cu phase with a crystallite size of 5 nm, well segregated spherical morphology and highest acidity of the resulting catalyst.[71] In our another study, waste fly ash was modified with Cu giving a very efficient catalyst (glycerol conversion = 37% with 84% 1,2-PDO selectivity) for glycerol

hydrogenolysis.[72] $CuAl_2O_4$ phase prepared at higher calcination temperature (800 ^oC) showed the best activity for glycerol hydrogenolysis to 1,2-PDO due to its highest reducibility and hydrogen mobility.[73] Compared to Cu/γ-Al_2O_3 and Cu/SiO_2 catalysts Cu/boehmite showed the highest activity and selectivity mainly due to the high surface concentration of active Cu clusters stabilized by boehmite, and Lewis acid sites of boehmite.[74]

Between precipitation gel (PG) and impregnation (IM) preparation methods for CuO/SiO_2 catalyst PG method gave higher copper dispersion and smaller metal particle size due to strong metal support interaction.[75] The stability of 200 h shown by this catalyst was due to the presence of some sodium which retards copper leaching .[76] A linear relationship between copper surface area and the activity was observed for Cu/SiO_2 catalyst prepared by incipient wetness and ion exchange methods.[77] Cu/SiO_2 catalysts prepared by homogeneous and heterogeneous deposition-precipitation methods affected the texture, structure and composition of the catalysts.[78] Cu in combination with Mg either in the form of MgO or Mg hydrotalcite ($Cu_{0.4}/Mg_{5.6}Al_2O_{8.6}$) has been also studied extensively for glycerol hydrogenolysis in which it was found that the co-precipitated catalysts gave better performance (72% glycerol conversion and 97.6% 1,2-PDO selectivity) due to the better dispersion of copper particles compared to the impregnated counterpart.[79-81] In case of Mg-hydrotalcite supported Cu catalysts, the basal spacing of hydrotalcite could be manipulated by reaction temperature variation, affecting the desorption of products and hence the selectivity pattern.[82] Mixed oxides of Mg, Al, Zn, N, Co and Cu in the form of hydrotalcites of different combinations were also studied for hydrogenolysis of glycerol, among which Cu/Zn/Al proved to be the most active with a 1,2-PDO selectivity of 93-94% at 14 bar hydrogen.[83]

Several non noble metals other than Cu were also explored as catalysts for hydrogenolysis of glycerol to 1,2-PDO. For example, Co/MgO calcined at higher temperature (600 ^oC) was found to be more active due to formation of $MgCo_2O_4$ spinel phase and a Mg-Co-O solid solution, which prevented the aggregation of Co particles under harsh conditions.[84] Cobalt nanowires and nanoparticles prepared by using stearic acid surfactant gave moderate glycerol conversion and 1,2-PDO selectivity at 220 ^oC and 30 bar H_2.[85] Among various Ni catalysts, Ni on NaX zeolite exhibited the best

performance because of its acidity.[86] Ce introduced in Ni catalyst and using carbothermal reduction method formed highly dispersed metallic Ni phase and the treatment with KBH_4 generated the phenolic groups that increased the acidity leading to the higher catalytic activity (63%) and 77% selectivity to 1,2-PDO. [87] A combination of SiO_2-Al_2O_3 support for Ni catalyst was more active than silica, alumina and carbon supports alone.[88]

Table 1.4. Supported and unsupported copper based catalysts for hydrogenolysis of glycerol

Sr. No.	Catalyst	Reaction conditions			Conv. (%)	Sel. (%)			Ref.
		Temp. (^oC)	Press. (bar)	T (h)		1,2-PDO	Acetol	EG	
1	Cu-Cr-Ba	250	200	4	-	85	-	-	44
2	Raney Cu	240	30	-	86	66	-	-	45
3	Cu/C	260	40	65	-	84	-	16	47
4	CuO/ZnO	180	80	90	20	100			48
5	Cu-Cr, Ni/C, Ni/SiO_2-Al_2O_3	200	13.8	24	55	85	-	-	49
6	Cu-Cr	240	-	-	91	-	91	-	50
7	Cu-Cr	220-230	Ambient		100	>50 (yield)	~35		51
8	Cu-Cr /C	210	41.4	10	51	96	-	-	52
9	Cu-Cr	220	80	12	80	84	-	-	53
10	Cu-Cr-Ba	220	52	5	34	84	3	4	54
11	Cu-Cr-Ba	220 220	52 41	5 -	34 65	84 91	3 ~5	4 <2	55

12	Cu-Cr (sol-gel)	210	41	5	47	75	5		56
13	Cu-Cr (Non-alkoxide sol-gel route)	210	41	10	32	54	8		57
14	Cu-Cr (0.5) (non-alkoxide sol-gel)	130	20	4	52	97	0.2		58
15	Cu:ZnO	200	41.9	12	17	29	-	3	61
16	Cu-ZnO (1:1)	200	60	6	2.6 TOF	94	-	6	62
17	CuO/ZnO-OG CuO/ZnO-CP	200	70	7	46 17	90 87	1 1	1 0	63
18	$Cu/ZnO/Ga_2O_3$	220	25	7	96	82	-	2	64
19	Cu/Al_2O_3, HY,HZSM, Hβ	200	36	10	35	93.9	-	-	65
20	$CuAg/Al_2O_3$; $CuZn/Al_2O_3$; $CuCr/Al_2O_3$	200	14.9	10	27 6 1	96 94 92	- - -	4 6 6	68
21	Cu-Al	220	70	5	38	91	4	5	69
22	Cu-Al	220	40	-	60	90	5	3	70
23	Cu-Al CAP(Na_2CO_3)	220	52	5	62	88	1	10	71
24	Cu /fly ash	220	52	5	37	84	4	3	72
25	$CuAl_2O_4$	220	50	12	90	83	-	-	73
26	Cu/boehmite	200	40	-	77	93	-	0.2	74
27	Cu/SiO_2 PG Cu/SiO_2 IM	200	90	12	73 26	94 95	Trace 0.3	2 2	75
28	Cu/SiO_2- Na	180	90	12	33	98.7	trace	0.7	76
29	Cu/SiO_2 IW Cu/SiO_2 IE	245 255	240 218	-	13 100	76 87	- 5	- 4	77

30	Cu/SiO_2 Hom-DP Het-DP	200	90	12	- 55 65	- 96 93	- - -	- 2 7	78
31	CuO-15 MgO-CP; CuO-15 MgO-CP + NaOH	180	30	20	72 82	98 96	- -	1.3 0.3	79
32	Cu/MgO	200	40	8	49.3	92	-	6	80
33	Cu/Mg–Al mixed-oxide	210	90	24	>95	85	-	-	81
34	Ni/NaX zeolites	200	60	10	95	72	-	11	86
35	Cu:Zn	200	20	16	37	92	3	3	89
36	$Cu/ZnO/Al_2O_3$; Ni/Al_2O_3	200	50 14.5	10	97 100	73 34	13 6	3 16	90
37	Cu/SBA-15	250	83	6-7	96	92	3	3	91
38	$Cu\text{-}STA/Al_2O_3$	240	60	-	90	90	-	4	92
39	Cu/Zn/Al	220	40	-	82	93	1	3	93
40	$Cu–ZnO/Al_2O_3$ (IWI)	250	32	19	80	90	10		94
41	Cu/Al_2O_3, $CuCr_2O_4$	200	50	24	59 30	79 68	7 3	1 0.5	95
42	Cu/ZnO/MOx (MOx =Al_2O_3, TiO_2, and ZrO_2)	240-300	14.5	1	100	10-20	75-80	20-35	96
43	Ce-Ni-SBA	200	24	8	50	29	-	-	97
44	CuAl-c-r	220	24	8	13	75	-	10	98
45	Cu/ Hectorite	200	40		61	>90			99
46	Raney Ni	230	40	9	74	54			100

47	Cu–Fe-500 (Cu/Fe=0.5) (Sol-gel)	190	41	10	95	47			101
48	$Cu_{0.4}/Zn_{0.6}Mg_{5.0}Al_2O_{8.6}$	180	20	10	78	99	-	1	102
49	Cu/Al_2O_3	180-300	1		100	88	9	-	103
50	Cu/Al_2O_3	200	50	24	76	96	1	1	104
51	Cu/Al_2O_3	205	50	23	89	94	-	-	105

Note: PG-precipitation gel method of catalyst preparation; IM- Impregnation method; OG- catalysts preparation by oxalate gel method; CP- by co-precipitation.

1.5.1.2. Supported noble metal catalysts

The noble metal catalysts reported for the glycerol hydrogenolysis to 1,2-PDO mainly include Rh, Ru, Pt, Pd and Au supported on various supports *viz.* carbon, SiO_2, Al_2O_3 , ZrO_2, TiO_2 and zeolites *etc*. the literature on which is given in **Table1.5** and the important findings are summarized below.

First report appeared in 1987, on homogeneous rhodium and ruthenium complexes [$Rh(CO)_2$ (acac)] (acac=acetylacetonate) together with tungstic acid for the hydrogenolysis of aqueous glycerol under very harsh conditions of 300 bar of syngas at 200 ^oC.[106] Shell used homogeneous palladium complex in a water-sulfolane mixture in presence of methane sulfonic acid to obtain 1-propanol, 1,2-PDO and 1,3-PDO in a 47 : 22 : 31 ratio.[107] Later, Ru complexes reported by Braca *et al.* [108] for hydrocarbonylation of glycerol were also used for glycerol hydrogenolysis under milder conditions (52 bar, 110 °C) but gave very low yields of 1,2- and 1,3-PDO (<5%).[109,110] The pioneering insights into glycerol hydrogenolysis to 1,2-PDO mechanism were made by Montassier *et al.* for supported Rh and Ru as well as other metallic catalysts.[111] Addition of tungstic acid (H_2WO_4) to supported Cu, Pd, Rh catalysts improved reaction rates and selectivity to glycerol hydrogenolysis products.[48]

A comparative activity studies of supported Rh, Ru, Pt and Pd catalysts for glycerol hydrogenolysis showed that 1,2-PDO selectivity was higher for 5% Ru/C than that for 5% Rh/Al_2O_3 catalyst.[112,113] In contrast to this Rh/SiO_2 exhibited both higher activity and selectivity compared to other catalysts.[114] The presence of solid acids such as Amberlyst enhanced the activity of Ru/C catalysts due to acceleration of the glycerol dehydration step while, control experiments using 1,2- and 1,3-PDO reaction mixture were reported in order to understand the mechanism of glycerol hydrogenolysis for the same catalysts.[115,116] Role of supports studied for Ru catalysts showed that zirconia was the best support for the highest activity while, SiO_2 support for Ru gave highest 1,2-PDO selectivity.[117] Between nitrate and chloride precursors of Ru used in the preparation of $Ru/\gamma\text{-}Al_2O_3$ catalysts, chloride precursor was found to be more active, but had tendency for excessive hydrogenolysis leading to the formation of propanols due to its higher Lewis acidity imparted by chloride ions.[118] For Ru/C catalyst in presence of ion-exchange resins (Amberlyst), the optimum temperature was 200 ^oC for the maximum 1,2-PDO selectivity while, increase in temperature led to increasing selectivity to condensation products.[119] One of the strongest solid acid used as a support for Ru was $Cs_{2.5}H_{0.5}[PW_{12}O_{40}]$(CsTPA), making an active bifunctional catalyst for the hydrogenolysis of glycerol and giving 1,2-PDO selectivity as high as 96%.[120] Several other solid acids explored were niobia, TPA supported on zirconia, and the cesium salt of TPA (also supported on zirconia) in presence of Ru/C catalyst for glycerol hydrogenolysis, but the maximum selectivity to 1,2-PDO obtained was only 60% for Nb_2O_5 and TPA/ZrO_2.[121,122]

The comparative study of Ru/C and Pt/C catalysts carried out for glycerol hydrogenolysis showed that the Ru/C was more active, although giving much less selectivity to 1,2-PDO, yielding more EG and methane instead. The addition of base (NaOH or CaO), led to increasing activity of Pt/C compared to that of Ru/C, which indicates that cleavage of C-C bond on the latter is catalyzed by metal and not by the added base.[123] Addition of bentonite to TiO_2 support for Ru/TiO_2 catalysts increased the glycerol conversion due to the increased acidity and dispersion of smaller (1.5 nm) Ru particles on the support.[124] In case of PtSn supported on SiO_2 catalyst prepared by surface organometallic chemistry (SOMC) technique with Sn/Pt ratio = 0.2, showed the

best performance due to 'Lewis acid sites' in the form of Sn^{+n} which would facilitate the C-OH adsorption and its subsequent C-O cleavage favoring the 1,2-PDO production.[125] The various Pd catalysts supported on CoO, Fe_2O_3, ZnO and NiO were prepared by co-precipitation and impregnation methods and tested for the glycerol hydrogenolysis in isopropanol and dioxane solvents. Among these catalysts best performance was obtained with co-precipitated Pd/CoO and Pd/Fe_2O_3 in batch as well as on large scale, as the co-precipitation allows metal-metal or metal-support interaction to a greater extent.[126] Recently, Pt supported on mesoporous solid acid Ti-W oxides, prepared by evaporation-induced self assembly (EISA) strategy having high surface area, large pore volume, uniform pore size and tunable W/Ti was used for hydrogenolysis of glycerol. The catalysts with 2 wt% $Pt/Ti_{90}W_{10}$-500s exhibited highest selectivity of 40.3% mainly to 1,3-PDO while 1,2-PDO was a minor product with 13.7% selectivity.[127] Ag/Al_2O_3 prepared by varying Ag loading and without prereduction step was reported for glycerol hydrogenolysis however, deactivation occurred due to Ag sintering under reduction conditions involving the presence of hydrogen, water and glycerol. The deactivated catalyst was regenerated by calcination in air, which redispersed the sintered Ag particles and might also burn off the coke formed.[128]

Table 1. 5. Supported noble metal catalysts for hydrogenolysis of glycerol to 1,2-PDO

Sr. No.	**Catalyst**	**Reaction conditions**			**Con. (%)**	**Sel. (%)**			**Ref.**
		Temp. (^oC)	**Press. (bar)**	**T (h)**		**1,2-PDO**	**Acetol**	**EG**	
1	Rh/C + H_2WO_4; Rh/Al_2O_3 + H_2WO_4	180	80	168	21 27	70 45	- -	- -	48
2	Ru/C; Ru/C+ H_2WO_4,	180 140	80 80	10 10	6 41	18 43	- -	- -	112

	Amberlyst,								
3	Rh/SiO_2 + Amberlyst; Rh/SiO_2	120	80	10	29 20	23 35	-	-	113
4	Ru/C; Amberlyst-70	180	80	10	7 50	50 73	-	40 20	116
5	Ru/SiO_2	240	80	5	22	61	2.4	29	117
6	Ru /C	180	80	24	43.3	66.7	0.5	23	119
7	$Ru/C+Nb_2O_5$	180	60	8	44.6	60.9	29.1	10	121
8	Ru/C+NaOH; Ru/C+CaO; Pt/C+NaOH; Pt/C+CaO	200	40	5	20 20 20 20	0.14 0.32 0.51 0.55	-	0.2	123
9	Ru/bentonite-TiO_2	150	20	7	70	81	-	10	124
10	PtSn (SOMC/M)	200	58	2	16	84	25	8	125
11	Pd/CoO	180	40	24	71	87	-	9	126
12	Pt/Ti_{80}-W_{20} (EISA)	180	55	12	18	14	-	14	127
13	Ag/Al_2O_3 (IW)	220	36	10	46	96		2	128
14	Ru/TiO_2; Ru/TiO_2+LiOH Li_2CO_3	170	30	12	66 90 80	48 87 82.3		26 8 8	129
15	Ru/Al_2O_3 + $Re_2(CO)_{10}$	160	80	8	53	50	-	8	130
16	Pt/ HLT	220	30	20	92	93.0	-	4	131
17	Ru/CNT(IM)	200	40	12	42.3	60.2		20	132

18	Pt/ASA	220	45	24	19	32	1.2	67	133
19	Ru/C+ Amberlyst-70 i)Single step ii)Two step	160	60	6-8	- 60 34	- 11 13	-	- 10 5	134
20	Re/SiO_{2c350}; $Ru–Re/SiO_2$-c350	160	80	- 8	1.7 51.7	44.4 44.8	-	11 6.4	135
21	Ru_2Fe_1/CNT	220	40	25	100	50	-	22	136
22	Ru-CaZnMg/Al (solid phase crystallization and impregnation)	180	32	18	58.5	85.5	-	15	137
23	Ru/SiO_2	240	80	5	22	61	-	-	138
24	$Pt/Nb_2O_5/Al_2O_3$+ Amberlyst-15	140	50	10	70-75	95	5		139
25	Pt/ ZnO	175	87	15	75	42	10	-	140
26	Pt/TiO_2	210	60	6	25	62	-	-	141

Note: HLT- Hydrotalcite; IPA- Iso-propylalcohol**;** IM- Impregnation**;** CP- Co-preciptation**;** SOMC- Surface organometallic chemistry on metals route**;** EISA- Evaporation-induced selfassembly; IW-Incipient wetness; ASA- Amorphous silica alumina.

1.5.1.3. Combination of copper and noble metal catalysts

In order to derive the combined advantages of both Cu and noble metals, several researchers explored mostly Ru, Rh, Pd metals along with Cu for selective

hydrogenolysis of glycerol to 1,2-PDO and this literature is summarized in **Table1.6**. Bimetallic Ru/Cu supported on ionic liquid modified bentonite was reported to give higher activity than monometallic copper catalyst, by Jiang *et al*.[142] The addition of Pd to Cu supported on layered double hydroxide increased glycerol conversion from 56% to 77% with 1,2-PDO yield of 90% at relatively low temperature and H_2 pressure conditions. The better performance of PdCu catalyst was attributed to H_2 spillover from Pd that assisted the conversion of glycerol over the Cu.[143] Similar results were obtained using Rh instead of Pd while, in alcohol medium both the catalyst system gave enhanced performance.[144] Hydrogen spillover effect was also observed in case of Ru-Cu nano-particles supported on carbon nanotubes which was responsible for much higher hydrogenolysis activity (99.8%) as compared to only Cu.[145] Incorporation of Cu with Ru supported on various supports *viz.* SiO_2, ZrO_2, zeolite Y (H and Na) was found to reduce the formation of ethylene glycol.[146] The amount of surface exposed Cu^0 and occluded hydrogen species was higher in case of added Pd to Cu-Cr catalysts giving higher glycerol conversion and complete 1,2-PDO selectivity.[147]

Table 1.6. Bimetallic copper and noble metal catalysts for hydrogenolysis of glycerol to 1,2-PDO

Sr. No.	**Catalyst**	**Reaction conditions**			**Con. (%)**	**Sel. (%)**			**Ref.**
		Temp. (^{o}C)	**Press. (bar)**	**T (h)**		**1,2-PDO**	**Acetol**	**EG**	
1	Ru-Cu /TMG-bentonite	230	80	18	100	85	-	8	142
2	Pd-Cu/ $MgAl_2O_{8.56}$	180	20	10	78	97	-	2	143
3	Rh- Cu/ $Mg_{5.6}Al_{1.98}O_{8.57}$	180	20	10	96	99	-	1	144

4	Cu-Ru/MWCNT	200	40	6	100	87	-	-	145
5	Ru–Cu/ ZrO_2	180	100	24	100	84	-	9.3	146
6	$Pd_{0.5}$–CuCr	220	40	18	90	95	-	-	147
7	Modified Ru/SiO_2	-	Ambient	-	55	26	27	46	148

1.5.2. Glycerol hydrogenolysis without external hydrogen

Generally, hydrogenation reactions involve insertion of molecular hydrogen from external source maintained at high pressure. This external source of hydrogen is obtained from fossil resources. Glycerol hydrogenolysis process is also based on use of such external hydrogen, the literature on which is summarized above. However, glycerol being an oxygenated molecule with C:O ratio of 1:1, it is capable of undergoing aqueous phase reforming (APR) to generate hydrogen.[149] Hence, the use of *in situ* generated hydrogen for the glycerol hydrogenolysis would provide alternative to high pressure fossil derived external hydrogen and would make the process safer and more sustainable, the detailed literature of which is summarized in **Table 1.7.** D'Hondt *et al.* first reported platinum catalyzed glycerol hydrogenolysis using *in situ* hydrogen generated by APR of glycerol, which gave 85% glycerol conversion with 64% selectivity to 1,2-PDO. [150] The recent report appeared on the use of combination of both Ru/Al_2O_3 and Pt/Al_2O_3 for *in situ* hydrogenolysis of glycerol, which was more active than the respective individual catalysts. [151] SiO_2 supported PtSn catalysts also showed efficient activity for *in situ* hydrogenolysis of glycerol with 59% 1,2-PDO selectivity.[152] Another variation of Pt catalysts involves Pt-nanoparticles supported on hydrotalcite (HT) which gave glycerol conversion of 98% with 74% 1,2-PDO selectivity. [153] Raney Ni catalyst used for *in situ* glycerol hydrogenolysis is an alternative to expensive Ru and Pt catalysts, but it was highly active towards C-C bond cleavage, resulting in increased selectivity to EG (32%) at the cost of 1,2-PDO selectivity (25%).[154] The best choice for *in situ* glycerol hydrogenolysis reported recently by Mane *et al.* is the non-noble and non-chromium Cu-

Al oxide catalyst.[155] This catalyst also presented consistent activity for a duration of 400 h for autogeneous hydrogenolysis of refined glycerol with 36% selectivity to 1,2-propanediol (1,2-PDO) and 75% with bio-glycerol feed.

Another option for glycerol hydrogenolysis without use of external hydrogen is to use hydrogen donor molecules such as 2-propanol, methanol, and formic acid. Musolino *et al.* first reported the selective transfer hydrogenolysis of glycerol to 1,2-PDO in presence of 2-propanol or ethanol over Fe_2O_3 supported Pd catalyst.[156] 2-Propanol and formic acid were commonly used as hydrogen donors for bimetallic Ni-Cu/Al_2O_3 catalysts in glycerol hydrogenolysis under N_2 pressure.[157-159]

Table 1.7. Hydrogenolysis of glycerol without external hydrogen

Sr. No.	**Catalyst**	**Reaction**			**Conv. (%)**	**Sel. (%)**			**Ref.**
		Temp. (^oC)	**N_2 Press. (bar)**	**T (h)**		**1,2-PDO**	**Acetol**	**EG**	
1	Pt/NaY	230	-	15	85	64	-	-	150
2	Raney Ni	180	-	1	100	43	-	-	151
3	Ru/Al_2O_3 + Pt/Al_2O_3	220	-	6	51	47	-	-	152
4	Pt/HT	225	35	3	98	70	-	-	153
5	PtSn/SiO_2	200	-	2	54	59	-	-	154
6	Cu-Al	220	-	-	90	55	22	2.5	155
7	Pd/Fe_2O_3	180	-	24	100	94	-	-	156
8	Ni—Cu/Al_2O_3 (sol-gel)	220	-	24	60	65	18		157
9	Ni–Cu/Al_2O_3	220	45	24	90	82	-	-	158
10	Ni–Cu/Al_2O_3	220	43	10	33.5	85.9	6.7	-	159

11	ZnO + NiMo	235	31 (Ar)	-	79	52 Yield	-	-	160
12	Cu/Mg/Al	210	-	-	95	92	-	-	161

1.5.3. Patented literature

Glycerol hydrogenolysis being a commercially important process, several catalyst and process patents also have been filed/granted and the important ones are summarized in **Table 1.8**.

Both homogeneous as well as heterogeneous catalyst systems have been patented which include noble metals, non-noble metals mainly Cu with and without Cr. Depending on the catalyst and reaction conditions, glycerol conversion and 1,2-PDO selectivity varied over a wide range.

Table 1.8. Patents on hydrogenolysis of glycerol to 1,2-PDO

Sr. No.	Patent No.	Inventor	Assignee	Highlights	Ref.
1	*US* 5214219, 1993	Casale *et al.*	Novamont S.p.A,Milan, Italy	Copper zinc catalysts 20-60% glycerol, > 200 ^{o}C, H_2 pressure 50-200 bar, conversion 6% - 100%, 27% - 80% 1,2-PDO.	**59**
2	*US* 5276181, 1994	Casale *et al.*		S-Ru in presence alkali and alkaline earth metal hydroxides and carbonate, 200 - 280 ^{o}C, 50 to 200 bar H_2, 6 - 100% conversion, 27 - 80% 1,2-PDO along with lactic acid.	**60**
3	*US* 4642394, 1987	Che *et al.*	Celanese Corporation, New York	**Syngas**, in basic organic solvent over homogeneous W and Gr. VIII catalysts, 75-250 ^{o}C, 68.9-103.4 bar H_2.	106
4	*US* 6080898, 2000	Drent *et al.*	Shell Oil Co	**Homogeneous Pd, Pt catalysts**, 50-250 ^{o}C, 2 - 100 bar H_2, 22 % 1,2-PDO, 47 % 1- propanol, 30 % 1,3-PDO.	107
5	*US* 5426249, 1995	Haas *et al.*	Degussa	Phosphoric acid coated Al_2O_3/TiO_2 catalyst at 250 - 340 ^{o}C and by hydrogenation over	162

				$Ni/Al_2O_3/SiO_2$, 20-120 ^oC, 1 - 20 bar H_2.	
6	*US* 5616817, 1995	Schuster *et al.*	BASF	CoO, CuO, MnO_2, MoO_3 with inorganic polyacids or hetero-polyacids, 200 –250 °C, 200–325 bar H_2, complete conversion, 95 % 1,2-PDO.	163
7	WO 98241, 2001	Bullock *et al.*	Du Pont	Ni/SiO_2 or Al_2O_3, 240–315 °C, 130–480 bar H_2, 70% 1,2-PDO, 15% EG, 11% degradation products.	164
8	*US* 6291725, 2001	Chopade *et al.*	Michigan State University (US), Battelle Memorial Institute, Pacific Noerhwest Laboratory (US).	Ru/ Al_2O_3, TiO_2 and C, 0.02 to 0.3 mole L^{-1} base, 34.4-137.9 bar H_2, 180-250 ^oC.	165
9	*WO* 03035582, 2002	Werpy *et al.*	Michigan State University	Re catalysts, 44% 1,2-PDO, 5% 1,3-PDO, 13% EG, 230 °C, 82 bar H_2.	166
10	*WO* 095536, 2005	Suppes *et al.*		Pd, Ni, Cu, Zn and Cr catalysts, conversion 69%, 72% 1,2-PDO, 200 ^oC, 14 bar H_2, 24 h.	167
11	*WO* 53705,	Suppes *et al.*	University of Missouri	Cr_2O_3 + CuO, 150-250 °C, 1-25 bar H_2,	168

	2007			complete conversion, 85%-95% propanediols.	
12	*WO* 99161, 2007	Henkelmann *et al.*	BASF	Cu catalysts, 100-350 ^{o}C, 100-325 bar H_2.	169
13	*WO* 89899, 2008	Achim *et al.*	Clariant Int. Ltd.	CuO + ZnO + MnO, 180-240 °C, 20-100 bar H_2	170
14	*US* 0103339, 2008	Bloom *et al.*	Archer Daniels Midland Company	Re-Ni /C or HC-1, alkaline medium, 82.7-110.3 bar H_2, 48-96% conversion, 36-55% 1,2-PDO.	171
15	*WO* 54701, 2009	Abhari *et al.*	Golden & Nelson	Ni/W, 550 °C, 110 bar H_2, 78% conversion, 100% 1,2-PDO.	172
16	*EP* 2540692 A2, 2011	Rabello *et al.*		Cu-Cr, 160°C-260°C, 4.9-49 bar H_2, 95% conversion, 90% 1,2-PDO.	173
17	*US* 0207972 A1, 2011	Brown *et al.*	Battelle Memorial Institute	Ni-La/C modified with ZrSc, ZrY, TiSc or TiY, 160-240 ^{o}C, 82.7-151.7 bar H_2, 50% 1,2-PDO, > 60-80% conversion.	174
18	*US* 0004029 A1, 2011	Chaudhari *et al.*		Pt-Re:Ru, Pt:Ru, Re:Ru, Pt:Re/Al_2O_3, C, SiO_2, zeolite, TiO_2, ZrO_2, ***in situ*** hydrogenolysis, 180-250 ^{o}C, 20-83% conversion, 26-53 mole%	175

				1,2-PDO.	
19	US 0071323 A1, 2011	Stankowiak *et al.*	Clariant Finance (BVI) Limited, Tortola (VG)	Raney Cu, Cu-Cr or CuO-ZnO, 200-220 ^{o}C, 50-90 bar H_2, 65-85% conversion, 60% 1,2-PDO.	176
20	*EP* 2 565 175 A1, 2011	Lemonidou *et al.*		Ru, Pt, Pd, or IB Group of metals [Cu and two oxidic components (ZnO and Al_2O_3)], **water as hydrogen source**, 200-300 °C, 10-100 bar **N_2**, 85% conversion, 39-45% 1,2-PDO.	177
21	EP 2 29 722 A2, 2011	Suppes *et al.*		Pd, Ni, Rh, Cu, Zn, Cr, **acetol** (80%) hydrogenation, 50-250 °C, 0.2-25 bar H_2.	178
22	WO 138643 A2, 2011	Rode *et al.*	Council of Scientific and Industrial Research	Cu-Cr promoted by Al, Zn and Ba and no-chromium Cu-Al catalysts for dehydration and hydrogenolysis of glycerol to acetol and 1,2-PDO, 180-240 ^{o}C, 20 bar N_2, 34.4 bar H_2.	179
23	*US* 8258351, 2012	Suzuki *et al.*	Kao Corporation, Tokyo , Japan	Cu/SiO_2, 210- 230 ^{o}C, 20-200 bar H_2.	180
24	*US*	Chaudhari *et al.*	University of	Ru/Al_2O_3, C, SiO_2,	181

	8252963, 2012		Kansas, US	zeolite, TiO_2, ZrO_2, 300 ^oC , 206.8 bar H_2.	
25	*US* 8252961 B2, 2012	Suppes *et al.*	University of Missouri, Columbia, US	Cu-Cr, 180-220 ^oC, 0.3-0.7 bar H_2. second step, 150-250 ^oC, 1-25 bar H_2.	182
26	*US* 8324434 B2, 2012	Molzahn *et al.*	Dow Global Technologies, LLC, (Midland), MI (US)	Cu-Cr, **non-aqueous** solvent (propylene glycol, dioxane *etc.*), 85% conversion, 139% 1,2-PDO, 204.7 ^oC, 0.281 H_2.	183

1.6. SCOPE AND OBJECTIVES OF THE THESIS

As clearly seen from above literature survey, several types of catalysts have been reported for glycerol hydrogenolysis with a major emphasis on noble metals and Cu-Cr catalyst systems. However, these suffer from drawbacks such as lower selectivity to 1,2-PDO and toxic nature of Cr respectively. Hence, there is still a need to design highly active and selective, inexpensive, non-hazardous and more stable catalyst for glycerol hydrogenolysis to 1,2-PDO.This can be attempted by fundamental understanding of roles of various components involved in the catalysts systems. For this purpose, several copper catalysts with and without chromium and promoters were prepared, thoroughly characterized by several techniques and evaluated for their activity performance in my Ph.D. work. The structure activity correlation enabled us to propose the plausible reaction pathways for glycerol dehydration and hydrogenolysis under different reaction conditions.

The specific objectives of this work are given below.

- Preparation of supported as well unsupported chromium and non-chromium Cu catalysts

- Influence of various promoters *viz.* Al, Ba and Zn and their composition on the activity and physicochemical properties of the copper chromite catalyst.
- Effect of pre-treatment conditions, precipitating agents and preparation procedure on activity and physico-chemical properties of the Cu-Al catalysts.
- Screening of the above prepared catalysts for glycerol hydrogenolysis in a batch operation
- Optimization of the reaction parameters and testing the stability of the best catalysts.
- Time on stream activity measurement in a continuous operation, of the selected catalyst.
- Use of waste fly ash as a catalyst for the liquid phase hydrogenolysis of glycerol.
- Activity testing of the noble as well as copper based catalysts for *in situ* hydrogenolysis of glycerol to 1,2-PDO under dehydration conditions.
- Effect of co-metals *viz.* Ba Mg, Zr, Zn and Al on acidity, reducibility and activity of copper catalysts for selective liquid phase dehydration of glycerol to acetol.
- Identification of active sites to develop structure-activity relationship and to propose plausible reaction pathways.

1.7. REFERENCES

1. A. Martin, U. Armbruster, H. Atia, *Eur. J. Lipid Sci. Technol.* **2012**, 114, 10-23.
2. U.S. Departmrnt of Energy, Report Top Value Added Chemicals from Biomass, **2004**.
3. J. D. Hooker, US Patent 027137, **2005**.
4. F. J. Luxem, US Patent 254387, **2004**.
5. H. Noureddini, US Patent 6015440, **2000**.
6. M. F. Pelly, WO Patent 085579, **2004**
7. P. Anand, R. K. Saxena, *New Biotechnol.* **2012**, 29, 199-205.
8. M. Canakci, J. V. Gerpen, *Transactions of the ASAE*, **2001**, 44, 1429-1436.
9. M. A. Dasari, M. J. Goff, G. J.Suppes, *J. American Oil Chemists' Society* **2003**, 80, 189-192.
10. C. W. Chiu, M. J. Goff, G. J. Suppes, *AIChE J.* **2005**, 51, 1274-1278.
11. L. Bournay, D. Casanave, B. Delfort, G. Hillion, J. A. Chodorge, *Catal. Today* **2005**, 106, 190-192.
12. J. Van Gerpen, *Fuel Proc. Technol.*, **2005**, 86, 1097-1107.
13. K. Chatterjee, K. Hall, S. Tell, Department of Chemical & Biomolecular Engineering, University of Pennsylvania, Senior Design Reports, **2011**.
14. http:..beag.ag,utk,edu/pp/biodiesel.pdf
15. F. Yang, M. A. Hanna, R. Sun, *Biotechnol. for Biofuels*, **2012**, 5, 13.
16. B. J. Kerr, W. A. Dozier III, K. Bregendahl, Nutritional value of crude glycerin for nonruminants. Proceedings of the 23rd Annual Carolina Swine Nutrition Conference Raleigh, NC, **2007**, 6.
17. M. J. Haas, A. J. McAloon, W. C. Yee, T. A., *Bioresour. Technol.* **2006**, 97, 671-678.
18. http://en.wikipedia.org/wiki/Glycerol
19. J. B. Rattray, *Inform*, **2006**, 17, 285.
20. http://en.wikipedia.org/wiki/Nitroglycerin
21. *Handbook of Chemistry and Physics (*Ed.: D. R. Lide), 87th edn., CRC Press, Boca Raton, FL, **2006.**

22. Why Glycerin USP?", The Soap and Detergent Association, **2000.**
23. *The Innovation Group Chemical Profile : Glycerin*
24. F. Jerome, Y. Pouilloux, J. Barrault, *ChemSusChem* **2008**, 1, 586-613.
25. M. Pagliaro, M. Rossi, *The Future of Glycerol,* RSC Publishing, Cambridge, UK, **2008**.
26. http://www.biodiesel.org/resources/pressreleases/gen/20091208_Urbanchuk%20study%20release%20w%20link _ final _ 120809% 20(2).pdf.
27. D. T. Johnson, K. A. Taconi, *Environ. Prog. Sus. Energy* **2007**, 26, 338-348.
28. M. Pagliaro, R. Ciriminna, H. Kimura, M. Rossi, C. D. Pina, *Eur. J. Lipid Sci. Technol.* **2009**, 111, 788-799.
29. C.-H. Zhou, J. N. Beltramini, Y.-X. Fana, G. Q. Lu, *Chem. Soc. Rev.* **2008**, 37, 527-549.
30. M. Pagliaro, R. Ciriminna , H. Kimura, M. Rossi, C. Della Pina, *Angew. Chem. Int. Ed.* **2007**, 46, 4434-4440.
31. A. Corma, S. Iborra, A. Velty, *Chem. Rev*. **2007**, 107, 2411-2502.
32. Y. Zheng, X. Chen, Y. Shen, *Chem. Rev.* **2008**, 108, 5253-5277.
33. A. Martin, U. Armbruster, I. Gandarias, P. L. Arias, *Eur. J. Lipid Sci. Technol.* **2013**, 115, 9–27.
34. A. Martin, M. Richter, *Eur. J. Lipid Sci. Technol.* **2011**, 113, 100-117.
35. J. ten Dam, U. Hanefeld, *ChemSusChem* **2011**, 4, 1017-1034.
36. A. Martin, U. Armbruster, H. Atia , *Eur. J. Lipid Sci. Technol.* **2012**, 114, 10-23.
37. J. A. Posada, L. E. Rincón, C. A. Cardona, *Bioresour. Technol.* **2012**, 111, 282-293.
38. J. Henkelmann, M. Becker, P. Wahl, G. Theis, S. Mauer, BASF, WO Patent 2007/099161 A1, **2007**.
39. C. Ellis, *Hydrogenation of Organic Substances*, 3rd ed., Van Nostrand Company, New York, **1930**, p. 564.
40. J. A. Monick, *Alcohols, Their Chemistry, Properties and Manufacture*, Reinhold Book Corporation, **1968**, p. 315.
41. http://www.cargill.com/news-center/news-releases/2007/NA3007798.jsp.
42. A. Wurtz, *Ann. Chim. Phys.,* **1859**, 55, 438.

43. I. MeHan, *Polyhydric Alcohols,* Spartan Books, Washington, D.C., **1962**, p. 46.
44. R. Connor, H. Adkins, *J. Am. Chem. Soc.* **1932**, 54, 4678-4690.
45. C. Montassier, D. Girau, J. Barbier, *Stud. Surf. Sci. Catal.* **1988**, 41,165-170.
46. C. Montassier, D. Giraud, J. Barbier, *Polyol Conversion by Liquid Phase Heterogenous Catalysis over Metals* (Eds.: M. Guisnet, *et al.*), Elsevier, Amsterdam, **1988**, p. 165.
47. C. Montassier, J. M. Dumas, P. Granger, J. Barbier, *Appl. Catal. A* **1995**, 121, 231-244.
48. J. Chaminand, L. Djakovitch, P. Gallezot, P. Marion, C. Pinel, C. Rosier, *Green Chem.,* **2004**, 6, 359-361.
49. M. A. Dasari, P.-P. Kiatsimkul, W. R. Sutterlin, G. J. Suppes, *Appl. Catal. A* **2005**, 281, 225-231.
50. C. W. Chiu, M. A. Dasari, G. J. Suppes, W. R. Sutterlin, *AIChE J.* **2006**, 52, 3543-3548.
51. C. W. Chiu, A. Tekeei, W. R. Sutterlin, J. M. Ronco, G. J. Suppes, *AIChE J.* **2008**, 54, 2456-2463.
52. C. Liang, Z. Ma, L. Ding, J. Qiu, *Catal. Lett.* **2009**, 130, 169-176.
53. N. D. Kim, S. Oh, J. B. Joo, K. S. Jung, J. Yi, *Top. Catal.,* **2010**, 53, 517-522.
54. R. B. Mane, A. A. Ghalwadkar, A. M. Hengne, Y. R. Suryawanshi, C.V. Rode, *Catal. Today* **2011**,164, 447-450.
55. C. V. Rode, A. A. Ghalwadkar, R. B. Mane, A. M. Hengne, S. T. Jadkar, N. S. Biradar, *Org. Process Res. Dev.* **2010**,14, 1385-1392.
56. Z. Xiao, C. Li , J. Xiu, X. Wang, C. T. Williams, C. Liang, *J. Mol. Catal. A* **2012**, 365, 24-31.
57. Z. Xiao, Z. Ma, X. Wang, C. T. Williams, C. Liang, *Ind. Eng. Chem. Res.* **2011**, 50, 2031-2039.
58. Z. Xiao, J. Xiu, X. Wang, B. Zhang, C. T. Williams, D. Su, C. Liang, *Catal. Sci. Technol.* **2013**, 3, 1108-1115.
59. B. Casale , A. M. Gomez, US Patent 5276181,**1994**.
60. B. Casale, A. M. Gomez, US Patent 5214219, **1993**.
61. S. Wang, H. C. Liu, *Catal. Lett.* **2007**, 117, 62-67.

62. S. A. Wang, Y. C. Zhang, H. C. Liu, *Chem. Asian J.* **2010**, 5, 1100-1111.
63. A. Bienholz, F. Schwab, P. Claus, *Green Chem.* **2010**, 12, 290-295.
64. A. Bienholz, R. Blume, A. Knop-Gericke, F. Girgsdies, M. Behrens, P. Claus, *J. Phys. Chem. C* **2011**, 115, 999-1005.
65. L. Y. Guo, J. X. Zhou, J. B. Mao, X. W. Guo, S. G. Zhang, *Appl. Catal. A* **2009**, 367, 93-98.
66. S. Sato, M. Akiyama, K. Inui, M. Yokota, *Chem. Lett.,* **2009**, 38, 560-561.
67. M. Akiyama, S. Sato, R. Takahashi, K. Inui, M. Yokota, *Appl. Catal. A* **2009**, 371, 60-66.
68. J- J. X. Zhou, L. Y. Guo, X. W. Guo, J. B. Mao, S. G. Zhang, *Green Chem.* **2010**, 12, 1835-1843.
69. R. B. Mane, A. M. Hengne, A. A. Ghalwadkar, S. Vijayanand, P. H. Mohite, H. S. Potdar, C.V. Rode, *Catal. Lett.* **2010**, 135,141-147.
70. R. B. Mane, C. V. Rode, *Org. Process Res. Dev.* **2012**, 16, 1043-1052.
71. R. B. Mane, S. E. Kondawar, P. S. Niphadkar, P. N. Joshi , K. R. Patil, C.V. Rode, *Catal. Today* **2012**, 198, 321.
72. C.V. Rode, R. B. Mane, A. S. Potdar, P. B. Patil , P. S. Niphadkar, P. N. Joshi, *Catal. Today* **2012**, 190, 31-37.
73. B. K. Kwak, D. S Park, Y. S. Yun, J. Yi, *Catal. Commun.* **2012**, 24 , 90-95.
74. Z. Wu , Y. Mao , M. Song , X. Yin , M. Zhang, *Catal. Commun.* **2013**, 32, 52-57.
75. Z. W. Huang, F. Cui, H. X. Kang, J. Chen, X. Z. Zhang, C. G. Xia, *Chem. Mater.* **2008**, 20, 5090-5099.
76. Z. W. Huang, F. Cui, H. X. Kang, J. Chen, C. G. Xia, *Appl. Catal. A* **2009**, 366, 288-298.
77. A. Bienholz, H. Hofmann, P.Claus, *Appl. Catal. A* **2011**, 391, 153-157.
78. Z. Huang, F. Cui, J. Xue, J. Zuo, J. Chen, C. Xia, *Catal. Today* **2012**,183, 42-51.
79. Z. Yuan, J. Wang, L.Wang, W. Xie, P.Chen, Z. Hou, X. Zheng, *Bioresour. Technol.* **2010**,101, 7088-7092.
80. Z. Yuan, L. Wang, J. Wang, S. Xia, P. Chen, Z. Hou, X. Zheng, *Appl. Catal. B* **2011**,101, 431-440.

81. M. Balaraju, K. Jagadeeswaraiah, P. S. Sai Prasad, N. Lingaiah, *Catal. Sci. Technol.* **2012**, 2, 1967-1976.
82. B. Zhao, C. Li, C. Xu, *Catal. Sci. Technol.* **2012**, 2, 1985-1994.
83. L. K. Meher, R. Gopinath, S. N. Naik, A. K. Dalai, *Ind. Eng. Chem. Res.* **2009**, 48, 1840-1846.
84. X. Guo, Y. Li, R. Shi, Q. Liu, E. Zhan,W. Shen, *Appl. Catal. A* **2009**, 371, 108-113.
85. Q. Liu, X. Guo, Y. Li, W. Shen, *Mater. Lett.* **2009**, 63, 1407-1409.
86. J. Zhao, W. Yu, C. Chen, H. Miao, H. Ma, J. Xu, *Catal. Lett.* **2010**, 134, 184-189.
87. W. Yu, J. Xu, H. Ma, C. Chen, J. Zhao, H. Miao, Q. Song, *Catal. Commun.* **2010**, 11, 493-497.
88. A. Marinoiu, G. Ionita, C.-L. Gaspar, C. Cobzaru, S. Oprea, *React. Kinet. Catal. Lett.* **2009**, 97, 315-320.
89. J. Zhou, J. Zhang, X. Guo, J. Mao,S. Zhang, *Green Chem.* **2012**, 14, 156-163.
90. L. Huang, Y.-L. Zhu, H.-Y. Zheng, Y.-W. Li, Z.-Y. Zeng, *J. Chem. Technol. Biotechnol.* **2008**, 83, 1670-1675.
91. J. Zheng, W. Zhu, C. Ma, Y. Hou, W. Zhang, Z. Wang, *Reac. Kinet. Mech. Cat.* **2010**, 99, 455-462.
92. S.-L. Hao, W. -C. Peng, N. Zhao, F.-K. Xiao, W. Weia, Y.-H. Sun , *J. Chem. Technol. Biotechnol.* **2010**, 85, 1499-1503.
93. Z. Zhou, X. Li, T. Zeng, W. Hong, Z. Cheng, W. Yuan, *Chin. J. Chem. Eng.* **2010**, 18, 384-390.
94. S. Panyad, S. Jongpatiwut, T. Sreethawong, T. Rirksomboon, S. Osuwan, *Catal. Today*, **2011**, 174, 59-64.
95. A. Wołosiak-Hnat, E. Milchert, G. Lewandowski, B. Grzmil, *Polish J. Chem. Technol.* **2011**, 13, 71-76.
96. Y. Feng, H. Yin, A. Wang, L. Shen, L. Yu, T. Jiang, *Chem. Eng. J.* **2011**,168 , 403-412.
97. I. Jiménez-Morales, F. Vila , R. Mariscal, A. Jiménez-López, *Appl. Catal. B* **2012**, 117– 118, 253-259.

98. F. Vila, M. López Granados, M. Ojeda, J.L.G. Fierro, R. Mariscal , *Catal. Today* **2012**, 187, 122-128.

99. T. Sánchez, P. Salagre, Y. Cesteros, A. Bueno-López, *Chem. Eng. J*. **2012** ,179, 302-311.

100. H. L. Hoşgün, M. Yıldız, H. F. Gerçel, *Ind. Eng. Chem. Res.* **2012**, 51, 3863-3869.

101. Z. Xiao, S. Jin, X. Wang, W. Li, J. Wang, C. Liang, *J. Mater. Chem.* **2012**, 22, 16598-16605.

102. S. Xia, R. Nie, X. Lu , L. Wang, P. Chen , Z. Hou, *J. Catal.* **2012**, 296,1-11.

103. Y. Feng, H. Yin, L. Shen, A. Wang, Y. Shen, T. Jiang, *Chem. Eng. Technol.* **2013**, *36*, 73-82.

104. A. Wolosiak-Hnat, E. Milchert, B. Grzmil, *Chem. Eng. Technol.* **2013**, 36, 411-418.

105. A. Wołosiak-Hnat, E. Milchert, G. Lewandowski, *Org. Process Res. Dev.* **2013**, 17, 701-713.

106. T. M. Che, US Patent 4642394, **1987**.

107. E. Drent, W. W. Jager, US Patent 6080898, **2000.**

108. G. Braca, A. M. R. Galletti, G. Sbrana, *J. Organomet. Chem.* **1991**, 417, 41-49.

109. M. Schlaf, P. Ghosh, P. J. Fagan, E. Hauptman, R. M. Bullock, *Angew. Chem. Int. Ed.* **2001**, 113, 4005-4008.

110. M. Schlaf, P. Ghosh, P. J. Fagan, E. Hauptman, R. M. Bullock, *Angew. Chem. Int. Ed.* **2001**, 40, 3887-3890.

111. C. Montassier, D. Giraud, J. Barbier, J. P. Boitiaux, *Bull. Soc. Chim. Fr*. **1989**, 2, 148-155.

112. Y. Kusunoki, T. Miyazawa, K. Kunimori, K. Tomishige, *Catal. Commun.*, **2005**, 6, 645-649.

113. T. Miyazawa, Y. Kusunoki, K. Kunimori, K. Tomishige, *J. Catal.*, **2006**, 240, 213-221.

114. I. Furikado, T. Miyazawa, S. Koso, A. Shimao, K. Kunimori, K. Tomishige, *Green Chem.* **2007**,9, 582-588.

115. T. Miyazawa, S. Koso, K. Kunimori, K. Tomishige, *Appl. Catal. A* **2007**, 318, 244-251.

116. T. Miyazawa, S. Koso, K. Kunimori, K. Tomishige, *Appl. Catal., A* **2007**, 329, 30-35.

117. E. S. Vasiliadou, E. Heracleous, I. A. Vasalos, A. A. Lemonidou, *Appl. Catal. B* **2009**, 92, 90-99.

118. B. Bachiller-Baeza, A. Guerrero-Ruiz, I. Rodriguez-Ramos, *J. Catal.* **2005**, 229, 439-445.

119. E. van Ryneveld, A. S. Mahomed, P. S. van Heerden, H. B. Friedrich, *Catal. Lett.* **2011**, 141, 958-967.

120. A. Alhanash, E. F. Kozhevnikova, I. V. Kozhevnikov, *Catal. Lett.* **2008**, 120, 307-311.

121. M. Balaraju, V. Rekha, P. S. Sai Prasad, B. L. A. Prabhavati Devi, R. B. N. Prasad, N. Lingaiah, *Appl. Catal. A* **2009**, 354, 82-87.

122. M. Balaraju, V. Rekha, B. L. A. Prabhavati Devi, R. B. N. Prasad, P. S. Sai Prasad, N. Lingaiah, *Appl. Catal. A* **2010**, 384, 107-114.

123. E. P. Maris, R. J. Davis, *J. Catal.* **2007**, 249, 328-337.

124. N. Hamzah, N. M. Nordin, A. H. A. Nadzri, Y. A. Nik, M. B. Kassim, M. A. Yarmo, *Appl. Catal. A* **2012**, 419– 420, 133-141.

125. M. L. Barbelli, G. F. Santori, N. N. Nichio, *Bioresour. Technol.* **2012**, 111, 500-503.

126. M. G. Musolino, L. A. Scarpino, F. Mauriello, R. Pietropaolo, *ChemSusChem* **2011**, 4, 1143-1150.

127. Y. Zhang, X.-C. Zhao, Y. Wang, L. Zhou, J. Zhang, J. Wang, A. Wang, T. Zhang, *J. Mater. Chem. A* **2013,** 1, 3724-3732.

128. J. Zhou, J. Zhang, X. Guo, J. Mao,S. Zhang, *Green Chem.* **2012**, 14, 156-164.

129. J. Feng, J. Wang, Y. Zhou, H. Fu, H. Chen, X. Li, *Chem. Lett.* **2007**, 36, 10, 1274

130. L. Ma, D. He , Z. Li, *Catal. Commun.* **2008**, 9, 2489-2495.

131. Z. Yuan, P. Wu, J. Gao, X. Lu, Z. Hou, X. Zheng , *Catal. Lett.* **2009**, 130, 261-265.

132. J. Wang, S. Shen, B. Li, H. Lin, Y. Yuan, *Chem. Lett.* **2009**, 38, 572-573.

133. I. Gandarias, P. L. Arias, J. Requies, M. B. Güemez, J. L.G. Fierro, *Appl.Catal. B* **2010**, 97, 248-256.

134. S. Bolado, R. E. Treviño, M. Teresa García-Cubero, G. González-Benito, *Catal. Comm.* **2010**, 12, 122–126.

135. L. Ma, D. He, *Catal. Today* **2010**, 149,148-156.

136. B. Li, J. Wang,Y. Yuan, H. Ariga, S. Takakusagi, K. Asakura, *ACS Catal.* **2011**, 1, 1521-1528.

137. S.-H. Lee, D. J. Moon, *Catal. Today* 2011, 174, 10-16.

138. E. S. Vasiliadou , A. A. Lemonidou, *Org. Process Res. Dev.* **2011**, 15, 925-931.

139. R. Rodrigues, N. Isoda, M. Gonçalves, F.C.A. Figueiredo, D. Mandelli, W.A. Carvalho, *Chem. Eng. J.* **2012**,198–199, 457–467

140. M. Checa, F. Auneau, J. Hidalgo-Carrillo, A. Marinas, J. M. Marinas, C. Pinel, F. J. Urbano, *Catal. Today* **2012**,196, 91-100.

141. S. N. Delgado, D. Yap, L. Vivier, C. Especel, *J. Mol. Catal. A* **2013**, 367, 89-98.

142. T. Jiang, Y. Zhou, S. Liang, H. Liu, B. Han, *Green Chem.* **2009**, 11, 1000-1006.

143. S. X. Xia, Z. L. Yuan, L. N. Wang, P. Chen, Z. Y. Hou, *Appl. Catal. A* **2011**, 403, 173-182.

144. S. Xia, Z. Yuan, L. Wang, P. Chen, Z. Hou, *Bioresour. Technol.* **2012**, 104, 814-817.

145. Z. Wu, Y. Mao, X. Wang, M. Zhang, *Green Chem.* **2011**, 13, 1311-1316.

146. H. Z. Liu, S. G. Liang, T. Jiang, B. X. Han, Y. X. Zhou, *CLEAN- Soil, Air, Water* **2012**, 40, 318-324.

147. N. D. Kim, J. R. Park, D. S. Park, B. K. Kwak, J. Yi, *Green Chem.* **2012**, 14, 2638-2646.

148. X. Liao, K. Li , X. Xiang, S.-G. Wang, X. She, Y. Zhu , Y. Li, *J. Ind. Eng. Chem.* **2012**, 18, 818-821.

149. G. W. Huber, J. W. Shabaker, J. A. Dumesic, *Science* **2003**, 300, 2075-2077

150. E. D'Hondt, S. Van de Vyver, B. F. Sels, P. A. Jacobs, *Chem. Commun.* **2008**, 6011-6012.

151. D. Roy, B. Subramaniam, R. V. Chaudhari, *Catal. Today* **2010**, 156, 31-37.

152. M. L. Barbelli, G. F. Santori, N. N. Nichio, *Bioresour. Technol.* **2012**, 111, 500-503.

153. C. Pendem, P. Gupta,N. Chaudhary, S. Singh, J. Kumar, T. Sasaki, A. Datta, R. Bal, *Green Chem.*, **2012**, 14, 3107-3113.

154. A. -Y. Yin, X. -Y. Guo, W. -L. Dai, K. -N. Fan, *Green Chem.* **2009**, 11, 1514-1516.

155. R. B. Mane, C. V. Rode, *Green Chem.* **2012**, 14, 2780-2789.

156. M. G. Musolino, L. A. Scarpino, F. Mauriello, R. Pietropaolo, *Green Chem.* **2009**, 11, 1511-1513.

157. I. Gandarias, P. L. Arias, J. Requies, M. El Doukkali, M. B. Güemez, *J. Catal.* **2011**, 282, 237-247.

158. I. Gandarias , J. Requies , P. L. Arias , U. Armbruster , A. Martin, *J. Catal.* **2012**, 290, 79-89.

159. I. Gandarias, P. L. Arias, Sara. G. Fernández, J. Requies, M. El Doukkali, M. B. Güemez, *Catal. Today* **2012**, 195, 22-31.

160. H. Jiye, L. Xiaoyu, F. Yiqiu , X. Songhai , P. Yan , Q. Minghua , F. Kangnian , Z. Xiaoxin , Z. Baoning, *Chinese J. Catal.* **2013,** 34, 1020-1026.

161. S. Xia, L. Zheng, L. Wang, P. Chen, Z. Hou, *RSC Adv.* **2013**, 3,16569-16576.

162. T. Haas, A. Neher, D. Arntz, H. Klenk ,W. Girke, US Patent 5426249, **1995.**

163. L. Schuster, M. Eggersdorfer, US Patent 5616817, **1995.**

164. R. M. Bullock, P. J. Fagan, E. M Hauptman, M. Schalf, WO Patent 98241, **2001.**

165. S. Chopade, D. Miller, J. Jackson, T. Werpy, J. Frye Jr, A. Zacher, US Patent 6291725, **2001.**

166. T. Werpy, J. Frye, A. Zacher , D. Miller, WO Patent 03035582, **2002**.

167. G. J. Suppes, W. R. Sutterling, M. A. Dasari, WO Patent 095536, **2005**.

168. G.J. Suppes, W. R. Sutterlin, WO Patent 53705, **2007**.

169. J. Henkelmann, M. Becker, P. Wahl, G. Theis , S. Mauer, WO Patent 99161, **2007**.

170. S. Achim , F. Oliver, WO Patent 89899, **2008.**

171. P. Bloom, US Patent 0103339, **2008**.

172. R. Abhari, WO Patent 54701, **2009**.

173. C. Rabello, M. Gomes, B. G.Siqueira, R. B. De Menezes, W. K. Huziwara, T. S. Yamada, L. M. M. De Oliveira, G. de C. Oliveira, W.V. C. Candido, EP Patent 2540692 A2, **2011**

174. H. M. Brown, J. G. Frye, D. M. Santosa, A.H. Zacher ,US Patent 0207972A1, **2011**.

175. R. V. Chaudhari, D. S. Roy, B. Subramaniam, US Patent 0004029 A1, **2011.**

176. A. Stankowiak, O. Franke, J. Appel, D. Buehring, O. Wachsen, US Patent 0071323 A1, **2011**.

177. A. Lemonidou, E. Vasileiadou, EP Patent 2565175 A1, **2011**.

178. G. J. Suppes, W. R. Sutterlin, M. A. Dasari, EP Patent 2298722 A2, **2011**.

179. C. V. Rode , A. M. Hengne, A. A. Ghalwadkar, R. B. Mane, P. H. Mohite, H. S. Potdar, WO Patent 138643 A2, **2011**.

180. N. Suzuki, M. Tamura, T. Mimura, US Patent 8258351, **2012**.

181. R. V. Chaudhari, D. S. Roy, B. Subramaniam, US Patent 8252963, **2012**.

182. G. J. Suppes, US Patent 8252961 B2, **2012.**

183. D. C. Molzahn, K. A. Burdett, W. L. Gibson, K. J. Kriel, J. E. McCreight, I. Mathur, US Patent 8324434 B2, **2012**.

Chapter 2

Experimental methods and physico-chemical characterization

Includes experimental procedures followed for the preparation of various catalysts, their characterization and activity testing for glycerol hydrogenolysis, dehydration and water gas shift reactions in both batch and continuous operations. Analytical methods used for identification of gaseous and liquid products are also described in this chapter.

2.1. INTRODUCTION

Activity of the prepared catalysts generally depends upon their textural properties such as surface area, particle and crystallite size, planes and/or phases of the active species, extent of reduction, acidity, morphology *etc.* These in turn depend upon their method of preparation procedures and the pretreatment conditions such as calcination and reduction particularly applicable to hydrogenation catalysts.[1,2] In order to understand the structure-activity correlation, detailed characterization of the calcined, reduced and recovered catalysts is also very crucial. Present chapter describes details of procedures followed for the preparation of various catalysts, catalyst characterization, activity testing of the prepared catalysts and the analytical methods used for gaseous and liquid product identification of glycerol hydrogenolysis, dehydration and water gas shift reactions.

2.2. MATERIALS

Refined glycerol (99%), was purchased from Merck Specialities, Mumbai, India while, bio-glycerol was obtained by transesterification of vegetable oil and methanol (1:6) in the presence of KOH. The assay of the bio-glycerol determined by GC was 48%, which was directly used without any pretreatment for making a feed concentration of 20 wt% aqueous solution. Ethylene glycol (EG), acetol, 1,2-Propanediol (1,2-PDO), and 2-propanol were purchased from Sigma– Aldrich, Bangalore, India. Nitrate precursors of copper, aluminium, barium, magnesium, zirconium, zinc and potassium, ammonium dichromate, 30% aqueous ammonia, and potassium carbonate were purchased from Loba Chemie, Mumbai, India. Sodium hydroxide (NaOH) and anhydrous sodium carbonate (Na_2CO_3) were purchased from Merck Specialties and S. d. Fine-Chem-Ltd., Mumbai, India, respectively. Zirconium oxychloride, ammonia solution, sulphuric acid, and hexane were purchased from Thomas Baker, India. Potassium hydroxide (KOH, 98%) and hydrochloric acid (HCl, 35.4%) were purchased from Loba Chemie, Mumbai, India. 3% Pt/C, SiO_2, and Al_2O_3 were purchased from Sigma-Aldrich, Bangalore, India.

Fly ash used here, was collected from the Parali Thermal Power Station of Ambajogai District, India. The chemical composition of the fly ash (on a dry wt% basis)

was 73.13% SiO_2, 21.18% Al_2O_3, 7.3% Fe_2O_3, 0.23% Na_2O, 1.72% CaO, 0.29% MgO, and 0.40% K_2O. Hydrogen and nitrogen gases of high purity (99.99%) were obtained from M/s. Inox Ltd. Mumbai, India.

2.3. CATALYST PREPARATION

2.3.1. Copper chromite (Cu-Cr)

Copper chromite catalysts were prepared by co-precipitation method by varying Cu-Cr composition and with the addition of various promoters like Al, Ba, Zn and their various combinations.[3] In a typical preparation procedure, the required amounts of each of nitrate precursors of copper [$Cu(NO_3)_2.3H_2O$] (Precursor 2) and of the respective promoters, Al, Zn or Ba were dissolved in deionized water (Promoter 1, 2). To this solution, the aqueous solution of ammonium chromate (Precursor 1) was added drop wise which was already prepared by drop wise addition of 30% aqueous ammonia to an aqueous solution of ammonium dichromate. Then reddish brown precipitate formed was separated by filtration and washed with deionized water. The obtained precipitate was dried in an oven at 100 ^oC for 5-8 h. A schematic of the preparation method is shown in **Figure 2.1** and a detailed percentage composition of the catalysts used for glycerol hydrogenolysis are given in **Table 2.1**.These catalysts were nominated as "NMT" catalysts.

2.3.2. Patented procedure for Cu-Cr with Ba as a promoter

Copper chromite catalyst was prepared according to the patented literature procedure in which barium was used as an additive and was designated as NMT-P.[4] In a typical preparation procedure, 0.01 moles (2.6 g) of barium nitrate was dissolved in 80 mL distilled water and warmed at 70 ^oC to obtain a clear solution. To this solution, 0.09 moles (21.8 g) of copper nitrate was added and the mixture was stirred at 70 ^oC until a clear solution was observed.

A solution of ammonium chromate prepared by dissolving 0.05 (12.6 g) moles of

ammonium dichromate in 60 mL of distilled water and adding 15 mL of the 30% aqueous ammonia was poured in to the warm solution of the nitrate in a thin stream under constant stirring. Stirring was continued for few minutes after which the reddish brown precipitate of copper barium ammonium chromate was obtained. The obtained precipitate after drying was then transferred into a beaker containing 75 mL of 10% acetic acid under stirring. After a few minutes, the stirring was stopped in order to settle down the residue for 10 min and then two- third of the spent acid was decanted and again replaced by 75 mL of fresh 10% acetic acid and this extraction was repeated for 2-3 times. The obtained residue was again extracted with distilled water for four times which was then filtered and dried at 110 ^{o}C.

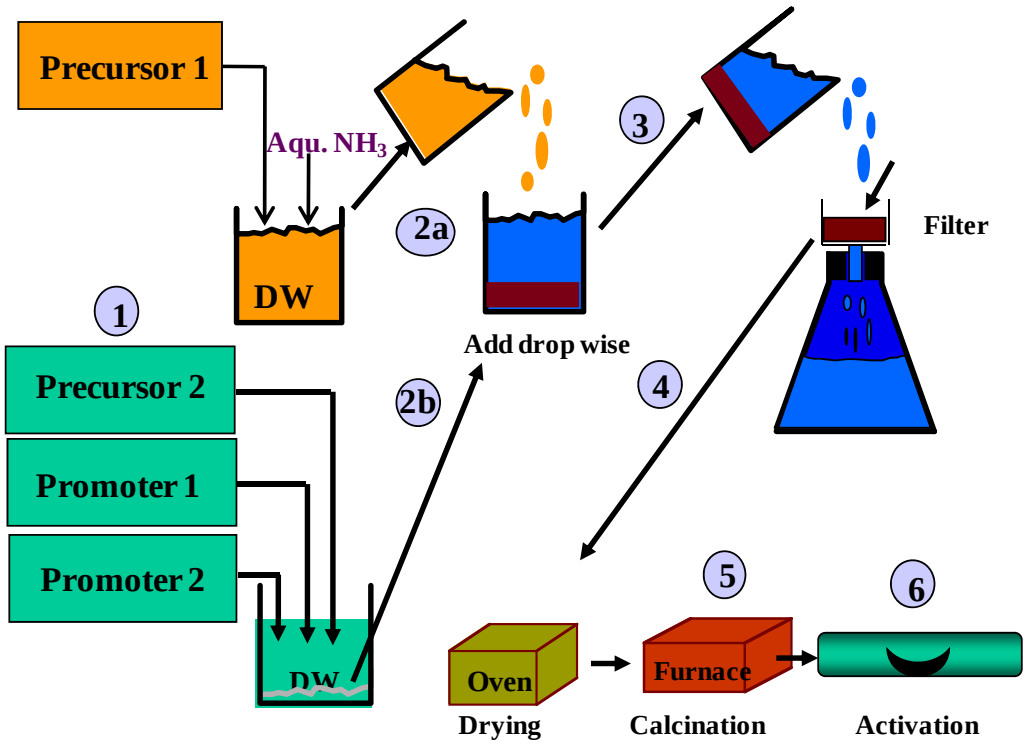

Figure 2.1. Preparation of copper chromite catalyst.

Table 2.1. Composition of Cu-Cr catalysts

Catalyst	Copper (%)	Chromium (%)	Promoters (%)		
			Ba	Al	Zn
NMT001	53	27	-	20	-
NMT002	30	31	-	39	-
NMT005	41	29	30	-	-
NMT006	66	34	-	-	-
NMT008	40	31	10	19	-
NMT011	54	30	-	-	16
T1	25	25	-	11	39
T2	25	25	-	39	11
T3	41	44	15	-	-
T4	41	19	40	-	-

2.3.3. Nano Cu-Al

The nano structured Cu–Al catalyst was prepared by a simultaneous co-precipitation and digestion method with co-addition of an equimolar (0.05 M) mixture of an aqueous solution of Cu $(NO_3)_2 \cdot 3H_2O$, $Al(NO_3)_3 \cdot 9H_2O$ and 0.2 M aqueous K_2CO_3 in a round bottom flask having 5–10 mL of water at room temperature.[5] After complete addition, the precipitate was digested further for 4–5 h and then filtered and washed with deionized water to remove the traces of potassium. The precipitate was dried in an oven at 100 °C for 5–8 h. A schematic of the preparation procedure is shown in **Figure 2.2.**

Following the same procedure described above, other Cu–Al catalysts were prepared by using different precipitating agents *viz.* KOH, NaOH and Na_2CO_3 and the

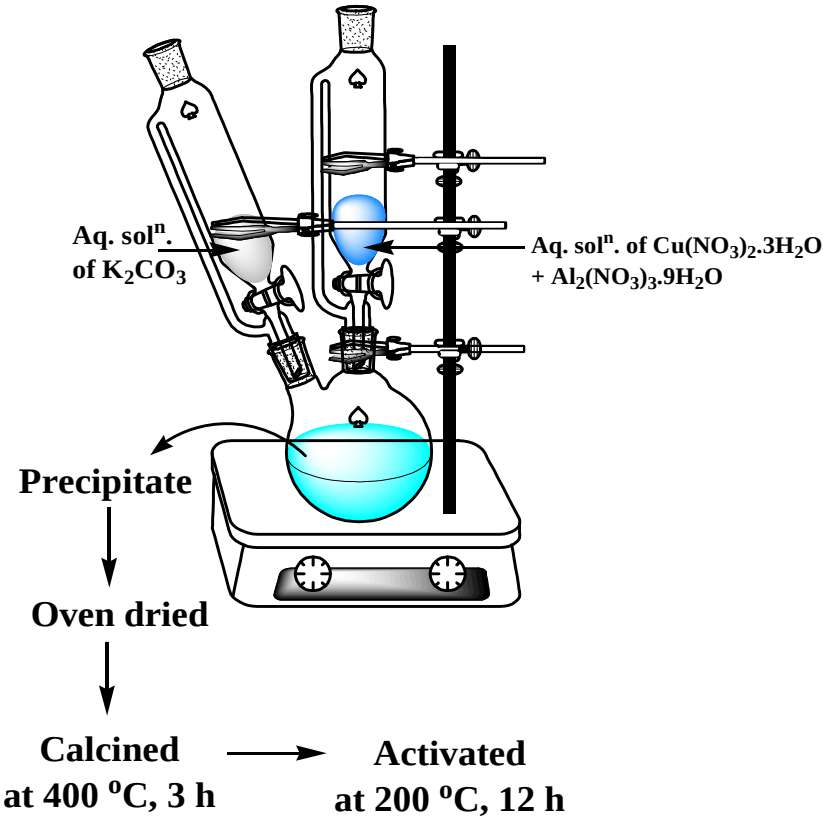

Figure 2.2. Preparation of nano Cu-Al catalyst.

final pH of the precipitate was maintained in a range of 8–9. The prepared catalysts were nominated as CAP (respective alkali formula) *e.g.* CAP (K_2CO_3), CAP (Na_2CO_3), CAP (NaOH), CAP (KOH).[6]

The catalysts with different at.% of Cu *viz.* 10, 30, 50, 70 and 80% were also prepared by the same simultaneous co-precipitation and digestion technique and were designated as Cu-Al-1, Cu-Al-3, Cu-Al-5, Cu-Al-7 and Cu-Al-8, respectively.[7] Copper catalysts with metals other than Al (Ba, Mg, Zr, Zn) were also prepared by simultaneous co-precipitation and digestion method. The prepared catalysts were nominated as Cu–Ba, Cu– Mg, Cu–Zr, and Cu–Zn. The Cu content was kept constant at 50 at.% in all these catalysts.[8]

2.3.4. Solid state fusion followed by precipitation

$Al(NO_3)_3 \cdot 9H_2O$ was mixed with NaOH flakes in the molar ratio of $Al(NO_3)_3 \cdot 9H_2O$: NaOH = 1:3. After drying, the resultant solid powder was heated at 550 ^oC in air for 2 h. The ground fused mass was then added to water (10 mL g^{-1} of fused mass) with constant stirring which was continued further for 1 h. To this, the required amount of 0.5 molar aqueous solution of $Cu(NO_3)_2 \cdot 3H_2O$ was added under constant stirring, to form a precipitate of Cu–Al having a mole ratio=1:1. An aq. NaOH solution was used to adjust the pH of ~9. The resultant slurry was further stirred for 3 h and the precipitate was recovered by filtration and washed with deionized water and dried at 80 ^oC for 8 h.[6] Following the same procedure, another catalyst was prepared by replacing NaOH by KOH and both the catalysts were designated as CAF (KOH) and CAF (NaOH), respectively.

2.3.5. Solid state fusion

A physical mixture of the $Al(NO_3)_3 \cdot 9H_2O$, $Cu(NO_3)_2 \cdot 3H_2O$ and KNO_3 was prepared in the molar ratio of 1:1:1 which was dissolved in a minimum quantity of water and dried. After drying, the ground powder was heated at 550 ^oC in air for 2 h and designated as CAF (KNO_3).[9]

2.3.6. Cu impregnated on parent fly ash (FA-1)

Catalyst was prepared by depositing copper nitrate on parent fly ash by a wet impregnation method, keeping the molar ratio of Al(present in the fly ash):Cu = 1:1. Prepared sample was dried at 80 ^oC for 8 h.[9]

2.3.7. Cu on fused fly ash by precipitation (FA-2)

First, fused fly ash was prepared by a typical solid state alkali metal hydroxide fusion method in which fly ash was initially mixed in a weight ratio of fly ash to KOH flakes of

1:1.2. After milling, the powder was poured into a stainless steel tray and heated at 550 ^{o}C in air for 1 h. The fused fly ash was then ground and used for Cu loading. To the above fused fly ash sample, water was added in the ratio 1:2 and the resulting slurry was aged for one day under stirring at room temperature. Finally, the required amount of 0.5 molar aqueous solution of Cu $(NO_3)_2{\cdot}3H_2O$ was added slowly to the fused fly ash slurry under constant stirring. The final pH of the slurry was adjusted to ~9 by adding KOH and stirring was further continued for 3 h. The precipitate formed was then filtered and washed with deionised water. The wet cake thus obtained was dried at 80 ^{o}C for 8 h. A schematic of the preparation procedure is shown in **Figure 2.3.**[9]

Following the similar procedure, the Cu content was varied in the range of (Al:Cu = 3:1–1:3) and the resultant samples were designated as FA-2 (3:1), FA-2 (2:1), FA-2 (1:1), FA-2 (1:2), FA-2 (1:3).

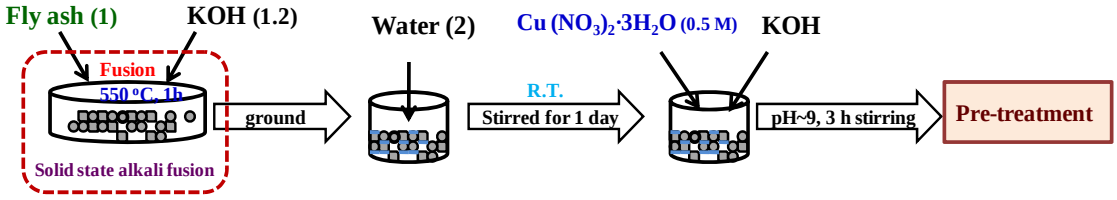

Figure 2.3. Preparation of Cu on fused fly ash catalyst.

2.3.8. Cu impregnated on acid treated fly ash (FA-3)

Parent fly ash sample was first sieved through 200 mesh size and the unburnt carbon present in the fly ash was removed by calcination at 800 ^{o}C for 2 h. The fly ash sample was further treated with 1 M hydrochloric acid (10 mL g^{-1}) under stirring for 10 h and then filtered, washed thoroughly with water until it was free from chloride. It was then dried at 120 ^{o}C. Cu was then deposited by wet impregnation on acid treated fly ash.[9]

2.3.9. Cu on acid treated fly ash by precipitation (FA-4)

Acid treated fly ash prepared as above (Section 2.3.8) was used for Cu deposition by a

precipitation method. 0.2 M potassium hydroxide was added slowly to the slurry of acid treated fly ash and 0.5 M $Cu(NO_3)_2 \cdot 3H_2O$ aqueous solution, until the pH of the solution reached ~9. The precipitate formed was further aged for 6 h at room temperature and then filtered, washed with deionised water and dried in a static air oven at 100 ^oC.[9]

2.3.10. 20% Cu impregnated on Al_2O_3

20% $Cu–Al_2O_3$ catalyst was prepared by a wet impregnation method, in which $Cu(NO_3)_2 \cdot 9H_2O$ (15.76 mmol) was dissolved in water to which alumina (39 mmol) was added and the slurry was stirred for 12 h. Thereafter excess water was removed on a rotavap and oven dried at 100 °C.[10]

All the catalysts prepared and used in this work were calcined under the conditions given in **Table 2.2.** The calcined samples were then reduced (activated) under H_2 flow at 200 ^oC for 12 h, prior to their use for the reactions.

Table 2.2. Calcination program

Temperature (^oC)	Ramp (^oC min.$^{-1}$)	Hold time (h)
100	10	1
200	10	1
300	10	1
400	10	3

2.3.11. Sulfated zirconia ($S–ZrO_2$)

For the preparation of sulfated zirconia ($S–ZrO_2$), 25 g of zirconium oxy-chloride ($ZrOCl_2.8H_2O$) was dissolved in doubly distilled water. To this clear solution, dilute aqueous ammonia was added drop-wise from a burette with vigorous stirring till the pH

of the solution reached 9. The obtained precipitate was washed with distilled water until free from chloride ions and dried at 120 ^{o}C for 24 h. A portion of the obtained hydrous zirconia sample was ground to fine powder and added to 1 M H_2SO_4 solution (30 mL) for 30 min. Excess water was evaporated on a water bath and the resulting sample was oven dried at 120 ^{o}C for 12 h and calcined at 650 ^{o}C for 4 h in air atmosphere and stored in vacuum desiccator.[8]

2.4. CHARACTERIZATION TECHNIQUES

2.4.1. Surface area measurement

The common method for measuring surface area of the catalyst is based on the theory developed by Brunauer, Emmett and Teller (BET) in 1938, considering the concept of multilayer adsorption. [11]

The isotherm points are transformed into the linear version of BET equation as given below:

$$\frac{1}{v\left[\left(\frac{P_0}{P}\right)-1\right]} = \frac{c-1}{v_m c}\left(\frac{P}{P_0}\right) + \frac{1}{v_m c} \qquad (2.1)$$

where,

P, P_0 = equilibrium and the saturation pressures of adsorbates at the temperature of adsorption,

v = adsorbed gas quantity (in volume units),

υ_m = monolayer adsorbed gas quantity,

c = BET constant, which is expressed by following equation.

$$c = \exp\left(\frac{E_1 - E_L}{RT}\right) \qquad (2.2)$$

where,

E_1 = heat of adsorption for the first layer,

E_L = heat of adsorption for the second and higher layers and is equal to the heat of

liquefaction.

Equation (2.1) is an adsorption isotherm and can be plotted as a straight line with 1 / v[(P_0 / P) − 1] on the y-axis and ϕ = P / P_0 on the x-axis according to the experimental results. This plot is called a BET plot. The linear relationship of this equation is maintained only in the range of 0.05 < P / P_0 < 0.35. The value of the slope (A) and the y-intercept (I) of the line are used to calculate the monolayer adsorbed gas quantity v_m and the BET constant c. The following equations for v_m and c can be used.

$$v_m = \frac{1}{A+I} \tag{2.3}$$

$$c = 1 + \frac{A}{I} \tag{2.4}$$

Total surface area (S_{total}) and a specific surface area (S_{BET}) are evaluated by the following equations,

$$S_{total} = \frac{v_m N s}{V} \tag{2.5}$$

$$S_{BET} = \frac{S_{total}}{a} \tag{2.6}$$

where,

v_m = units of volume which are also the units of the molar volume of the adsorbate gas,

N = Avogadro's number,

s = adsorption cross section of the adsorbing species,

V = molar volume of adsorbate gas and

a = mass of adsorbent (g)

The BET surface area and pore volume of the catalyst samples were determined by a N_2 adsorption–desorption technique using a Quantachrome Quadrasorb automatic volumetric instrument.

2.4.2. X-ray diffraction (XRD)

Powder X-ray diffraction uses X-rays to investigate and quantify the crystalline nature of materials by measuring the diffraction of X-rays from the planes of atoms within the

material.[12] It is sensitive to both the types and relative position of atoms in the material as well as the length scale over which the crystalline order persists. It can, therefore, be used to measure the crystalline content of materials; identify the crystalline phases present (including the quantification of mixtures in favourable cases); determine the spacing between lattice planes and the length scales over which they persist; and to study preferential ordering and epitaxial growth of crystallites. In essence, it probes length scales from approximately sub angstroms to a few nm and is sensitive to ordering over tens of nanometres.

This method involves the interaction between the incident monochromatized X-rays (like Cu Kα or Mo Kα source) with the atoms of a periodic lattice of the solid material.[13] In materials with regular structure (*i.e.* crystalline), the scattered X-rays undergo constructive and destructive interference. This is the process of diffraction. The diffraction of X-rays by crystals is described by Bragg's Law:

$$n\lambda = 2d\sin\theta \tag{2.7}$$

where,

n = 1, 2, 3 (integer called order of the diffraction)

λ = wavelength of the X-rays, Å

d = distance between two lattice planes, Å,

θ = angle (deg.) between the incoming X-rays and the normal to the reflecting lattice plane.[14]

The interplanar distances or *d*-spacings are calculated from the values of the peaks observed from the above Bragg's equation. The width of diffraction peaks carries information on the dimensions of the reflecting planes. For crystals with size below 100 nm, line broadening occurs due to incomplete destructive interference in scattering directions where the X-rays are out of phase. The crystallite size can be calculated from the Debye- Scherrer equation, as given below:

$$D_{hkl} = k\lambda / \beta\cos\theta \tag{2.8}$$

where,

D_{hkl} = volume averaged particle diameter, Å

k = Scherrer's constant (0.9)

λ = X-ray wavelength, Å

β = full width at half maximum (FWHM), radian.

θ = diffraction angle, deg.

For example, the crystallite size of the prepared Cu-Cr-Ba catalyst was calculated from XRD data **(Chapter 3, Figure 3.1)** as follows:

Data: λ = 1.54178 Å; β (FWHM) = 0.1224 deg.; θ = 43.4 ^{o} (β and θ were measured from XRD graph)

Particle size (D) = (0.9 x 1.54178)/ [0.1224 x 3.14/180 x Cos (43.4/2)] = 698.73 Å

X-ray powder diffraction patterns of all the catalysts reported in this thesis were recorded on a P Analytical PXRD system (Model X-Pert PRO-1712), using Ni filtered Cu Kα radiation (λ= 0.154 nm) as an X-ray source (current intensity, 30 mA; voltage, 40 kV) and an X-accelerator detector. The samples were scanned in a 2θ range of 10–80 ^{o}. The species present on the surface were identified by their characteristic 2θ values of the relevant crystalline phase.

2.4.3. Transmission electron microscopy (TEM)

Transmission electron microscopy uses high energy electrons (up to 300 kV accelerating voltage) which are accelerated to nearly the speed of light. The electron beam behaves like a wave front with wavelength about a million times shorter than light waves. When an electron beam passes through a thin-section specimen of a material, electrons are scattered. A sophisticated system of electromagnetic lenses focuses the scattered electrons into an image or a diffraction pattern, or a nano-analytical spectrum, depending on the mode of operation. Each of these modes offers a different insight about the

specimen. The imaging mode provides a highly magnified view of the micro- and nanostructure and ultimately, in the high resolution imaging mode a direct map of atomic arrangements can be obtained (high resolution EM = HREM). Crystal structure can also be investigated by high-resolution transmission electron microscopy (HRTEM), also known as phase contrast. When utilizing a field emission source and a specimen of uniform thickness, the images are formed due to differences in phase of electron waves, which is caused by specimen interaction.[15] Image formation is given by the complex modulus of the incoming electron beams. As such, the image is dependent on the number of electrons hitting the screen, making direct interpretation of phase contrast images more complex. However, this effect can be used to an advantage, as it can be manipulated to provide more information about the sample, such as in complex phase retrieval techniques.

The diffraction mode (electron diffraction) displays accurate information about the local crystal structure called selected area electron diffraction (SAED).[16] By adjusting the magnetic lenses such that the back focal plane of the lens rather than the imaging plane is placed on the imaging apparatus to generate a diffraction pattern. For thin crystalline samples, this produces an image that consists of a pattern of dots in the case of a single crystal, or a series of rings in the case of a polycrystalline or amorphous solid material. For the single crystal case, the diffraction pattern is dependent upon the orientation of the specimen and the structure of the sample illuminated by the electron beam. This image provides the investigator with information about the space group symmetries in the crystal and the crystal's orientation to the beam path. This is typically done without utilising any information but the position at which the diffraction spots appear and the observed image symmetries. More complex behaviour in the diffraction plane is also possible, with phenomena such as Kikuchi lines arising from multiple diffraction within the crystalline lattice.

The nano analytical modes [x-ray and electron spectrometry or energy-dispersive X-ray spectroscopy (EDS)] tells us which elements are present in the tiny volume of material. It can also be used to obtain chemical and electronic information at the sub-nanometer scale.

In this work, the transmission electron microscopy (TEM) analysis was performed

on a Jeol Model JEM 1200 electron microscope operated at an accelerating voltage of 120 kV. A small amount of specimen was prepared by ultrasonically suspending the powder sample in ethanol, and drops of the suspension were deposited on a carbon coated copper grid dried at room temperature before analysis.

2.4.4. Scanning electron microscope (SEM) and energy dispersive X-ray (EDX) techniques

In scanning electron microscopy (SEM), an electron beam is scanned across the sample's surface. It allows direct observations of topography and morphological features with high resolution and depth of field than optical microscope.[17] When the electrons strike the sample, a variety of signals are generated, and it is the detection of specific signals which produces an image or a sample's elemental composition. The three signals which provide the greatest amount of information in SEM are the secondary electrons (SE), backscattered electrons (BSE), and X-rays.

Secondary electrons are emitted from the atoms occupying the top surface and produce a readily interpretable image of the surface. The contrast in the image is determined by the sample morphology. A high resolution image can be obtained because of the small diameter of the primary electron beam.

Backscattered electrons are primary beam electrons which are 'reflected' from atoms in the solid. The contrast in the image produced is determined by the atomic number of the elements in the sample. The image will therefore show the distribution of different chemical phases in the sample. Because these electrons are emitted from a depth in the sample, the resolution in the image is not as good as for secondary electrons.

Interaction of the primary beam with atoms in the sample causes shell transitions which result in the emission of an X-ray. The emitted X-ray has an energy characteristic of the parent element. Detection and measurement of the energy permits elemental analysis (Energy Dispersive X-ray Spectroscopy or EDS). EDS can provide rapid qualitative, or with adequate standards, quantitative analysis of elemental composition with a sampling depth of 1-2 microns. X-rays may also be used to form maps or line profiles, showing the elemental distribution in a sample surface.

The chemical composition and morphology of the sample were determined by energy dispersive X-ray (EDX) attached to SEM (JEOL JSM 500).

2.4.5. Inductively coupled plasma atomic emission spectroscopy (ICP-AES)

Inductively coupled plasma atomic emission spectroscopy (ICP-AES), also referred to as inductively coupled plasma optical emission spectrometry (ICP-OES), is an analytical technique used for the detection of trace metals. It is a type of emission spectroscopy that uses the inductively coupled plasma to produce excited atoms and ions that emit electromagnetic radiation at wavelengths characteristic of a particular element.[18,19] The intensity of this emission is indicative of the concentration of the element within the sample.

The Cu content was determined from inductive coupled plasma (ICP) analysis with a Spectro 165 high resolution ICP-OES Spectrometer (model no. ARCOSFHS 12). 25 mg of catalyst was treated with aqua regia (HNO_3–HCl = 1 : 3) at 60 °C on a sand bath for 2 h and the obtained solid was dissolved in 50 mL distilled water.

2.4.6. X-ray photoelectron spectroscopy (XPS)

XPS is a quantitative spectroscopic technique that measures the elemental composition, empirical formula, chemical state and electronic state of the elements that exist within a material. XPS spectra are obtained by irradiating a material with a beam of X-rays while simultaneously measuring the kinetic energy and number of electrons that escape from the top 1 to 10 nm of the material being analyzed.[20] XPS requires ultra-high vacuum (UHV) conditions. XPS is also known as Electron Spectroscopy for Chemical Analysis (ESCA), an abbreviation introduced by Kai Siegbahn's research group.

XPS are based on the photoelectron effect. An atom absorbs a photon of energy $h\nu$; then a core or valence electron with binding energy E_b is ejected with kinetic energy.

$$E_k = h\nu - E_b - \varphi \quad (2.9)$$

$$E_b = h\upsilon - E_k \quad (2.10)$$

where,

E_k = kinetic energy of the photoelectron,

h = Planck's constant,

v = frequency of the exciting radiation,

E_b = binding energy of the photoelectron with respect to the Fermi level of the sample,

φ = work function of the spectrometer.

Routinely, X-ray sources are Mg Kα (1253.6 eV) and Al Kα (1486.3 eV). XPS detects all elements with an atomic number (Z) of 3 (lithium) and above. It cannot detect hydrogen (Z = 1) or helium (Z = 2) because the binding energy of these electrons is so small compared to the excitation energy of the x-ray photon and hence, the absorption efficiency is very small.

A typical XPS spectrum is a plot of the number of electrons detected (sometimes per unit time) (Y-axis, ordinate) versus the binding energy of the electrons detected (X-axis, abscissa). Each element produces a characteristic set of XPS peaks at characteristic binding energy values that directly identify each element that exist in or on the surface of the material being analyzed. These characteristic peaks correspond to the electron configuration of the electrons within the atoms, *e.g.,* 1s, 2s, 2p, 3s, *etc.* The number of detected electrons in each of the characteristic peaks is directly related to the amount of element within the area (volume) irradiated. To generate atomic percentage values, each raw XPS signal must be corrected by dividing its signal intensity (number of electrons detected) by a "relative sensitivity factor" (RSF) and normalized over all of the elements detected. XPS detects only those electrons that have actually escaped into the vacuum of the instrument. The photo-emitted electrons that have escaped into the vacuum of the instrument are those that originated from within the top 10 to 12 nm of the material. All of the deeper photo-emitted electrons, which were generated as the X-rays penetrated 1– 5 micrometers of the material, are either recaptured or trapped in various excited states within the material.

X-Ray photoelectron spectroscopy (XPS) data of different catalysts were collected on a VG Scientific ESCA-3000 spectrometer using a non-monochromatised Mg Kα radiation (1253.6 eV) at a pressure of about 1×10^{-9} Torr (pass energy of 50 eV,

electron takeoff angle 55) and overall resolution ~0.7 eV determined from the full width at half maximum of the $4f_{7/2}$ core level of the gold surface. The error in the binding energy values were within 0.1 eV. The binding energy values were charge-corrected to the C1s signal (285.0 eV).

2.4.7. Extended X-ray absorption fine structure (EXAFS) and X-ray absorption near edge structure (XANES)

X-ray Absorption Spectroscopy (XAS) includes both Extended X-Ray Absorption Fine Structure (EXAFS) and X-ray Absorption Near Edge Structure (XANES). XANES data indicate the absorption peaks due to the photo absorption cross section in the X-ray Absorption Spectra (XAS) observed in the energy region. EXAFS gives detailed local structure information *viz.* atomic identity, co-ordination number and bond distance while, XANES reveals the oxidation state and electronic environment of atoms. XANES, also known as near edge X-ray absorption fine structure (NEXAFS). NEXAFS is synonymous with XANES, but NEXAFS by convention is usually reserved for soft X-ray spectroscopy (photon energy less than 1000 electron volts). NEXAFS is generally used when applied to surface and molecular science, while XANES is used in most other fields.[21]

In the EXAFS, the fine structure in the X-ray absorption spectra in the high energy range extending from about 150 eV beyond the ionization potential is a powerful tool to determine the atomic pair distribution (*i.e.* interatomic distances) with a time scale of about 10−15 s. In fact, the final state of the excited photoelectron in the high kinetic energy range (150-2000 eV) is determined only by single backscattering events due to the low amplitude photoelectron scattering.

In the XANES region, starting from about 5 eV beyond the absorption threshold, because of the low kinetic energy range (5-150 eV), the photoelectron backscattering amplitude by neighbouring atoms is very large so that multiple scattering events become dominant in the XANES spectra.

The different energy range between XANES and EXAFS can be also explained in a very simple manner by the comparison between the photoelectron wavelength and the

interatomic distance of the photoabsorber-backscatterer pair. The photoelectron kinetic energy is corelated with the wavelength by the following relation:

$$E_{kinetic} = h\nu - E_{binding} = \hbar^2k^2 / 2m = (2\pi)^2\hbar^2 / (2m\lambda^2) \quad (2.11)$$

that means that for high energy, the wavelength is shorter than interatomic distances and hence, the EXAFS region corresponds to a single scattering regime while, for lower E larger than interatomic distances, XANES region is associated with a multiple scattering regime.

X-ray absorption near edge structure (XANES) and extended X-ray absorption fine structure (EXAFS) measurements were performed using a synchrotron radiation ring at BL-9C, Photon Factory, KEK Tsukuba, Japan with a Si (111) double-crystal monochromator in transmission mode at room temperature. The spectra were analyzed by the UWXAFS package.[22] The XANES spectra were normalized by the edge jump to be unity. After background subtraction, k-weighted EXAFS functions in the k range of 20–110 nm were Fourier transformed into R-space. The spectrum was fitted in the corresponding k-space of the R range 0.10–0.20 nm. The backscattering amplitudes and phase shifts were calculated by the FEFF8 code.[23]

2.4.8. Fourier transform infrared spectroscopy (FT-IR)

FT-IR is the preferred method of infrared spectroscopy. In infrared spectroscopy, IR radiation is passed through a sample. Some of the infrared radiation is absorbed by the sample and some of it is passed through(transmitted). These absorptions are resonant frequencies, i.e. the frequency of the absorbed radiation matches the transition energy of the bond or group that vibrates. The energies are determined by the shape of the molecular potential energy surfaces, the masses of the atoms, and the associated vibronic coupling. The resulting spectrum represents the molecular absorption and transmission, creating a molecular fingerprint of the sample. It has been widely used for structural analysis, chemical compound identification and monitoring of changes occurring during the course of a chemical reaction.[24]

IR spectra were recorded on a Perkin-Elmer (SpectrumOne) FT-IR instrument. The pellets for analysis were prepared by mixing 2 mg of the catalyst with 150 mg of KBr. FTIR spectra were recorded between 400 to 4000 cm^{-1} with accumulation of 20 scans and 4 cm^{-1} resolution.

2.4.9. Thermogravimetric and differential thermal analysis (TG and DTA)

Thermogravimetric analysis or thermal gravimetric analysis (TGA) is a method of thermal analysis in which changes in physical and chemical properties of materials are measured as a function of increasing temperature (with constant heating rate), or as a function of time (with constant temperature and/or constant mass loss).[25] TGA is commonly used to determine selected characteristics of materials that exhibit either mass loss or gain due to decomposition, oxidation, or loss of volatiles (such as moisture). Common applications of TGA are (1) material characterization through analysis of characteristic decomposition patterns, (2) studies of degradation mechanisms and reaction kinetics, (3) determination of organic content in a sample, and (4) determination of inorganic (*e.g.* ash) content in a sample, which may be useful for corroborating predicted material structures or simply used as a chemical analysis.

Differential thermal analysis (or DTA) is a thermo analytical technique, similar to differential scanning calorimetry. In DTA, the material under study and an inert reference are made to undergo identical thermal cycles, while recording any temperature difference between sample and reference.[26] This differential temperature is then plotted against time, or against temperature (DTA curve or thermogram). Changes in the sample, either exothermic or endothermic, can be detected relative to the inert reference. Thus, a DTA curve provides data on the transformations that have occurred, such as glass transitions, crystallization, melting and sublimation. The area under a DTA peak is the enthalpy change and is not affected by the heat capacity of the sample.

Thermogravimetric analysis (TGA/DTA) was performed on Perkin-Elmer TGA-7 analyzer at a 20 $^{o}C\ min^{-1}$ scan rate in nitrogen atmosphere.

2.4.10. Temperature programmed desorption of ammonia (NH_3-TPD)

Ammonia-TPD technique is generally used to determine the acidity and acid strength of the solid catalysts and involves monitoring surface or bulk interaction between the solid catalyst and its gaseous environment *via* continuous analysis of the gas phase composition as the temperature is raised linearly with time.[27] Instrument used for ammonia-TPD study consists of a sample holder charged with the catalyst in a furnace that can be temperature programmed and a thermal conductivity detector (TCD) to measure the NH_3 gas in the gas mixture before and after interaction.

Ammonia temperature programmed desorption (TPD) measurements of all the catalysts were carried out on a Micromeritics- 2720 (Chemisoft TPx) instrument. In order to evaluate the acidity of the catalysts, ammonia TPD measurements were carried out by (i) pre-treating the samples from room temperature to 300 ^oC under helium flow rate of 25 mL min^{-1}, (ii) adsorption of ammonia at 50 ^oC and (iii) desorption of ammonia with a heating rate of 10 ^oC min^{-1} starting from the adsorption temperature to 700 ^oC. The (%) distribution of acidic sites was calculated by measuring the area of desorption peaks in a low and high temperature regions.

2.4.11. Pyridine FT-IR technique

Pyridine FT-IR is the most widely used technique for determining the nature of acidic sites *i.e.* BrØnsted and/or Lewis present on the catalyst surface.[28] For pyridine, according to Knouzinger[29] the ring vibration modes of 19b and 8a are most affected by the nature of intermolecular interactions *via* the nitrogen lone pair electrons. These two modes are observed at **1440-1447** and **1580-1600** cm^{-1}, respectively, for hydrogen-bonded pyridine, at **1535- 1550** and about **1640** cm^{-1} for the pyridinum ion, and at **1447-1464** and **1600** to **1634** cm^{-1} for pyridine coordinatively bonded to Lewis acid sites.[30] The catalyst having BrØnsted acidity shows a peak at 1540 cm^{-1}, while the peak at 1450 cm^{-1} can be assigned to Lewis acidity.

In this thesis, Pyridine-IR spectra were recorded on a Shimadzu FT-IR 8000 attached with a SSU (Second sampling unit) using 20 mg of the catalyst sample. The

sample was placed in a sample cup and 20 mL of pyridine was injected in N_2 flow. Desorption of pyridine was recorded in a temperature range of 100–375 ^oC.

2.4.12. Temperature programmed desorption of carbon dioxide (CO_2-TPD)

CO_2 -TPD technique is generally used to determine the basicity and basic strength of the solid catalysts and involves monitoring surface or bulk interaction between the solid catalyst and its gaseous environment *via* continuous analysis of the gas phase composition as the temperature is raised linearly with time.

The temperature-programmed desorption of CO_2 (CO_2-TPD) was carried out using a Quantachrome Autosorb-1C sorption unit. 0.1 g of activated catalyst sample was heated at a rate of 10 ^oC min^{-1} to 110 ^oC under a He flow (30 mL min^{-1}) and was maintained at this temperature for 1 h in order to remove the surface impurities. After cooling to room temperature under He flow, the sample was exposed to a mixture of 30% CO_2/He for 1.5 h. Subsequently, the sample was purged with He for 30 min and then heated to 700 °C at a rate of 10 °C min^{-1}.

2.4.13. Temperature programmed reduction (TPR)

TPR is a widely used tool for the characterization of metal oxides, mixed metal oxides, and metal oxides dispersed on a support. The TPR method yields quantitative information of the reducibility of the oxide's surface, as well as the heterogeneity of the reducible surface.[31,32] The reduction of the metal oxide M_xO_y by H_2 is shown in **Equation 2.12.** TPR is a method in which a reducing gas mixture (typically 3% to 17% hydrogen diluted in argon or nitrogen) flows over the sample. A thermal conductivity detector (TCD) is used to measure changes in the thermal conductivity of the gas stream. The TCD signal is then converted to concentration of the active gas using a level calibration. Integrating the area under the concentration *vs.* time (or temperature) profile yields total gas consumed.

$$MxOy + yH_2 \rightarrow xM + yH_2O \qquad (2.12)$$

Temperature-programmed reduction (TPR) experiments were carried out using Quantachrome Autosorb-1C sorption unit, Micromertics-2720 model (Chemisoft TPx), and BEL-CAT (BEL Japan Inc.). In a typical TPR experiment, prior to the reduction in the TPR, the catalyst (~25 mg) was pretreated by heating under a stream of argon (25 mL min^{-1}) at 200 °C for 30 min to remove the moisture and surface impurities present on the sample and was then cooled to room temperature. Reduction was carried out at a heating rate of 5 °C per minute up to a temperature of 500 °C under a flow of 5% H_2/ Ar at a rate of 30 cm^3 min^{-1}.

2.4.14. Nitrous oxide (N_2O) chemisorption

The chemisorption techniques are mainly used to evaluate the free metal specific surface area and degree of metal dispersion. Metal surface areas are usually determined by selective chemisorption of a suitable probe molecule (*e.g.* CO, H_2, O_2). A lot of experimental techniques for the determination of Cu metal areas are based on the dissociative chemisorption of nitrous oxide (N_2O).[33]

N_2O-chemisorption was conducted in an AutoChem II 2920 (Micromeritics). The surface area of Cu metal was measured by a N_2O surface titration method. Prior to the N_2O titration, the fresh samples with 0.1 g were reduced at 250 ^oC for 2 h with 10 % H_2/Ar flow. The consumption of N_2O and the release of N_2 on the metallic Cu sites (N_2O + 2Cu = Cu_2O + N_2) was measured at 60 ^oC by a thermal conductivity detector (TCD). The surface area of metallic Cu was calculated by assuming 1.46 × 1019 Cu atoms m^{-2} with a molar ratio of 0.5 for N_2O/Cus (Cu atom on surface).

2.5. CATALYST ACTIVITY MEASUREMENT

2.5.1. Hydrogenolysis and dehydration of glycerol in a batch reactor

All the batch hydrogenolysis and dehydration experiments were carried out in a 300 mL capacity stirred autoclave supplied by Parr Instruments Co. USA, which was equipped with heating arrangement, overhead stirrer, thermo well, internal cooling coil, gas inlet

and outlet, liquid sampling valve, safety rupture disc, pressure gauge as well as transducer for digital pressure display, separate automatic controller to control the temperature, agitation speed, solenoid valve and high temperature cut off module. Water circulation through the internal cooling loop equipped with automatic cut-off arrangement controlled the temperature inside the reactor with an accuracy of ±1^{o}C. A schematic of the batch slurry reactor set-up is shown in **Figure 2.4.**

In a typical hydrogenolysis experiment, required amount of substrate was charged into the reactor. Total volume of the liquid phase was always kept to 100 mL by adding appropriate solvent and the required amount of catalyst was charged in an autoclave

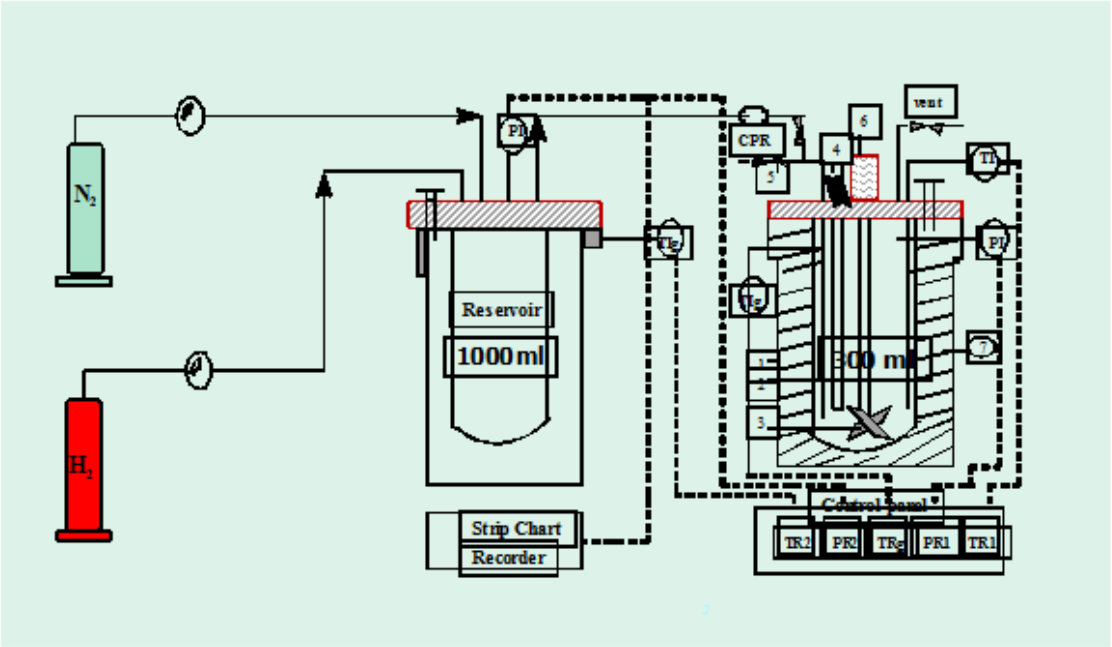

Figure 2.4. Schematic of a batch reactor set-up.

(1) Reactor (2) Stirrer shaft (3) Impeller (4) Cooling water (5) Sampling valve (6) Magnetic stirrer (7) Electric furnace.

TI: Thermocouple, **PI**: Pressure transducer, **TIg**: Thermocouple for gas, **N_2**: Nitrogen cylinder, **H_2**:Hydrogen gas cylinder, **PR**: Pressure regulator, **CPR**: Content pressure regulator, **TR1**: Reactor temperature indicator, **PR1**: Reactor pressure indicator, **TR2**: Reservoir temperature Indicator, **TRg**: Gas temperature indicator, **PR2**: Reservoir pressure indicator.

carefully and reactor vessel was closed. The contents were first flushed 2-3 times with N_2 gas for the removal of trapped air and then flushed with H_2. Then the temperature was ramped to the required value. After attaining the desired temperature, the system was pressurized with H_2 gas to the desired value. Initial liquid sample was withdrawn before switching on the stirrer and the progress of the reaction was monitored by observing the pressure drop in the reservoir as a function of time. When the reaction was over, as indicated by a constant H_2 pressure on the pressure display, the reactor was cooled to room temperature and excess H_2 gas was vented out safely and the reactor contents were discharged. Liquid samples were withdrawn at regular time intervals for the analysis using gas chromatography.

Typical hydrogenolysis conditions were: temperature, 220 ^oC; glycerol concentration, 20 wt%; catalyst loading, 1 g; and hydrogen pressure, 35-70 bar. The dehydration experiments were carried out under the same conditions except that H_2 was replaced by N_2 atmosphere.

2.5.2. Hydrogenolysis and dehydration of glycerol in a continuous fixed bed reactor

Continuous hydrogenolysis of glycerol was carried out in a bench scale, high-pressure, fixed-bed reactor supplied by M/s Geomechanique, France. A schematic of the reactor setup is shown in **Figure 2.5.** This reactor set up consisted of a stainless steel single tube of 0.34 m length and 1.5×10^{-2} m inner diameter. The reactor was heated by two tubular furnaces whose zones (TIC1 and TIC2) were independently controlled at the desired bed temperature. The reactor was provided with mass flow controllers, pressure indicator, and controller (PIC) devices and two thermocouples to measure the temperature at two different points. A storage tank was connected to the high-pressure liquid chromatography (HPLC) pump through a volumetric burette to measure the liquid flow rate. The pump had a maximum capacity of 3×10^{-4} m^3 h^{-1} under a pressure of 100 bar. The gas-liquid separator was connected to other end of the reactor through a condenser. The powdered catalyst was pelletized in the form of pellets of 1×10^{-2} m diameter and cut into 4 pieces each having 0.5×10^{-3} m diameter (**Figure 2.6**). Twenty three g of the pelletized catalyst was charged in to the reactor. The section of 7×10^{-2} m above and 0.16

m below the catalyst bed was packed with carborundum as an inert packing, thus providing the catalyst bed of 0.11 m. Before starting the actual experiment the reactor was flushed thoroughly, first with N_2 and then with H_2 at room temperature. The liquid feed was "switched on" along with step wise pressurizing the reactor with H_2. After the reactor reached the operating pressure and was kept at that value for 1 h to obtain the constant liquid flow rate. Liquid samples were withdrawn at regular intervals of time. Liquid samples were analyzed by GC.

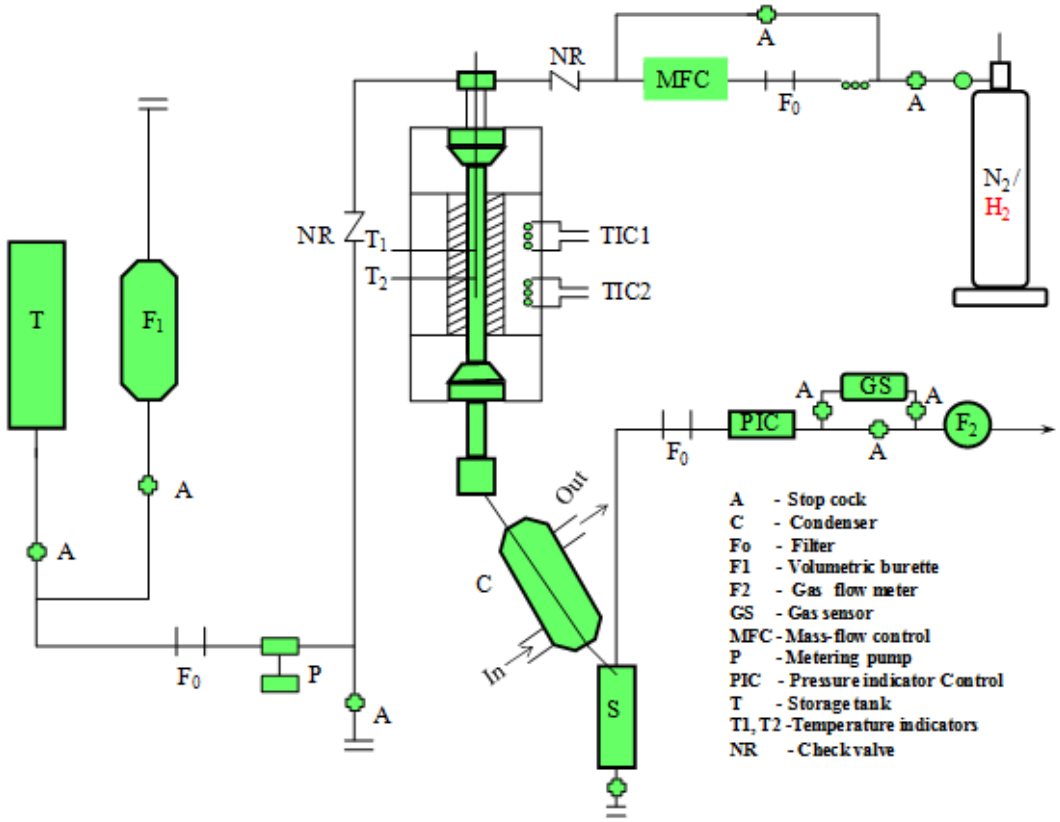

Figure 2.5. Schematic of a continuous fixed bed reactor set-up.

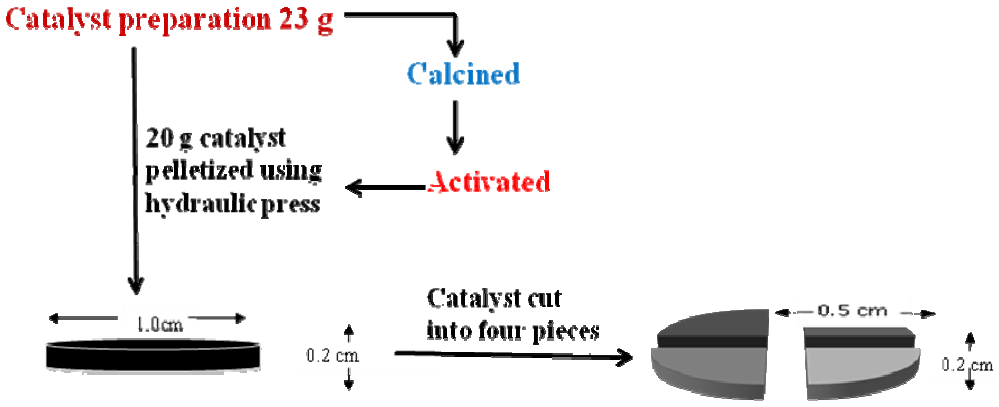

Figure 2.6. Schematic of catalyst pellet preparation.

2.5.3. Water gas shift reaction (WGSR) in a fixed-bed micro-tubular quartz reactor

Activity tests for WGSR were carried out from 200 to 400 ^{o}C under atmospheric pressure in a fixed-bed micro-tubular quartz reactor with an inner diameter of 4 mm. The catalyst charge was 48 mg. T-union was employed at the exit of quartz reactor to install a thermocouple. A thermocouple was inserted into the catalyst bed to measure the reaction temperature. Prior to each catalytic measurement, the catalyst was reduced in 5% H_2/N_2 from room temperature to 200 ^{o}C at a heating rate of 3.3 ^{o}C min^{-1} and the temperature was maintained for 2 h. The simulated reformed gas consisted of 6.5 vol.% CO, 7.1 vol.% CO_2, 0.7 vol.% CH_4, 42.4 vol.% H_2, 28.7 vol.% H_2O, and 14.5 vol.% N_2. The feed $H_2O/(CH_4 + CO + CO_2)$ ratio was fixed at 2.0 due to the fact that a H_2O/CH_4 ratio is typically 3.0 in steam reforming of methane (SRM: $H_2O+CH_4 = 3H_2+CO$) to avoid coke formation.[34]

A gas hourly space velocity (GHSV) of 36,201 h^{-1} was used to screen the catalysts in this study. Water was fed using a syringe pump and was vaporized at 150 ^{o}C upstream of the reactor. The reformed gas was chilled, passed through a trap to condense the residual water, and then flowed to the on-line micro-gas chromatograph (Agilent 3000).

2.6. ANALYTICAL METHODS

Glycerol and its hydrogenolysis and dehydration liquid products such as 1,2-propanediol, acetol, ethylene glycol, 1,3-propanediol, 1-propanol, 2-propanol and methanol were analysed by gas chromatograph. The details of the analytical method are given below.

Conditions:

- GC : Varian 3600
- Column: Capillary HP-FFAP (Free fatty acid phase column)
- Column details: 30 m length x 0.53 mm i.d. x 1 μm film thickness.
- Column stationary phase: Polyethylene glycol (highly polar)
- Carrier: He
- Detector: FID
- Injector temp.: 250 ^{o}C
- Detector temp.: 300 ^{o}C
- Total run time: 34.00 min.
- Injection volume: 1μL.
- Oven temperature program (**Table 2.3**)

Table 2.3. GC oven temperature program

Sr. No.	Ramp	Temp. (^{o}C)	Hold time (min)
1	-	80	2
2	5	190	10

A typical chromatogram of the reaction products of glycerol hydrogenolysis is shown in **Figure 2.7** and retention times are given in **Table 2.4.**

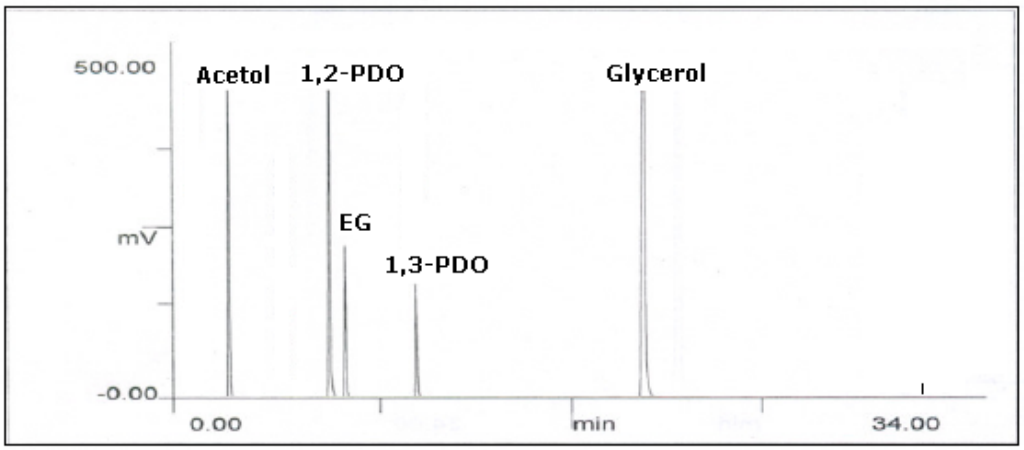

Figure 2.7. GC of glycerol hydrogenolysis products.

Table 2.4. Retention time of each of reference standards

Reference standard	Retention time (R_t) (min)
Acetol	2.1
1,2-PDO	6.5
EG	7.25
1,3-PDO	10.4
Glycerol	20.4

For some of the experiments carried out in this work, the liquid samples were also analyzed by GC (Model-Shimadzu GC-2025) equipped with an auto sampler (Model AOC-20i) and FID detector on a capillary FFAP (Free Fatty Acid Phase) (30 m length × 0.53 mm i.d. ×1 µm film thickness) column. The details of the analytical conditions are given below.

Conditions:

- GC : Shimadzu 2025
- Injector temp. : 300 ^{o}C
- Detector temp.: 300 ^{o}C

- Carrier gas: He
- Injection mode: Split
- Split ratio : 30.0
- Pressure : 4.1 psi
- Column flow : 4.48 ml min^{-1}
- Make up flow: 30 ml min^{-1}
- H_2 flow: 40 mL min^{-1}
- Air flow: 400 mL min^{-1}
- Injection volume: 1uL
- Oven temperature program (**Table 2.5**):

Table 2.5. GC oven temperature program

Sr. No.	Ramp	Temp. (^oC)	Hold time (min)
1	**-**	**90**	**1**
2	**20**	**140**	**1**
3	**5**	**180**	**3**
4	**15**	**200**	**10**

A typical chromatogram shown in **Figure 2.8.**

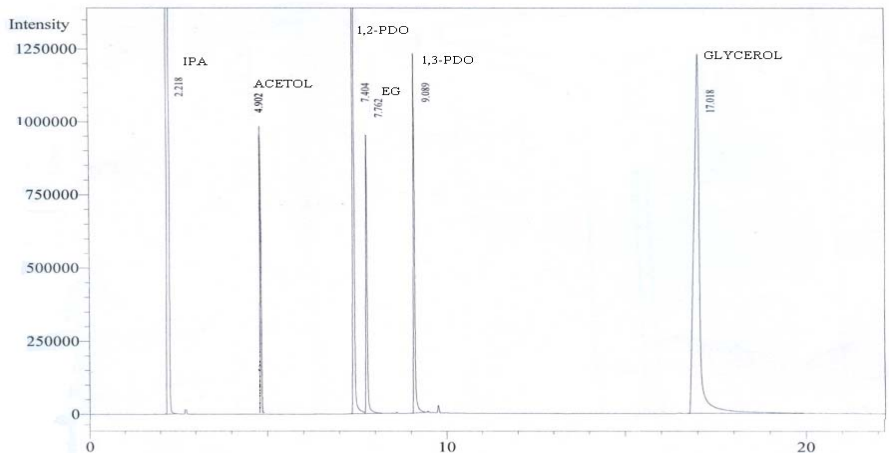

Figure 2.8. GC of glycerol hydrogenolysis products.

The liquid products formed were also confirmed by GC-MS analysis (Schimadzu GC-2010 Plus).

Gas analysis of gaseous products formed by glycerol aqueous phase reforming were carried out using a Chemito 8610 GC fitted with packed Porapac-Q column (2 m) connected to the thermal conductivity detector (TCD) detector. The reformed gas used in water gas shift reaction was analysed by the on-line micro-gas chromatograph (Agilent 3000).

The various terms used in this thesis are defined as follows.

$$\text{Conversion}(\%) = \frac{\text{Initial conc. of substrate} - \text{final conc. of substrate}}{\text{Initial conc. of substrate}} \times 100 \quad (2.13)$$

$$\text{Selectivity}(\%) = \frac{\text{Conc. of desired product formed}}{\text{Total conc. of all the products formed}} \times 100 \quad (2.14)$$

$$\text{Carbon selectivity}(\%) = \frac{\text{Moles of individual product formed} \times \text{number of C atoms}}{\text{Moles of glycerol feed} \times \text{conversion} \times 3} \times 100 \quad (2.15)$$

$$\text{Yield}(\%) = \frac{\text{Conversion} \times \text{selectivity}}{100} \quad (2.16)$$

$$\text{TOF}\ (h^{-1}) = \frac{\text{Concn. of substrate consumed}}{[\text{Concn. of catalyst (active metal)}](t)} \quad (2.17)$$

$$\text{Atom economy}(\%) = \frac{\text{Mass of atoms in desired product}}{\text{Mass of atoms in reactants}} \times 100 \quad (2.18)$$

$$\text{Liquid hourly space velocity (LHSV, } h^{-1}) = \frac{\text{Reactant liquid flow rate}}{\text{Reactor volume}} \quad (2.19)$$

$$\text{Gas hourly space velocity (GHSV, } h^{-1}) = \frac{\text{Reactant gas flow rate}}{\text{Reactor volume}} \quad (2.20)$$

$$\text{Contact time}(h) = \frac{\text{Catalyst loading (W in g)}}{\text{Feed rate (F in g } h^{-1})} \quad (2.21)$$

2.7. REFERENCES

1. T. J. Marks,"*Introduction: Polymerization*," Proceedings of the National Academy of Sciences of the United States of America, 103, 42, **2006,** p.15288.
2. H. Topsøe, *J. Catal.* **2003,** 216, 155-164.
3. R. V. Chaudhari, R. Jaganathan, S. T. Chaudhari, C. V. Rode, US Patent 7037877, **2006**.
4. J. Henkelmann, M. Becker, J. Bürkle, P. Wahl, G. Theis, S. Maurer, WO 2007099161 A1, **2007**.
5. R. B. Mane, A. M. Hengne, A. A. Ghalwadkar, S. Vijayanand, P. H. Mohite, H. S. Potdar, C.V. Rode, *Catal. Lett.* **2010**, 135,141-147.
6. R. B. Mane, S. E. Kondawar, P. S. Niphadkar, P. N. Joshi , K. R. Patil, C.V. Rode, *Catal. Today* **2012**, 198, 321-329.
7. R. B. Mane, D.-W. Jeong, A. Malawadkar, H.-S. Roh, C.V. Rode *ChemCatChem* communicated, 2013.
8. R. B. Mane, A. Yamaguchi, A. Malawadkar, M. Shirai, C. V. Rode, *RSC Adv.* **2013,** 37, 16499-16508.
9. C.V. Rode, R. B. Mane, A. S. Potdar, P. B. Patil , P. S. Niphadkar, P. N. Joshi, *Catal. Today* **2012**, 190, 31-37.
10. R. B. Mane, C. V. Rode, *Green Chem.* **2012**, 14, 2780-2789
11. S. Brunauer, P. H. Emmett, E. Teller, *J. Am. Chem. Soc.* **1938**, 60, 309-319.
12. R. W. G. Wyckoff, *Crystal Structures*, 2nd ed., Wiley, New York, **1964.**
13. J. W. Niemantsverdriet, *Spectroscopic Methods in Heterogeneous Catalysis*, VCH, Weinheim, **1993**, p.82.
14. W. H. Bragg, W. L. Bragg, *The Crystalline State*, Vol. 1, McMillan, New York, **1949**.
15. E. Kirkland, *Advanced computing in Electron Microscopy,* Springer. ISBN 0-306-45936-1, **1998**.
16. J. Duan, S. Yang, H. Liu, J. Gong, H. Huang, X. Zhao, R. Zhang, Y. J. Du, *Am. Chem. Soc.* **2005**, 127, 6180-6181.

17. G. Lawes, *Scanning Electron Microscopy and X-Ray Microanalysis*, John Wiley and Sons Ltd., Chichester, **1987**.
18. A. Stefánsson, I. Gunnarsson, N. Giroud, *Anal. Chim. Acta* **2007**, 582, 69–74.
19. J. M. Mermet, *J. Anal. At. Spectrom.* **2005**, 20, 11–16.
20. X. D. Wu, D. Dijkamp, S. B. Ogale, A. Inam, E. W. Chase, P. F. Miceli, C. C. Chang, J. M. Tarascon, T. Venkateshan, *Appl. Phys. Lett.* **1987**, 51, 861-863.
21. A. L. Ankudinov, B. Ravel, J. J. Rehr, S. D. Conradson, *Phys. Rev. B* **1998**, 58, 7565-7576.
22. E. A. Stern, M. Newville, B. Ravel, Y. Yacoby and D. Haskel, *Phys. B* **1995**, 208–209, 117–120.
23. A. L. Ankudinov, B. Ravel, J. J. Rehr and S. D. Conradson, *Phys. Rev. B: Condens. Matter Mater. Phys.* **1998**, 58, 7565–7576.
24. J. Hagen, *in Industrial catalysis*, 2nd edition, Wiley-VCH, Germany, **2006**, p. 215.
25. A. W. Coats, J. P. Redfern, *Analyst* **1963**, 88, 906–924.
26. H. K. D. H. Bhadeshia *Thermal analyses techniques. Differential thermal analysis*,University of Cambridge, Material Science and Metallurgy.
27. Y. Kamiya, Y. Ooka, C. Obara, R. Ohnishi, T. Fujita, Y. Kurata, K. Tsuji, T. Nakajyo, T. Okuhara, *J. Mol. Catal. A* **2007**, 262, 77-85.
28. E. Modrogan, M. H. Valkenberg, W. F. Hoelderich, *J. Catal*. **2009**, 261,177-187.
29. H. Knouzinger, *Adv. Catal.* **1976**, 25,184-271.
30. M. C . Kung , H. H. Kung, *Catal . Rev.-Sci. Eng.* **1985**, 27, 425-460.
31. G. S. Sewell, E. van Steen, C.T. O'Connor, Catal. Lett. 37 (1996) 255.
32. H. Knöuzinger in *Handbook of Heterogeneous Catalysis* (Eds.: G. Ertl, H. Knöuzinger, J. Weitkamp.), Vol. 2, Wiley-VCH, Weinheim, **1997**, p. 676.
33. J. L.Lemaitre, P. G. Menon, F. Delannay in *The measurements of catalyst disperdion' Characterization of heterogeneous catalysts*, F. Delannai, M. Dekker Inc., New York, Cap. 7, **1984**, pp. 266-299
34. H.-S. Roh, H. S. Potdar, D.-W. Jeong, K. Kim, J. Shim, W. Jang, K. Y. Koo, W. L. Yoon, *Catal. Today* **2012**, 185, 113-118.

Chapter 3

Role of promoters and process optimization studies for hydrogenolysis of glycerol to 1,2-propanediol over copper chromite catalysts

Various copper chromite catalysts with and without promoters were prepared by co-precipitation and digestion technique and the role of promoters (Al, Ba and Zn) was investigated for hydrogenolysis of glycerol to 1, 2-propanediol (1, 2-PDO) in both batch and continuous operations. Catalyst screening studies showed that Cu-Cr-Ba was the best catalyst. Its higher activity performance was explained based on its detailed caharcatrization by XRD and NH_3-TPD techniques. This catalyst was found to be active for more than 800 h in a continuous operation also.

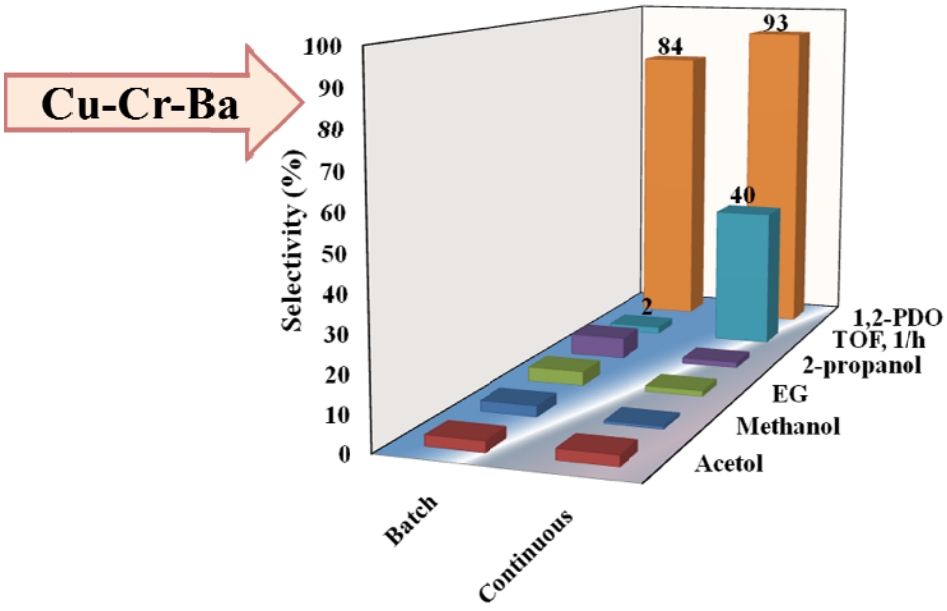

Catal. Today **2011, 164, 447 -450**

Org. Process Res. Dev. **2010, 14, 1385-1392**

3.1. INTRODUCTION

Catalytic production of 1,2- propanediol (1,2-PDO) is one of the most attractive downstream applications of glycerol which is a main byproduct of biodiesel formation as already discussed in chapter 1 (**section 1.1.1**).[1,2] The commercial route for 1,2-PDO involves the hydration of petroleum based propylene oxide derived by either chlorohydrin process or the hydroperoxide process both of which are multistep processes and generate HCl. Hence, catalytic hydrogenolysis of glycerol to 1,2-PDO is a sustainable process utilizing a renewable feedstock as well as substantially improves the process economics of the bio-diesel manufacture.

Glycerol hydrogenolysis has been studied using various catalyst systems involving both noble metals such as Rh, Ru, Pt, Pd as well as other transition metals mainly copper, chromium and zinc in combination with each other or supported on active carbon, SiO_2, Al_2O_3.[3-5] Among noble metals, ruthenium on carbon in presence of amberlyst resin gave glycerol conversion of 79% with the highest selectivity of 82% to 1,2- PDO at 120 ^oC and 80 bar initial H_2 pressure for 10 h.[6,7] However, higher reaction pressure, longer reaction time and the formation of byproducts such as ethylene glycol due to C–C bond cleavage favoured by Ru make this catalyst system unviable from process point of view. Although sulfur addition to Ru/C catalyst increased the selectivity to 1,2-PDO, the glycerol conversion was limited to only 45%.[8,9] In the case of Pt catalyst, in spite of its higher activity for the glycerol hydrogenolysis, it gave higher selectivity to lactate.[10] Since, copper is responsible for selective cleavage of C-O bond without affecting C-C bond, and also it is much cheaper than Ru or Pt, more attention has been focused on copper based catalysts for glycerol hydrogenolysis. Glycerol hydrogenolysis was first reported using copper and zinc catalysts under very high pressure and temperature conditions (150 bar; 240-272 ^oC) with 75-85% selectivity to 1,2-PDO while > 25 % were cracked products such as ethylene glycol (EG), ethanol, methanol and lactic acid. [10,11] Chaminand *et al.* [12] reported glycerol conversion of 20% with > 90% selectivity to 1,2 -PDO, using Cu-ZnO in presence of tungstic acid in 92 h. Bifunctional Cu-ZnO catalysts were also proposed to obtain 84% selectivity to 1,2-PDO with 23% glycerol conversion in 12 h.[13] Sato *et al.*[14] showed that Cu/Al_2O_3 materials could effectively catalyze the dehydration of glycerol to produce hydroxyacetone in a

hydrogen flow where 1, 2-PDO was formed as a by-product. Schuster and Eggersdorfer, and Cameron *et al.*[15,16] reported a catalyst system comprising of cobalt, manganese, molybdenum, along with copper and an inorganic polyacid for achieving a 95% yield of 1,2-PDO under severe conditions of 250 bar pressure and 250 ^{o}C for glycerol hydrogenolysis.

Copper along with chromium forms a copper chromite (Cu-Cr) system which is also well studied for hydrogenation as well as for the decomposition or dehydration of alcohols. [17-19,20] After the first report of copper chromite catalyst by Fleckenstein *et al.* [21] for glycerol hydrogenolysis at very high pressure (250 bar), several reports have appeared using various types of copper chromite catalysts.[22-24] Commercial as well as proprietary copper chromite systems are also reported for which the reaction conditions could be much milder such as 200 ^{o}C and 14 bar H_2 pressure.[21,25] Another possibility with this catalyst system is that by altering the composition and reaction conditions, very high selectivity to intermediate acetol (80%) with 86% glycerol conversion can be achieved. It is well known that one or more metals from groups II and III are usually incorporated as promoters in copper chromite catalyst systems. These promoters play a vital role in enhancing the catalyst activity as well as the product selectivity particularly in case of glycerol hydrogenolysis, in which the first step involves the acid catalyzed dehydration to acetol [22] and also for controlling the formation of degradation products such as EG, methanol, 1-propanol *etc*. However, it is evident from the literature that most of the work on various catalyst systems including the promising one such as copper chromite has been carried out using a batch reactor operation. Although few reports describe the continuous dehydration/hydrogenolysis of glycerol, reaction conditions are very harsh and/or the major product formed was acetol along with considerable formation of unidentified side products. Continuous process for the production of a commodity product like 1,2-PDO will be highly desirable from commercialization point of view. However, performance of the same catalyst would differ considerably in a continuous operation from that in a batch mode.

In this chapter, the additive effect of each promoter such as Al, Ba and Zn separately and with their combinations, on the activity and selectivity of copper chromite catalysts for hydrogenolysis of glycerol was studied.[26,27] Primarily, promoters such as

Al, and Zn were chosen owing to their Lewis acidity to facilitate the first step glycerol dehydration to acetol. While Ba having less acidic characteristics was expected to show poor activity. Surprisingly among these catalysts, Cu-Cr with barium as a promoter showed the highest performance which was then used to carry out further studies *viz.* (i) the product distribution and a systematic comparison of batch and continuous process for glycerol hydrogenolysis; (ii) to optimize the process conditions for a continuous operation; (iii) to study the catalyst life.[28]

3.2. EXPERIMENTAL

Copper chromite catalyst with different promoters (Al, Zn and Ba) was prepared by a co-precipitation method and the detail experimental procedure of their preparation has been described in chapter 2 (section 2.3.1). The catalysts were characterizaed by XRD and NH_3-TPD techniques according to the procedure described in sections 2.4.2 and 2.4.10. The activity testing of prepared catalysts was carried out in batch as well as continuous operation for hydrogenolysis glycerol to 1,2-PDO following the experimental procedure described in sections 2.5.1 and 2.5.2. Liquid samples were analyzed by GC (Varian 3600) equipped with a flame ionization detector and a capillary column (HP-FFAP 30 m, 0.53 mm, 1 μm).

3.3. RESULTS AND DISCUSSION

3.3.1. Role of promoters

Figure 3.1 shows XRD patterns of the various activated Cu-Cr catalyst samples without and with Al, Ba and Zn promoters. In all these samples, content of Cu as well as that of different promoters were kept constant at 52% and 30%, respectively. Copper chromite without any promoter showed predominant peaks at 2θ values of 43.2^o (111) and 50.1^o (200) [29] which could be attributed to metallic Cu while two small peaks at 35.4^o (111) and 38.4^o (111) showed the presence of CuO.[13] While, the XRD spectrum of the Ba promoted copper chromite catalyst showed peaks at 2θ values of 22.4^o (111), 25.4^o (210),

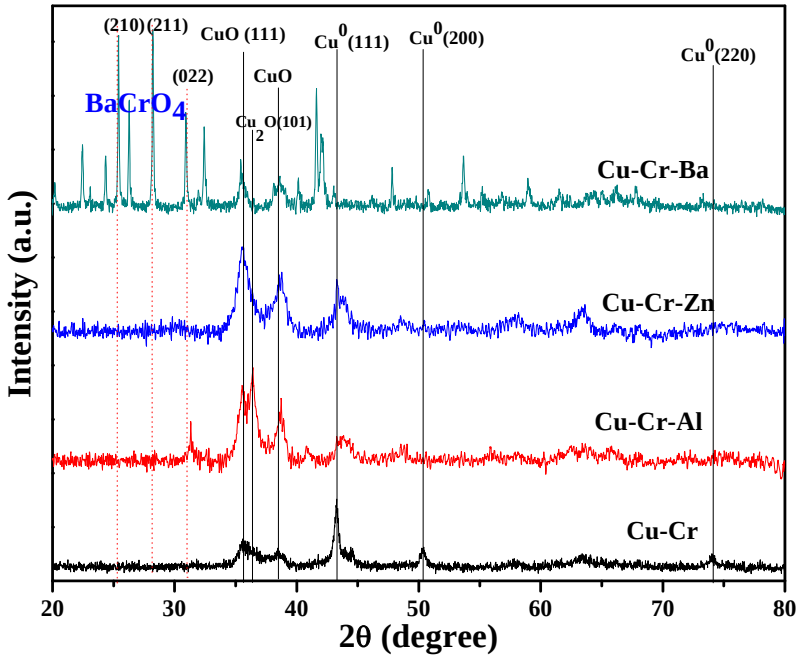

Figure 3.1. XRD patterns of Cu-Cr catalysts with and without promoters.

28.2° (211), 30.9° (112), 41.6° (113), 41.9° (203) and 43° (410) which correspond to $BaCrO_4$ phase.[30] A peak at 2θ value of 43.2° was due to metallic Cu while, no peak corresponding to CuO or Cu_2O was observed. Al promoted Cu-Cr showed a major peak at 2θ of 36.4° (101) which was due to Cu_2O phase and two minor broad peaks at 2θ of 35.4° (111) and 38.4° (111) for CuO. Cu-Cr catalyst with Zn also showed the presence of CuO with only small amount of metallic copper. This clearly showed that the presence of Ba was responsible for stabilizing metallic Cu phase in copper chromite catalysts which is mainly responsible for hydrogenolysis of glycerol as indicated by the activity results shown in **Figure 3.2.**

It is also interesting to note that crystallite sizes obtained from diffraction peak for metallic Cu (2θ = 43.2°) phase in Cu-Cr catalysts without and with promoters varied as follows: 156 nm (Cu-Cr) > 149 nm (Cu-Cr-Zn) > 95 nm (Cu-Cr-Al) > 69 nm (Cu-Cr-Ba). Thus Ba was found to be responsible for inhibiting the aggregation which also has been reported earlier.[31] The inhibition of aggregation by Ba leading to a stable catalyst activity which was evidenced by time on stream activity of >7 fold than that of only Cu-Cr catalyst for continuous hydrogenolysis of glycerol, as shown in **Figure 3.3.** The first

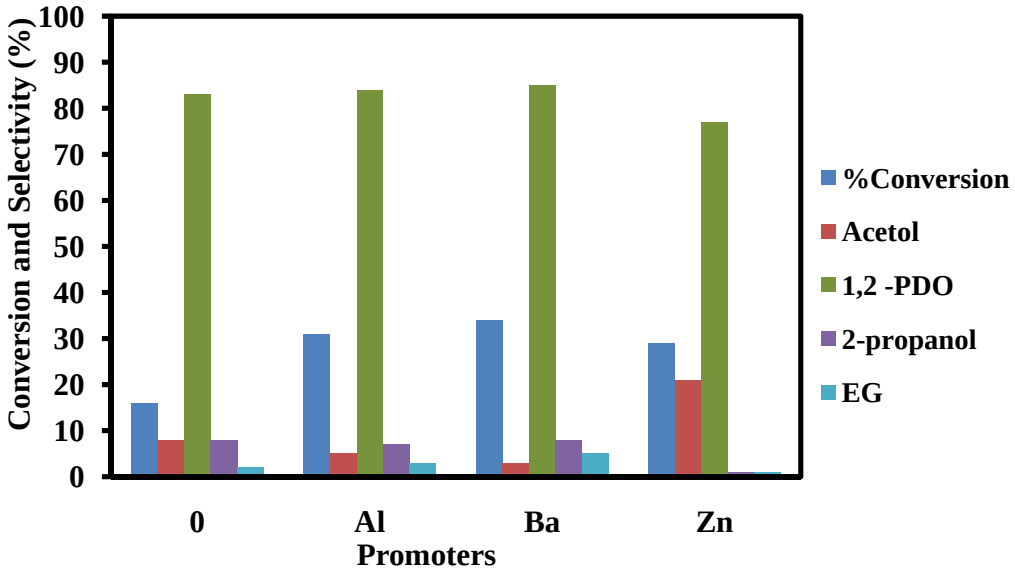

Figure 3.2. Effect of promoters on glycerol hydrogenolysis.

Reaction conditions: Temperature, 220 ^{o}C; 20 wt% glycerol; H_2 pressure, 52 bar; solvent, 2-propanol; catalyst, 1g; reaction time, 5 h.

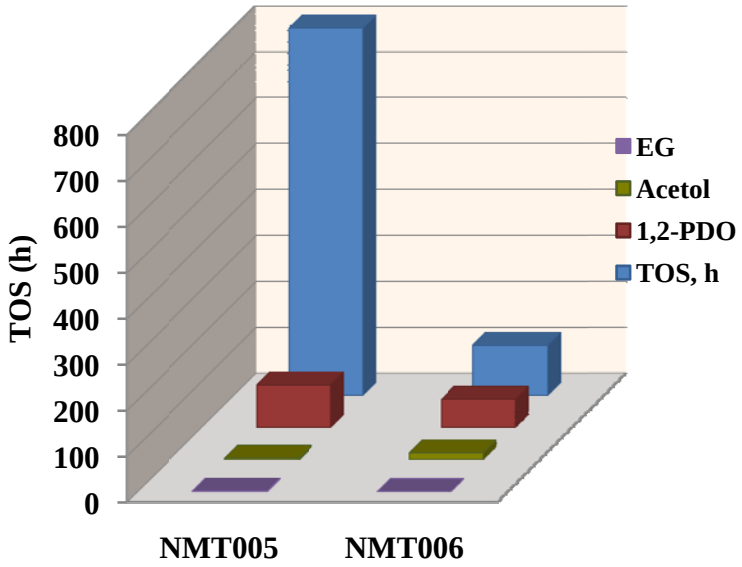

Figure 3.3. Time on stream activity of Cu-Cr-Ba (NMT005) and Cu-Cr (NMT006) catalysts.

Reaction conditions: Temperature, 220 ^{o}C; catalyst wt., 23 g; solvent, 2-propanol; 20 wt% glycerol; feed flow rate, 30 mL h^{-1}; H_2 flow rate, 10NL h^{-1}; H_2 pressure, 40 bar.

step of glycerol hydrogenolysis involves its dehydration to acetol which is said to be catalyzed by acid sites of the catalyst/support. Hence, the strength and nature of acid sites of our catalysts were also determined by NH_3-TPD and the results are presented in **Table 3.1.** Cu-Cr catalyst showed the least acidity (0.3414 mmol NH_3 g^{-1}) while, Cu-Cr-Ba (NMT005) sample showed the highest acidity (1.2444 mmol NH_3 g^{-1}). Although, both Al and Ba promoters showed similar acidity in lower temperature region (50-200 ^oC), acidity for Ba promoted sample increased substantially in higher temperature region (200- 400 ^oC) which corresponds to the reaction temperature used in this work.

Table 3.1. Ammonia TPD results of Cu-Cr catalysts with different promoters

Sr. No.	Catalyst	Promoter	NH_3 desorbed region wise			Total NH_3 desorbed (mmol g^{-1})
			50-200 (^oC)	200-400 (^oC)	400-700 (^oC)	
1	NMT006	Nil	0.0208	0.2299	0.0907	0.3414
2	NMT001	Al	0.1255	0.3743	0.3562	0.856
3	NMT005	Ba	0.1255	0.8684	0.2505	1.2444
4	NMT011	Zn	0.0910	0.3452	0.3494	0.7856

Hence activity of Ba promoted catalyst was also found to be higher than that for Al promoted catalyst. It was observed that Cu-Cr without any promoter showed the least activity (16% conversion) towards glycerol hydrogenolysis (**Figure 3.2**). While, Cu-Cr catalyst with barium showed highest glycerol conversion of 34% in comparison with the other promoters such as aluminium and zinc which gave about 31 and 29% glycerol conversion respectively. From the activity results and characterization of catalysts described above, the highest activity of barium promoted Cu-Cr catalyst was mainly due to the following reasons. (i) Higher acidity responsible for catalyzing the first step of dehydration of glycerol to acetol, more efficiently. (ii) Formation of $BaCrO_4$ phase that inhibits the growth of crystallites contributing to prolonged catalyst activity under high

temperature reaction conditions.[31]

Since, Ba was found to be the best promoter, effect of barium content was also studied in the range of 15-40% and the results are shown in **Figure 3.4.** It was observed that the activity increased with the increase in barium content up to 30%, after which it decreased substantially (from 34 to < 20% conversion) for higher barium content of 40%. XRD pattern of the catalysts with different Ba content showed the decrease in diffraction

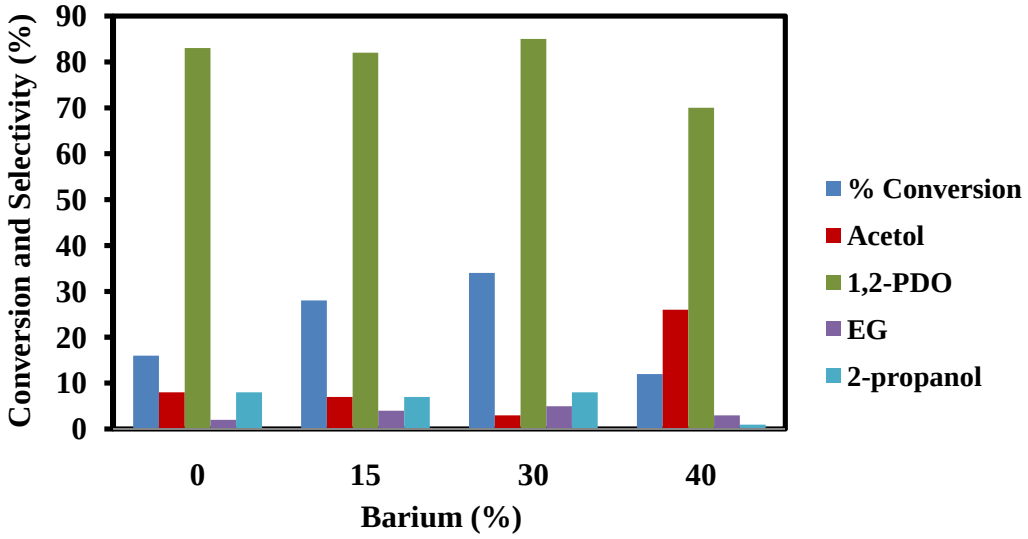

Figure 3.4. Effect of Ba content on glycerol hydrogenolysis.
Reaction conditions: Temperature, 220 ^{o}C; 20 wt% glycerol; H_2 pressure, 52 bar; solvent, 2-propanol; catalyst, 0.01g mL^{-1}; reaction time, 5 h.

peak intensity for metallic Cu phase with increase in Ba content upto 30% where as at higher 40% Ba content diffraction peak for metallic Cu phase diminished **(Figure 3.5)**. This could be due to fact that the critical concentration of Ba exists beyond which the $BaCrO_4$ inhibits the migration of Cu from the bulk to the surface hence decreasing the hydrogenation activity. Ba content beyond 40% also affected the selectivity pattern. With increase in Ba content from 30 to 40%, acetol selectivity increased substantially from < 5% to 25% and at the same time 1, 2-PDO selectivity decreased from 84 % to 70% (**Figure 3.4**).

As the Ba content increased, the enhanced acidity (**Table 3.2**) was responsible for

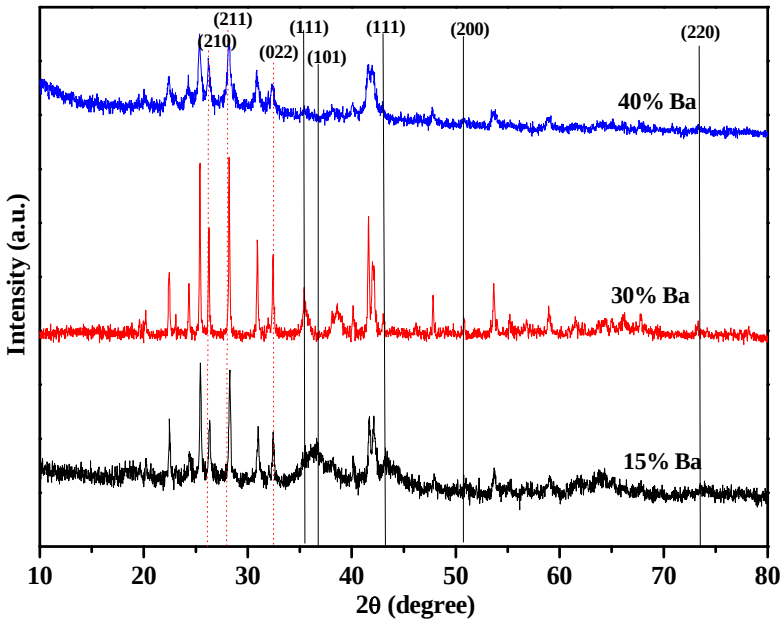

Figure 3.5. XRD patterns of Cu-Cr catalyst with different barium content.

the dehydration of glycerol to acetol while the second step of acetol hydrogenation was retarded due to less number of Cu atoms on the catalyst surface. As can be seen from **Figure 3.3** and also discussed above, time on stream activity of Ba containing Cu-Cr catalyst (NMT005) showed much higher activity and stability than Cu-Cr catalyst without a promoter (NMT006) confirms that the choice of an appropriate promoter is necessary for a stable activity under reaction conditions.

Table 3.2. Ammonia TPD results of Cu-Cr catalysts with different Ba content

Sr. No.	Catalyst	Ba	NH_3 desorbed region wise			Total NH_3 desorbed ($mmolg^{-1}$)
			50-200 °C	200-400 °C	400-700 °C	
1	NMT006	0	0.0208	0.2299	0.0907	0.3414
2	T-3	15	0.0241	0.1713	0.2866	0.482
3	NMT005	30	0.1255	0.8684	0.2505	1.2444
4	T-4	40	0.0610	0.6675	0.5843	1.3128

Since, the activity achieved was almost double for Cu-Cr catalyst containing both Al and Ba as promoters (**Figure 3.2**), effect of combination of both these promoters together (NMT008) on the activity was also evaluated and the results are shown in **Table 3.3**. Surprisingly, 1, 2-PDO selectivity obtained for NMT008 catalyst was much lower (71%) than the catalysts containing a single promoter. Lowering in 1, 2-PDO selectivity for a catalyst containing both Al and Ba promoters was mainly due to the formation of

Table 3.3. Activity of Cu-Cr catalysts with promoter combinations

Catalyst	Promoters (%)			Conversion (%)	Selectivity (%)			
	Al	Ba	Zn		Acetol	1,2- PDO	EG	2-propanol
NMT006	-	-	-	16	8	83	2	8
T-2	39	-	11	34	4	90	1	5
T-1	11	-	39	17	6	85	5	4
NMT008	19	10	.	26	16	71	10	3

Reaction conditions: Temperature, 220 ^{o}C; 20 wt% glycerol; H_2 pressure, 52 bar; solvent, 2-propanol; catalyst, 1g ; reaction time, 5 h.

cracked product like ethylene glycol (10%) from glycerol and also due to accumulation of an intermediate acetol (selectivity 16%) indicating slower kinetics of acetol hydrogenation. Al and Zn promoters were chosen mainly due to their Lewis acid characteristic that was expected to play an important role in the glycerol hydrogenolysis, since it involves the first step of acid catalyzed dehydration of glycerol to acetol. Very interesting results were obtained over the Cu-Cr catalysts with Al and Zn promoters together, *e.g.* higher Al at.% (39%) in T-2 catalyst gave higher glycerol conversion (34%) and 1,2-PDO selectivity (90%) than T-1 catalyst with higher Zn at.% (39%). This may be due to the higher acidity of Al compared to Zn which helps to catalyze glycerol

dehydration to acetol.

3.3.2. Comparison of batch and continuous operations over Cu-Cr-Ba catalyst

Since Cu-Cr catalyst with Ba as a promoter was found to be highly efficient for glycerol hydrogenolysis to 1,2-PDO compared to other promoters, the further studies were carried out focusing on (i) the product distribution for glycerol hydrogenolysis in a batch reactor; (ii) evaluation of time on stream activity and product distribution for continuous glycerol hydrogenolysis; (iii) optimization of reaction conditions in both batch and continuous glycerol hydrogenolysis and to compare their performances for both batch and continuous glycerol hydrogenolysis were carried out using Cu-Cr-Ba catalyst.

The effects of temperature, H_2 pressure, liquid and gas flow rates and glycerol concentration on the conversion of glycerol and the product selectivities were also investigated. The range of reaction conditions used for this study is given in **Table 3.4.** The specifications of Cu-Cr catalyst with Ba as a promoter used for continuous glycerol hydrogenolysis operation are given in **Table 3.5**.

Table 3.4. Range of operating conditions

Parameter	Range	
	Batch	**Continuous**
Initial concentration of glycerol, wt%	20-60	20-60
Solvent	2-propanol	2-propanol
Temperature (^oC)	180-240	180-240
H_2 pressure (bar)	35-70	20-60
Catalyst wt (g)	0.8 - 2	23
Liquid velocity, LHSV (h^{-1})	-	0.78-2.34
Gas velocity, GHSV (h^{-1})	-	434-1304
Catalyst packing length (m)	-	0.11
Particle diameter (m)	-	0.004
Density of the catalyst (kg m^{-3})	-	1685

Table 3.5. Specifications of Cu-Cr-Ba catalyst

Type	**Cu-Cr-Ba**
Form	Pellets
Size (m)	0.005 X 0.002
Surface area ($m^2 g^{-1}$)	54.24
Bulk density ($g mL^{-1}$)	1.35

3.3.2.1. Batch reactor performance

3.3.2.1.1. Product distribution

Figure 3.6 shows the conversion, selectivity *vs.* time profile for liquid phase glycerol hydrogenolysis over Cu-Cr-Ba catalyst in 2-propanol at 220 ^{o}C, pH_2 of 52 bars for 5 h. Glycerol conversion increased from 10 to 34 % with increase in reaction time from 1 to

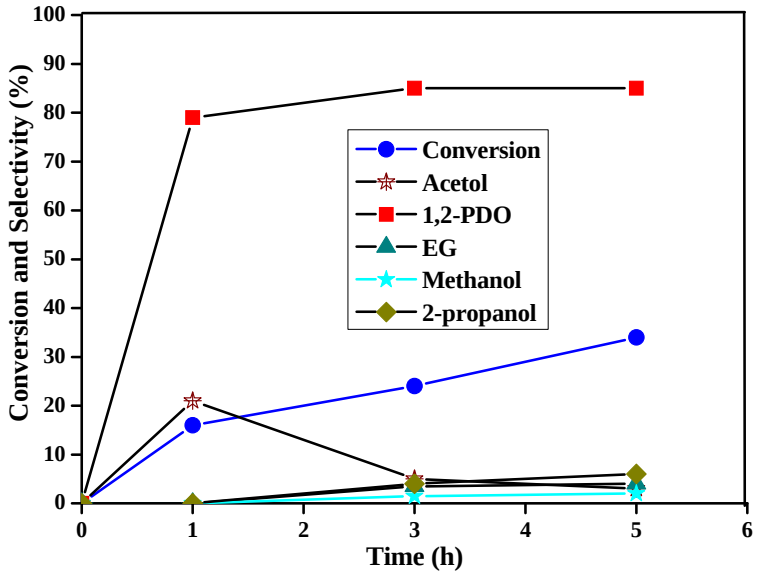

Figure 3.6. Conversion and selectivity *vs.* time profile of glycerol hydrogenolysis in a batch reaction.

Reaction conditions: Temperature, 220 ^{o}C; 20 wt% glycerol; H_2 pressure, 52 bar; solvent, 2-propanol; catalyst, 1 g; reaction time, 5 h.

5 h beyond which no effect of reaction time was observed on the conversion levels. For Cu-Cr catalysts, usually very long reaction times of > 12 h are reported [22] however; our catalyst gave a maximum conversion of 34% within a very short reaction time of 5 h. Another novelty of our catalyst was that the highest selectivity of > 84 % to 1,2-PDO was achieved and from the beginning of the reaction it was ~>4 times higher than that of the intermediate dehydration product, acetol indicating that the hydrogenation of acetol to 1,2-PDO is a very fast reaction. The highest selectivity of acetol formed was ~ 20% in one h, after which it started decreasing and was stable at ~ 5%. The only side products formed under the conditions of the present work were ethylene glycol, methanol and 2-propanol.

Two separate hydrogenolysis experiments starting with 1,2-PDO and glycerol were carried out using *n*-butanol as a solvent, in order to confirm the pathway of formation of 2-propanol and ethylene glycol. In case of hydrogenolysis of 1,2-PDO, the only product formed was 2-propanol confirming that it was a product of further hydrogenolysis of primary -OH and no cleavage products were formed from 1,2-PDO. As shown in **Figure 3.7**, glycerol hydrogenolysis gave 2-propanol, ethylene glycol and methanol along with acetol (minor) and 1,2-PDO as a major product. It was interesting to note that (**Figure 3.7**), the selectivity to 1,2-PDO reached a maximum value of 86% in about 2 h, after which it marginally decreased to 84% due to onset of formation of 2-propanol. This indicates that after a certain critical concentration of 1,2-PDO was reached, with a longer contact time its further hydrogenation to 2-propanol started. Also the formation of ethylene glycol was due to cleavage of C-C bond directly from glycerol and not from the 1,2-PDO while, 2-propanol was formed at the cost of excessive hydrogenolysis of 1,2-PDO.[32] As expected, methanol formation was also observed due to the hydrogenation of formaldehyde formed during C-C bond cleavage to give ethylene glycol.

These results as well as no formation of the gaseous product viz. methane, justify the reaction pathway for the hydrogenolysis of glycerol shown in **Scheme 3.1**.

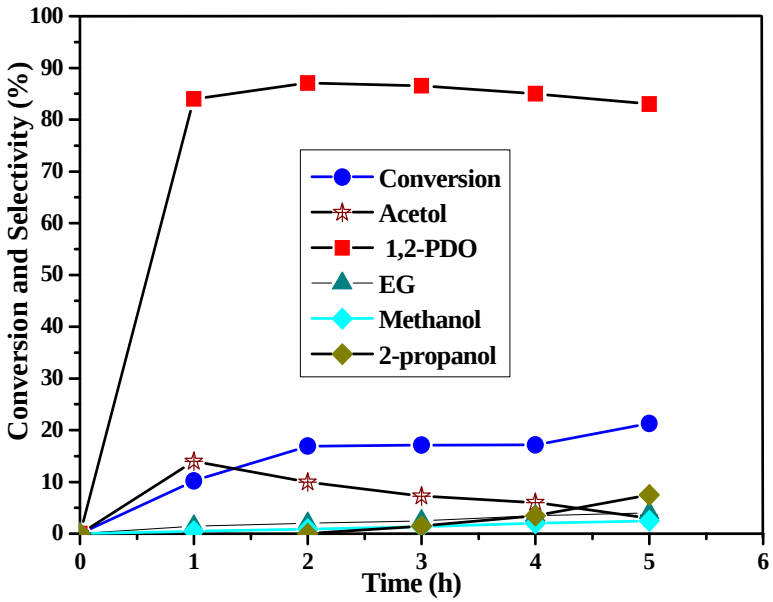

Figure 3.7. Conversion and selectivity *vs.* time profile of glycerol hydrogenolysis in batch reaction using *n*-butanol solvent.

Reaction conditions: Temperature, 220 ^{o}C; 20 wt% glycerol; H_2 pressure, 52 bar; solvent, *n*-butanol; catalyst, 1g; reaction time, 5 h.

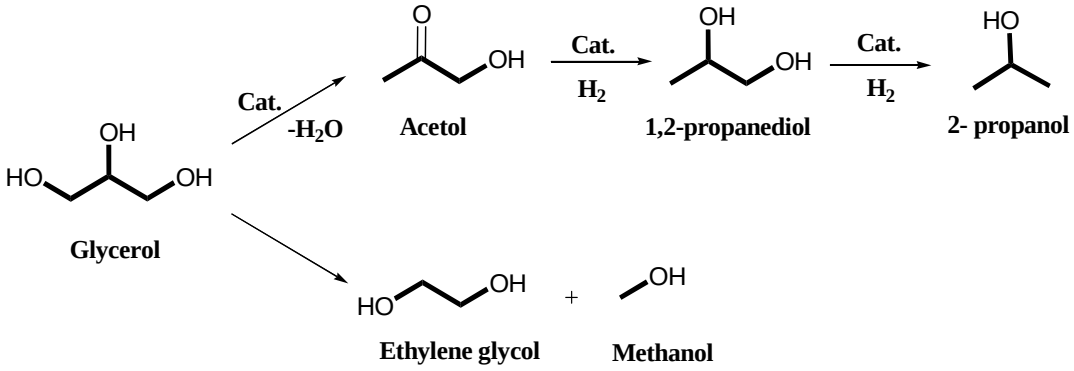

Scheme 3.1. Reaction pathway for hydrogenolysis of glycerol over Cu-Cr-Ba catalyst.

3.3.2.1.2. Effect of temperature

The effect of temperature on both glycerol conversion and 1,2-PDO selectivity was

studied in the temperature range of 180-240 °C, for Cu-Cr -Ba catalyst and the results are shown in **Figure 3.8.** Glycerol conversion increased from 18 to 43% with increase in temperature from 180 to 240 °C. As expected, the selectivity to 1,2-PDO decreased from 86 to 78% due to the excessive hydrogenation of 1,2-PDO favored at higher temperature to give 2-propanol. Also the selectivities to ethylene glycol and methanol increased from 0 to 6%, and 0 to 4% respectively, indicating that the degradation due to C-C cleavage of glycerol was more facile at high temperature.

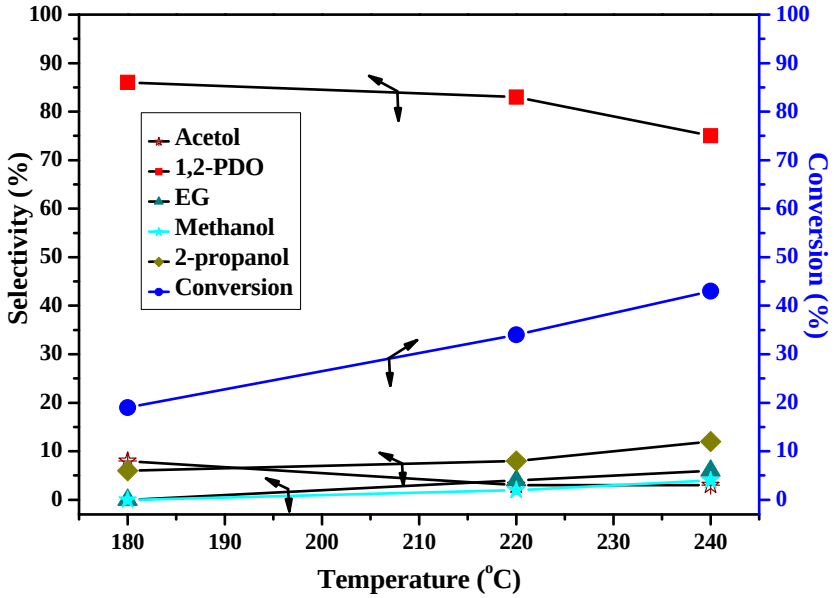

Figure 3.8. Effect of temperature on conversion and selectivity.

Reaction conditions:, 20 wt% glycerol; H_2 pressure, 52 bar; solvent, 2-propanol;catalyst, 1g; reaction time, 5 h.

An Arrhenius plot was also obtained as shown in **Figure 3.9**, from which the activation energy was estimated to be 147.5 kJ mol^{-1} K^{-1}.

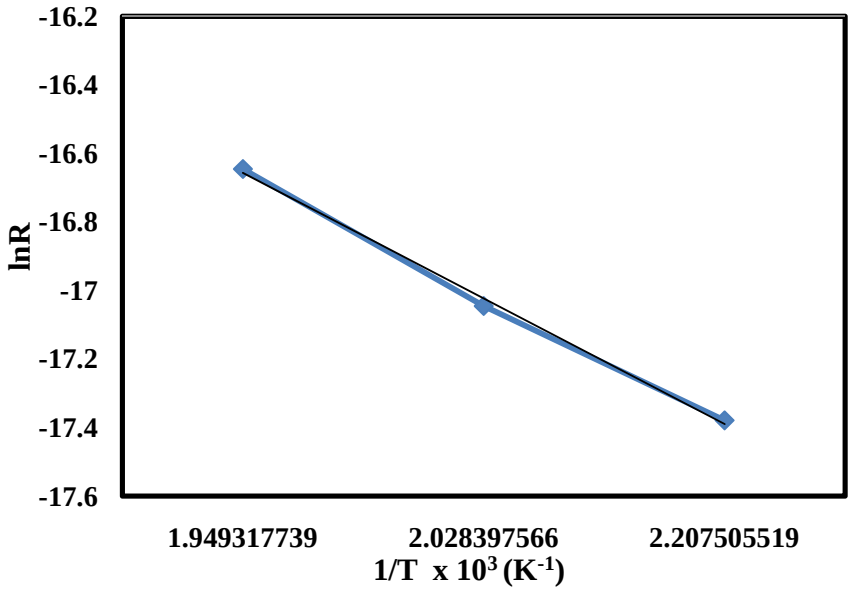

Figure 3.9. Plot of lnR *vs*. 1/T.

Reaction conditions: 20 wt% glycerol; H_2 pressure, 52 bar; solvent, 2- propanol; catalyst, 1g; reaction time, 5 h.

3.3.2.1.3. Effect of pressure

The results of effect of hydrogen pressure on glycerol hydrogenolysis studied at a constant temperature of 220 ^{o}C are shown in **Figure 3.10**. Glycerol conversion decreased marginally from 34% to 28% with increase in H_2 pressure from 35 to 67 bars indicating that the hydrogen atoms at a higher pressure compete with the re-adsorption of an intermediate acetol, for the active sites causing the decrease in conversion. Increase in hydrogen pressure in the higher range from 50 to 67 bars resulted in decreasing the selectivity to 1,2–PDO from 84 to 77% due to enhanced further hydrogenation of 1,2-PDO to 2-propanol. It is interesting to note that an increase in H_2 pressure did not affect the selectivity to the degradation product EG because copper is responsible for selective cleavage of C-O bond without affecting C-C bond. This was also confirmed by the study of catalyst loading effect discussed below.

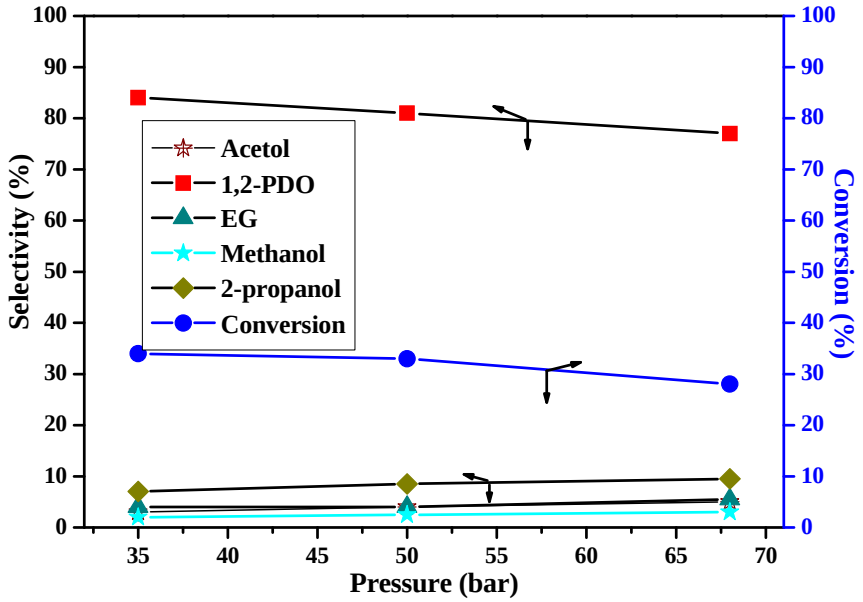

Figure 3.10. Effect of H_2 pressure.

Reaction conditions: 20 wt% glycerol; temperature, 220 ^{o}C; solvent, 2-propanol; catalyst, 1 g; reaction time, 5 h.

3.3.2.1.4. Effect of catalyst loading

The effect of catalyst loading on the hydrogenolysis reaction was studied in the range of 0.8- 2.0 g at 220 ^{o}C and 52 bar of hydrogen pressure, and the results are presented in **Figure 3.11**. It was observed that the conversion of glycerol increased from 31 to 47% with increase in catalyst weight from 0.8 to 2 g. Selectivity to 1, 2- PDO initially increased from 81 to 84% for an increase in catalyst weight from 0.8 to 1 g, while at the same time acetol selectivity decreased, indicating that rate of hydrogenation of acetol to 1,2-PDO increased at higher catalyst loading. The selectivity to the degradation product EG remained constant, irrespective of the catalyst loading, confirming that copper based catalyst does not favour C-C bond cleavage.

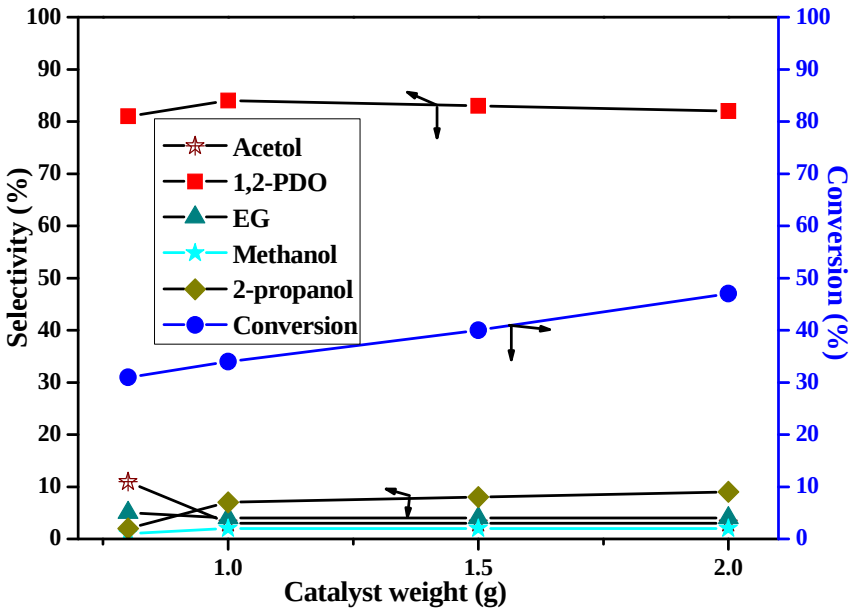

Figure 3.11. Effect of catalyst loading.

Reaction conditions: 20 wt% glycerol; temperature, 220 ^{o}C; H_2 pressure, 52 bar; solvent, 2-propanol; reaction time, 5 h.

3.3.2.1.5. Effect of glycerol loading

Effect of glycerol concentrations on the conversion of glycerol and selectivity pattern was also studied in the range of 20-60 wt% glycerol, and the results are shown in **Figure 3.12.** The conversion of glycerol decreased drastically from 34 to 11% while the selectivity to 1,2-PDO marginally decreased from 84 to 82% with increase in glycerol loading from 20-60 wt%. Interestingly, ethylene glycol selectivity increased by twice (from 3 to 6%), while that of 2-propanol decreased substantially from 7 to 3% as the concentration of glycerol increased from 20 to 60 wt%. Hence, 20 wt% of glycerol was found to be the optimum glycerol concentration. The substantial decrease in glycerol conversion could be due to the limiting number of catalytic sites at higher glycerol concentration. Miyazawa *et al.* also reported a high glycerol conversion at lower glycerol concentration of 10%.[6]

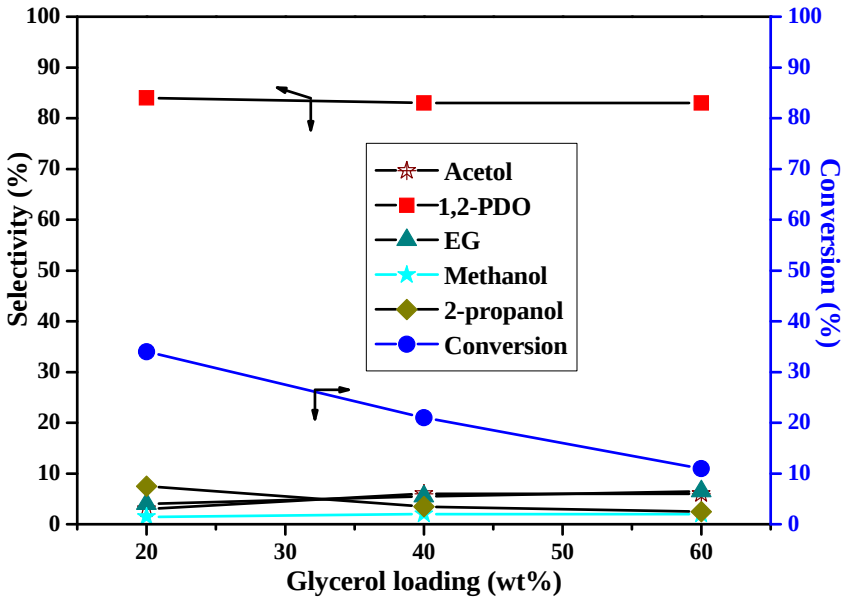

Figure 3.12. Effect of glycerol loading.

Reaction conditions: Temperature, 220 ^{o}C; H_2 pressure, 52 bar; catalyst, 1 g; solvent, 2-propanol; reaction time, 5 h.

3.3.2.2. Continuous reactor performance

Time on stream activity of Cu-Cr-Ba catalyst was also evaluated for the continuous hydrogenolysis of glycerol. **Figure 3.13** shows that this catalyst gave an excellent performance for 800 h for continuous operation in 2-propanol under 220 ^{o}C, and 52 bar hydrogen pressure conditions, with an average glycerol conversion of ~ 65% and > 91% selectivity to 1,2-PDO. The product distribution pattern studied in 2-propanol solvent is shown in **Figure 3.14.** The consistent performance of the catalyst was without any deactivation-reactivation cycle indicating that the activity of the catalyst was being maintained by *in situ* activation in a continuous flow of hydrogen and also resulted in higher activity (>65% conversion) as compared to that in a batch operation (34% conversion).

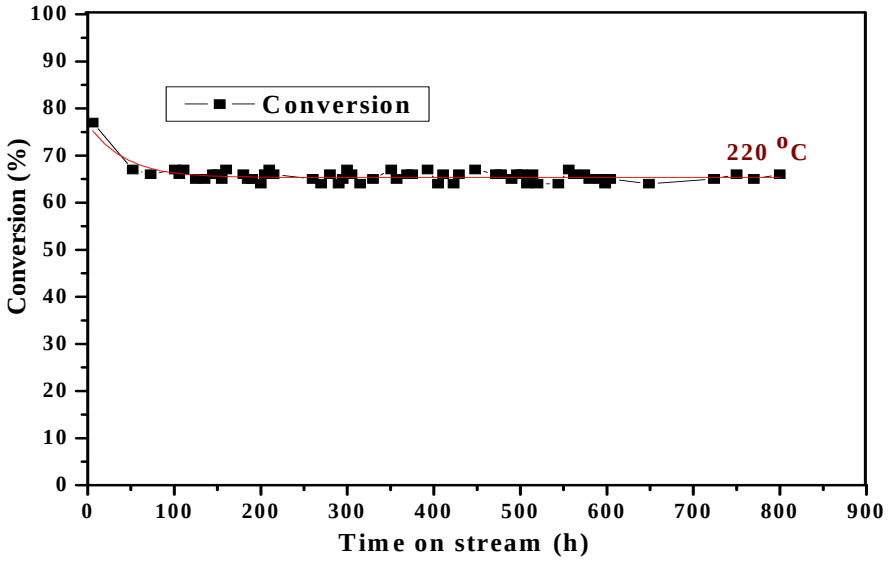

Figure 3.13. Time on stream activity for continuous glycerol hydrogenolysis.

Reaction conditions: Catalyst wt, 23 g; solvent, 2-propanol; 20 wt% glycerol; feed flow rate, 30 mL h^{-1}; H_2 flow rate, 10 NL h^{-1}; H_2 pressure, 40 bar; temperature, 220 ^oC.

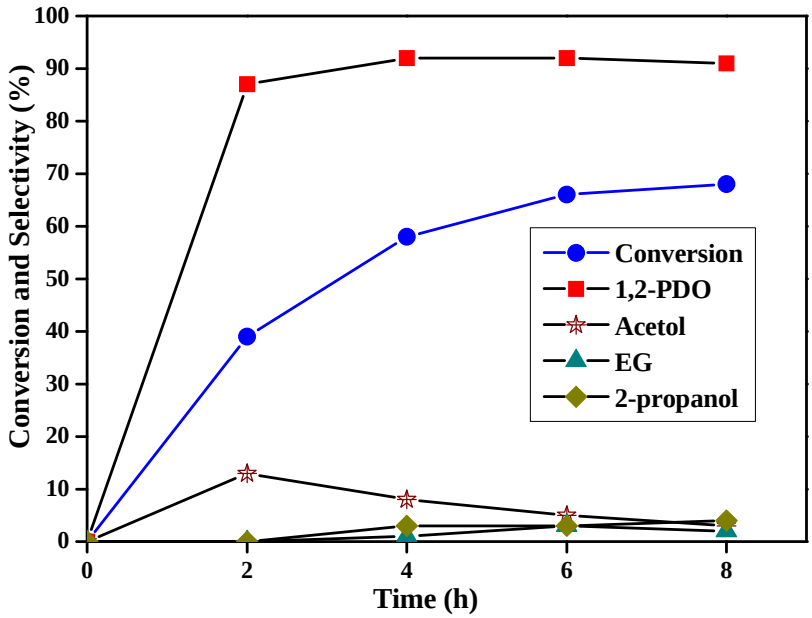

Figure 3.14. Conversion and selectivity *vs.* time profile for continuous glycerol hydrogenolysis.

Reaction conditions: Catalyst wt, 23 g; solvent, 2-propanol; 20 wt% glycerol; feed flow rate, 30 mL h^{-1}; H_2 flow rate, 10 NL h^{-1}; H_2 pressure, 30 bar; temperature, 220 ^oC.

As shown by a conversion and selectivity *vs.* time profile in **Figure 3.15,** formation of 2-propanol was again confirmed by a separate glycerol hydrogenolysis experiment in *n*-butanol solvent. Interestingly, much less (<2%) formation of EG was observed in the continuous glycerol hydrogenolysis due to the lower contact time (1.3 h) as compared to that in case of a batch operation (5 h). The lower EG formation also led to a very negligible (<0.8%) formation of methanol in the continuous operation and hence could not be shown in conversion and selectivity *vs.* time profiles. The effects of various reaction parameters on glycerol conversion and the selectivity pattern are discussed below.

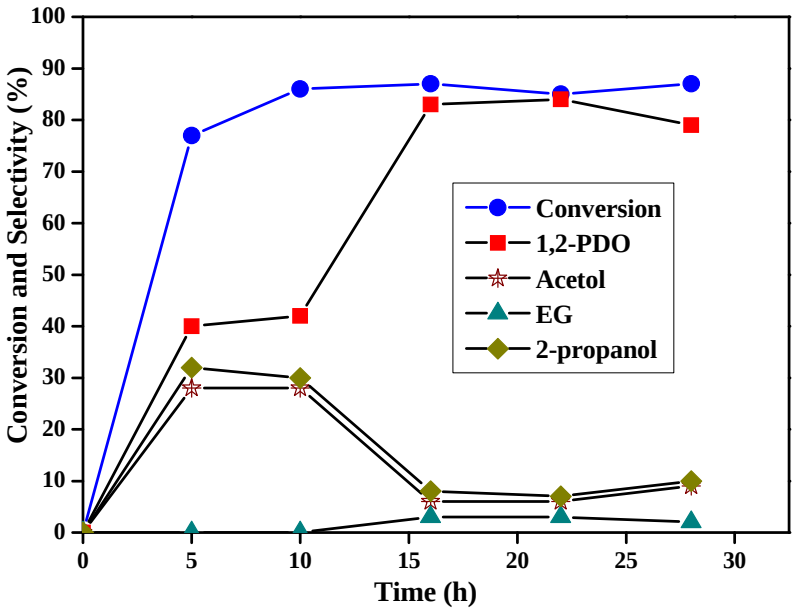

Figure 3.15. Conversion and selectivity *vs.* time profile for continuous glycerol hydrogenolysis in *n*-butanol.

Reaction conditions: Catalyst wt, 20 g; solvent, *n*-butanol; 20 wt% glycerol; feed flow rate 30 mL h^{-1}; H_2 flow rate, 10 NL h^{-1}; H_2 pressure, 30 bar; temperature, 220 ^oC.

3.3.2.2.1. Effect of liquid flow rate

The effect of liquid flow rate on conversion of glycerol was studied in the range of 18-54 mL h^{-1}, under constant temperature, H_2 pressure, and gas flow rate conditions and the

results are shown in **Figure 3.16.** With increase in liquid flow rate from 18 to 54 mL h^{-1}, glycerol conversion decreased proportionately. The reason for this decrease in conversion is the reduction in residence time of glycerol in the reactor with an increase in the liquid flow rate. Therefore, less time was available for the intimate contact of H_2 with liquid glycerol and the catalyst pellets, thus inhibiting the substrate diffusion. At lower liquid flow rate, catalyst particles were partially wetted; therefore, there would be direct contact of gas-phase reactant and catalyst surface which increases the reaction rate. Subsequently at higher liquid flow rate, the increased wetted fractions of catalyst surface would slow down the reaction rate. Similar observation was reported for continuous hydrogenation of 2-butyne -1,4-diol by Rode *et al*. [33]

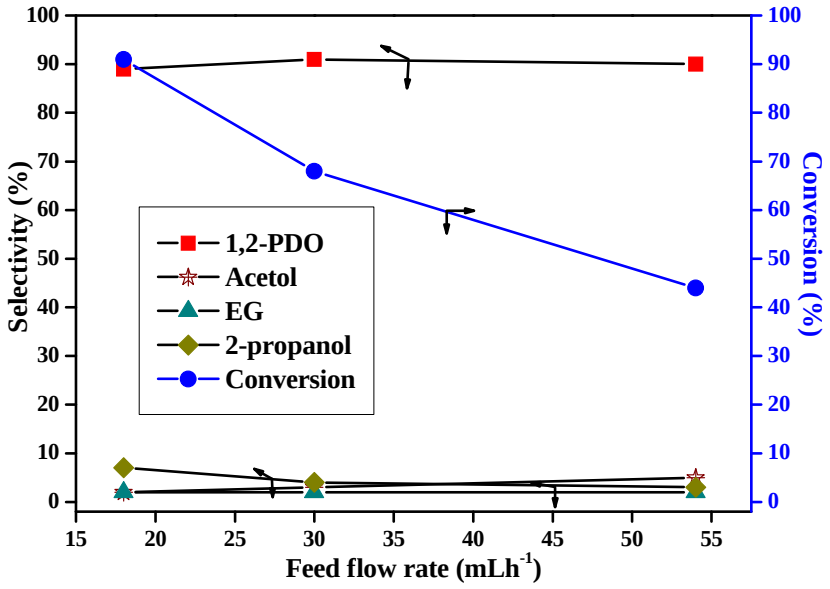

Figure 3.16. Effect of liquid flow rate.

Reaction conditions: Catalyst wt, 23 g; solvent, 2-propanol; 20 wt% glycerol; H_2 flow rate, 10 NL h^{-1}; pressure, 40 bar; temperature, 220 ^oC.

3.3.2.2.2. Effect of H_2 pressure

The effect of H_2 pressure was studied at constant temperature of 220 ^oC in the range of 20-60 bar H_2 pressure, and the results are shown in **Figure 3.17.** Unlike the results in a

batch operation, **(Figure 3.10)**, glycerol conversion increased from 64 to 74% with increase in H_2 partial pressure from 20 to 60 bar, in a continuous operation. At higher H_2 pressure, *in situ* reactivation of the catalyst could be more efficient, leading to higher glycerol conversion. 1, 2-propanediol selectivity initially increased from 82 to 91% while the selectivity to acetol decreased from 10 to 3% with increase in H_2 pressure from 20 to 40 bar, indicating higher hydrogenation rate at higher H_2 pressure.

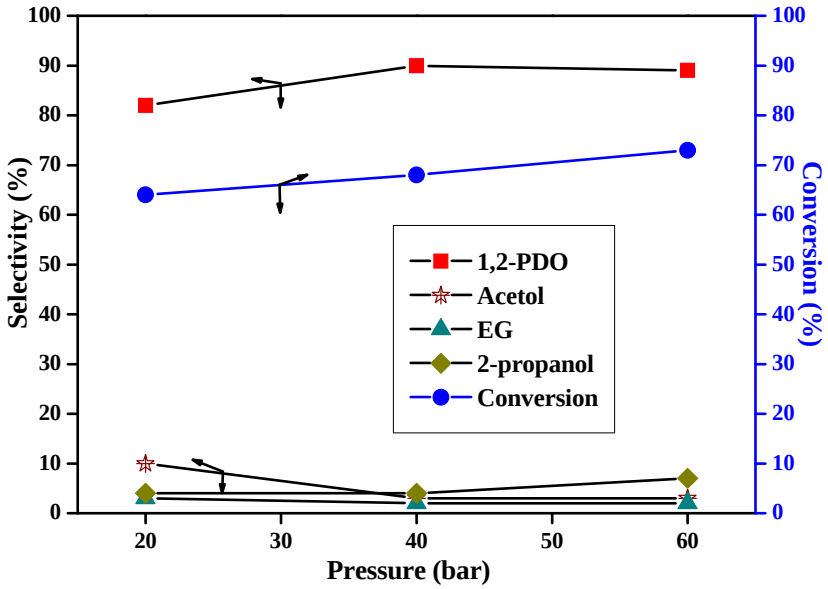

Figure 3.17. Effect of hydrogen pressure.

Reaction conditions: Catalyst wt, 23 g; solvent, 2-propanol; 20 wt% glycerol; feed flow rate, 30 mL h^{-1}; H_2 flow rate, 10 NL h^{-1}; temperature, 220 ^oC.

3.3.2.2.3. Effect of gas (H_2) flow rate

Effect of hydrogen gas flow rate on glycerol hydrogenolysis was studied in the range of 10 -30 NL h^{-1} under constant temperature and pressure conditions. From **Figure 3.18**, it was observed that there was no any effect of H_2 flow rate on glycerol conversion. The product selectivities also remained constant since the change in H_2 flow rate did not affect the reaction rate to a considerable extent.

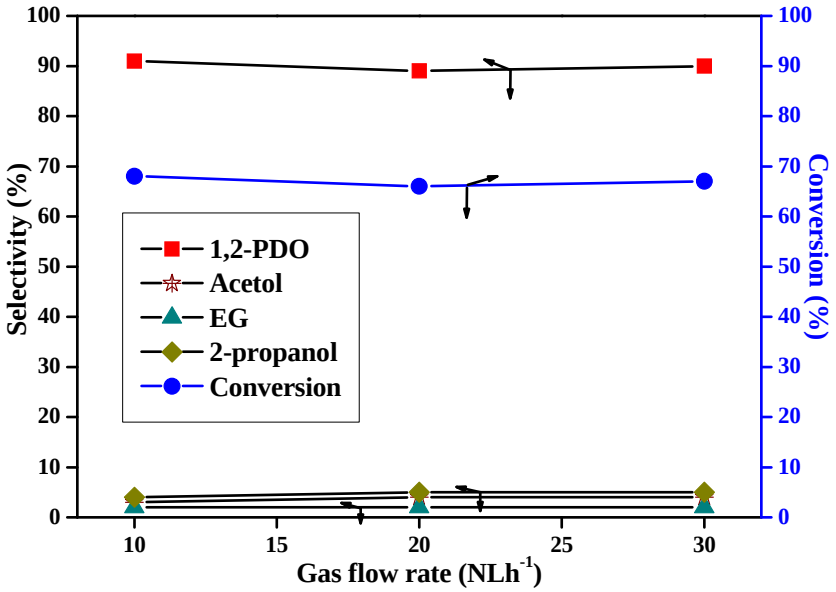

Figure 3.18. Effect of gas flow rate.

Reaction conditions: Catalyst wt, 23 g; solvent, 2-propanol; 20 wt% glycerol; feed flow rate, 30 mL h^{-1}; H_2 pressure, 40 bar; temperature, 220 ^oC.

3.3.2.2.4. Effect of temperature

Temperature effect was studied over the range of 180-220 ^oC by keeping other parameters constant. It was observed from **Figure 3.19** that reaction temperature had a considerable effect on the conversion of glycerol. However, as compared to the batch operation, the effect of temperature on the glycerol conversion was highly predominant in a continuous operation as evidenced by about more than 6 times increase in glycerol conversion (from 13 to 87%) as temperature increased from 180-220 ^oC while the selectivity to 1, 2 -propanediol decreased marginally from 95 to 86% correspondingly increasing the selectivity to the cracking product such as ethylene glycol.

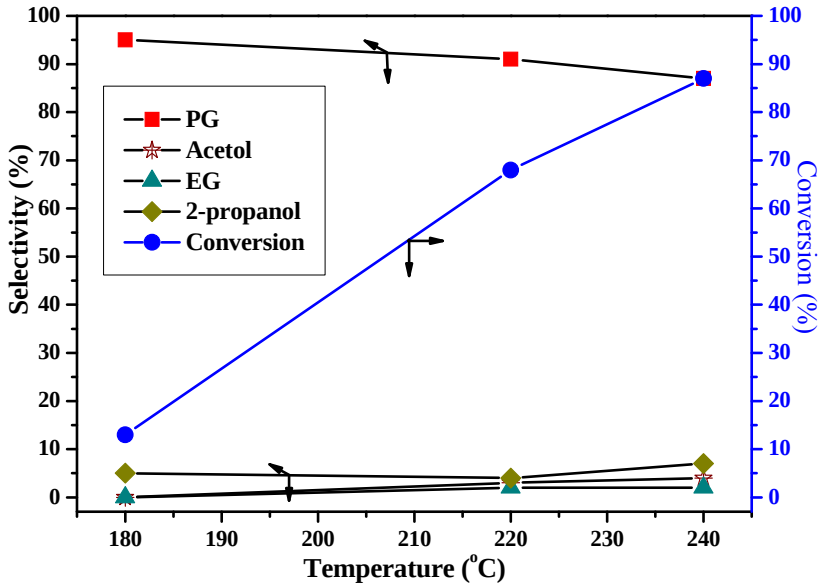

Figure 3.19. Effect of temperature.

Reaction conditions: Catalyst wt, 23 g; solvent, 2-propanol; 20 wt% glycerol; feed flow rate, 30 mL h^{-1}; H_2 flow rate, 10NL h^{-1}; H_2 pressure, 40 bar.

3.3.2.2.5. Effect of glycerol loading

Effect of glycerol loading was also studied by varying wt% of glycerol from 20 to 60% in liquid feed and the results are shown in **Figure 3.20**. Although similar to the batch operation, glycerol conversion initially decreased from 68 to 40% with increase in concentration from 20 to 40 wt%, it remained constant for further increase in glycerol loading up to 60 wt%. Thus, the effect of glycerol loading on the catalyst activity was much milder in a continuous operation, which could be due to the fact that the continuous flow of hydrogen leads to the catalyst surface renewal inhibiting the strong adsorption of the substrate. Another observation different from that in batch operation was that the selectivity to 1,2-PDO remained constant at 90% with initial increase in glycerol loading from 20 to 40% and then decreased to 85 % with further increase in glycerol loading up to 60%. At this glycerol loading corresponding formation (~ 10%) of other side products was observed.

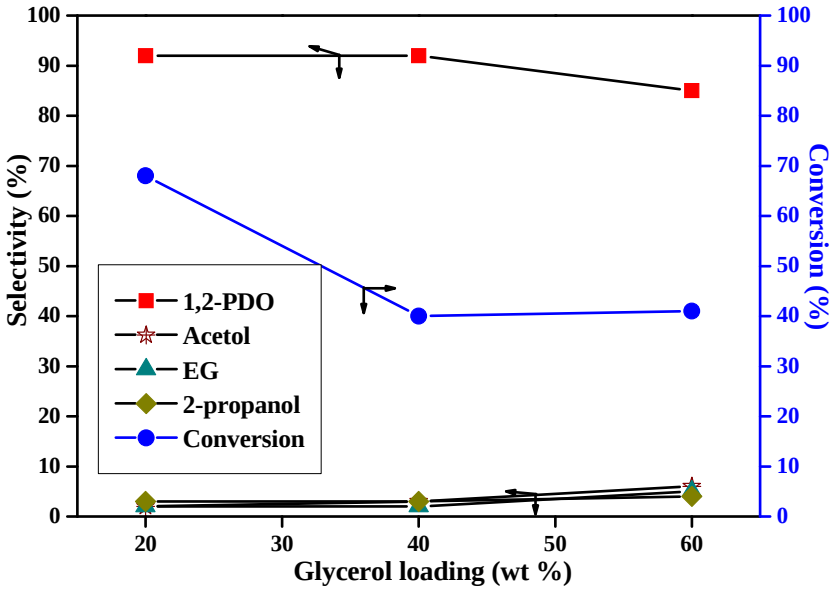

Figure 3.20. Effect of glycerol loading.

Reaction conditions: Catalyst wt, 23 g; solvent, 2-propanol; feed flow rate, 30 mL h^{-1}; H_2 flow rate, 10 NL h^{-1}; H_2 pressure, 40 bar; temperature, 220 ^oC.

3.4. CONCLUSIONS

- The role of promoters in copper chromite catalysts was found to be very important in determining the activity as well as the selectivity in hydrogenolysis of glycerol.
- Effect of three promoters *viz.* Al, Zn and Ba was studied individually as well as in combination with each other for the hydrogenolysis of glycerol.
- Cu-Cr catalyst with Ba as a promoter showed the highest conversion of 34% with highest selectivity of 85% to 1, 2-PDO in a batch operation while in a continuous operation it gave still higher conversion of 65% with a higher (>7 fold) catalyst stability as compared to Cu-Cr catalyst without any promoter.
- Highest activity and selectivity with Ba was mainly due to enhanced acidity catalyzing the first step of dehydration of glycerol to acetol and due to $BaCrO_4$ phase stabilizing the crystallite size of Cu^0 at a lower value of 69 nm than that compared to ~ 150 nm incase of bare Cu-Cr catalyst.

- In continuous operation, Cu-Cr -Ba catalyst gave time on stream (TOS) activity of 800 h for glycerol hydrogenolysis to 1,2-PDO without any deactivation-activation cycle.
- Product distribution studies in a batch operation confirmed that 2-propanol was formed due to excessive hydrogenation of 1,2-PDO while the C-C bond cleavage in glycerol led to the formation of ethylene glycol and methanol.
- Higher selectivity of >90% to 1,2-PDO was achieved in a continuous operation than that in a batch operation (84%) due to elimination of formation of ethylene glycol.
- Study of effect of process conditions in a continuous operation revealed that glycerol conversion and selectivity to 1,2-PDO increased from 65 to 74% and from 82 to 91 % respectively, with increase in H_2 partial pressure from 20 to 60 bar, while the selectivity to acetol decreased from 10 to 3% indicating higher hydrogenation rate at higher H_2 pressure.

3.5. REFERENCES

1. A. Corma, S. Iborra, A. Velty, *Chem. Rev.* **2007,** 107, 2411-2425.
2. A. Behr, J. Eilting, K. Irawadi, J. Leschinski, F. Lindner, *Green Chem*. **2008**, 10, 13-30.
3. I. Furikado, T. Miyazawa; S. Koso, A. Shimao, K. Kunimori, K. Tomishige, *Green Chem.* **2007,** 9, 582-588.
4. L. Ma, D. H. He, Z. P. Li, *Catal. Commun.* **2008**, 9, 2489-2495.
5. D. G. Lahr, B. H. Shanks, *J. Catal.* **2005,** 232, 386-394.
6. T. Miyazawa, Y. Kusunoki, K. Kunimori, K. Tomishige, *J. Catal.* **2006,** 240, 213-221.
7. T. Miyazawa, S. Koso, K. Kunimori, K. Tomishige, *Appl. Catal. A* **2007,** 318, 244-251.
8. Miyazawa, T.; Koso, S.; Kunimori, K.; Tomishige, K. *Appl. Catal., A* **2007**, 329, 30-35.
9. I. Furikado, T. Miyazawa, S. Koso, A. Shimao, K. Kunimori, K. Tomishige, *Green Chem.* **2007,** 9, 582-588.
10. B. Casale, A. Gomez, US Patent 5214219, **1993.**
11. B. Casale, A. M.Gomez, US Patent 5276181, **1994.**
12. J. Chaminand, L. Djakovitch, P. Gallezot, P. Marion, C.Pinel, C. Rosier, *Green Chem.* **2004**, 6, 359-361.
13. S. Wang, H. C. Liu, *Catal. Lett.* **2007**, 117, 62-67.
14. S. Sato, M. Akiyama, R. Takahashi, T. Hara, K. Inui, M. Yokota, *Appl. Catal. A* **2008,** 347, 186-191.
15. L. Schuster, M. Eggersdorfer, US 5616817, **1997.**
16. D. C. Cameron, N. E. Altaras, M. L.Hoffman, A. J. Shaw, *Biotechnol. Prog.* **1998**, 14, 116-125.
17. C. L.Thomas,; "Catalytic Processes and Proven Catalysts," *Academic Press, New York,* **1970.**
18. H. Zhenga, J. Yanga, Y. Zhub, G. Zhaob, *React. Kinet. Catal. Lett.* **2004,** 82, 263-269.

19. R. Jaganathan, S. T. Chaudhari, C. V.Rode, R. V.Chaudhari, *Ind. Eng. Chem. Res.* **1998,** 37, 2099-2106.
20. R. Rao, A. Dandekar, R. T. K. Baker, M. A. Vannice, *J. Catal.* **1997,** 171, 406-419.
21. T. Fleckenstein, G. Glebel, F. J. Carduck, DE Patent 4302464, **1994**.
22. M. A. Dasari, P. P. Kiatsimkul, W. R. Sutterlin, G. J. Suppes, *Appl. Catal. A* **2005**, 281, 225-231.
23. C. W. Chiu, M. A. Dasari, G. J.Suppes, *AIChE J.* **2006**, 52, 10, 3543-3548.
24. C. Chiu, A.Tekeei, W. R. Sutterlin, J. M. Ronco, G. J. Suppes, *AIChE J.* **2008** 54, 9, 2456-2463.
25. G. Suppes, W. Suttterlin, M. A. Dasari, WO Patent 2005095536 A2, **2005.**
26. R. B. Mane, A. A. Ghalwadkar, A. M. Hengne, Y. R. Suryawanshi, C.V. Rode, *Catal. Today* **2011**,164, 447 **-450.**
27. R. B. Mane, C. V. Rode, Catalytic recycling of glycerol formed in biodiesel production, *Recycling and Reuse of Materials and Their Products, Advances in Materials Science* book series (Edis.: S. Thomas), Apple Academic Press, Inc, , Vol. 3, Chapter 2, **2013**, p.9.
28. C. V. Rode, A. A. Ghalwadkar, R. B. Mane, A. M. Hengne, S. T. Jadkar, N. S. Biradar, *Org. Process Res. Dev.* **2010**,14, 1385-1392.
29. J. Pike, S.-W. Chan, F. Zang, X. Wang, J. Hanson, *Appl. Catal. A* **2006**, 303, 273-277.
30. Y.Yan, Q.-S. Wu, L. Li, Y.-P. Ding, *Crystal Growth & Design* **2006**, 6, 769-773.
31. V. R. Choudhary, S. G. Pataskar, *Thermochimica. Acta.* **1985**, 95, 87-98.
32. Y. Kusunoki, T. Miyazawa, K. Kunimori, K. Tomishige, *Catal. Commun.* **2005,** 6, 645-649.
33. C. V. Rode, P. R. Tayade, J. M. Nadgeri, R. Jaganathan, R. V. Chaudhari, *Org. Process Res. Dev.* **2006**, 10, 278-284.

Chapter 4

Non-noble, non-chromium nano Cu-Al catalyst for aqueous phase glycerol hydrogenolysis and dehydration

Non-chromium Cu-Al nano catalyst prepared by simultaneous co-precipitation and digestion method without any template or stabilizer, showed three times higher activity than the bulk Cu-Cr catalyst for hydrogenolysis of glycerol in both 2-propanol and water solvents. Cu_2O phase formed after reduction was found to stabilize the particle size in a narrow range of 7-11 nm by inhibiting the sintering of copper particles under reaction conditions. The same catalyst was also found to catalyze the direct hydrogenolysis of glycerol to 1,2-PDO. Time on stream activity (TOS) of our Cu-Al-5 catalyst for both continuous hydrogenolysis and dehydration of glycerol was found to be 400 h with an average conversion of 65% and 90% respectively. In glycerol dehydration, Cu-Al-5 catalyst showed the highest activity and acetol selectivity in water medium while, in 2-propanol as a reaction medium, transfer hydrogenation led to the formation of 1,2-PDO (10-38%).

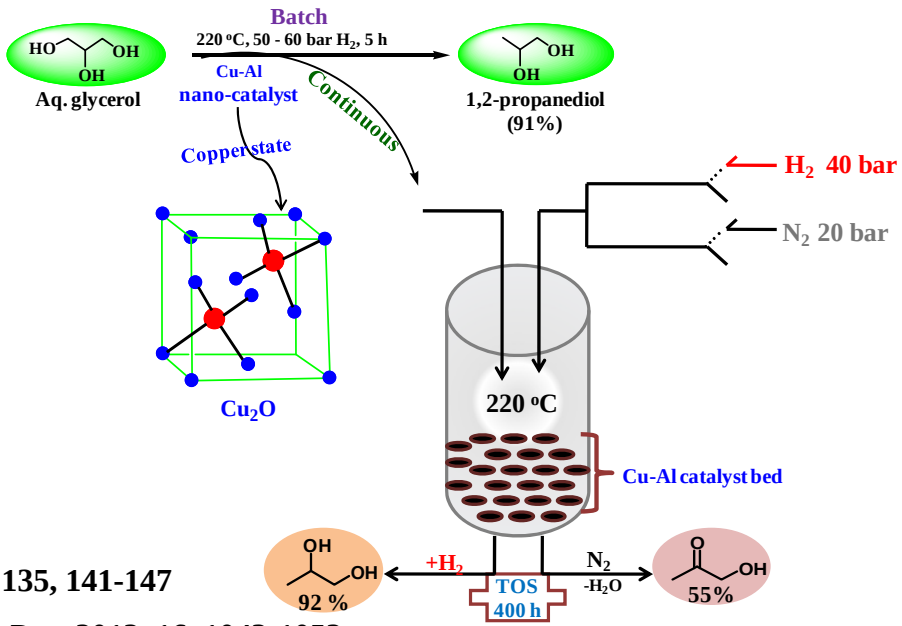

***Catal. Lett.* 2010, 135, 141-147**

***Org. Process Res. Dev.* 2012, 16, 1043-1052**

4.1. INTRODUCTION

Glycerol hydrogenolysis to 1,2-PDO proceeds through two distinct pathways, (i) glycerol dehydration to acetol (on acid sites) followed by its hydrogenation to 1,2-PDO (on metal sites) (**pathway A, Scheme 4.1**), (ii) and through dehydrogenation-dehydration-hydrogenation in presence of a base (**pathway B, Scheme 4.1**).[1-6]

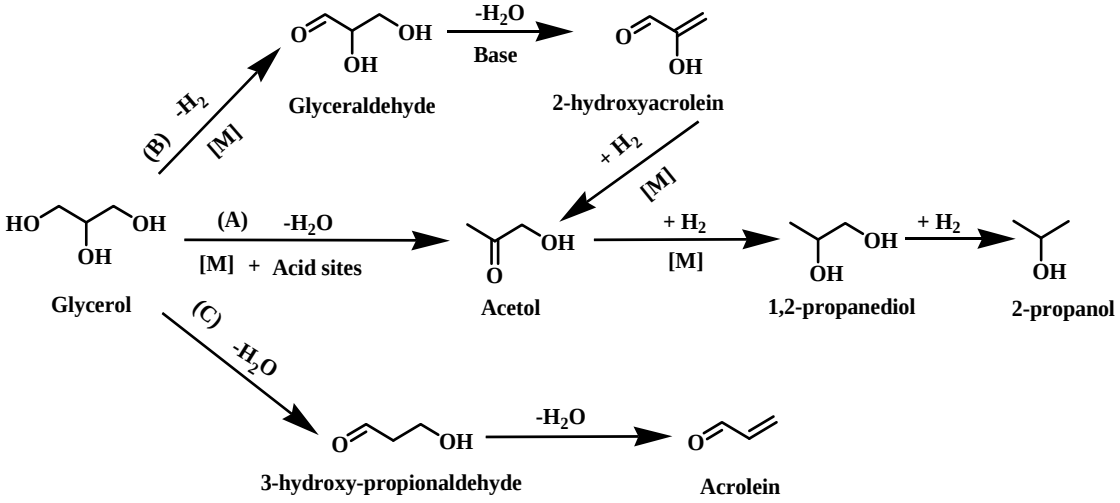

Scheme 4.1. Parallel and series reaction network in glycerol hydrogenolysis.

Pathway C (**Scheme 4.1**) is also possible for glycerol dehydration leading to formation of acrolein through 3-hydroxy-propionaldehyde intermediate however, it is catalyzed by strong BrØnsted acid sites.

In pathway A, acetol is a first step dehydration product while in pathway B, acetol is obtained indirectly through glyceraldehyde. Therefore, the first route *via* acetol to 1,2-PDO is generally preferred as acetol although an intermediate, has wide range applications in hydrogen production by catalytic steam reforming,[7] pyruvaldehyde synthesis through oxidation[8] and as a starting material in various organic transformations.[9,10] Secondly, acetol can be hydrogenated in a separate step with complete selectivity to 1,2-PDO. Catalyst systems reported for glycerol hydrogenolysis *via* acetol can be broadly classified into two types *viz.* supported noble metals and other transition metals either supported or in their mixed oxide forms. Among noble metals Ru, Rh, Pt, Au have been extensively studied which were found to be highly active in

direct cleavage of both C-C and C-O bonds; thus, formation of ethylene glycol (EG) and methane are competing byproducts with 1,2-PDO.[11,12] As Cu catalysts are well-known for selective C-O bond hydrogenation, glycerol hydrogenolysis to 1,2-PDO is preferred over Cu in combination with other non-noble metals, particularly Cr, Zn, Ba and Al.[13-16] Dasari *et al.* reported 20 wt% aqueous glycerol hydrogenolysis over various commercial copper-chromite catalysts with 54.8% glycerol conversion and 85% selectivity to 1,2-PDO,[17] while copper-chromite catalysts synthesized by template preparation resulted in enhancing 1,2-PDO selectivity to 96% using 40 wt% aqueous glycerol.[18] A systematic study of various promoters in Cu-Cr catalysts showed that the presence of Ba up to 30% in Cu-Cr gave higher activity and stability (> 7 -fold) as compared to Cu-Cr without any promoter. The better performance of Ba promoted catalyst was found to be due to enhanced acidity and $BaCrO_4$ phase formation stabilizing the Cu^0 particle size at 69 nm (as discussed in chapter 3). However, toxicity associated with Cr in these catalysts necessitates the development of new generation of catalysts. Among non-Cr catalysts, Cu-ZnO catalyst was first evaluated in presence of a solid acid by Chaminand *et al.* to give 1,2-PDO selectivity >90% with a very low conversion of 20% inspite of longer reaction time (92 h). [19] Although a shorter reaction time (12 h) was reported by Wang and Liu for the Cu/ZnO catalyst, conversion was restricted to 22.5% with only 83.6% selectivity to 1,2-PDO.[20] Recently, highest selectivity of 93% to 1, 2-PDO was achieved with 34% glycerol conversion for Cu-ZnO catalyst in 16 h reaction time.[21] Although, Cu-ZnO catalyst system could be acceptable due to elimination of chromium, but longer reaction times make it unpractical from process point of view. In spite of the fact that production of a high-volume product like 1,2-PDO would be commercially viable with only continuous process, very few reports are available on process optimization. Some of these studies include gas phase glycerol hydrogenolysis over Cu-Zn-Al catalysts and Cu/Al_2O_3 catalysts giving 96-100% glycerol conversion with 1,2-PDO selectivity > 90%.[22,23] However, these studies were carried out under gas phase conditions requiring a preheating step, at very low WHSV/LHSV conditions and also the catalyst stability in terms of time on stream activity has not been specified.

Hence, the main objective of present work was to develop highly efficient non-chromium nano (Cu-Al) catalysts by the reduction of cubic spinel-type phases, which

contain excess copper ions that will exhibit good catalytic performance and do not require any promoter for the glycerol hydrogenolysis. As per the expectation, our non chromium Cu-Al nano catalyst (7-11 nm) exhibited > two fold activity as compared to the bulk Cu-Cr catalyst (>25 nm, by TEM) with the highest selectivity of 91% to 1, 2-PDO for aqueous phase hydrogenolysis of glycerol in a very short reaction time of 5 h.[24] The catalyst was completely characterized for its physico-chemical properties based on which the observed activity results have been discussed. Effect of various reaction parameters on conversion of glycerol and selectivity to 1, 2-PDO has also been reported for the nanostructured Cu- Al catalyst. Further Cu-Al catalyst was used to investigate the activity performance for continuous dehydration of glycerol to acetol in an inert atmosphere and also for direct glycerol hydrogenolysis to 1,2-PDO, separately.[25] This study is highly desirable from process point of view since, acetol can be first obtained and further hydrogenated over the same catalyst with complete selectivity to both the products. For this purpose, a detail study was carried out on comparison of performances of various copper catalysts with and without chromium for (i) dehydration and hydrogenolysis of glycerol to acetol and 1,2-PDO respectively, in a batch reactor; (ii) effect of aqueous and organic solvents; (iii) performance study of the best non-chromium Cu-Al catalyst in a continuous process for both dehydration and hydrogenolysis of aqueous glycerol; (iv) comparison of product distribution in batch and continuous operations; (v) catalyst stability in terms of time on stream (TOS) activity of Cu-Al catalysts.

4.2. EXPERIMENTAL

Nano Cu-Al catalyst of different compositions and Cu-Cr catalyst with different promoters (Ba, Al, Zn) were prepared by simultaneous co-precipitation and digestion technique and the details of which has been described in chapter 2 (section 2.3.1-2.3.3). Cu-Cr catalyst without Ba was designated as NMT006 while another one containing Ba prepared by patented procedure was designated as NMT-P.[26] Copper contents of NMT006 and NMT-P catalysts were 67 and 60% respectively. The catalysts were characterized by HR-TEM, XRD and NH_3-TPD and the detailed characterization procedure is described in chapter 2 (sections 2.4.3, 2.4.2, 2.4.10). The activity of

prepared Cu-Al and Cu-Cr catalysts for dehydration and hydrogenolysis of glycerol to acetol and 1,2-PDO respectively was carried out in batch as well as continuous operations and experimental procedure is described in chapter 2 (sections 2.5.1, 2.5.2).

4.3. RESULTS AND DISCUSSION

4.3.1. Catalyst characterisation

TEM images of the reduced Cu-Al (having composition of 50:50) nano catalyst shows an aggregation of the metal particles, the size of which was estimated to be ~10 nm **(Figure 1, a)**. SAED in **Figure 1 (b)** shows the diffraction planes as (110), (111), (311), (204) which correspond to acicular CuO nano particles.[27] TEM of bulk NMT006 **(Figure 1, c)** clearly shows the higher extent of aggregation of metal particles from which the particle size was found to be in the range of 25-30 nm.

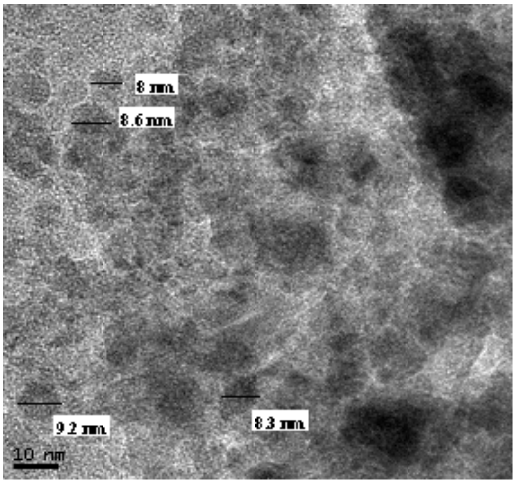

(a)

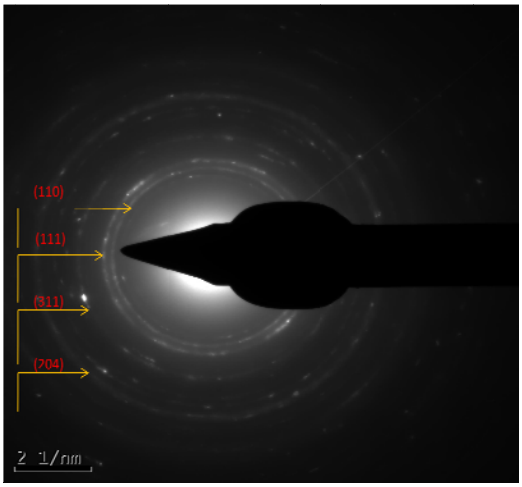

(b)

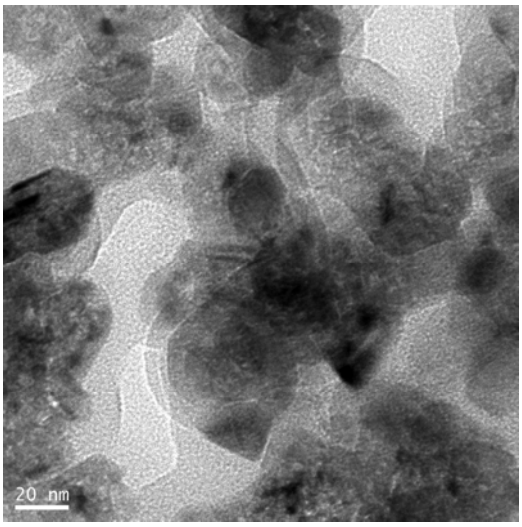

(c)

Figure 4. 1. (a) HR-TEM image of nano Cu-Al catalyst (b) SAED image showing planes of Cu (110), (111), (311) and (204) (c) HR-TEM image of bulk NMT006.

Figures 4.2 (**a**) and (**b**) show the XRD patterns of nano Cu- Al catalyst and the bulk NMT006 catalysts respectively, at various stages of preparation. The XRD patterns after calcination for both Cu-nano (A1 in **Figure 4.2, a**) as well as bulk NMT006 catalysts (B1 in **Figure 4.2, b**) showed dominant peaks at 2θ values of 35.46^o ($\bar{1}$11) and 38.7^o (111) corresponding to CuO phase.[20]After reduction of NMT006 in hydrogen, narrow well defined peaks appeared at 2θ = 43.36^o (111), 50.96^o (200), and 74.5^o (220) which correspond to metallic Cu phase (B2 in **Figure 4.2, b**).[28] While, reduced nano catalyst shows broader peaks at 2θ = 36.54^o (111) and 43.36^o (111) which were assigned to Cu_2O and metallic Cu phases respectively, indicating the inadequate reduction of Cu in nano catalyst. Both these phases were also confirmed by their corresponding small peaks at 2θ = 29.5 (110), 61.4 (220) and 2θ = 50.4 (200), 74.1 (200) respectively. This also confirms that CuO in nano Cu-Al catalyst undergoes the sequential reduction, first to Cu_2O cubic phase as a stable intermediate and then to Cu^0.[27] The XRD of used samples of both nano Cu-Al and NMT006 showed the high intensity peaks corresponding to metallic Cu with increased crystallinity and very small peak of Cu_2O phase indicating higher extent of reduction and aggregation of Cu species under reaction conditions. Using Scherrer equation, the crystallite sizes of fresh and used nano catalyst were found to be 7 and 11

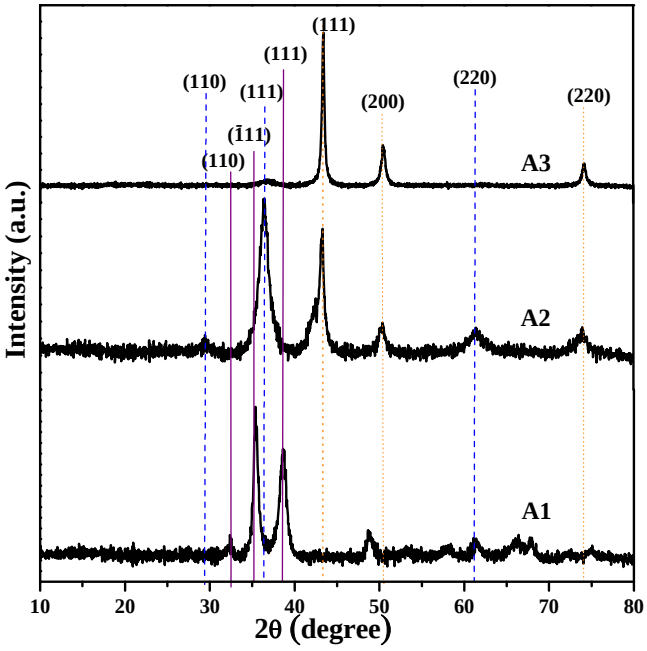

(a)

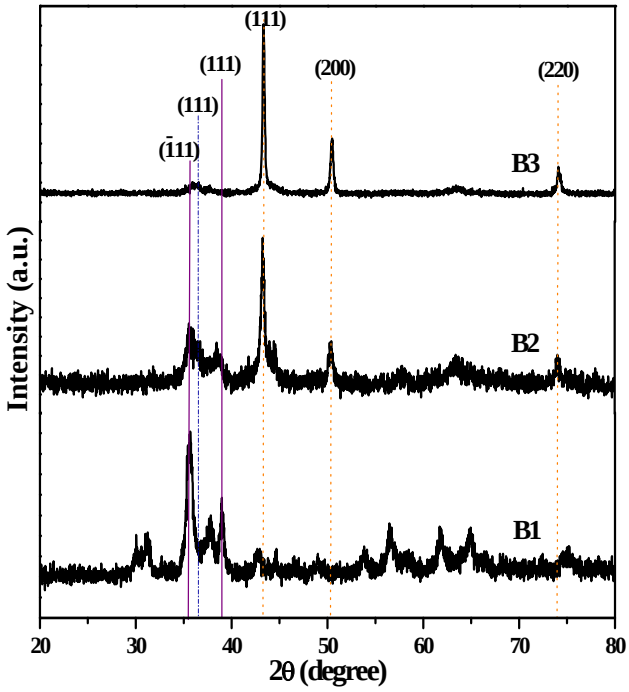

(b)

Figure 4.2. (a) XRD pattern of nano Cu-Al catalyst: (A1) calcined, (A2) reduced, (A3) after reaction (b) XRD pattern of NMT006 catalyst :(B1) calcined, (B2) reduced, (B3) after reaction.

nm while, those of bulk catalysts were 24 and 42 nm respectively. This shows that the extent of aggregation for nano Cu-Al catalyst was much less than that observed for the bulk catalyst under reaction conditions which could be due to the presence of Cu_2O species in the nano catalyst.

Since, the first step of glycerol hydrogenolysis involves its dehydration to acetol; the strength and nature of acid sites of our catalysts were determined by NH_3-TPD. **Table 4.1** shows the values of ammonia adsorbed and distribution of acidic sites of nano Cu-Al, NMT006 and NMT-P catalyst samples. The nano Cu- Al catalyst shows the highest total concentration of acidic sites as 1.567 mmol g^{-1} among all the three catalysts indicating that hydrogenolysis of glycerol proceeds through acetol *via* dehydration (**Scheme 4.1 (A)**) without needing a separate acidic catalyst.

Table 4.1. Ammonia TPD results of nano Cu-Al, NMT006 and NMT-P[26] catalyst

Catalyst	NH_3 adsorbed (mmol g^{-1})	Distribution of acidic sites (mmol g^{-1})		
		50-200 °C	200-400 °C	400-700 °C
Nano Cu- Al	1.567	0.145	0.910	0.512
NMT006	0.3414	0.0208	0.2299	0.0907
NMT-P	1.184	0.145	0.910	0.129

4.3.2. Catalyst activity

The results of liquid phase glycerol hydrogenolysis in 2-propanol at 220 °C over different copper catalysts are presented in **Table 4.2.** Cu-Al nano catalyst showed the highest activity (turn over frequency, TOF = 2.96 h^{-1}) with 88% selectivity to 1, 2 –PDO and 7% to acetol, while NMT006 catalyst showed the lowest activity (TOF, 0.92 h^{-1}) with 74% selectivity to 1, 2- PDO and 24 % to acetol. Bulk catalysts (NMT006 and NMT-P) showed >20% selectivity to acetol due to lower rate of hydrogenation of acetol. The activity of Cu- Al nano catalyst was almost five fold higher than the bulk Cu-Cr catalysts reported in the literature.[17,20] The novelty of our catalysts was that the formation of degradation product *viz.* ethylene glycol was much lower (≤ 5%) than that compared to

the bulk copper catalysts reported in the literature for which ethylene glycol along with methanol, propanols and gaseous products to the extent of > 50% were formed.[17,20] Also, the major side product formed was only the acetol which eventually undergoes hydrogenation to give 1, 2- PDO.

Table 4.2. Hydrogenolysis of glycerol in 2-propanol

Catalyst	TOF (h^{-1})	Conversion (%)	Selectivity (%)		
			1,2-PDO	Acetol	EG
Cu-Al	2.96	47	88	7	5
NMT006	0.92	16	74	24	2
NMT-P	1.26	24	63	32	5

Reaction conditions: 23 wt% glycerol (100 mL); H_2 pressure, 70 bar, catalyst, 0.8 g; temperatura, 220 ^oC; reaction time, 5 h.

Table 4.3 shows the activity results of various catalysts for the hydrogenolysis of glycerol using water as a solvent. Cu-Al nano catalyst showed the highest (TOF, 2.63 h^{-1}) activity and selectivity (91%) to 1, 2 -PDO. Activity as well as selectivity to 1, 2-PDO decreased drastically for bulk Cu-Cr catalysts (NMT006 and NMT-P) in comparison with Cu-Al nano catalyst. The drop in selectivity to 1, 2 -PDO was mainly due to the accumulation of an intermediate, acetol indicating slower kinetics of acetol hydrogenation to 1, 2- PDO over bulk Cu-Cr catalyst. The activity and selectivity exhibited by Cu- Al nano catalyst in water was almost comparable to that in 2-propanol solvent indicated the better water tolerance of the Cu-Al nano catalyst hence, aqueous glycerol solution can be directly used as a feed for its selective hydrogenolysis to 1, 2-PDO.

The highest activity of the Cu-Al nano catalyst for glycerol hydrogenolysis could be due to the following two reasons. (1) The higher acidic sites as shown by ammonia

Table 4.3. Hydrogenolysis of glycerol in water

Catalyst	TOF (h^{-1})	Conversion (%)	Selectivity (%)		
			1,2-PDO	Acetol	EG
Cu-Al	2.63	38	91	4	5
NMT006	0.51	9	55	44	1
NMT-P	0.94	11	38	68	<0.01

Reaction conditions: 20 wt% glycerol (100 mL); H_2 pressure, 70 bar; catalyst, 0.8 g; temperatura, 220 ^oC; reaction time, 5 h.

TPD results. As the glycerol hydrogenolysis is a two step process, the first step being dehydration of glycerol to acetol followed by the hydrogenation to give 1, 2- PDO. Aluminium present in our nano catalyst gets converted to alumina during calcination step which is normally responsible for higher acidity leading to faster dehydration to form acetol. Sato *et al.* [29] proposed that alumina supported copper as well as pure copper was an effective catalyst for the dehydration of glycerol to acetol under inert conditions, and (2) acetol thus formed undergoes probably a very fast hydrogenation to 1, 2-PDO, catalyzed by nano size Cu^0. The nano size Cu^0 was stabilized due to the inhibition of sintering by Cu_2O, the presence of which is evidenced by the XRD pattern **(Figure 4.2 a)**. Huang *et al.* also have suggested that the Cu^{1+} formed during the reduction treatment, although catalytically inactive in glycerol reaction, helps to inhibit the sintering of copper particles during the reaction.[30] While NMT006 catalyst **(Figure 4.2 b)** consists of pure metallic copper phase *i.e.* Cu^0, the Cu^{1+} species in Cu-Al nano catalyst formed due to alumina is responsible for the higher catalytic activity due to the stabilization of the catalyst by inhibiting the sintering of active species.

Further studies on effect of process parameters *viz.* temperature, catalyst loading, glycerol concentration, hydrogen pressure and catalyst stability on glycerol conversion and 1,2-PDO selectivity were carried out over nano Cu-Al catalyst in aqueous medium,

are discussed below.

4.3.2.1. Effect of temperature

Figure 4.3 shows the influence of reaction temperature on conversion and selectivity pattern in glycerol hydrogenolysis over Cu-Al nano catalyst. Glycerol conversion increased from 29 to 76% with increase in temperature from 200 to 240 ^{o}C. Maximum conversion of 76% was obtained at 240 ^{o}C however, selectivity to 1, 2-PDO decreased marginally from 93 to 89% with a corresponding increase in the selectivity to ethylene glycol from 6 to 10%, indicating that the higher temperature favoured degradation products due to C-C bond cleavage.

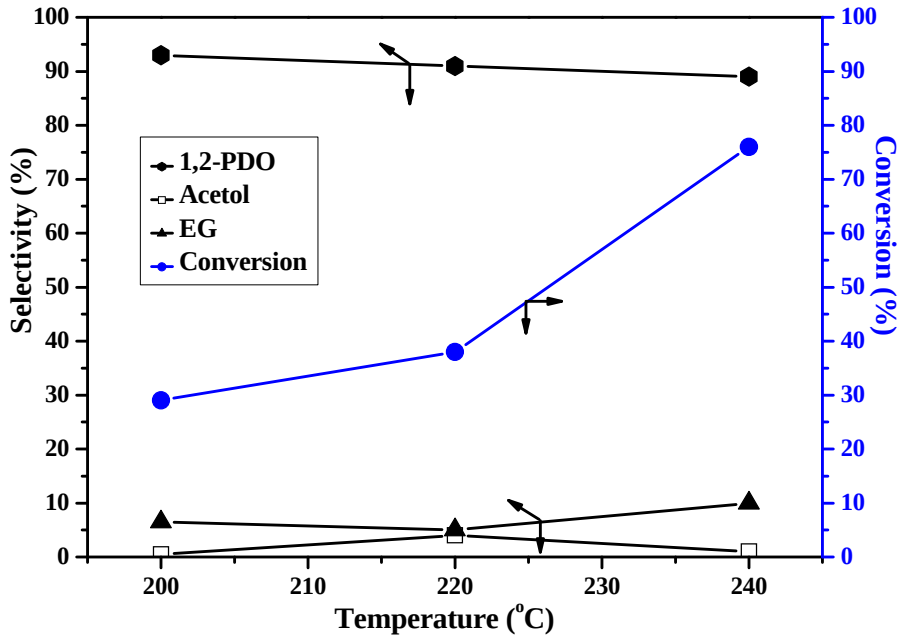

Figure 4.3. Effect of temperature.

Reaction conditions: 20 wt% aqueous glycerol (100 mL); H_2 pressure, 70 bar; catalyst, 0.8 g, reaction time, 5 h.

4.3.2.2. Effect of catalyst loading

Figure 4.4 shows the effect of catalyst loading on glycerol conversion and selectivity for hydrogenolysis of glycerol at 220 ^{o}C. It was found that conversion of glycerol increased almost three fold with increase in catalyst loading from 0.4 to 1.6 g. The selectivity to 1, 2 -PDO slightly decreased at higher catalyst loading due to formation of degradation products. The increase in conversion with increase in catalyst loading could be due to more availability of the active sites on the catalyst surface for the reaction which also leads to excessive hydrogenation of 1, 2- PDO to lower alcohols.

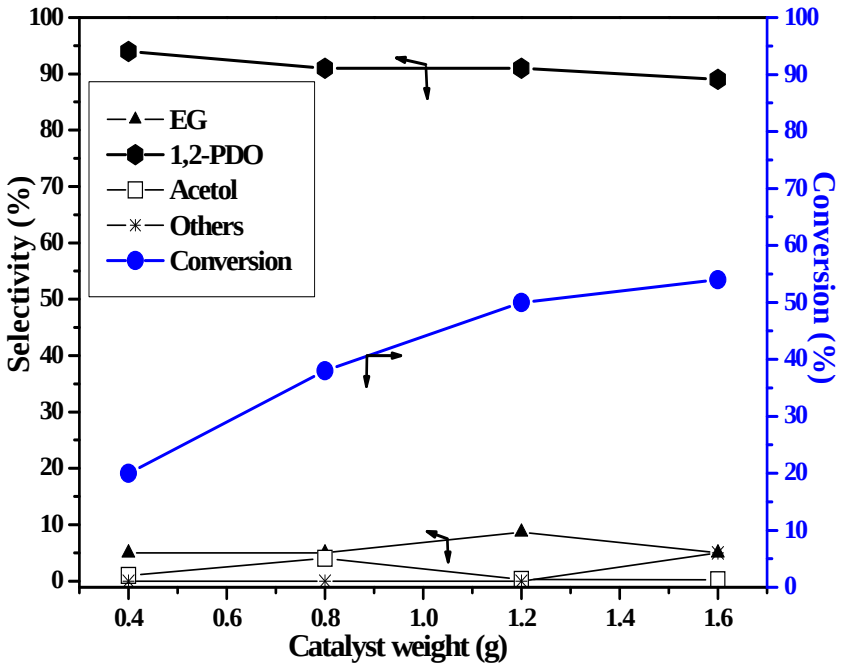

Figure 4.4. Effect of catalyst loading.

Reaction conditions: 20 wt% aq. glycerol (100 mL); H_2 pressure,70 bar; temperature, 220 ^{o}C; reaction time, 5 h.

4.3.2.3. Effect of glycerol concentration

In order to achieve maximum productivity of 1, 2-PDO, the effect of aqueous glycerol concentration on the conversion was also studied. **Figure 4.5** shows that conversion of glycerol increased from 38 to 45% with increase in glycerol concentration upto 60 wt% beyond which it decreased drastically to 23%. This is because the limiting number of catalyst active sites was available since the catalyst concentration was constant. Substrate inhibited kinetics at higher glycerol concentration could be another explanation for the decrease in conversion beyond 60% glycerol concentration. Similar observation was reported in case of butynediol hydrogenation also.[31] There was no significant effect of glycerol concentration on the selectivity pattern. For the highest glycerol loading of 60%, Cu-Al nano catalyst showed several fold (>10) higher activity (TOF, 10.2 h^{-1}) than the bulk copper catalysts. [17,20]

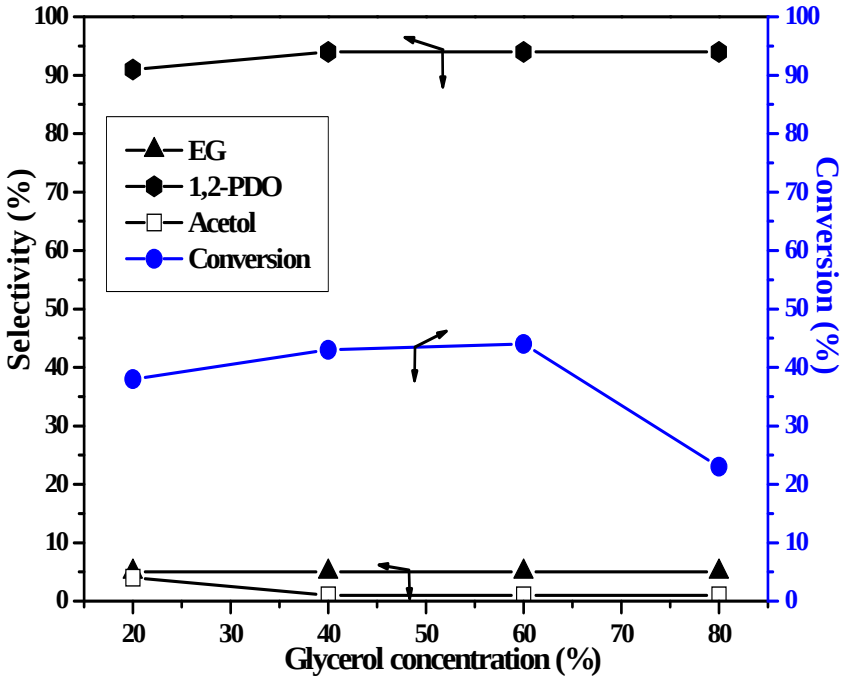

Figure 4.5. Effect of glycerol concentration.

Reaction conditions: H_2 pressure, 70 bar; catalyst, 0.8 g; temperature, 220 ^oC; reaction time, 5 h.

4.3.2.4. Effect of hydrogen pressure

The results of effect of H_2 pressure on glycerol hydrogenolysis studied at a constant temperature of 220 ^oC are shown in **Figure 4.6**. Glycerol conversion increased from 23 to 38% as the hydrogen pressure increased from 35 to 70 bar. The increase in conversion was due to the higher availability of hydrogen at the catalyst surface at higher H_2 pressure. It is interesting to note that the selectivity to 1,2-PDO and acetol was not affected with change in H_2 pressure.

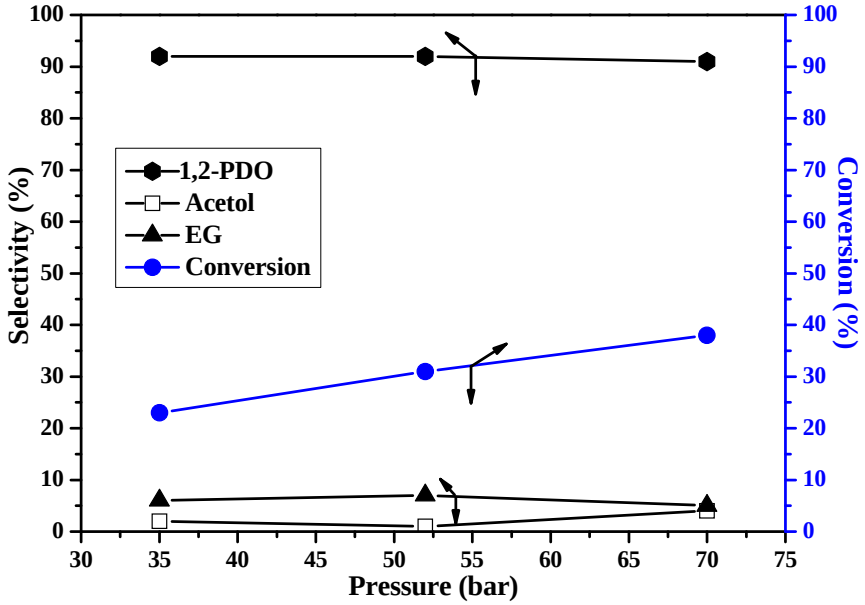

Figure 4.6. Effect of hydrogen pressure.

Reaction conditions: 20 wt% glycerol aqueous (100 mL); catalyst, 0.8 g; temperature, 220 ^oC, reaction time, 5 h.

4.3.2.5. Catalyst recycle study

In order to establish the reusability of catalyst for glycerol hydrogenolysis reaction, the catalyst was filtered after the first reaction and washed with a solvent. Then it was dried in oven at 110 ^oC and regenerated under hydrogen and used for the subsequent hydrogenolysis of glycerol. This procedure was followed for two subsequent hydrogenolysis reactions and the results are shown in **Figure 4.7.** Our Cu-nano catalyst

showed significant activity even after the second recycle in terms of TOF. The turn over frequency of Cu- nano catalyst decreased from 2.96 to 2.27 h^{-1} which could be mainly due to the handling losses of the catalyst as well as metal sintering under reaction conditions of high temperature (220 ^{o}C) for long time duration (5 h).

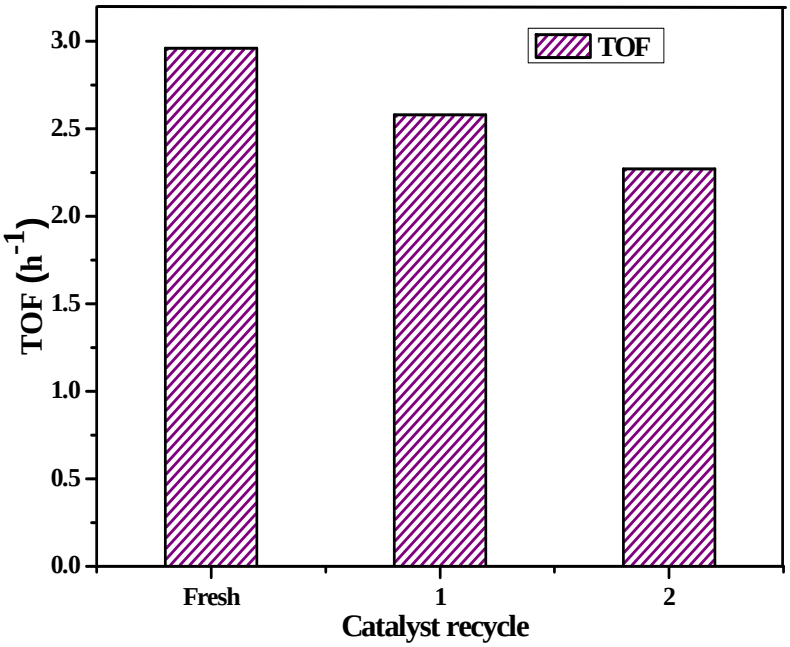

Figure 4.7. Catalyst recycle study.

Reaction conditions: 20 wt% aq. glycerol (100 mL); H_2 pressure, 70 bar; catalyst, 0.8 g; temperature, 220 ^{o}C; reaction time, 5 h.

4.3.3. Activity comparison with other catalysts

In order to demonstrate the unique efficiency of our Cu-Al catalyst, its hydrogenolysis activity was compared with various other copper catalysts with chromium. The Cu-Al composition was also optimized by varying Cu-Al ratios. The results of activity comparison of all these catalysts in water as well as in 2-propanol are shown in **Tables 4.4 and 4.5** respectively and the results are discussed below.

4.3.3.1. Catalyst screening in water

As can be seen from **Table 4.4,** among various Cu-Cr catalysts screened for glycerol hydrogenolysis in water, only Cu-Cr with Ba as a promoter (**NMT005, Table 4.4**) showed glycerol conversion of 20% with 56% selectivity to 1,2-PDO and 44% selectivity to acetol. Other Cu-Cr catalysts with and without promoters (NMT006-NMT011, **Tables 4.2 and 4.4**) showed very poor hydrogenolysis activity (6-10% conversion, **Tables 4.2 and 4.4**) in water. In case of all Cu-Cr catalysts, 1, 2-PDO selectivity obtained was in the range of 54-65% , and the balance was acetol without any other byproducts.

Table 4.4. Catalyst screening for hydrogenolysis of glycerol to 1,2-PDO in aqueous medium

Catalyst	Composition	Conversion (%)	Selectivity (%)			
			1,2-PDO	Acetol	EG	Others
Cu-Al-5	50:50	38	91	4	5	0
Cu-Al-7	70:30	45	60	1	2	37
Cu-Al-3	30:70	51	85	6	3	5
NMT005	Cu, Cr, Ba	20	56	44	0	0
NMT008	Cu, Cr , Al, Ba	8	65	35	0	0
NMT011	Cu, Cr, Zn	10	54	46	0	0

Reaction conditions: Catalyst wt, 0.8 g; temperature, 220 ^{o}C; pressure, 69 bar; 20 wt% glycerol; reaction time, 5 h.

On the other hand, Cu-Al with varying compositions showed much higher hydrogenolysis activity than any other Cu-Cr catalyst in water in the following order: Cu-Al-3> Cu-Al-7> Cu-Al-5 (**entries 1-3, Table 4.4**). The lowest 1,2-PDO selectivity of 60% observed for Cu-Al-7 catalyst was due to formation of other byproducts to the extent of 37% which could be due to higher content of Cu, whereas the highest 1,2-PDO

selectivity achieved was 91% with 38% glycerol conversion for a catalyst having equimolar composition of Cu and Al (Cu-Al-5) with acetol and EG as the only byproducts. The reason for the best performance of Cu-Al-5 catalyst is due to the presence of both surface acidity and metal sites as discussed above. Conversion, selectivity *vs* time profile (**Figure 4.8)** shows that with increase in reaction time, 1,2-PDO selectivity increased from 75 to 91% within the first hour of reaction at the cost of acetol confirming glycerol hydrogenolysis proceeds through the acetol intermediate. Although lower content of Cu (30 mol%) in Cu-Al-3 catalyst showed the highest glycerol conversion, 1,2-PDO selectivity obtained was less than that for Cu-Al-5 (**Table 4.4)**. Hence, Cu-Al-5 catalyst was chosen as the best catalyst for further studies on glycerol hydrogenolysis.

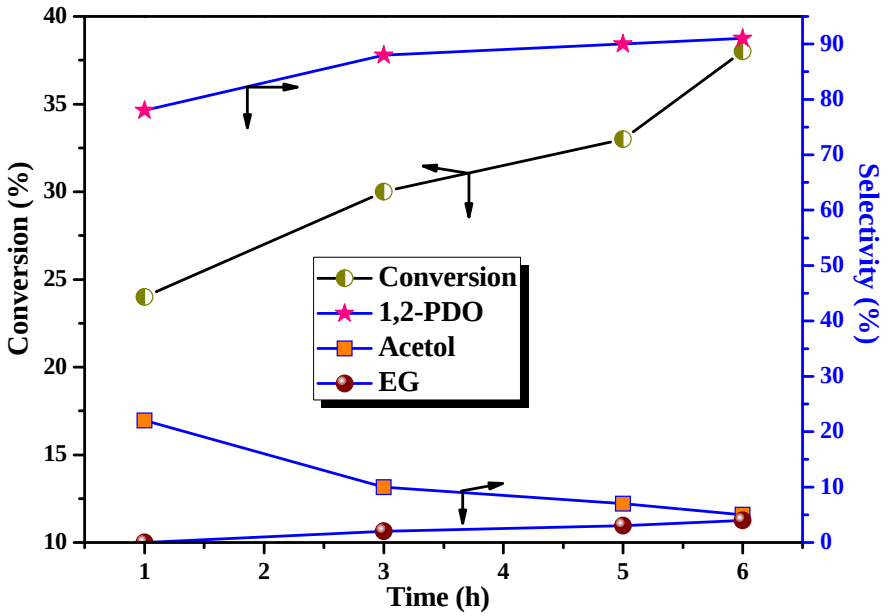

Figure 4.8. Conversion and selectivity *vs* time profile of aqueous glycerol hydrogenolysis in a batch reactor.

Reaction conditions: Catalyst wt, 0.8 g; temperature, 220 ^{o}C; pressure, 69 bar; 20 wt% aqueous glycerol.

4.3.3.2. Catalyst screening in 2-propanol

As can be seen from **Table 4.5**, the catalyst activity for glycerol hydrogenolysis in 2-propanol solvent showed a trend of Cu-Al-7 > Cu-Al-5> Cu-Al-3; however, in all cases higher conversions were observed. As high as 69% glycerol conversion was achieved over Cu-Al-7 catalyst having a maximum Cu content of 70 mole %. The selectivity to 1,2-PDO was in the range of 88-90% with slight variation due to either more accumulation of acetol or due to higher formation of byproducts, depending on the Cu content of the catalysts. Cu-Cr catalysts showed much higher hydrogenolysis activities in 2-propanol than those shown in water (**Table 4.4**); nevertheless, activities were lower than those of Cu-Al catalysts, the obvious reason being the higher hydrogen solubility in 2-propanol than that in water. Among the Cu-Cr catalysts, Ba containing catalyst (NMT005) showed the highest activity (34% conversion) and 1,2-PDO selectivity (84%). NMT008 catalyst having Al in combination with Ba gave the highest EG selectivity while, NMT011 containing Zn gave highest dehydration product acetol affecting the 1,2-PDO selectivity.

Table 4.5. Catalyst screening for hydrogenolysis of glycerol to 1,2-PDO in 2-propanol

Catalyst	Composition	Conversion (%)	Selectivity (%)			
			1,2-PDO	Acetol	EG	Others
Cu-Al-5	50:50	47	88	7	5	0
Cu-Al-7	70:30	69	90	4	4	2
Cu-Al-3	30:70	42	91	4	2	2
NMT005	Cu, Cr, Ba	34	84	3	5	8
NMT008	Cu, Cr , Al, Ba	26	71	17	10	2
NMT011	Cu, Cr, Zn	29	77	19	1	3

Reaction conditions: Catalyst wt, 0.8 g; temperature, 220 ^{o}C; pressure, 69 bar, 20 wt % aqueous glycerol, reaction time, 5 h.

4.3.4. Continuous glycerol hydrogenolysis over Cu-Al-5 catalyst

As water is supposed to be a green solvent and Cu-Al-5 catalyst showed an optimum performance (**Table 4.4**), further studies on product distribution, TOS activity and studies on effect of process parameters in a continuous operation for both glycerol hydrogenolysis and dehydration were carried out using this catalyst the specifications of which, are given in **Table 4.6.** The effects of temperature, H_2 pressure, liquid and gas flow rates and glycerol concentration on the conversion of glycerol and the product selectivities were also investigated. The range of reaction conditions used for this study are given in **Table 4.7.**

Table 4.6. Specifications of Cu-Al-5 catalyst

Catalyst	Cu-Al-5
Form	Pellets
Size (m)	0.005 X 0.002
Surface area ($m^2 g^{-1}$)	31.37/56.63
Bulk density (g mL^{-1})	1.05
Cu-Al composition	50:50

The product distribution over a longer period of reaction was necessary in order to ascertain if the catalyst activity was constant in an acceptable range as well as any byproducts get accumulated which could be undesirable from continuous process point of view. As can be seen from **Figure 4.9,** the initial glycerol conversion decreased from 85% to 65% after the first 30 h beyond which it remained constant at that value. The initial 1,2-PDO selectivity obtained was 92% which remained almost constant over the period of time as shown in **Figure 4.9.** Acetol selectivity obtained in the beginning of the continuous run was about 7% (**Figure 4.9**) as against much higher acetol selectivity of ~20% in a batch operation (**Figure 4.8**). TOS activity of this catalyst in **Figure 4.10** shows the consistent performance of 60% glycerol conversion with 1,2-PDO selectivity of 90% for 400 h at 220 ^oC and 40 bar H_2 pressure.

Table 4.7. Range of operating conditions

Parameter	Range	
	Dehydration	**Hydrogenolysis**
Initial concentration of glycerol (wt%)	10-40	20-60
Solvent	Water	Water
Temperature (^{o}C)	180-240	180-240
Pressure (bar)	20 N_2	21-62 H_2
Catalyst wt (g)	20	20
Liquid velocity, LHSV (h^{-1})	0.3-2.7	0.3-2.7
Gas velocity,GHSV (h^{-1})	500	500
Catalyst packing length (m)	0.13	0.13
Particle diameter (m)	0.005	0.005
Density of the catalyst (kg m^{-3})	1050	1050

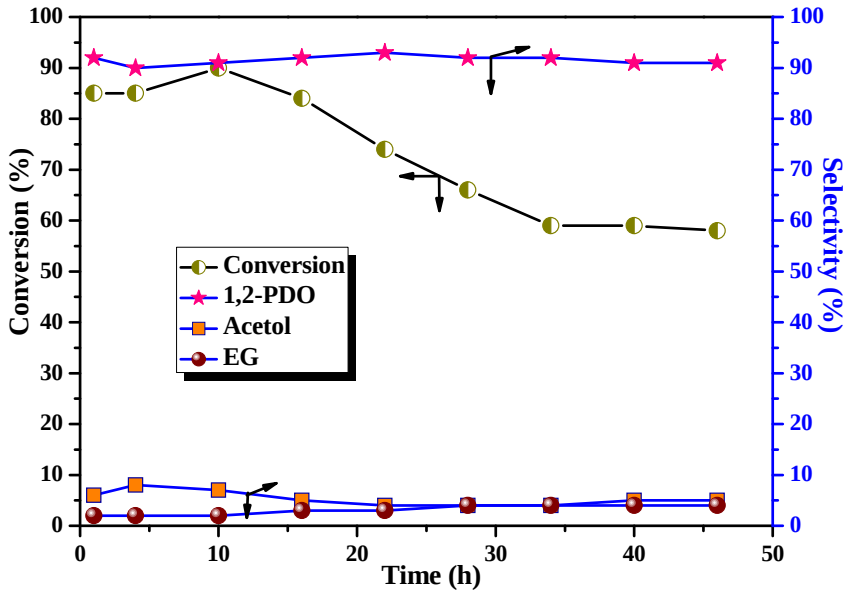

Figure 4.9. Conversion and selectivity *vs* time profile of aqueous glycerol hydrogenolysis in a continuous fixed bed reactor.

Reaction conditions: Catalyst wt, 20 g; temperature, 220 ^{o}C; pressure, 40 bar; 20 wt% aqueous glycerol; GHSV, 500 h^{-1}; LHSV , 1.5 h^{-1}.

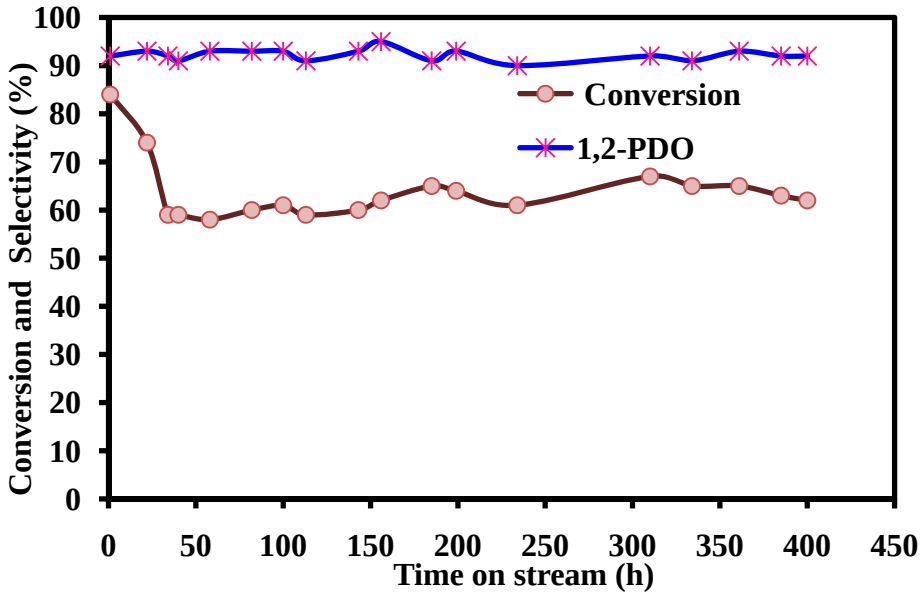

Figure 4.10. Time on stream activity of Cu-Al-5 catalysts for continuous hydrogenolysis of aqueous glycerol.

Reaction conditions: Catalyst wt, 20 g; temperature, 220 ^{o}C; pressure, 40 bar; 20 wt% aqueous glycerol; GHSV, 500 h^{-1}; LHSV, 1.5 h^{-1}.

Further studies on effect of process parameters on glycerol conversion and 1,2-PDO selectivity are discussed below.

4.3.4.1. Effect of H_2 pressure

Figure 4.11 shows the effect of H_2 pressure in the range of 20-62 bar at a constant temperature of 220 ^{o}C on global rate of reaction. Initially, as the pressure increased (upto 42 bar) the rate of reaction also increased linearly to a maximum value and decreased sharply with further increase in H_2 pressure upto 62 bar. The initial increase in the rate of reaction upto 42 bar pressure indicates a first order kinetics with respect to hydrogen. The enhancement of activity with higher H_2 pressure could be also due to *in situ* activation of the catalyst. Beyond 42 bar pressure, competitive hydrogen adsorption seems to be predominant hence a sharp decline in hydrogenation rate was observed. Glycerol conversion and selectivity dependence on H_2 pressure (**Figure 4.12**) shows that initially

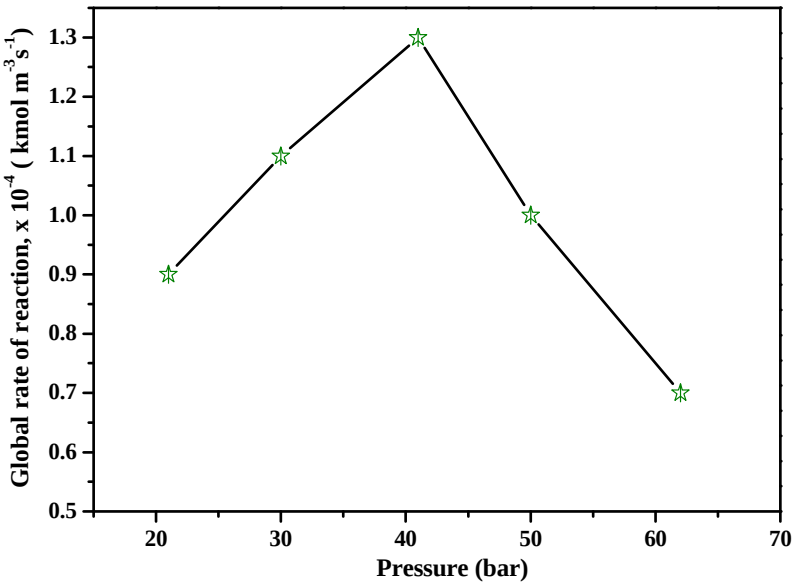

Figure 4.11. Effect of H_2 pressure on global rate of aqeous glycerol hydrogenolysis.

Reaction conditions: Catalyst wt, 20 g; temperature, 220 ^{o}C; 20 wt% aqueous glycerol, GHSV, 500 h^{-1}; LHSV, 1.5 h^{-1}.

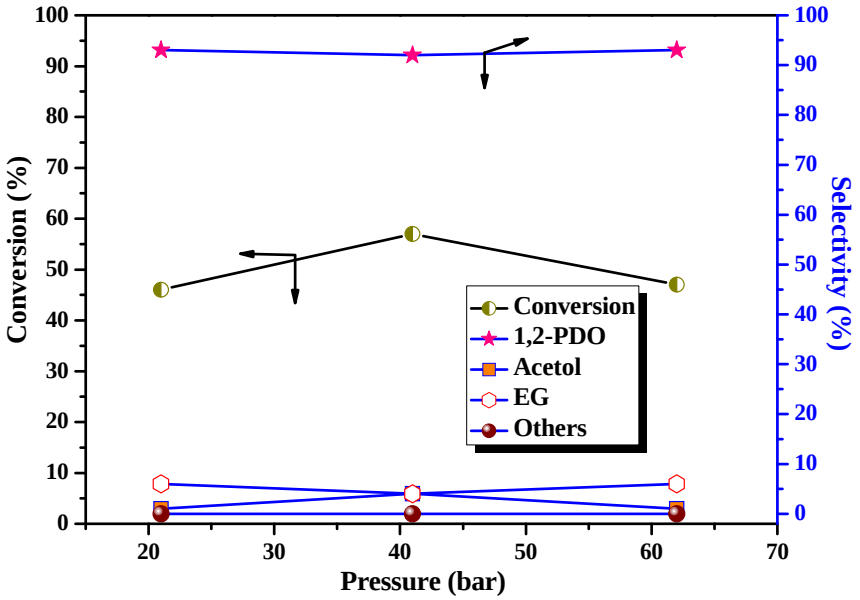

Figure 4.12. Effect of H_2 pressure on conversion and product selectivity in aqueous glycerol hydrogenolysis.

Reaction conditions: Catalyst wt, 20 g; temperature, 220 ^{o}C; 20 wt% aqueous glycerol, GHSV, 500 h^{-1}; LHSV, 1.5 h^{-1}.

the conversion increased from 44 to 57% with increase in H_2 pressure from 20 to 40 bar while it decreased to again 44% with further increase in H_2 pressure upto 62 bar. Selectivity to 1,2-PDO remained constant at 92% irrespective of H_2 pressure as EG formation is strongly catalyst dependant rather than kinetic dependant. Acetol and EG were the only major byproducts over the range of H_2 pressure studied in this work.

4.3.4.2. Effect of liquid flow rate

The effect of liquid flow rate on rate of glycerol hydrogenolysis and product selectivity was studied in the range of 18-54 mL h^{-1} keeping other reaction parameters constant. **Figure 4.13** shows that increase in flow rate from 18 to 30 mL h^{-1} increased the rate of hydrogenolysis linearly from 0.74 to 1.3 X 10^{-4} kmol $m^{-3}s^{-1}$. While, further increase in liquid flow rate from 32 to 54 mL h^{-1} decreased the rate of hydrogenolysis. In the lower range of liquid flow rate (18-30 mL h^{-1}), catalyst particles were partially wetted resulting into a direct contact of gas phase reactant and catalyst surface (already wetted internally due to capillary forces) which increased the reaction rate. With increase in the liquid flow rate beyond a certain value (>30 mL h^{-1}, in this case) causes complete wetting of the catalyst particle hence expected to retard the reaction rate due to enhanced liquid-solid resistance.[32,33] 1,2-PDO selectivity was found to remain constant at 91% irrespective of the liquid flow rate. The effect of liquid flow rate in terms of contact time (W/F, h) on glycerol conversion was also studied and the results are shown in **Figure 4.14.** It was found that conversion increased from 27 to 60% with increase in contact time from 0.35 to 0.6 h beyond which it remained constant upto contact time of 1.07 h. On comparison of **Figures 4.13 and 4.14**, highest productivity of 1,2-PDO can be achieved at the optimum liquid flow rate of 30 mL h^{-1}.

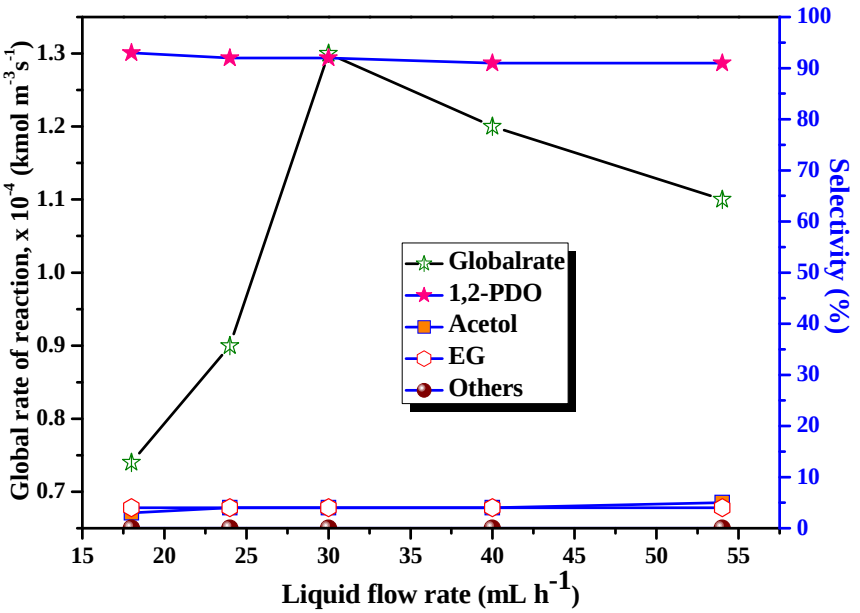

Figure 4.13. Effect of liquid flow rate on global rate and product selectivity in glycerol hydrogenolysis.

Reaction conditions: Catalyst wt, 20 g; temperature, 220 ^{o}C; pressure, 40 bar; 20 wt% aqueous glycerol; GHSV, 500 h^{-1}.

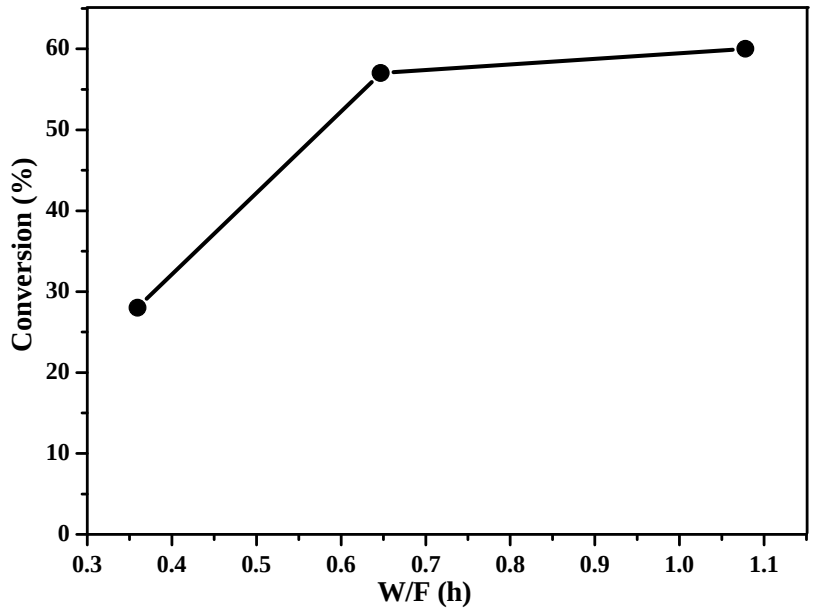

Figure 4.14. Effect of contact time, W/F on glycerol conversion.

Reaction conditions: Catalyst wt, 20 g; temperature, 220 ^{o}C; pressure, 40 bar; 20 wt% aqueous glycerol; GHSV, 500 h^{-1}.

4.3.4.3. Effect of glycerol loading

Figure 4.15 shows the dependence of rate of glycerol hydrogenolysis on glycerol loading in the range of 20-60 wt%, at 220 ^{o}C and 40 bar H_2 pressure. Similar to the trend observed for the effect of hydrogen pressure, the rate of hydrogenolysis increased steeply by three folds with increase in glycerol loading from 20-40 wt% while, it decreased dramatically for glycerol loading > 40 wt%. This indicates that the substrate gets strongly adsorbed at higher concentration on the active sites and needs to be considered for design purposes. In order to achieve the maximum productivity, effect of glycerol loading on conversion and product selectivity was also studied in the range of 20-60 wt%, the results of which are shown in **Figure 4.16.** Glycerol conversion increased from 53 to 67% with increase in glycerol loading upto 40 wt%, beyond which it decreased substantially (30%) while, no appreciable change in product selectivities was observed.

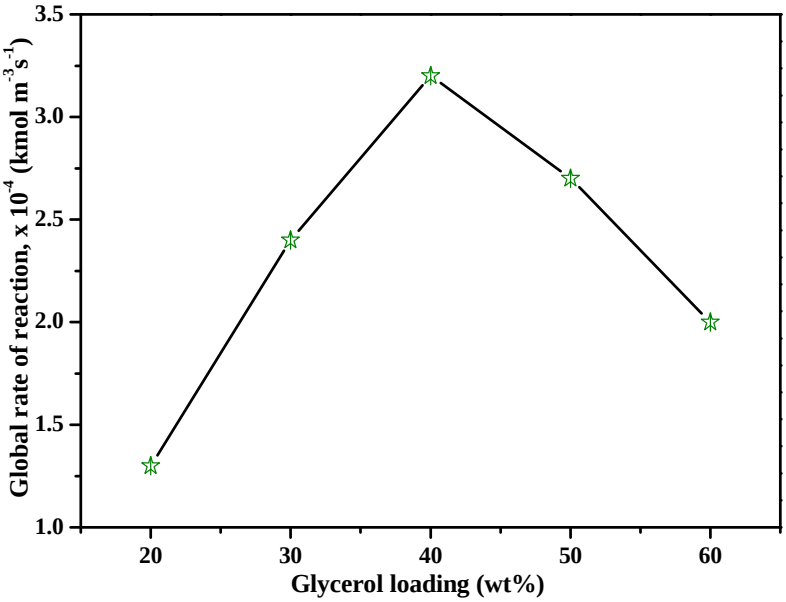

Figure 4.15. Effect of glycerol loading on global rate of aqueous glycerol hydrogenolysis.

Reaction conditions : Catalyst wt, 20 g; temperature, 220 ^{o}C; pressure, 40 bar; GHSV, 500 h^{-1}; LHSV, 1.5 h^{-1}.

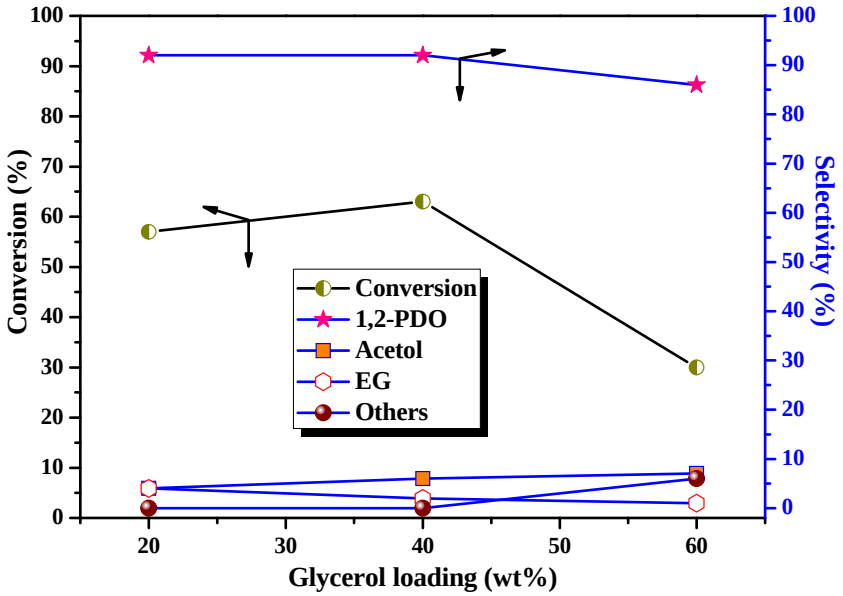

Figure 4.16. Effect of glycerol loading on conversion and product selectivity in aqueous glycerol hydrogenolysis.

Reaction conditions : Catalyst wt, 20 g; temperature, 220 ^{o}C; pressure, 40 bar; GHSV, 500 h^{-1}; LHSV, 1.5 h^{-1}.

4.3.4.4. Effect of temperature

Figure 4.17 shows the effect of temperature on glycerol conversion and product selectivity respectively. Significant increase in glycerol conversion from 20 to 84% was observed with increase in temperature from 180 to 240 ^{o}C. Although 1,2-PDO slectivity remained constant (~93%) for increase in glycerol conversion with increase in temperature upto 220 ^{o}C **(Figure 4.17)**, it drastically decreased from 94 to 78% with further increase in temperature to 240 ^{o}C. This decrease in 1,2-PDO selectivity at highest temperature was due to increased acetol (4-10%), and other byproducts (0-11%). Other byproducts include acetaldehyde, formaldehyde and 2-propanol formed from acetol and 1,2-PDO due to C-C cleavage and excess hydrogenation respectively. Increase in acetol selectivity at higher temperature indicates glycerol dehydration is more favorable than acetol hydrogenation which is also in accordnce with the thermodynamic feasibility

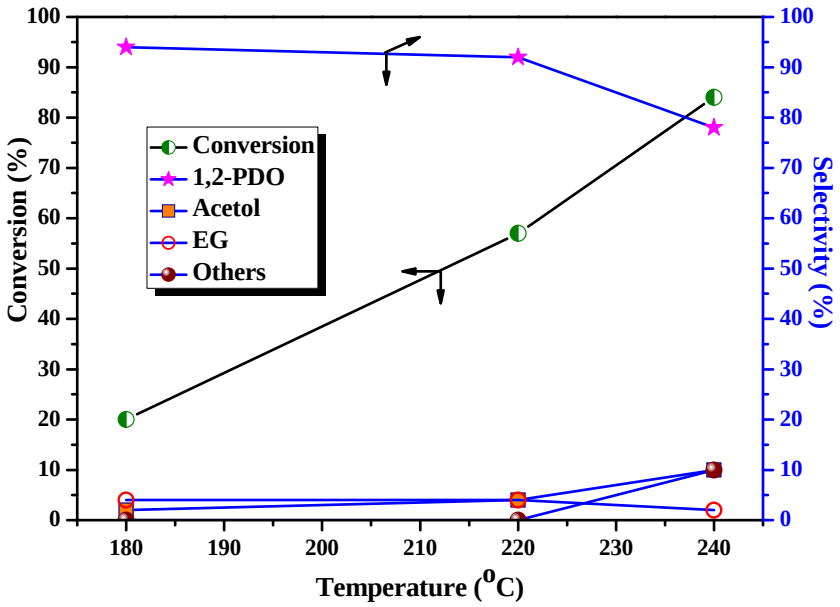

Figure 4.17. Effect of temperature on conversion and product selectivity in aqueous glycerol hydrogenolysis.

Reaction conditions : Catalyst wt, 20 g; pressure, 40 bar; 20 wt% aqueous glycerol; GHSV, 500 h^{-1}; LHSV, 1.5 h^{-1}.

criteria.[34] The optimum temperature was found to be 220 ^{o}C as the highest selectivity of 92% was achieved for 1,2-PDO with minium formation of acetol, EG and others at that temperature. The activation energy evaluated from the Arrhenius plot (**Figure 4.18**) was found to be 80 kJ mol^{-1} K^{-1} indicating that the glycerol hydrogenolysis reaction over the present catalyst is kinetically controlled. It is also to be noted that for the same catalyst, activation energy for dehydration of glycerol (38 kJ mol^{-1} K^{-1}) was much less than that observed for the hydrogenolysis of glycerol, indicating that glycerol dehydration is much faster than the hydrogenolysis reaction.

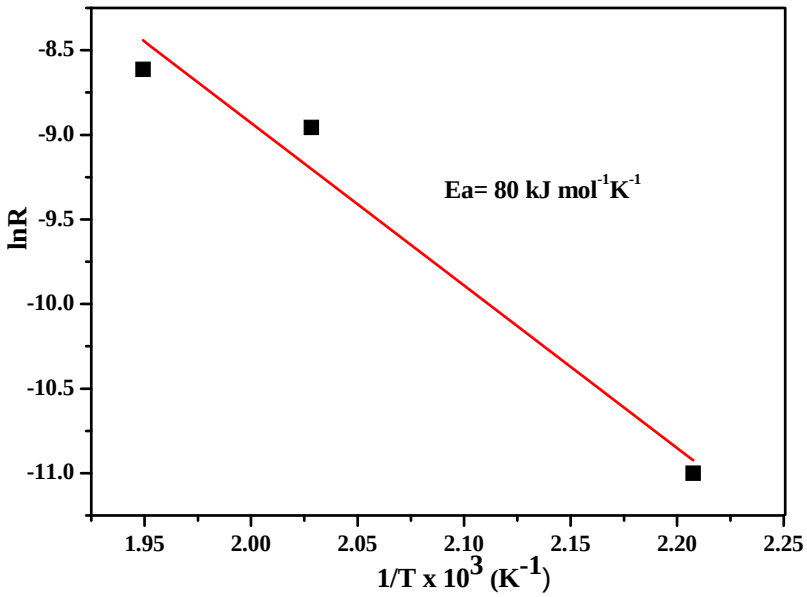

Figure 4.18. Plot of lnR *vs* 1/T for aqueous glycerol hydrogenolysis.

Reaction conditions: Catalyst wt, 20 g; pressure, 40 bar; 20 wt% aqueous glycerol; GHSV, 500 h^{-1}; LHSV, 1.5 h^{-1}.

4.3.5. Glycerol dehydration

Since, the first step of glycerol hydrogenolysis involves dehydration to acetol, which is also a commercially important product (section 4.1) it was thought appropriate to study the liquid phase glycerol dehydration separately over those catalysts used for glycerol hydrogenolysis in this work. As shown in **Scheme 4.1** (**Pathway C**) glycerol dehydration under gas phase conditions usually carried out under severe temperature and acidic conditions give acrolein as the major product compared to acetol formation under liquid phase dehydration conditions.[35] While gas phase glycerol dehydration has been extensively studied, very few reports are available on liquid-phase dehydration of glycerol to acetol. It is interesting to note that dehydration of glycerol takes place efficiently even in water; hence, the performance of the same catalyst was studied in both water and 2-propanol and the results are discussed below. All the dehydration experiments were carried out under N_2 atmosphere.

4.3.5.1. Catalyst screening in water

As shown in **Table 4.8**, Cu-Cr catalysts with and without promoters showed a low activity (3-8% conversion) with complete selectivity to acetol for glycerol dehydration in water, while in case of Cu-Al catalysts, activity and acetol selectivity were influenced by the Cu:Al composition. For Cu-Al composition of 30:70, highest conversion of 26% was obtained however, for both lowest as well as highest Cu contents, formation of other byproducts was observed. Since no byproduct formation was observed in case of Cu-Al ratio = 50:50, this was chosen for further studies on glycerol dehydration. The better performance of Cu-Al-5 catalyst for the glycerol dehydration to acetol was mainly due to its highest surface acidity determined by NH_3-TPD (0.1873 mmol g^{-1}) as compared to Cu-Al-7 and Cu-Al-3 catalysts having acidity of 0.0533 mmol g^{-1} and 0.177 mmol g^{-1}, respectively. Nevertheless, formation of minor 1,2-PDO over Cu-Al catalysts in water medium could be due to *in situ* hydrogenation reaction.

Table 4.8. Catalyst screening for dehydration of glycerol to acetol in water under ambient conditions.

Catalyst	Composition	Conversion (%)	Selectivity (%)		
			Acetol	1,2-PDO	Others
Cu-Al-5	50:50	17	93	7	0
Cu-Al-7	70:30	23	89	4	7
Cu-Al-3	30:70	26	92	2	6
NMT005	Cu, Cr, Ba	3	100	0	0
NMT006	Cu, Cr	<5	100	0	0
NMT008	Cu, Cr , Al, Ba	8	100	0	0
NMT011	Cu, Cr, Zn	5	100	0	0

Reaction conditions: Catalysts wt, 0.8 g; temperature, 220 ^oC; pressure, N_2 ambient; 20 wt % glycerol, reaction time, 3 h.

4.3.5.2. Catalyst screening in 2-propanol

Dehydration reaction involves the formation of water hence, it is important to assess the role of water itself in dehydration of glycerol. For this purpose, the catalysts screened for aqueous glycerol dehydration were also further evaluated under similar conditions in 2-propanol solvent and the results are shown in **Table 4.9.** It was very interesting to note that several fold increase in glycerol conversion was observed for both Cu-Cr as well as Cu-Al catalysts in 2-propanol solvent. Similar to dehydration in water, Cu-Al catalysts showed higher activity than that of Cu-Cr catalysts however, with increasing Cu content from 30 to 70% (mole basis) glycerol conversion increased from 46-86%. For highest Cu content of 70 mole %, acetol selectivity was as low as 18% due to formation of by-products up to 70% comprising mainly glycerol/ acetol alkylation products. While in case of Cu-Cr catalysts with and without promoter glycerol conversion remained constant in the range of 34-38% however, acetol selectivity achieved was as high as 90%. The lower selectivity to acetol over Cu-Al catalyst was due to formation of 1,2-PDO (10-38%) as a result of transfer hydrogenation of acetol in 2-propanol solvent.[36] It is clear from the

Table 4.9. Catalyst screening for dehydration of glycerol to acetol in 2-propanol under ambient conditions.

Catalyst	Composition	Conversion (%)	Selectivity (%)			
			Acetol	1,2-PDO	EG	Others
Cu-Al-5	50:50	70	54	38	8	0
Cu-Al-7	70:30	86	18	10	2	70
Cu-Al-3	30:70	46	50	29	3	17
NMT006	Cu, Cr	37	86	14	0	0
NMT008	Cu, Cr , Al, Ba	34	90	8	2	0
NMT011	Cu, Cr, Zn	38	55	7	0	38

Reaction conditions: Catalysts wt,0.8 g; temperature,220 ^{o}C; pressure, N_2 ambient; 20 wt% glycerol, reaction time, 3 h.

above results that Cu-Al catalyst system in water gave a very clean product distribution (acetol selectivity > 90%). This was also confirmed by conducting the dehydration experiment over Cu-Al-5 in water for a longer period of 12 h (**Figure 4.19**), which also showed a consistent acetol selectivity of ~95% with marginal increase in glycerol conversion of 17 to 20%. Hence, further studies on glycerol dehydration were carried out over Cu-Al-5catalyst in water medium.

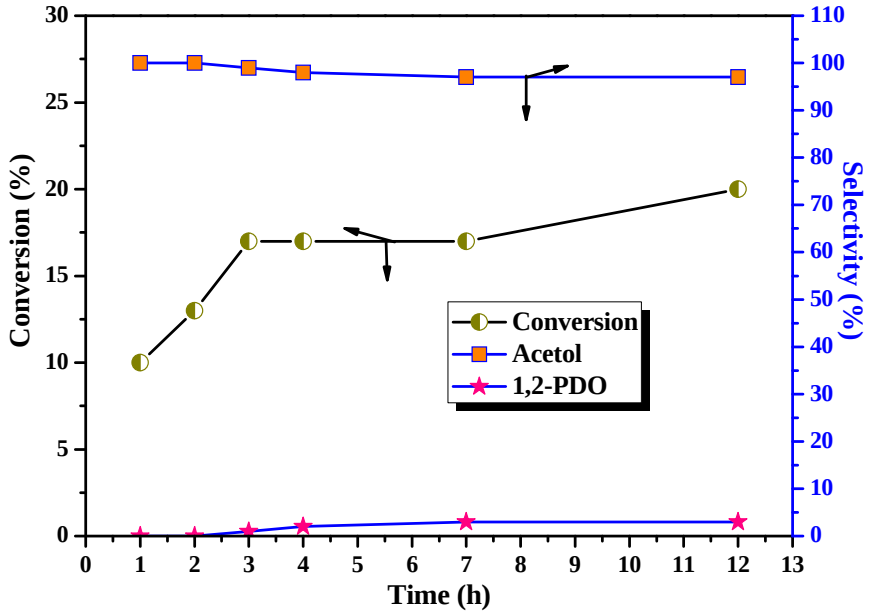

Figure 4.19. Conversion and selectivity *vs* time profile of aqueous glycerol dehydration in a batch reactor.

Reaction conditions: Catalyst wt, 0.8 g, temperature, 220 ^{o}C; pressure, N_2 ambient; 20 wt% aqueous glycerol, 12 h.

4.3.6. Continuous glycerol dehydration over Cu-Al-5 catalyst

TOS activity of our Cu-Al-5 catalyst was also evaluated for continuous glycerol dehydration. **Figure 4.20** shows a consistent performance of Cu- Al-5 catalyst for 400 h in water at 220 ^{o}C under N_2 pressure of 20 bar with an average glycerol conversion of 92% and acetol selectivity in the range of 45-55%. However, unlike the product

distribution in a batch operation **(Figure 4.19)** acetol selectivity was restricted to 54% in a continuous operation as shown in **Figure 4.20.**

As can be seen from the conversion, selectivity *vs.* time profile **(Figure 4.21)**, the major byproduct formed was 1,2-PDO to the extent of 30% while, others included propionic acid, acetic acid, acetaldehyde, propionaldehyde and 2-propanol formed upto 15%. The substantial formation of 1,2-PDO was due to *in situ* hydrogenation of acetol as the hydrogen availability was possible due to aqueous phase reforming (APR) of

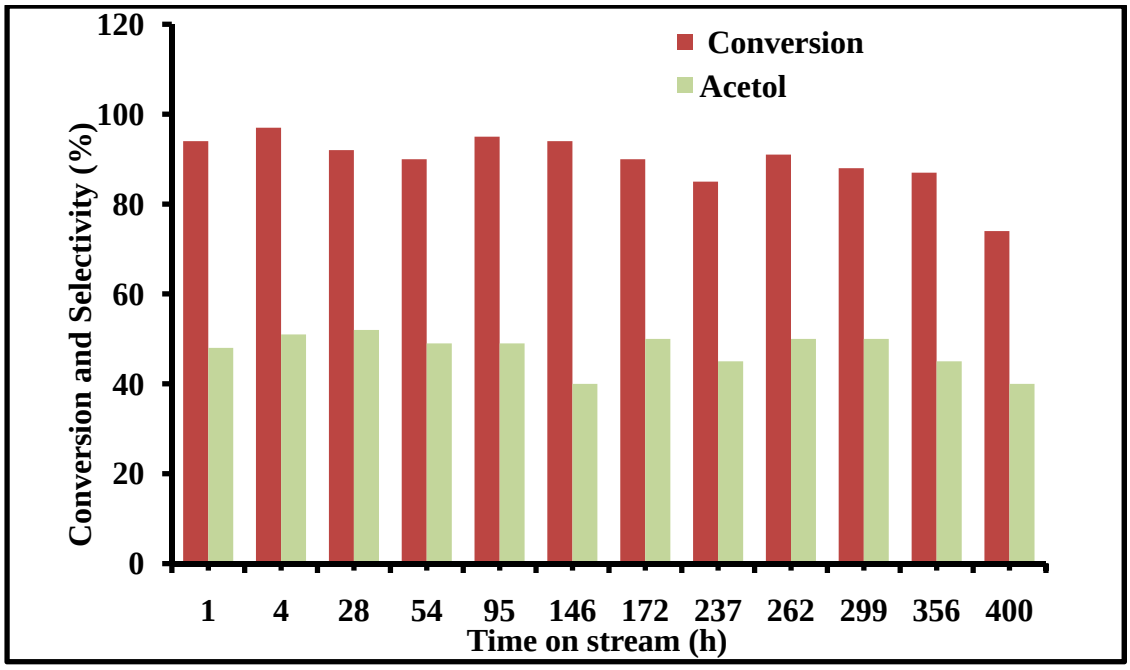

Figure 4.20. Time on stream activity of Cu-Al-5 catalysts for dehydration of aqueous glycerol under inert atmosphere.

Reaction conditions: Catalyst wt, 20 g; temperature, 220 ^{o}C; pressure, 20 bar; 20 wt% aqueous glycerol, GHSV, 500 h^{-1}; LHSV, 1.53 h^{-1}; 400 h.

glycerol. [37]The formation of 1,2-PDO and several other byproducts can be explained by C-C cleavage, isomerization of acetol and excessive hydrogenation of 1,2-PDO as shown in **Scheme 4.2.** The effects of various reaction parameters on global rate of glycerol dehydration, conversion and selectivity pattern are discussed below. These studies were

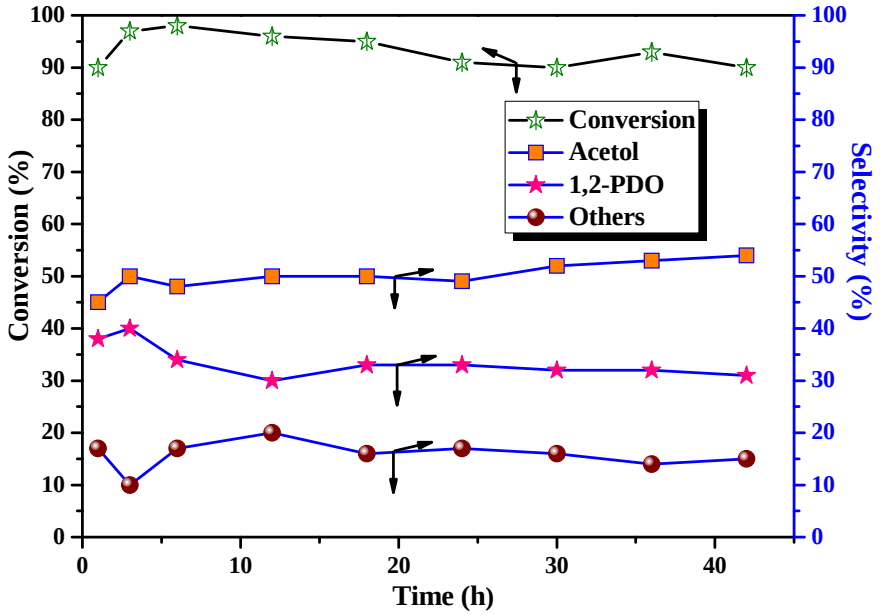

Figure 4.21. Conversion and selectivity *vs* time profile of aqueous glycerol dehydration in a continuous fixed bed reactor.

Reaction conditions: Catalyst wt, 20 g; temperature, 220 ^{o}C; pressure, 20 bar; 20 wt% aqueous glycerol, GHSV, 500 h^{-1}; LHSV, 1.53 h^{-1}; 400 h.

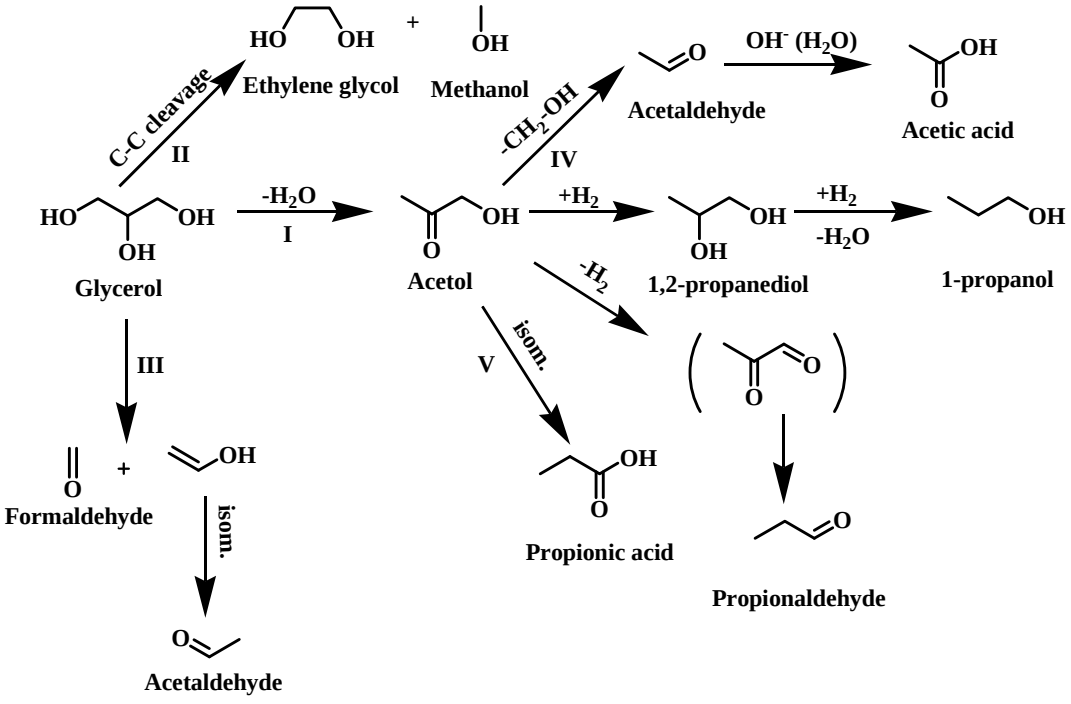

Scheme 4.2. C-O, C-C cleavage and isomerization products of glycerol over Cu-Al catalyst under dehydration conditions.

conducted in a single continuous run after establishing the TOS of the catalyst for more than 250 h. Each parameter effect was continued for 24 h under steady state conditions and a standard run was conducted after every 24 h to ensure the original activity of the catalyst.

4.3.6.1. Effect of liquid flow rate

The effect of liquid flow rate on global rate of dehydration, glycerol conversion and the product selectivities was carried out in the range of 18-54 mL h^{-1}, and the results are shown in **Figure 4.22**. Initially, the global rate of dehydration increased by about 50% with an increase in the liquid flow rate from 18 to 30 mL h^{-1}, whereas with a further increase in liquid flow rate to 54 mL h^{-1}, a marginal increase in the overall dehydration rate was observed. The increase in liquid flow rate would wet more surface area of the catalyst particle resulting into higher liquid-solid mass transfer coefficient, thus causing a

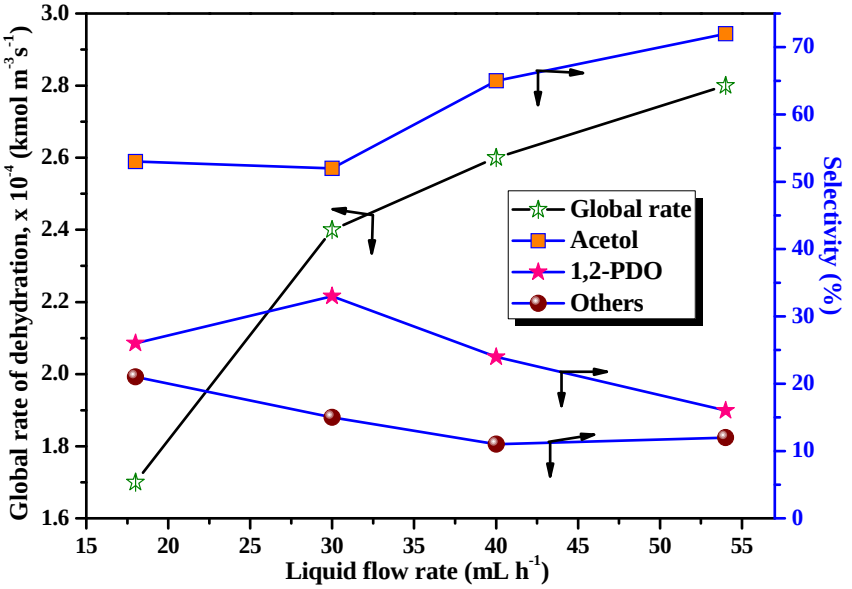

Figure 4.22. Effect of liquid flow rate on global rate of glycerol dehydration and product selectivity.

Reaction conditions: Catalyst wt, 20 g; temperature, 220 ^{o}C; pressure, 20 bar; 20 wt% aqueous glycerol;GHSV,500 h^{-1}.

higher overall rate of dehydration which is a liquid-solid reaction. More interestingly, the product distribution varied with the change in liquid flow rate as evidenced by increase in acetol selectivity from 55 to 70% with increase in flow rate by three fold (from 18 to 54 mL h^{-1}). 1,2-PDO selectivity initially increased from 22 to 30% with increase in flow rate from 18 to 30 mL h^{-1} beyond which it decreased to a minimum value of 15% at highest flow rate of 54 mL h^{-1}. With increase in liquid flow rate, contact time reduced hence, the readsorption of acetol might not take place thus retarding its further hydrogenation to 1,2-PDO. The selectivity to other byproducts also stabilized at a minimum value of 10 % for the highest flow rate of 54 mL h^{-1}. The novel feature of this study was that the optimum selectivity to both acetol (55%) and 1,2-PDO (30%) could be achieved for a flow rate of 30 mL h^{-1} of 20% aqueous glycerol.

4.3.6.2. Effect of glycerol loading

Figure 4.23 shows the dependence of the overall rate of dehydration and the selectivity behaviour of acetol, 1,2-PDO and other byproducts on glycerol loading. The overall rate of dehydration sharply increased (> 70%) with initial increase in glycerol loading from

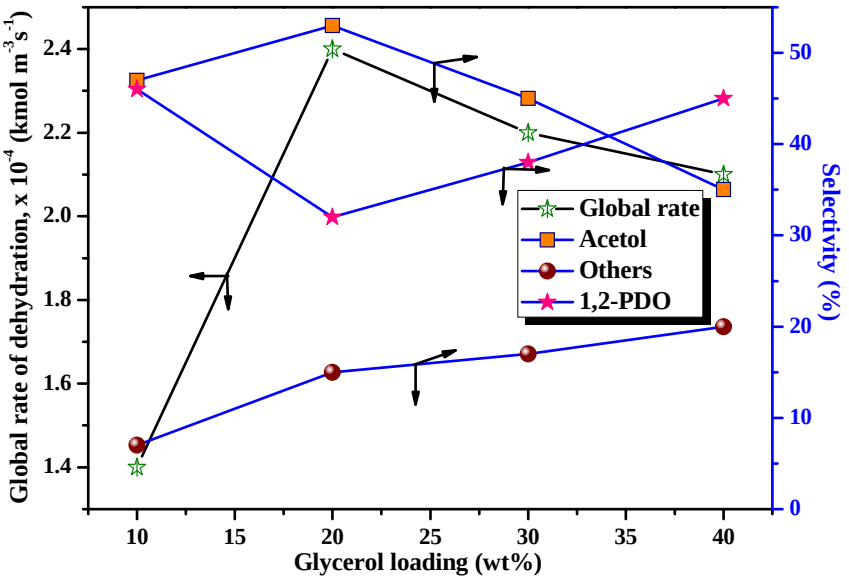

Figure 4.23. Effect of glycerol loading on global rate of aqueous glycerol dehydration and product selectivity.

Reaction consitions: Catalyst wt, 20 g; temperature, 220 ^{o}C; N_2 pressure, 20 bar; GHSV, 500 h^{-1}; LHSV, 1.53 h^{-1}.

10 to 20 wt% while, further increase in glycerol loading to 40 wt% decreased the rate of dehydration as well as acetol selectivity from 2.35 to 2.1 kmol $m^{-3}s^{-1}$ and from 55 to 35 % respectively. The initial increase in glycerol loading to 20 wt% obviously caused the higher concentration of glyecrol on the catalyst surface leading to higher dehydration rate. Similarly, acetol selectivity first increased from 45 to 55% with increasing the glycerol loading from 10 to 20 wt% and then decreased to as low as 35% at the highest glycerol loading of 40 wt%. The lowering of acetol selectivity accompanied with increase in 1,2-PDO selectivity due to higher rate of glycerol APR at higher concentration of glycerol. Increase in glycerol loading also caused an increase in the selectivity to other byproducts. Hence the optimum glycerol loading was found to be 20 wt% for which highest selectivity to acetol achieved was 55%.

4.3.6.3. Effect of temperature

The effect of temperature on both glycerol conversion and acetol selecrivity was studied in the temperature range of 140 -240 ^{o}C for Cu-Al-5 catalyst. It was found that glycerol conversion remained almost constant (32-35%) for the temperature range of 180 to 200 ^{o}C and then reached the maximum of 91% at 220 ^{o}C. Acetol selectivity remained more or less contant at 52% up to 220 ^{o}C beyond which it slightly dropped down to 40% at 240 ^{o}C due to formation of higher extent of byproducts. The activation energy was found to be 38 kJ $mole^{-1}$ K^{-1} as estimated from the Arrhenius plot (**Figure 4.24**) for dehydration of glycerol over Cu-Al-5 catalyst.

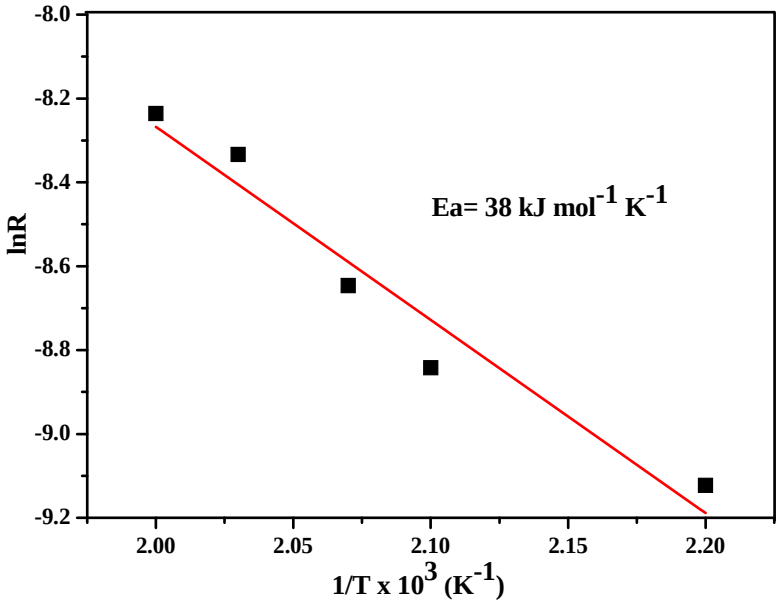

Figure 4.24. Plot of lnR vs 1/T for glycerol dehydration.

Reaction conditions: Catalyst wt, 20 g; N_2 pressure, 20 bar; 20 wt% aqueous glycerol; GHSV, 500h^{-1}; LHSV, 1.53 h^{-1}.

4.4. CONCLUSIONS

- Highest TOF of 10.3 h^{-1} was achieved with Cu- Al nano (7-11 nm) non-chromium copper catalyst for the hydrogenolysis of aqueous glycerol (60 wt % in 100 mL). Major product formed was 1, 2- propanediol (91% selectivity) while the only degradation product formed was ethylene glycol (< 5%).
- Presence of Cu_2O as evidenced by XRD, in the Cu-nano catalyst helps to inhibit the sintering of the active phase (Cu^0) under reaction conditions leading to higher activity of the Cu-nano catalyst. Ammonia TPD results indicated higher acidity (1.567 mmol g^{-1}) of the non-chromium catalyst which is responsible for the hydrogenolysis of glycerol *via* dehydration pathway without using any acid catalyst.

- Glycerol conversion increased from 29 to 76% with increase in temperature from 200 to 240 ^{o}C. Nano Cu-Al catalyst was also found to be active even after the second recycle indicating its excellent stability under reaction conditions.
- Studies on effect of process parameters on conversion-selectivity behaviour and global rates of continuous hydrogenolysis and dehydration of aqueous glycerol over a non chromium copper catalyst was carried out.
- The same catalyst also gave a TOS activity of 400 h for continuous hydrogenolysis of glycerol with an average glycerol conversion of 65% and >90% selectivity to 1,2-PDO.
- A dramatic enhancement in glycerol conversion (>4-fold) was observed with a rise in temperature from 180 to 240 ^{o}C however, 1,2-PDO selectivity dropped down to 78% at the highest temperature.
- The activation energy of 80 kJ $mol^{-1}K^{-1}$ for hydrogenolysis reaction showed that hydrogenolysis is much slower than the dehydration reaction (E = 38 kJ $mol^{-1}K^{-1}$).
- Among other parameters, negative order kinetics appeared to follow at higher H_2 pressure, while a higher feed flow rate decresed the glycrol conversion due to an enhanced liquid-solid mass transfer coefficient. Optimum glycerol loading for hydrogenolysis was found to be 40 wt% of glycerol, beyond which the conversion sharply declined from 67 to 30%.
- At an optimum glycerol loading of 20 wt% and 220 ^{o}C, acetol selectivity in a continuous dehydration process under inert atmisphere incresed from 55 to 70 % with 3- fold increse in the flow rate due to the decrease in the contact time.

4.5. REFERENCES

1. M. N. Bertero, R. C. Apesteguia, J. A. Marchi, *Appl. Catal. A* **2008,** 349,100-109.
2. F. Wang, L. J. Dubois, W. Ueda, *J. Catal.* **2009,** 268, 260-267.
3. F. Wang, J. L. Dubois, W. Ueda, *Appl. Catal. A* **2010,** 376, 25-32.
4. Z. L. Yuan, P. Wu, J. Gao, Y. X. Lu, Y. Z. Hou, M. X. Zheng, *Catal. Lett.* **2009,** 130, 261-265.
5. L. Z. Yuan, J. H. Wang, L. N.Wang, W. H. Xie, P. Chen, Z. Y. Hou, X. M. Zheng, *Bioresour. Technol.* **2010,** 101, 7088–7092.
6. Z. L. Yuan, L. N. Wang, J. H. Wang, S. X. Xia, P. Chen, Z. Y. Hou, X. M. Zheng, *Appl. Catal. B* **2011,** 101, 431-440.
7. M. C. Ramos, A. I. Navascue´s, L. Garcı´a, R. Bilbao, *Ind. Eng. Chem. Res.* **2007,** 46, 2399-2406.
8. M. Ai, K. Ohdan, *Bull. Chem Soc. Jpn.* **1999,** 72, 2143-2148.
9. J. Paradowska, M. Rogozinska, J. Mlynarski, *Tetrahedron Lett.* **2009,** 50, 1639-1641.
10. X. Wu, Z. Ma, Z Ye, S. Qian, G. Zhaob, *Adv. Synth. Catal.* **2009,** 351,158-162.
11. E. S. Vasiliadou, E. Heracleous, I. A. Vasalos, A. A. Lemonidou, *Appl. Catal. B* **2009**, 92, 90-99.
12. C. Montassier, J. C. Menezo, J. Naja, J. Barbier, J. M. Dominguez, P. Sarrazin, B. Didillon, *J. Mol. Catal.* **1994,** 91, 107-117.
13. A. Bienholz, F. Schwab, P. Claus, *Green Chem.* **2010,** 12, 290-295.
14. M. C. Tessie, US Patent 4642394, **1987.**
15. E. Drent, W. W. Jager, US Patent 6080898, **2000.**
16. G. J. Suppes, W. R. Sutterlin, WO Patent 2007053705, **2007.**
17. M. A. Dasari, P. P. Kiatsimkul, W. R. Sutterlin, G. J. Suppes, *Appl. Catal. A* **2005**, 281, 225-231.
18. C. Liang, Z. Ma, L. Ding, J. Qui, *Catal. Lett*. **2009,** 130, 169-176.

19. J. Chaminand, L. Djakovitch, P. Gallezot, P. Marion, C. Pinel, C. Rosierb, *Green Chem.* **2004,** 6, 359-361.
20. S. Wang, H. Liu, *Catal. Lett.* **2007**, 117, 62-67.
21. M. Balaraju, V. Rekha, P. S. S. Prasad, R. B. N. Prasad, N. Lingaiah, *Catal. Lett.* **2008,** 126, 119-124.
22. C. W. Chiu, A. Tekeei, W. R. Sutterlin, J. M. Ronco, G. J. Suppes. *AIChE J.* **2008,** 54, 2456-2463.
23. M. Akiyama, S. Sato, R. Takahashi, K. Inui, M. Yokota, *Appl. Catal. A* **2009,** 371, 60-66.
24. R. B. Mane, A. M. Hengne, A. A. Ghalwadkar, S. Vijayanand, P. H. Mohite, H. S. Potdar, C. V. Rode, *Catal. Lett.* **2010,** 135, 141-147.
25. R. B. Mane, C. V. Rode, *Org. Process Res. Dev.***2012,** 16, 1043-1052.
26. J. Henkelmann, M. Becker, J. Bürkle, P. Wahl, G. Theis, S. Maurer, WO Patent 2007099161 A1, **2007.**
27. J. Pike, S.-W. Chan, F. Zhang, X. Wang, J. Hanson, *Appl. Catal. A* **2006,** 303, 273-277.
28. R. B. C. Pillai, *Catal. Lett.* **1994,** 26, 365-371.
29. S. Sato, M. Akiyama, R.Takahashi, T. Hara, K. Inui, M. Yokota, *Appl. Catal. A* **2008,** 347,186-191.
30. Z. Huang, F. Cui, H. Kang, J. Chen, X. Z. Zhang, C. G. Xia, *Chem. Mater.* **2008,** 20,5090-5099.
31. M. M. Telkar, C. V. Rode, V. H. Rane, R. Jagannathan, R .V. Chaudhari, *Appl. Catal. A* **2001**, 216, 13-22.
32. M. V. Rajashekharam, R. Jagannthan, R. V. Chaudhari, *Chem. Eng. Sci*. **1998**, 53, 787-805.
33. R. V. Chaudhari, R. Jagannthan, S. P. Mathew, *AIChE J.* **2002**, 48, 110-125.
34. L. Huang, Y. L. Zhu, H. Y. Zheng, Y. W. Li, Z. Y. Zeng, *J. Chem. Technol. Biotechnol.* **2008,** 83, 1670-1675.
35. B. Katryniok, S. Paul, V. Belli`ere-Baca, P. Reye, F. Dumeignil, *Green Chem.* **2010,** 12, 2079-2098.

36. M. G. Musolino, L. A. Scarpino, F. Mauriello, R. Pietropaolo, *Green Chem.* **2009,** 11, 1511-1513.

37. R. D. Cortright, R. R. Davda, J. A. Dumesic, *Nature* **2002**, 418, 964-967.

Chapter 5

Effect of preparation parameters of Cu catalysts on their physico-chemical properties and activities for glycerol hydrogenolysis

Cu based catalysts were prepared by three methods *viz.* (i) co-precipitation, (ii) alkali fusion followed by precipitation and (iii) direct solid state fusion. The changes in the phase formation, morphology, crystallite size, extent of aggregation, strength and nature of acid sites were observed due to variations in precipitating agents and also their order of addition. The catalyst prepared by co-precipitation using Na_2CO_3 showed the predominant presence of metallic Cu phase with a crystallite size of 5 nm, well segregated spherical morphology and highest acidity in the reduced sample. These intrinsic properties contributed to achieve the highest glycerol conversion of 62% and 1,2-PDO selectivity of 88% in glycerol hydrogenolysis.

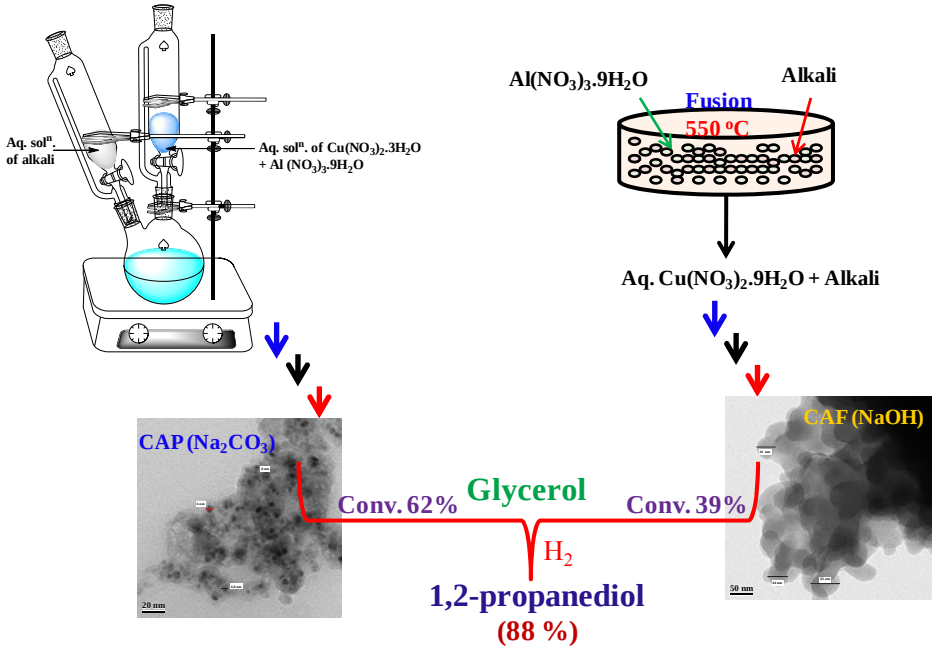

***Catal. Today* 2012, 198, 321-329**

5.1. INTRODUCTION

The cost effectiveness of the non noble Cu catalysts is an added advantage for commercialization.[1] Highly dispersed Cu prepared in several ways has been used in number of reactions *viz.* steam reforming, hydrogenation, ester hydrogenolysis, reduction of NOx, oxidation of CO and hydrocarbons.[2-4] Copper in combination with other transition metals *viz.* Al, Zn, Mg, Ag and Cr as mixed metal oxides or on various supports were reported for the glycerol hydrogenolysis to 1,2-PDO under mild reaction conditions. Bienholz *et al.* reported Cu/SiO_2 catalysts prepared by incipient wetness and ion exchange techniques and found that the stable copper catalyst with high surface area was desirable for higher glycerol conversion and 1,2-PDO selectivity.[5] 1,2-PDO selectivity (94%) was found to be similar for Cu/SiO_2 catalyst prepared by both precipitation-gel and impregnation method. However, the former method gave higher catalyst activity with 73% conversion and stability due to strong copper-support interaction, high copper dispersion and presence of NaOH that reduces the catalyst leaching.[6] Homogeneous dispersion of copper in the solid base matrix such as hydrotalcite (Cu/MgAlO) obtained by co-precipitation method also resulted in enhancement of activity (80%) and selectivity to 1,2-PDO (98.2%).[7] Copper chromite catalysts prepared by co-precipitation method also showed higher activity and selectivity as compared to impregnation method for glycerol hydrogenolysis to 1,2-PDO. [8] Along with SiO_2 and Cr_2O_3 supports, Al_2O_3 was also found to be an efficient support for Cu catalyst giving 96% glycerol conversion and 96.7% 1,2-PDO selectivity for continuous operation. [9] Copper on more acidic supports like various zeolites showed inferior performance than Al_2O_3 due to the higher acidity of zeolites forming acrolein instead of acetol intermediate. The strong CuO-support interaction was also observed preventing the oxide reduction to metallic Cu.[10] Although co-impregnation of silver with Cu/Al_2O_3 facilitated the *in situ* reduction of copper but showed the lower activity compared with parent pre-reduced Cu/Al_2O_3 catalyst.[11]

It is clear from the above discussion that the stability and activity of the active sites for glycerol hydrogenolysis not only depend on the preparation methods but also on the preparation parameters used in the same method *viz.* pH, precipitating agent, co-metal and the type of support.[12,13] As per our knowledge, there are no reports on use of various precipitating agents as well as on fusion method except the recent work on pretreated fly

ash for glycerol hydrogenolysis.[14] Such a study will evolve an optimized preparation method that can enhance the catalyst activity and selectivity to the desired product in reactions involving highly functional substrates, intermediates and products such as glycerol hydrogenolysis.

In continuation of our work on various Cu catalysts, [14-17] we discuss here (i) the effect of precipitating agents in co-precipitation method, (ii) comparison of co-precipitation and fusion methods, (iii) detailed physico-chemical characterization and (iv) the activity of the prepared catalysts for glycerol hydrogenolysis.[18] The catalysts were characterized by X-ray diffraction (XRD), N_2 adsorption-desorption, thermo gravimetric analysis (TG/DTA), X-ray photoelectron spectroscopy (XPS), high resolution transmission electron microscope (HR-TEM), temperature-programmed reduction (TPR), and NH_3 temperature-programming desorption (NH_3-TPD). The observed activity results were explained based on characterization data.

5.2. EXPERIMENTAL

Cu-Al catalysts using different precipitating agents *viz.* KOH, NaOH and Na_2CO_3 were prepared by simultaneous co-precipitation and digestion technique and the detailed experimental procedures for their preparation have been described in chapter 2 (section 2.3.3). The prepared cataysts were nominated as CAP (respective alkali formula) *e.g.* CAP (NaOH). The catalyst prepared by using K_2CO_3 as a precipitating agent and thoroughly washed with water during filtrarion till free from potassium, was designated as CAP (K_2CO_3F). Cu-Al catalyst was also prepared by direct addition of 0.05 M of each of copper and aluminium nitrates to the solution of Na_2CO_3 taken in the round bottom flask. This catalyst was designated as CAP (Na_2CO_3R). Cu-Al catalysts prepared by solid state fusion followed by precipitation using KOH and NaOH were designated as [CAF (KOH) and CAF (NaOH)], respectively while, that prepared by solid state fusion with KNO_3 was named as [CAF (KNO_3)]. The details of all the preparation procedures are described in chapter 2 (sections 2.3.4 and 2.3.5). The catalysts were characterized by various techniques which are also described in chapter 2 (section 2.4). The activity of the prepared catalysts was evaluated for glycerol hydrogenolysis to 1,2-PDO in a batch reactor as detailed in chapter 2 (section 2.5.1).

5.3. RESULTS AND DISCUSSION

5.3.1. Catalyst characterization

In both, co-precipitation and solid state alkali fusion methods of preparation of Cu-Al catalyst various bases were used with an objective to vary the physico-chemical properties of the catalysts. Hence, a detailed characterization of the prepared catalysts at different stages of calcination and reduction is discussed below.

XRD patterns of calcined catalyst samples prepared by co-precipitation and fusion methods are shown in **Figure 5. 1**. Samples prepared by co-precipitation using both Na_2CO_3 and K_2CO_3 showed almost identical amorphous nature while, use of KOH as a precipitant gave the crystalline material. The co-precipitation by Na and K-carbonates is known to give the molecular precursors such as $Cu_2(OH)_2CO_3$ having both amorphous and crystalline nature and crystalline $Cu(OH)_2$ and to a small extent of CuO. [19,28] In the present work, the amorphous nature of the calcined sample shown by XRD indicates the interdiffusion of Cu and Al during calcination at 400°C. In a reverse co-

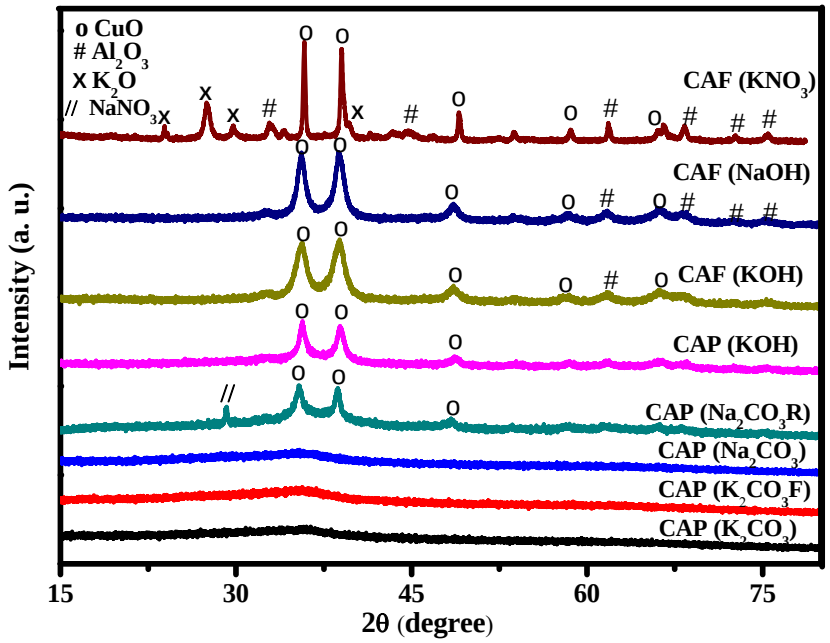

Figure 5.1. XRD patterns of calcined catalyst samples.

precipitation (*i.e.* adding both Cu and Al nitrate solutions to the solution of Na_2CO_3), crystalline nature of the sample (CAP Na_2CO_3R) was due to different nucleation conditions provided by a large volume of the precipitant as compared to that of simultaneous addition of the later. Higher crystallinity was also observed in co-precipitation carried out with KOH, due to formation of corresponding crystalline metal hydroxides which after calcination gave crystalline CuO. All the samples prepared by co-precipitation with carbonates and hydroxides showed reflections at $2\theta = 35.5^o$ (002), 38.73^o (111) and 48.7^o (202) corresponding to CuO phase [JCPDS File no.s 80-1917, 80-1917]. An additional peak at $2\theta = 29.3^o$ (104) observed for CAP (Na_2CO_3R) sample was attributed to $NaNO_3$ phase [JCPDS File no. 79-2056]. The presence of such Na species was also reported for the Cu/SiO_2 catalyst prepared by precipitation-gel method using NaOH.[6] The extent of residual Na present in our catalyst was found to be ~ 3 wt% by EDAX which was the highest among all the catalysts (< 0.5%) prepared in this work. Hence, it showed a significant enhancement of the catalyst activity as discussed later. The catalyst samples prepared by solid state alkali fusion (CAF KOH; CAF NaOH) followed by precipitation also showed higher degree of crystallinity. This can be explained by first, the formation of γ-alumina phase under high temperature (550 ^oC) conditions of fusion followed by precipitation resulting into dispersion of crystalline CuO.[20,21] XRD (**Figure 5.1**) of these samples clearly showed a peak at $2\theta = 61.7^o$ (122) assigned to γ-alumina phase [JCPDF File no.85-1337] along with typical CuO peaks. Still higher crystallinity was observed in the sample prepared by only solid state fusion of nitrates of Cu, Al and K. XRD of this sample (CAF KNO_3) showed additional peaks at $2\theta = 32.75^o$ (002), 43.3^o (113), 44.6^o (311), 61.7^o (122), 66.6^o (214), 72.8^o (420), 75.5^o (314) and 23.8^o (111), 27.6^o (200), 29.7^o (200), 39.6^o (220) attributable to Al_2O_3 [JCPDS File no.s 86-1410, 82-1468, 85-1337] and K_2O [JCPDS File no.s 77-2151, 77-2176], respectively. This clearly indicates the formation of distinct oxide phases of Cu, Al and K. The observed difference in XRD patterns of the same catalyst prepared by using different precipitating agents following the same procedure was due to the formation of different molecular precursors during preparation. This study was also carried out by the TG-DTA analysis discussed later.

XRD patterns of reduced catalyst samples prepared by co-precipitation and fusion

methods are shown in **Figures 5.2** (**a**) **and** (**b**) respectively. In all the samples, peaks at 2θ = 36.54° (111) [JCPDS File no.78-2076] and those at 2θ = 43.3° (111), 50.4° (200) and 74.2° (220) [JCPDS file no. 85-1326] were assigned to Cu_2O and metallic Cu respectively (**Figure 2, a**). These peaks with higher intensities indicate higher crystallinity as compared to that of the calcined samples (**Figure 5.1**). The appearance of

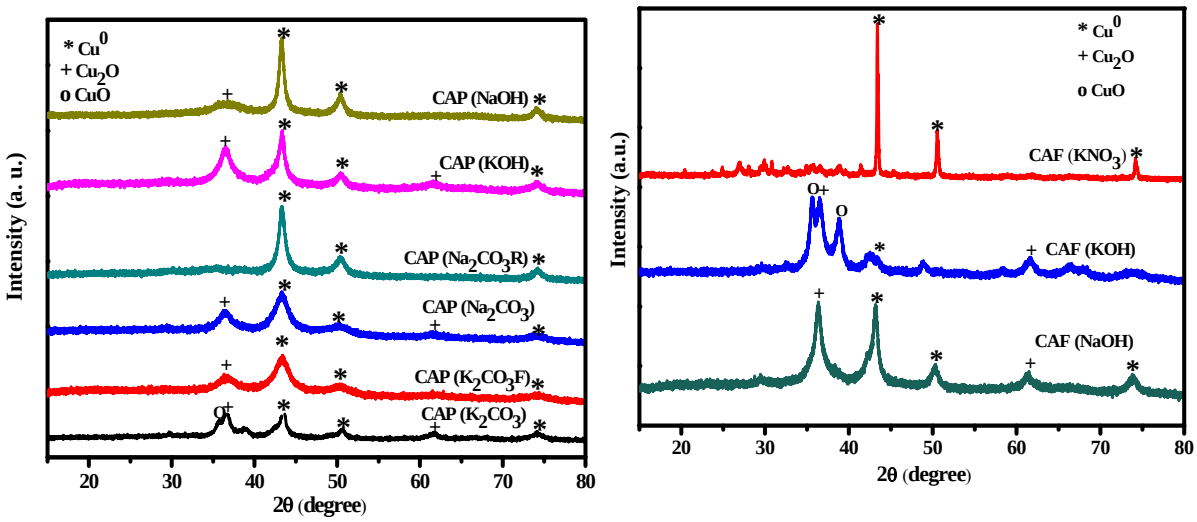

(a) **(b)**

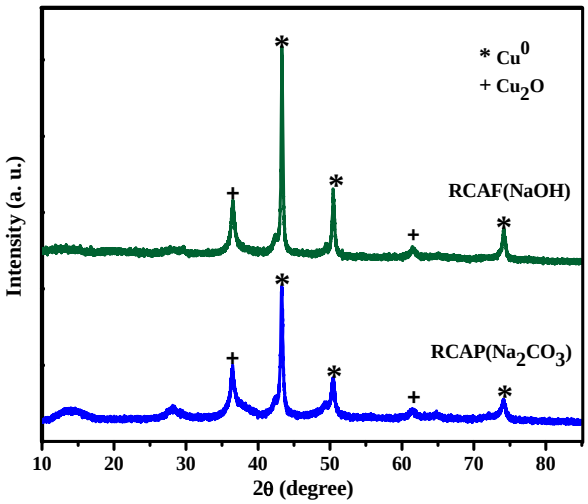

(c)

Figure 5.2. XRD patterns of reduced catalyst samples (a) and (b) prepared by co-precipitation and fusion respectively, (c) recovered after the reaction.

Cu_2O along with Cu^0 phase was due to the sequential reduction of CuO to Cu^0 *via* Cu_2O during H_2 activation at 200 ^oC. Among these samples, CAP (K_2CO_3) showed a peak at $2\theta = 35.5^o$ due to CuO phase indicating its incomplete reduction as compared to the other samples. The co-existence of metallic Cu and partially reduced Cu could be possible either separately as a layer of Cu_2O on metallic Cu with oxygen vacancies exposing Cu_2O or as Cu_2O/Cu^0 interfacial sites.[22] Interestingly, the sample prepared by reverse addition (CAP Na_2CO_3R) showed only the metallic Cu indicating formation of easily reducible CuO species.[19] Depending on the type of alkali metal used, XRD of the samples prepared by alkali fusion followed by precipitation (CAF NaOH and CAF KOH) showed different XRD patterns (**Figure 5.2, b**). CAF (NaOH) sample showed the presence of Cu_2O and Cu^0 phases while CAF (KOH) sample showed the presence of CuO phase predominantly rather than Cu^0 also indicating lower extent of reduction in the later. The sample prepared by KNO_3 fusion showed the presence of only metallic Cu. The reason for this could be the formation of easily reducible CuO phase, as discussed above. XRD patterns of the recovered catalysts which gave the highest activity (discussed later) showed the retention of Cu_2O and Cu^0 phases similar to the fresh catalysts (**Figure 5.2, c**). This indicates that the fresh catalysts did not undergo any significant changes under the reaction conditions.

The crystallite sizes of various activated samples determined by the Scherrer equation and BET surface area are presented in **Table 5.1**. Among the precipitated samples, minimum crystallite size of 5 nm could be obtained with Na_2CO_3 precipitant and K free sample while higher crystallite size of 12 nm was observed for K_2CO_3 precipitant. As seen from **Figure 5.2** (**a**), the residual Na and K affect the extent of reduction of CuO and also the sample having Cu^{1+} helps to stabilize the crystallite size.[13,24] While, a similar crystalite size of 12 to 13 nm was observed for the samples precipitated by alkali metal hydroxides which was higher than that of prepared by Na_2CO_3 precipitant. Intrestingly, the surface areas of samples using alkali metal hydroxides were more than twice than those of using carbonate precipitant. Another observation made was that the higher surface areas were obtained in these cases inspite of their higher crystalite sizes (**entries 5, 6 Table 5.1**). This could be explained by the fact that crystalite sizes are of well disperesed Cu only while, BET measurement represents the total surface area of the

material and not of the Cu alone. The samples prepared by alkali fusion followed by precipitation also showed the surface areas in a range of 127-149 m^2g^{-1}, while the sample prepared by only fusion showed the least surface area and highest crystallite size of 9.6 m^2g^{-1} and 42 nm respectively. In the later case, the high temperature fusion caused the aggregation of the neighboring particles resulting into highest crystallite size and thereby decrease in surface area. [23]

Table 5.1. BET surface areas and crystallite sizes of prepared catalysts

Sr. No.	Catalysts	BET surface area (m^2 g^{-1})	Crystallite size by XRD (nm)
1	CAP (K_2CO_3)	57	12
2	CAP (K_2CO_3F)	51	5
3	CAP (Na_2CO_3)	57	5
4	CAP (Na_2CO_3R)	47	11
5	CAP (KOH)	124	12
6	CAP (NaOH)	104	13
7	CAF (KOH)	127	-
8	CAF (NaOH)	149	14
9	CAF (KNO_3)	9.6	42

The thermal analyses involved the TG and DTA measurements of the representative 'as prepared' samples in order to understand the pathways of formation of various precursors depending on the preparation methods. The DTA curve of CAP (K_2CO_3) shown in **Figure 5.3** (**a**) indicates the loss of water molecule evident from the first endothermic peak at 100 ^oC followed by another endothermic peak around 190 ^oC due to the water/hydroxyl loss from the lattice. The broad exothermic peak between 200-700 ^oC represents the transformation of Cu hydroxide/nitrate to CuO. TG was flat after 700 ^oC suggesting the formation of stable CuO. The DTA curve (**Figure 5.3, b**) of CAP (Na_2CO_3) closely matched with that of CAP (K_2CO_3) except that the weight loss was

observed in the region of 500-700 °C due to hydroxyl carbonate species.[17] The initial region of the DTA curve of CAF (KOH) showed the close resemblance with those of CAP (K_2CO_3) and CAP (Na_2CO_3) indicating the formation of similar molecular precursors. However, next endothermic peak at 260 °C was due to the dehydration of $Cu(OH)_2$ to a highly stable CuO.[24]

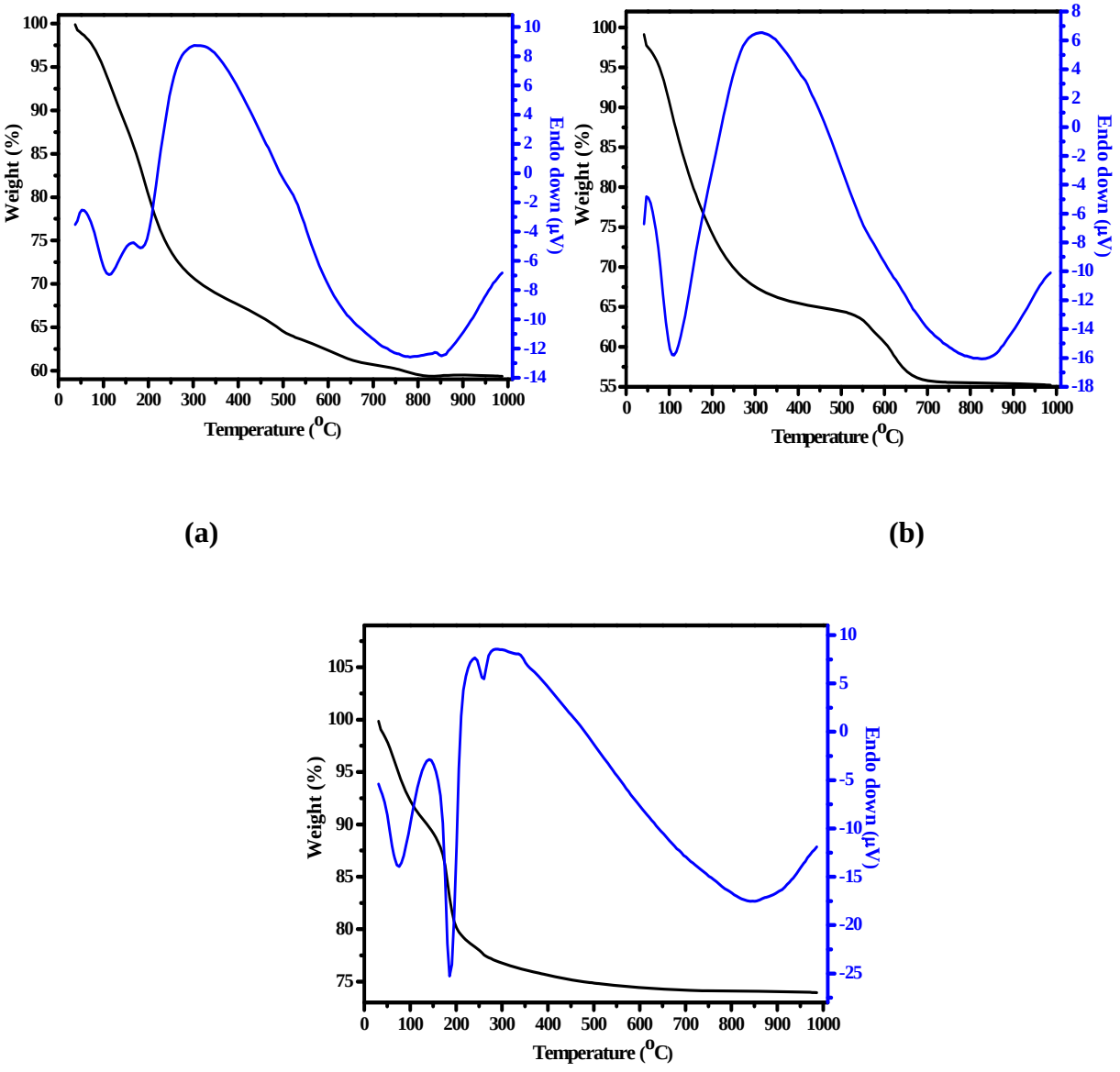

Figure 5.3. TG-DTA curves of various catalyst samples (a) CAP (K_2CO_3) (b) CAP (Na_2CO_3) (c) CAF (KOH).

Cu 2*p* XPS of the reduced catalysts, CAP (Na_2CO_3), CAF (NaOH) and CAP (K_2CO_3) showing highest and lowest activity respectively, are shown in **Figure 5.4.** The Cu $2p_{3/2}$ peaks in CAP (Na_2CO_3) and CAF (NaOH) observed at 932.6 eV and Cu $2p_{1/2}$ at 952.5 eV were assigned to metallic Cu.[25] The absence of any satellite peaks although indicates that the Cu mostly present in the reduced form on the surface, the possibility of Cu^{1+} cannot be ruled out as the binding energies of Cu^0 and Cu^{1+} are indistinguishable. This observation also matches with the XRD results discussed above. On the other hand, CAP (K_2CO_3) showed a broad peak in the range of 932-935 eV along with a satellite peak at 940-946 eV was indicative of CuO along with metallic Cu. The incomplete reduction of CuO to metallic Cu adversely affected its performance as compared to CAP (Na_2CO_3) catalyst. Al 2*p* XPS showed the shift in B. E. from 73 eV in Al_2O_3 to 74.6 eV (**Figure 5.4, b**) confirming the interaction between Al and Cu species to form mixed oxides. It was well reported that the surface spinel $CuAl_2O_4$ species were easily formed upto 300 ^oC.[25]

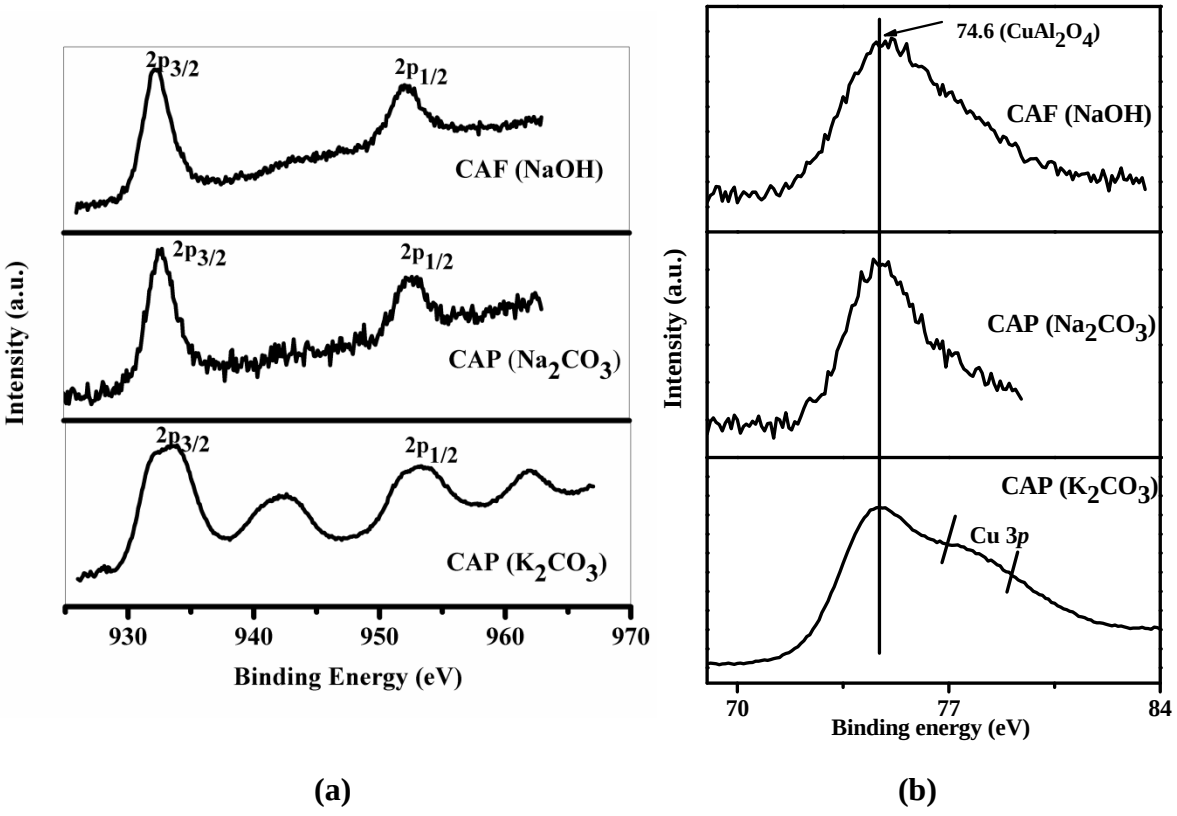

Figure 5.4. XPS spectra of reduced samples (a) Cu 2*p* and (b) Al 2*p*.

TEM images of selected samples prepared by co-precipitation, fusion followed by precipitation showing highest hydrogenolysis activity and that prepared by only fusion which showed the least activity are shown in **Figures 5.5 (a)- (c)**. Two distinct features

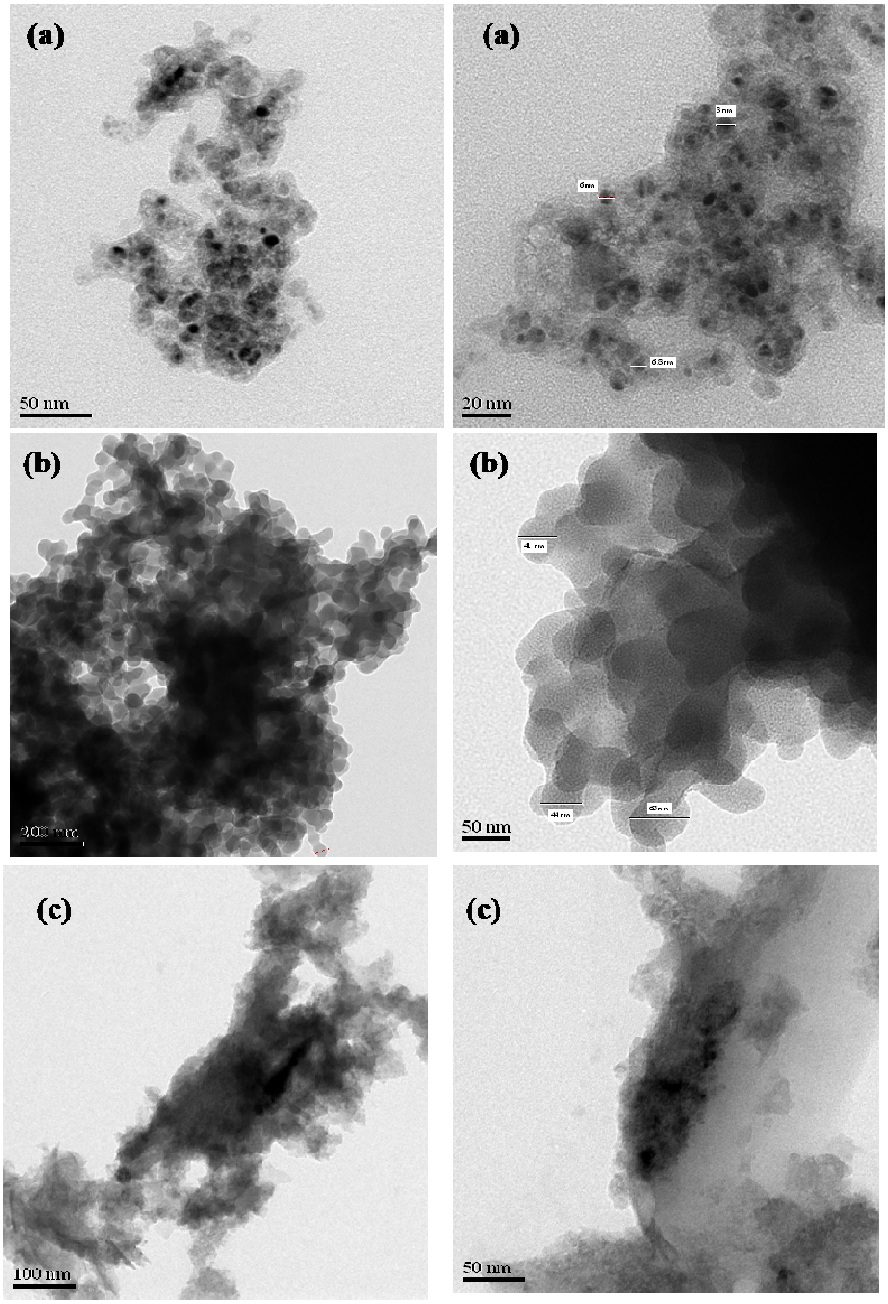

Figure 5.5. HR- TEM images at different resolutions (a) CAP (Na_2CO_3) (b) CAF (NaOH) (c) CAF (KNO_3).

observed from TEM images are that the catalyst prepared by precipitation (CAP Na_2CO_3) showed the spherical morphology (**Figure 5.5, a**) with a particle size of 6-8 nm as against no definite morphology and higher extent of aggregation of the sample prepared by only fusion (CAF KNO_3). The aggregation of the particles was due to the high temperature fusion also evidenced by sample CAF (NaOH) as seen in **Figure 5.5** (b). This has been also directly reflected on their activity performance as discussed later (**Tables 5.3, 5.4**).

The reduction behavior of the reduced catalyst samples was studied by H_2- TPR characterization and the respective profiles are shown in **Figure 5.6.** The reduction peak in all the samples in the range of 200- 300 ^oC was assigned to the reduction of bulk CuO. However, in case of CAP (Na_2CO_3) and CAF (KOH), a hump at lower temperature was observed due to either reduction of surface CuO and/or sequential reduction of Cu^{2+} to Cu^{1+} and then to Cu^0. [26] These results also matched very well with the XRD patterns which also showed the presence of Cu_2O (**Figures 5.2, a and b**). The extent of H_2 consumed by CAP (Na_2CO_3) was the maximum (**Figure 5.6.**) indicating the presence of more number of unreduced Cu species. The presence of Na in a certain concentration could be affecting the extent of Cu reduction. [6] While, in case of reverse addition

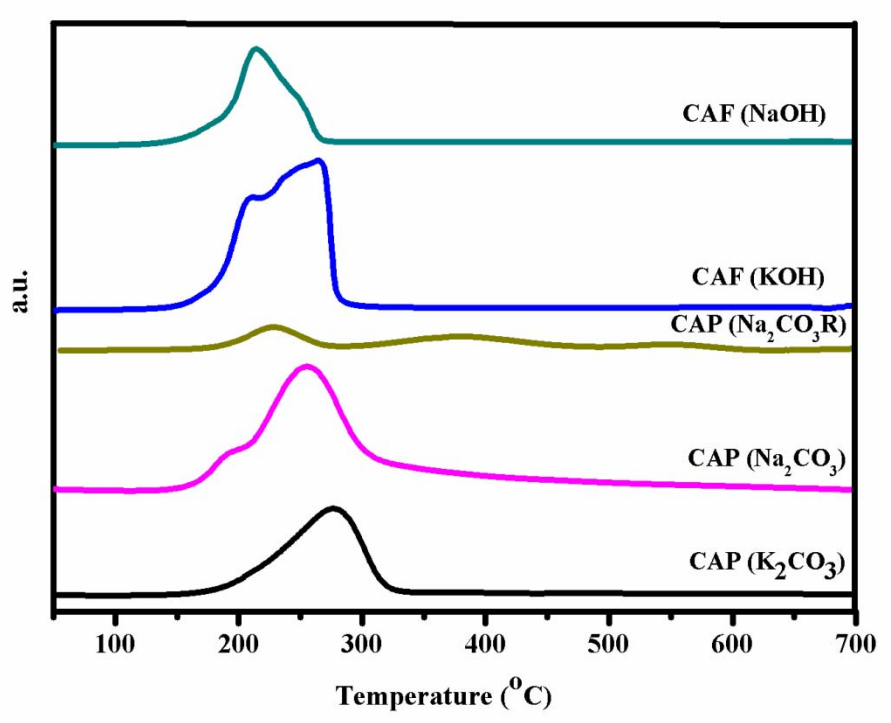

Figure 5.6. H_2-TPR profiles of various catalysts.

procedure (CAP Na_2CO_3R) the amount of hydrogen consumed was the least indicating almost complete reduction of CuO. The difference in hydrogen consumption observed in TPR characterization for the same precipitant was due to variation in preparation procedure and precursor formation. H_2 consumed in TPR of CAF (KOH) was also higher obviously due to the presence of more than one unreducible Cu species as seen from **Figure 5.6.** This also commensurate with XRD (**Figure 5.2**) and lowest activity results.

The acidity of the catalyst plays a significant role in glycerol hydrogenolysis which involves first step of acid catalyzed dehydration to acetol. Hence, the strength and nature of acid sites of our catalysts were determined by NH_3-TPD and the results are shown in **Table 5.2.** The distribution of acid sites were observed in low (50-200 ^oC), medium (200-400 ^oC) and high (400-700 ^oC) temperature regions which can be correlated with Lewis (200-400 ^oC) and BrØnsted acidity (400-700 ^oC) respectively.[27] CAP (Na_2CO_3) catalyst showed the highest total concentration of acidic sites as 0.2293 mmol g^{-1} among all the catalysts having maximum medium strength acid sites followed by CAP (Na_2CO_3R) catalyst (**entry 3, Table 5.2**). Its maximum acidity could be due to two reasons: (i) lower residual Na content (0.17 wt %) as evidenced by EDAX and

Table 5.2. NH_3- TPD results of prepared catalysts

Sr. No.	Catalysts	Total NH_3 desorbed (mmol g^{-1})	Distribution of acidic sites (mmol g^{-1})		
			50-200 ^oC	200-400 ^oC	400-700 ^oC
1	CAP (K_2CO_3)	0.1873	0.0615	0.1127	0.0129
2	CAP (K_2CO_3F)	0.1730	0.0422	0.1032	0.0275
3	CAP (Na_2CO_3)	0.2293	0.0181	0.1483	0.0628
4	CAP (Na_2CO_3R)	0.1796	0.0214	0.1263	0.0318
5	CAP (KOH)	0.1773	0.0296	0.1476	-
6	CAP (NaOH)	0.1785	0.0381	0.1340	0.0062
7	CAF (KOH)	0.123	0.0847	0.0327	0.0054
8	CAF (NaOH)	0.1305	0.0367	0.0937	-
9	CAF (KNO_3)	0.168	0.0025	0.0887	0.0768

(ii) contribution of mixed oxide phases to the surface acidity is known due to defective structures.[28] Although same base Na_2CO_3 was used in both the cases, acid strength decreased in case of CAP (Na_2CO_3R) catalyst due to change in the order of addition of precursors causing higher formation of NaOH and slight lowering in acidity (**entry 4, Table 5.2**). The change in cation from Na^+ to K^+ also lowered the acid strength, fitting to the trend of alkali metals. [29] Acid strengths of both CAP (NaOH) and CAP (KOH) were lower than that of CAP (Na_2CO_3). The samples prepared by fusion method invariably showed lower acid strengths than those of prepared by precipitation. The activity trend was also according to the acidity particularly, of the medium acid sites which is discussed later.

5.3.2. Catalyst activity

The activity results of the catalysts prepared by co-precipitation and those prepared by fusion are presented in **Tables 5.3 and 5.4**, respectively. Among the precipitated catalysts, CAP (Na_2CO_3) and (Na_2CO_3R) (entries, 4 and 5**, Table 5.3**) showed the highest conversion of 62-63% with 1,2-PDO selectivity of 88%. The activity of these catalysts was also much higher than that of reported Cu catalysts in combination with Cr and Ba which gave glycerol conversion of 34% with 1,2-PDO selectivity of 85% in 2-propanol solvent.[17,27] The highest activity of the present Cu-Al catalysts was due to several reasons as discussed here. The presence of mainly Cu^0 species as evidenced by XRD and XPS (**Figures 5.2 and 5.4**, respectively), were responsible for catalyzing glycerol hydrogenolysis. These samples also showed the minimum crystallite size in a range of 5-11 nm (**Table 5.1**). TEM results (**Figure 5.5**) revealed that the CAP (Na_2CO_3) catalyst having well defined spherical morphology without any aggregation that contributes to its highest activity. In addition, the highest acidity of this catalyst in the medium range (200-400 ^oC) is responsible for the efficient first step dehydration to acetol necessary for 1,2-PDO formation. Similar activity trend (58% conversion) was exhibited by CAP (KOH) which also had crystallite size of 12 nm (**Table 5.1**) with majority of Cu in the metallic form (**Figure 5.2**). The interesting observation was that although the surface areas of carbonate precipitated samples were 50% less than those of the hydroxide precipitated

Table 5.3. Activity results of catalysts prepared by co-precipitation for hydrogenolysis of glycerol

Sr. No.	Catalysts	Conversion (%)	Selectivity (%)			
			1,2-PDO	Acetol	EG	2-propanol
1	CAP (K_2CO_3)	38	91	4	4	1
2	CAP (K_2CO_3F)	36	87	1.5	10	0.5
3	CAP (K_2CO_3)[a]	38	88	2	9	1
4	CAP (Na_2CO_3)	62	88	1	10	1
5	CAP (Na_2CO_3R)	63	88	1	10	1
6	CAP (KOH)	58	88	1	10	1
7	CAP (NaOH)	51	87	1	10	2

Reaction conditions: Glycerol, 20 wt%; solvent, water; catalyst, 1 g ; temperature, 220 ^oC; H_2 pressure, 52 bar; reaction time, 5 h; total reaction volume, 100 mL.

[a] before reaction externally 0.9 M NaOH was added in charge (20 wt% aq. glycerol solution) .

Table 5.4. Activity results of catalysts prepared by fusion for hydrogenolysis of glycerol

Sr. No.	Catalysts	Conversion (%)	Selectivity (%)			
			1,2-PDO	Acetol	EG	2-propanol
1	CAF (KOH)	5	74	16	8	2
2	CAF (NaOH)	39	88	4	7	1
3	CAF (KNO_3)	15	84	13	1	2

Reaction conditions: Glycerol, 20 wt%; solvent, water; catalyst, 1 g; temperature, 220 ^oC; H_2 pressure, 52 bar; reaction time, 5h; total reaction volume, 100mL

samples, their activities were almost similar. This indicates not only the surface area but

also other physico-chemical properties such as reduced metal species, distribution and strength of acid sites, crystallite size, and morphology are also important for the catalytic activity. As the catalyst in the present work were prepared using alkali metal carbonates and hydroxides, the effect of free alkali (0.9 M NaOH) on glycerol hydrogenolysis was also studied. The same conversion of 38% obtained for CAP (K_2CO_3) and CAP (K_2CO_3)[a] (**entry 3, Table 5.3**) clearly showed no effect of free alkali unlike reported for supported noble metal catalysts. [30] The product distribution for all the catalysts showed 1,2-PDO selectivity in the range of 87-91%, with major byproduct as ethylene glycol (EG) except in case of CAP (K_2CO_3) catalyst which showed the appreciable formation of acetol.

The samples prepared by fusion method showed substantially lower glycerol hydrogenolysis activity than those prepared by precipitation method. The activity order of the samples prepared by fusion was: CAF (NaOH) > CAF (KNO_3) > CAF (KOH) (**Table 5.4**). The highest activity (39% conversion) of CAF (NaOH) sample was again due to the well defined morphology as shown in **Figure 5.5.** However, considerable aggregation of the particles was also observed which resulted into lower activity as compared to the CAP (NaOH) sample. The intermediate activity of 15% conversion was shown by CAF (KNO_3) inspite of the prominent presence of metallic Cu (XRD, **Figure 5.2, b**). The major causes of its poor activity were its ill-defined morphology (**Figure 5.5, c**), bigger crystallite size of 42 nm and very low surface area of 9.6 m^2g^{-1} (**Table 5.1**). Almost negligible activity (5% conversion) was shown by CAF (KOH) catalyst mainly because of very low extent of reduction of CuO and Cu_2O to metallic Cu (**Figure 5.2, b**), inspite of its higher surface area. The activity pattern of fusion samples was quite different from that of precipitated samples. Although the major product formed was 1,2-PDO, its selectivity was affected due to higher formation of acetol along with EG and 2-propanol.

As the co-precipitated CAP (Na_2CO_3) catalysts showed higher activity for glycerol hydrogenolysis, its stability was also established by its recycle studies. As seen from **Figure 5.7,** CAP (Na_2CO_3) catalyst showed consistent activity even after third recycles with slight decrease in glycerol conversion from 62 to 59%, due to the handling losses of the catalyst. The product selectivity was not affected during catalyst recycle study.

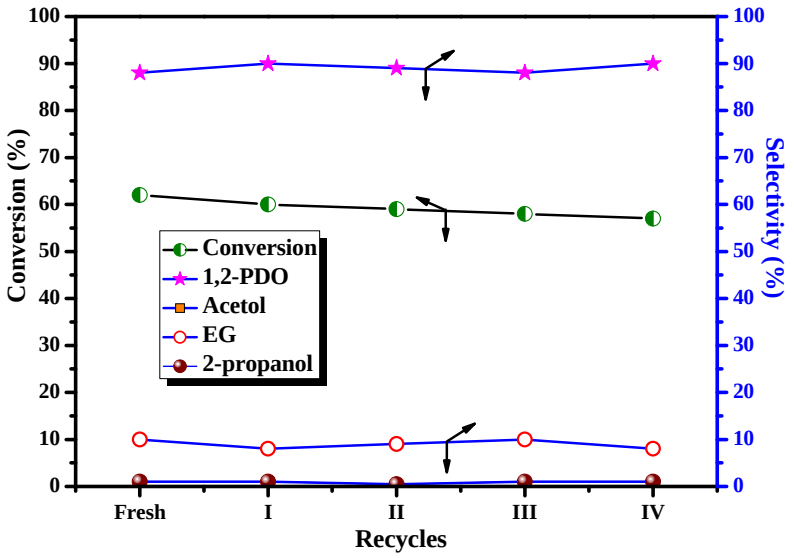

Figure 5.7. Catalyst recycle study.

Reaction conditions: Glycerol, 20 wt. %; solvent, water; catalyst, 1 g; temperature, 220 ^{o}C; H_2 pressure, 52 bar; reaction time, 5 h; total reaction volume, 100 mL.

From the above discussion, catalysts prepared by co-precipitation method were found to be superior than those prepared by fusion method.

5.4. CONCLUSIONS

The effect of precipitating agents was systematically investigated in co-precipitation and solid state fusion followed by precipitation methods for Cu catalysts used in glycerol hydrogenolysis to 1,2-PDO. These catalysts were thoroughly characterized by various techniques such as XRD, BET, TG-DTA, XPS, TEM, H_2-TPR and NH_3-TPD. The important finding of our study was that not only the surface area but also other physico-chemical properties such as reduced metal species, distribution and strength of acid sites, crystallite size, and morphology were important for the catalytic activity. The distinct characteristics of various catalysts prepared in this work are:

- Catalyst prepared using Na_2CO_3 as a precipitant (CAP Na_2CO_3) showed predominantly metallic Cu with a crystallite size of 5 nm while the one prepared with K_2CO_3 showed CuO phase along with Cu^0 having crystallite size of 12 nm.

- XRD of the samples prepared by alkali fusion followed by precipitation (CAF NaOH and CAF KOH) also showed different phases depending on the type of alkali metal used. *E.g.* CAF (NaOH) sample showed the presence of both Cu_2O and Cu^0 phases while CAF (KOH) sample showed the presence of CuO phase predominantly, indicating its incomplete reduction.
- TEM analysis revealed that (CAP Na_2CO_3) catalyst having the spherical morphology with a particle size of 6-8 nm as against no definite morphology and higher extent of aggregation for (CAF KNO_3) catalyst.
- The samples prepared by fusion method invariably showed lower acid strengths than those of prepared by precipitation. Among all the catalysts, CAP (Na_2CO_3) catalyst showed the maximum acid sites (0.1483 mmol g^{-1}) in the temperature region used for hydrogenolysis.
- The change in cation from Na^+ to K^+ also lowered the acidity, fitting into the trend of alkali metals.

Due to its unique characteristics, CAP (Na_2CO_3) showed the highest conversion of 62-63% with 1,2-PDO selectivity of 88%. Among the catalysts prepared by fusion, CAF (NaOH) gave reasonable activity (39% conversion) that was again due to the well defined morphology nevertheless, co-precipitation method proved to be better in giving highly efficient Cu catalyst system.

5.5. REFERENCES

1. E. S. Vasiliadoua, A. A. Lemonidou , *Appl. Catal. A* **2011,** 396, 177-185.
2. H. Kobayashi, N. Takezawa, C. Minochi, *J. Catal.* **1981,** 69, 487-494.
3. D. F. Jin, B. Zhu, Z.Y. Hou, J. H. Fei, H. Lou, X. M. Zheng, *Fuel* **2007,** 86, 2707-2713.
4. V. Z. Fridman, A. A. Devydov, *J . Catal.* **2000,** 195, 20-30.
5. A. Bienholz, H. Hofmann, P. Claus, *Appl. Catal. A* **2011,** 391, 153-157.
6. Z. W. Huang, F. Cui, H. X. Kang, J. Chen, C. G. Xia, *Appl. Catal. A* **2009,** 366, 288-298.
7. Z. L. Yuan, L. N. Wang, J. H. Wang, S. X. Xia, P. Chen, Z. Y. Hou, X. M. Zheng, *Appl. Catal. B* **2011,** 101, 431-440.
8. N. D. Kim, S. Oh, J. B. Joo, K. S. Jung, J. Yi, *Top. Catal.* **2010,** 53, 517-522.
9. M. Akiyama, S. Sato, R. Takahashi, K. Inui, M. Yokota, *Appl. Catal. A* **2009,** 371, 60-66.
10. L. Y. Guo, J. X. Zhou, J. B. Mao, X. W. Guo, S. G. Zhang, *Appl. Catal. A* **2009,** 367, 93-98.
11. J. J. X. Zhou, L. Y. Guo, X. W. Guo, J. B. Mao, S. G. Zhang, *Green Chem.* **2010**, 12, 1835-1843.
12. Ch. Sivaraj, B. R. Rao, M. R. Hussain, P. K. Rao, in P. K. Rao (Ed.), Proc. 2nd Indo-Soviet Seminar on *Recent Advances in Catalysis and Catalytic Reaction Engineering*, Hyderabad, India, November **1986,** p. 492.
13. Z. Huang, F. Cui, H. Kang, J. Chen, X. Zhang, C. Xia, *Chem. Mater.* **2008,** 20, 5090-5099.
14. C.V. Rode, R. B. Mane, A. S. Potdar, P. B. Patil , P. S. Niphadkar, P. N. Joshi, *Catal. Today* **2012**, 190, 31-37.
15. C.V. Rode, A. A. Ghalwadkar, R. B. Mane, A. M. Hengne, S.T. Jadkar, N. S. Biradar, *Org. Process Res. Dev.* **2010,** 14,1385-1392.
16. R. B. Mane, A. M. Hengne, A. A. Ghalwadkar, S. Vijayanand, P. H. Mohite, H. S. Potdar, C. V. Rode, *Catal. Lett.* **2010,** 135, 141-147.

17. R. B. Mane, A. A. Ghalwadkar, A. M. Hengne, Y. R. Suryawanshi, C.V. Rode, *Catal. Today* **2011,**164, 447-450.
18. R. B. Mane, S. E. Kondawar, P. S. Niphadkar, P. N. Joshi, K. R. Patil, C. V. Rode, *Catal. Today* **2012,** 198, 321-329.
19. R. O. Idem, N. Bakshi, *Ind. Eng. Chem. Res.* **1994,** 33, 2047-2055.
20. G. K. Chuah, S. Jaenicke, T. H. Xu, *Micro. Meso. Mater.* **2000,** 37, 345-353.
21. M. F. R. Founda, R. S. Amin, M. M. Selim, *Thermochimica Acta.* **1989,** 141, 277-291.
22. E. E. Miro, E. A. Lombardo, J. O. Petunchi, *J. Catal.* **1987,** 104, 176-185.
23. B. Pacewska, M. Keshr, *Thermochimica Acta.* **2002,** 385, 73-80.
24. J. W. Patterson, R. E. Bolce, D. Marani, *Environ. Sci. Technol.* **1991,** 25, 1780-1787.
25. A. Wolberg, J. F. Roth, *J. Catal.* **1969,** 15, 250-255.
26. P. A. Kumar, M. P. Reddy, L. K. Ju, B. Hyun-Sook, H. H. Phil, *J. Mol. Catal. A* **2008,** 291, 66-74.
27. N. A. S. Amin, D. D. Anggoro, *J. Natural Gas Chem.* **2003,** 12, 123-134.
28. M. M. Gunter, T. Ressler, B. Bems, C. Buscher, T. Genger, O. Hinrichsen, M. Muhler, R. Schlogl, *Catal. Lett.* **2001,** 71, 37-44.
29. O. Ilgen, A. N. Akin, *Turk. J. Chem.* **2009,** 33, 281-287.
30. E. P. Maris, R. J. Davis, *J. Catal.* **2007,** 249, 328-337.

Chapter 6

Copper modified waste fly ash as a promising catalyst for glycerol hydrogenolysis

Several catalyst formulations using waste fly ash along with Cu were prepared and characterized by XRD, BET and TEM. These catalysts were also evaluated for the first time for hydrogenolysis of glycerol to 1,2-propanediol (1,2-PDO). The fly ash pretreated by alkali using the fusion method and impregnated with Cu showed an excellent activity and stability for glycerol hydrogenolysis. Due to pretreatment with alkali at high temperature, transformation of α-quartz to the tridymite phase of SiO_2 occurred. More importantly, use of alkali either during the pretreatment or the Cu loading step resulted in a high dispersion on the surface which was responsible for higher glycerol conversion and 1,2-PDO selectivity. The effects of temperature, Cu loading and solvent on glycerol conversion and product selectivities were also studied in this work.

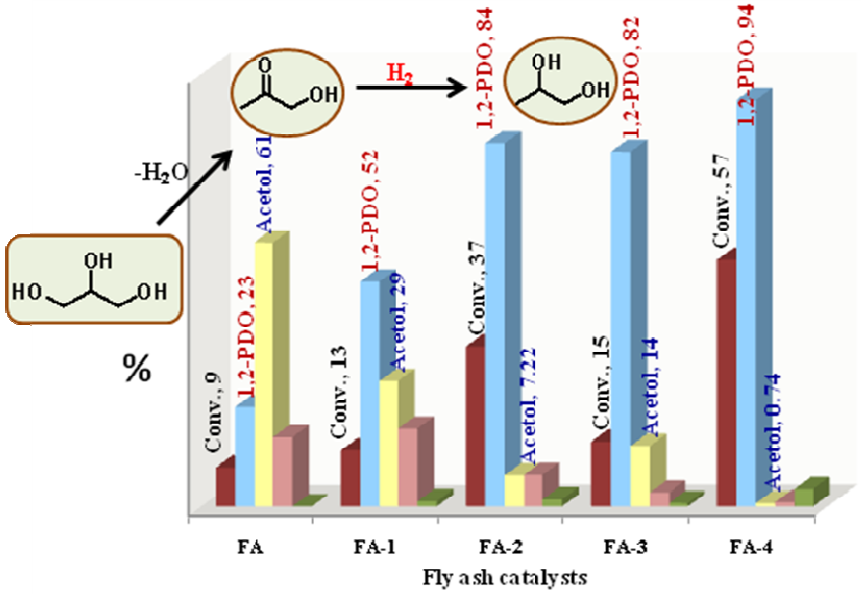

***Catal. Today* 2012, 190, 31-37**

6.1. INTRODUCTION

In continuation of our work on a bi-functional Cu-Al nano catalyst for selective hydrogenolysis of glycerol to 1,2-propanediol,[1-3] we thought of exploring the use of waste fly ash by incorporating Cu, as an efficient catalyst system for glycerol hydrogenolysis. Coal combustion for power generation results in huge amounts of fly ash as a waste material. Fly ash is mainly composed of SiO_2 (~70%) and Al_2O_3 (~21%) and since it is formed after high temperature combustion possesses high thermal stability, which make it as a good catalyst support. In addition, minor components of other metal oxides such as Fe_2O_3, TiO_2, CaO, MgO, K_2O, and Na_2O present in the fly ash could also be used as effective catalyst components. [4,5] Until now, fly ash has been used for the synthesis of zeolites as well as for catalyzing deep oxidation, condensation and NO reduction reactions.[6-8] To date, there has been no published report on fly ash being used as a catalyst for hydrogenolysis of glycerol. Therefore, the main objective of the present investigation was to utilise the alumina content present in the fly ash for the preparation of Cu modified catalyst for hydrogenolysis of glycerol to 1,2-PDO.[9] For this purpose, waste fly ash was modified by two methods *viz.* solid state fusion with alkali metal hydroxide and acid treatment followed by Cu deposition by impregnation and precipitation methods. Among these catalysts, Cu impregnated fused fly ash (Al:Cu=1:1) showed the highest activity and 1,2-PDO selectivity (>85%) in glycerol hydrogenolysis. This study will be useful in establishing the reuse of the waste material such as fly ash as a catalyst for hydrogenolysis of renewable glycerol to 1,2-PDO.

6.2. EXPERIMENTAL

The parent fly ash (FA) was subjected to solid state alkali metal hydroxide fusion and acid pretreatment methods. These pretreated fly ash samples were modified by incorporating copper with respect to fixed Al content in the fly ash by impregnation and precipitation methods. The details of the preparation methods are given in chapter 2 (sections 2.3.6-2.3.9). The copper modified fly ash catalysts prepared by different methods were designated as FA-1 (Cu on parent fly ash), FA-2 (Cu on fused fly ash), FA-

3 (Cu on acid treated fly ash by wet impregnation), FA-4 (Cu on acid treated fly ash by precipitation). The catalysts were characterized by various techniques and a detailed characterization procedure is described in chapter 2 (section 2.4). The activity testing of prepared catalysts for glycerol hydrogenolysis to 1,2-PDO was carried out in a batch reactor and its detailed experimental procedure is described in chapter 2 (section 2.5.1).

6.3. RESULTS AND DISCUSSION

6.3.1 Catalyst characterization

Powder XRD patterns of parent fly ash showed the presence of characteristic peaks of crystalline phase of α-quartz [JCPDS File no. 86-1630], mullite and hematite [10] which were also present in Cu modified fly ash samples FA-1, FA-3, and FA-4 (**Figure 6.1, a**). This indicates that fly ash remained unchanged after acid pretreatment as well as copper loading by impregnation and precipitation methods. The high content of SiO_2 in fly ash exists in a very stable form and acts as a support for the metal loaded (in this case Cu) on it. Although the packing of sample holder was uniform for all the samples, the Cu loaded fused fly ash (FA-2) sample showed comparatively low intensity of the diffraction lines of α-quartz and complete disappearance of diffraction lines of mullite and hematite phases. This sample also showed appearance of a new peak at $2\theta = 29.11^{o}$ (223) which could be attributed to the tridymite SiO_2 phase [JCPDS File no. 86-0681]. Partial transformation of α-quartz to tridymite in our case could be due to the solid state reaction of silica with KOH during fusion pretreatment of fly ash at 550 ^{o}C. Similar phase transformations with alkali metal salt pretreatment at high temperatures have been reported in the literature. [11-13] XRD patterns **(Figure 6.2)** of varying Cu loadings on FA-2 also showed the transformation of α-quartz to the tridymite phase indicating the alkali treatment under high temperature is the main cause for such phase transformation.

In order to investigate phases of Cu in samples FA-1, FA-2, FA-3 and FA-4, XRD patterns were expanded in the 2θ region = $30\text{-}55^{o}$ **(Figure 6.1, b).** Samples FA-1 and FA-3 exhibited diffraction peaks at $2\theta = 35.46^{o}$ (002), 36.54^{o} (111) and 43.56^{o} (111) which could be assigned to CuO [JCPDS File no. 80-1917], Cu_2O [JCPDS File no.78-

2076] and metallic copper [JCPDS File no. 85-1326] reflections respectively.[1] FA-4 sample showed strong diffraction peaks at 2θ = 35.46° and 38.7° corresponding to (002) and (111) planes of CuO while, a peak at 2θ = 36.54° could be attributed to Cu_2O (111) phase and a peak at 2θ = 50.1° (200) was corresponding to metallic copper. FA-2 sample showed very broad diffraction peaks at 2θ = 35.46° (002), 36.54° (111), 43.56° (111), 74.13° (220) indicating that Cu existed in different phases. In all the samples, the

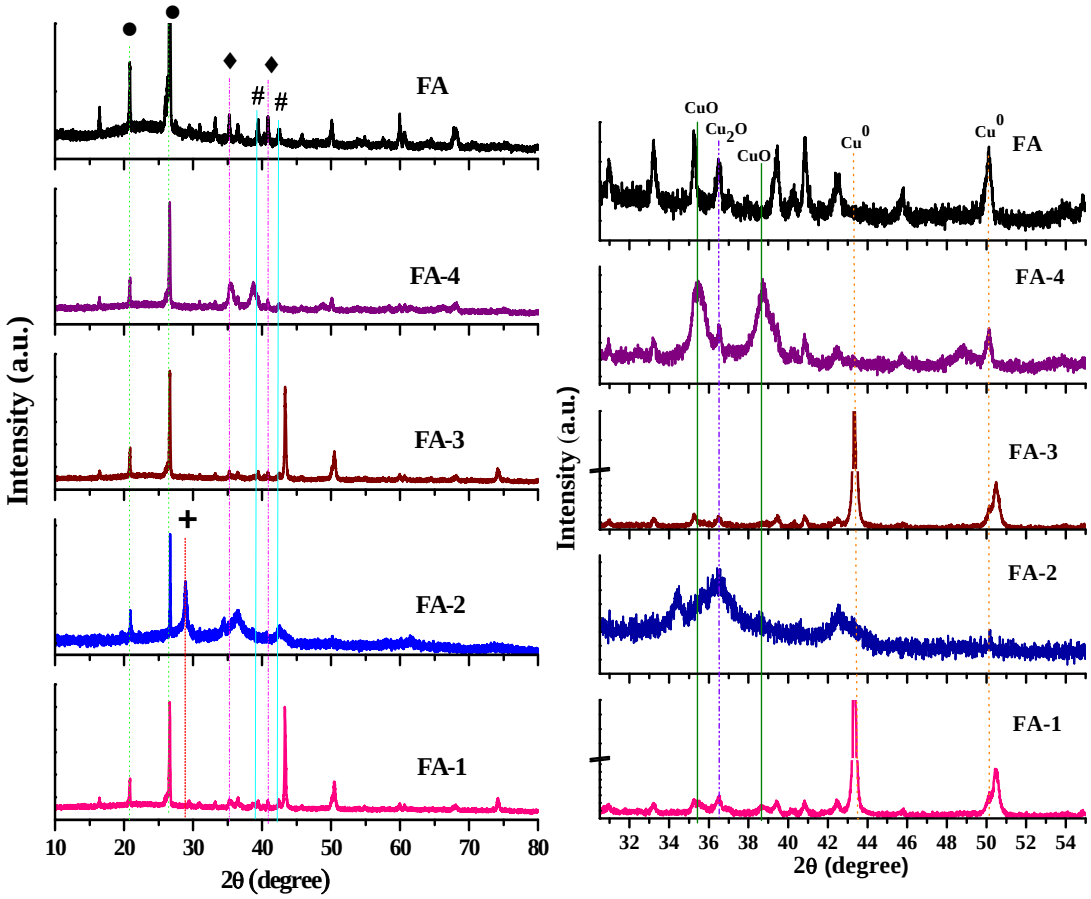

(a) **(b)**

Figure 6.1. XRD patterns of (a) parent fly ash and Cu-modified fly ash samples, (●) ∝-quartz, (#) mullite, (♦) hematite and (+) tridymite (b) expanded XRD in the range of 30-55°.

presence of different phases of Cu indicates the stepwise reduction of CuO to Cu^0 during reduction. However, the extent of reduction varied depending on the pretreatment and Cu loading procedures. The lower intensities of peaks for metallic copper in the FA-2 and FA-4 samples indicate very high dispersion of smaller Cu particles due to their pretreatment and the Cu loading methods employed such as highly basic conditions (solid state KOH reaction and co-precipitation using KOH, respectively). Under these conditions, the fly ash surface mainly comprising SiO_2 is negatively charged favoring adsorption of Cu cations resulting in highly dispersed Cu species on the surface.[14] This higher dispersion has also led to higher activities of FA-2 and FA-4, as discussed later.

As shown in **Figure 6.2**, increasing Cu loading in FA-2 resulted in increasing crystallinity of metallic Cu. Other interesting features were the distinct appearance of Cu_2O along with Cu^0 in the FA-2 (1:2) sample and the lowering intensity of tridymite phase of SiO_2 for the highest Cu content (FA-2, 1:3) due to higher surface coverage by Cu species.

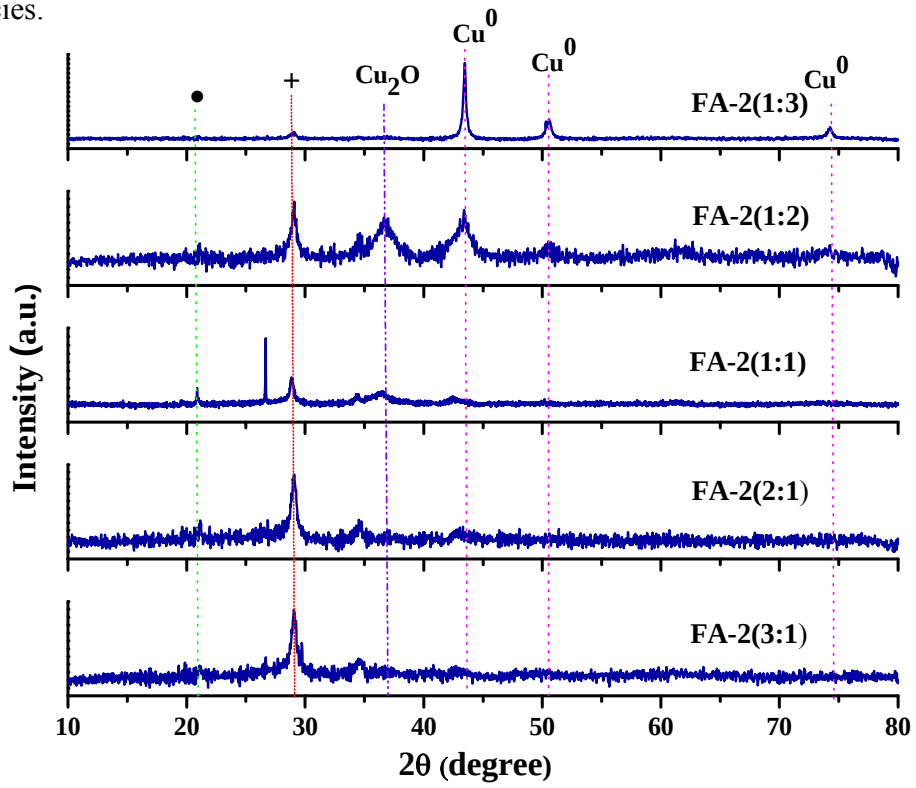

Figure 6.2. XRD patterns of Cu loaded fused fly ash with different Al: Cu ratios, (+) tridymite, (●) α-quartz .

As shown in **Table 6.1**, BET surface areas of various fly ash samples with the same Cu loading (Al : Cu=1:1) showed the trend as FA-4>FA-2>FA-1>FA-3>FA. Parent fly ash (FA) showed the minimum surface area of 31 m^2g^{-1} which systematically increased with Cu loading depending on the method of fly ash pretreatment and Cu loading procedure. The effect of use of alkali either in fusion pretreatment procedure or in Cu loading procedure on enhancement in surface area has been distinctly observed (entries FA-2 and FA-4) while Cu loading on parent fly ash and on acid treated fly ash showed similar surface areas (entries FA-1 and FA- 3). The higher surface areas of both FA-2 and FA-4

Table 6.1. BET surface areas of fly ash and Cu modified fly ash catalyst samples.

Catalyst	Al:Cu ratio	BET surface area ($m^2 g^{-1}$)
FA	--	31
FA-1	1:1	43
FA-2	1:1	61
FA-3	1:1	40
FA-4	1:1	113
FA-2 (3:1)	3:1	44
FA-2 (2:1)	2:1	52
FA-2 (1:2)	1:2	41
FA-2 (1:3)	1:3	39

indicate the excellent dispersion of Cu which is also confirmed by their activity results. Between the two, FA-4 showed the highest surface area of 113 m^2 g^{-1} owing to its high temperature (800 ^oC) pretreatment for removal of carbon and its amorphous nature as seen from the XRD pattern **(Figure 6.1, b)**. Interesting observations regarding the surface areas of fused fly ash with varying Cu loadings were made and the results are shown in **Table 6.1**. Among these samples, with increase in Cu loading (entries, FA-2 (3:1) to FA-2 (1:1)) surface area also increased gradually from 44 to 61 m^2g^{-1} up to a certain Cu loading value beyond which further increase in Cu loading caused decrease in surface

area from 61 to 39 m^2g^{-1}. For lower Cu loading, the impregnating precursor solution was of lower concentration which might diffuse faster without filling all the pores and not initiating the crystallization process. Increasing concentration of impregnating precursor solution increased the number of nuclei for crystallization hence, the crystal surface area was proportional to the Cu loading. However, with further increase in precursor concentration though the number of crystallites remained same, the crystallite size increased leading to lower surface area.[15]

TEM images of parent fly ash catalyst (**Figure 6.3, a**) shows an irregular rod like structure having a polycrystalline nature. Diffraction planes obtained from SAED (**Figure 6.3, b**) were (101), (104), (104) reflections corresponding to quartz [JCPDS File no. 86-1630], hematite [JCPDS File no. 86-1410] and corundum [JCPDS File no. 86-0550] phases of silicon, iron oxides and aluminium, respectively. This is in accordance with the XRD studies discussed above.

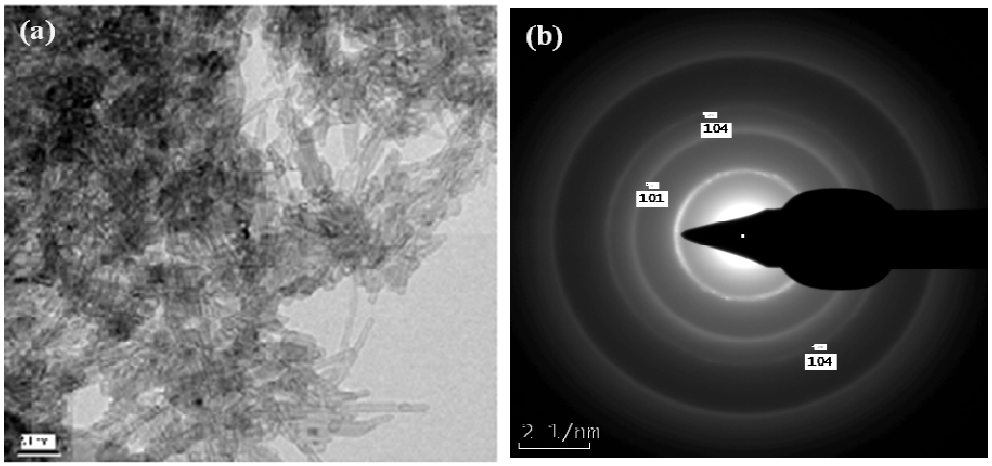

Figure 6.3. a) TEM of parent fly ash (FA) b) SAED showing diffraction planes.

TEM images of fused fly ash with varying Al: Cu ratios are shown in **Figures 6.4** (**a**)**,** (**c**) **and** (**e**). In case of both the lowest and the highest Cu loadings, irregular morphology was observed (**Figures 6.4, a and e**) while for FA-2 (1:2) sample rod like morphology was observed as evidenced by the dimensions (99.67nm X 51.82 nm) shown by the marked particle in **Figure 6.4** (**c**). A well defined morphology could be due to stabilization of Cu particle size by the presence of Cu^{1+} as evidenced by XRD (**Figure**

6.2).[1] The SAED diffraction pattern of FA-2 (1:1) presented in **Figure 6.4** (**b**) confirms the crystalline nature of the particles exhibiting diffraction planes (220), (111), associated with metallic copper [JCPDS File no. 85-1326] and (311) for copper aluminate. The SAED pattern of FA-2 (1:2) presented in **Figure 6.4** (**d**) shows diffraction planes as (311), and both (111), (220) corresponding to copper aluminate [JCPDS File no.78-1605]

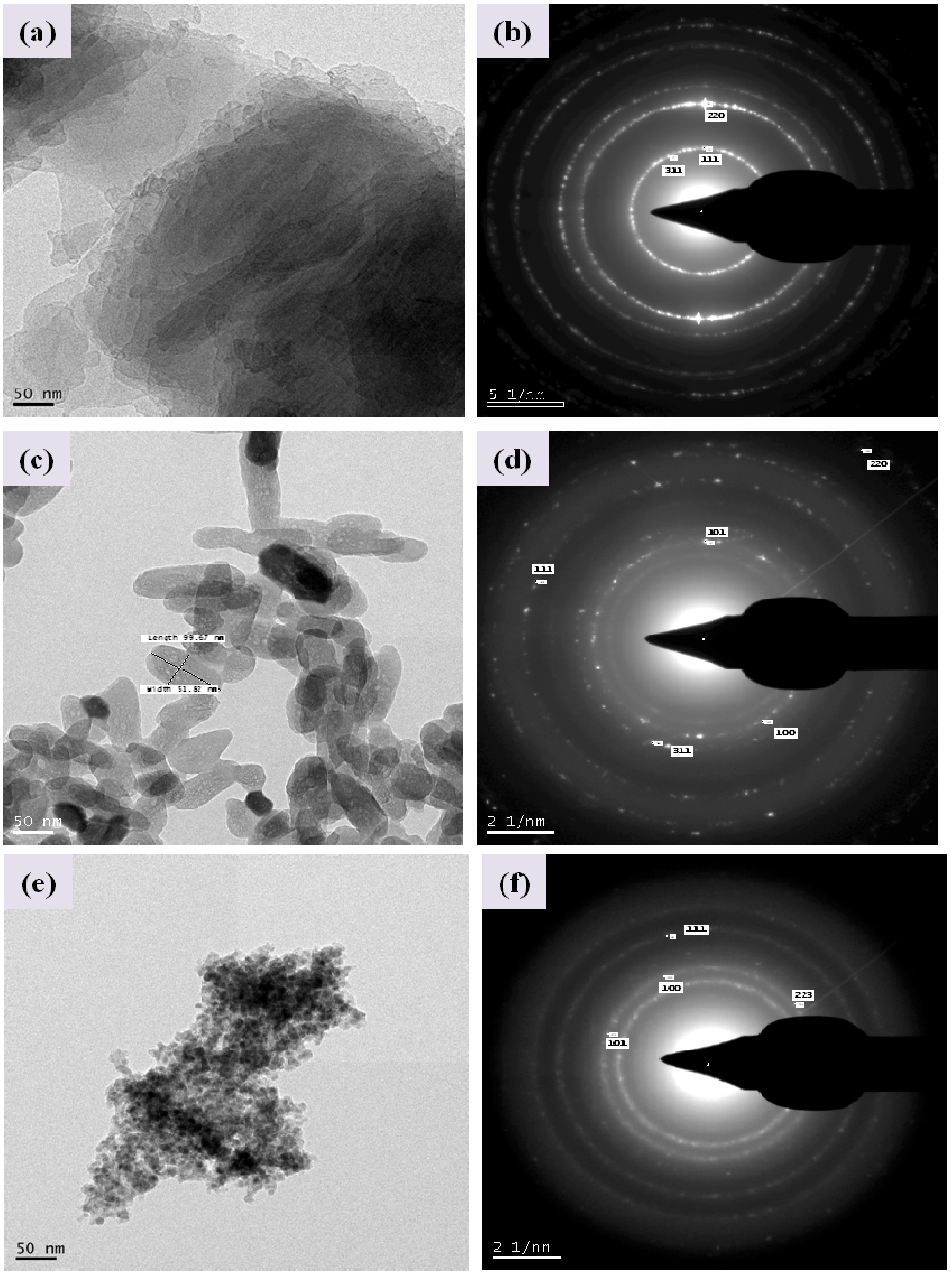

Figure 6.4. TEM images of fused fly ash samples a) FA-2 (1:1), c) FA-2 (1:2), e) FA-2 (1:3) and SAED of b) FA-2 (1:1), d) FA-2 (1:2), f) FA-2 (1:3).

and metallic copper, respectively. The SAED pattern of FA-2 (1:3) presented in **Figure 6.4 (f)** shows crystalline nature of particles having diffraction planes as (100) and (101) corresponding to α-quartz [JCPDS File no. 86-1630], and (223) corresponding to tridymite [JCPDS File no. 86-0681] and metallic copper. Comparison of SAED patterns of fused fly ash with varying Al: Cu ratios shows that the extent of Cu loading might lead to the exposure of different surface terminated planes of metallic copper which might affect the glycerol hydrogenolysis activity.

6.3.2. Catalyst activity

Figure 6.5 shows the screening of parent fly ash and various Cu loaded pretreated fly ash catalyst samples for the hydrogenolysis of glycerol. The reproducibility of the catalytic data was confirmed by repeated experiments, within ±7% error bar. Parent fly ash without any pretreatment and Cu loading showed the least activity (9% conversion) for hydrogenolysis of glycerol. Since, fly ash contains alumina and silica as expected, higher selectivity to acetol the product of glycerol dehydration was obtained.[1] Surprisingly, hydrogenation as well as C-C cleavage products 1, 2-PDO and ethylene glycol (EG) respectively, were also formed which could be due to presence of other components particularly MgO, CaO, Na_2O and K_2O although in minor proportions.[16,17] The other byproducts identified were methanol and 2-propanol however, these are shown together as unknowns since their formation was in a range of 0.1-2%. Under the present set of conditions carbon selectivities were found to be >80%. Cu impregnated fly ash catalyst (FA-1) showed a marginal increase in glycerol conversion (13%) with substantial increase in 1,2-PDO selectivity to 50%. In this case (FA-1), ethylene glycol formation was also to the extent of 15% due to C-C cleavage. Among other pretreated fly ash loaded with Cu catalysts, FA-4 showed the highest conversion of ~57% and a 1, 2-PDO selectivity as high as ~94% without formation of any acetol and ethylene glycol. The high activity of FA-4 must be due to the excellent dispersion of Cu^0 on the surface as evidenced by its surface area of 113 m^2g^{-1} (**Table 6.1**) and the low intensity peaks in XRD (**Figure 6.1, a**). However after the reaction, separation of brown coloured Cu particles was observed in the case of FA-4, indicating its lower stability under the

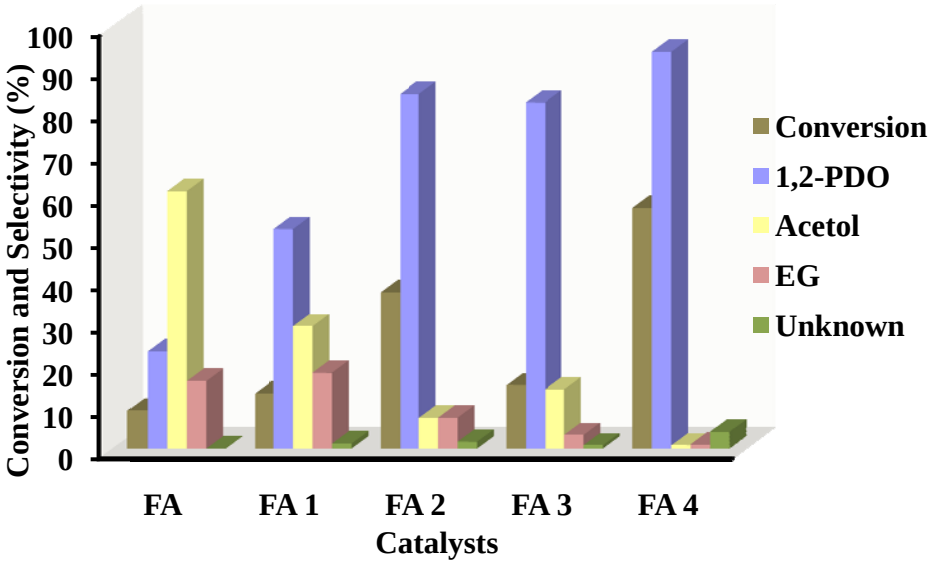

Figure 6.5. Catalyst screening for glycerol hydrogenolysis.

Reaction conditions: Glycerol, 20 wt%; 2-propanol, 80 wt%; catalyst, 1 g; temperature, 220 ^{o}C; H_2 pressure, 52 bar; reaction time, 5 h; total reaction volume, 100 mL.

reaction conditions. Further studies on the characterization of the recovered catalyst are required to ascertain the leaching of Cu. The second best performance was observed for alkali fused fly ash impregnated with Cu (FA-2) giving a glycerol conversion of 37% with 84% selectivity to 1, 2-PDO along with formation of both acetol and ethylene glycol (< 10%). The activity of FA-2 also could be due to its higher surface area (61 $m^2 g^{-1}$) and better dispersion of Cu on the surface. Acid pretreated fly ash impregnated with Cu (FA-3) did not show any appreciable increase in activity as compared to non- pretreated fly ash impregnated with Cu (FA-1). This is also consistent with its surface area of 40 $m^2 g^{-1}$, which is similar to that of FA-1 and lower than those of FA-4 and FA-2. These results for the various Cu-fly ash catalysts clearly indicate that the fly ash pretreatment with alkali caused excellent dispersion of Cu phase on the surface leading to higher activity for selective glycerol hydrogenolysis.

Further studies such as the role of solvent, Cu loading and temperature effects on glycerol conversion and 1,2-PDO were investigated using FA-2 due to its stability under reaction conditions. Glycerol conversion decreased by almost half (20%) in water with same 1,2-PDO selectivity (85%) as compared to that in 2-propanol and hence, 2-propanol

is a suitable solvent for glycerol hydrogenolysis.

The effect of Cu loading was studied by varying Cu content in the range of 0.33-3 fold with respect to Al content in the fly ash and the results are shown in **Figure 6.6.** An increase in Cu loading by two fold (Al: Cu, 1:2) resulted in marginal increase in both glycerol conversion from 37 to 42% and 1,2-PDO selectivity from 84 to 90%. With further increase in Cu loading by 3 folds, glycerol conversion decreased below 27% with 1,2-PDO selectivity remaining constant at 90%. The higher Cu content might have resulted in lower dispersion of Cu on the surface as discussed above. Decreasing Cu loading by half (Al: Cu, 1:0.5) caused a substantial decrease in glycerol conversion to below 10% as well as a marginal decrease in 1,2-PDO selectivity to <82%. Further decrease in Cu content (Al: Cu, 1:0.33) did not affect glycerol conversion but caused a decrease in 1,2-PDO selectivity (<70%) with substantial accumulation of acetol and formation of EG and other products. The performance of the lowest Cu containing fly ash

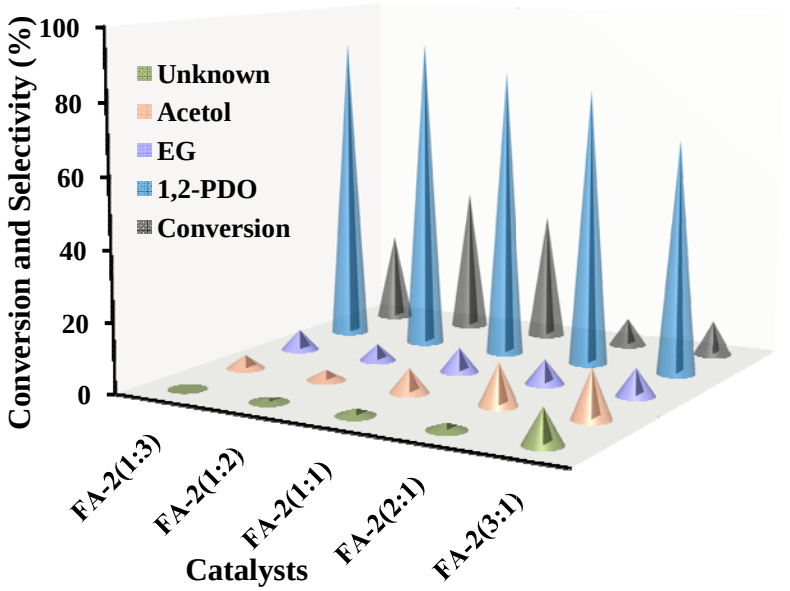

Figure 6.6. Effect of Al:Cu ratio in Cu modified fused fly ash on glycerol hydrogenolysis.

Reaction conditions: glycerol, 20 wt%; 2-propanol, 80 wt%; catalyst, 1 g; temperature, 220 ^{o}C; H_2 pressure, 52 bar; reaction time, 5 h; total reaction volume, 100 mL.

catalyst was similar to that of parent fly ash without Cu (**Figure 6.5**) indicating that the minimum Cu content required for the optimum performance was equimolar to the Al content in the fly ash.

Figure 6.7 shows the effect of temperature on glycerol conversion and 1, 2-PDO selectivity for the FA-2 (1:1) catalyst. As temperature was increased from 200 to 220 ^{o}C, conversion of glycerol increased from 14 % to 37% with a slight decrease in 1, 2-PDO selectivity from 84-80%. With a further increase in temperature to 240 ^{o}C, an increase in glycerol conversion from 37% to 54% occurred which was accompanied by a significant decrease in selectivity of 1,2-PDO from 85% to 77%. Thus, 220 ^{o}C was considered as an optimum temperature for hydrogenolysis of glycerol to 1,2-PDO for Cu modified fly ash catalyst.

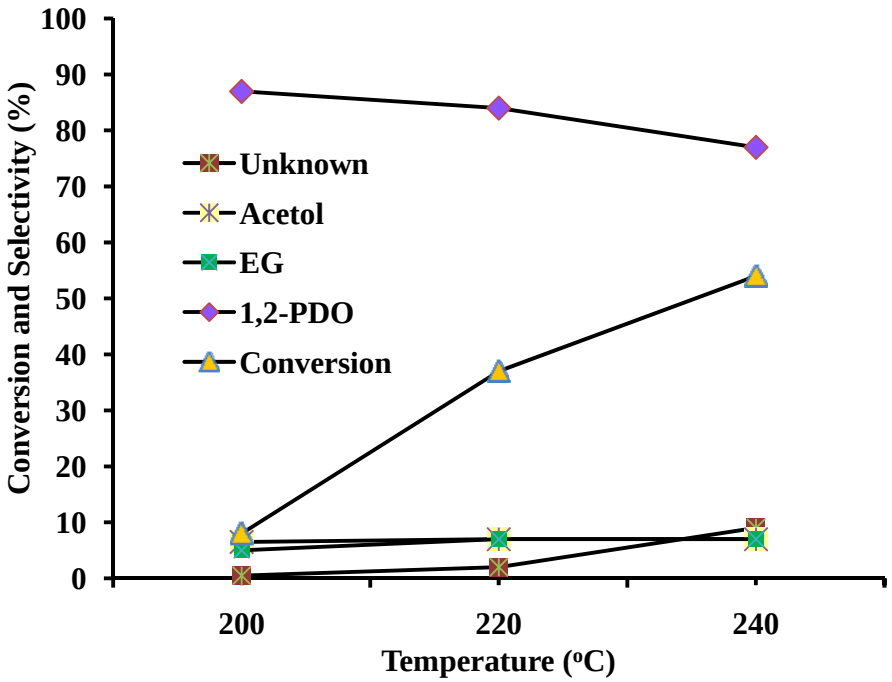

Figure 6.7. Effect of temperature on glycerol hydrogenolysis.

Reaction conditions: Glycerol, 20 wt%; 2-propanol, 80 wt%; catalyst, 1 g; H_2 pressure, 52 bar; reaction time, 5 h; total reaction volume, 100 mL.

6.4. CONCLUSIONS

- The waste fly ash in its original form showed measurable activity for glycerol dehydration to acetol due to its inherent content of components such as Al_2O_3, MgO, K_2O, Na_2O *etc*.
- In order to enhance the hydrogenolysis activity of waste fly ash, it was further modified systematically in two ways: (i) by alkali /acid pretreatment with the aim to increase its surface area and (ii) loading an active glycerol hydrogenolysis catalyst such as Cu.
- Cu impregnated non-pretreated fly ash was responsible for the accumulation of first step glycerol dehydration and C-C cleavage products acetol and EG, respectively. However, alkali pretreated fused fly ash with Cu (FA-2, Al:Cu=1:1) showed the highest activity and 1,2-PDO selectivity (>85%) in glycerol hydrogenolysis.
- The higher and stable activity of FA-2 was due to transformation of α-quartz to the tridymite phase of SiO_2 and very high dispersion of Cu on to its surface as characterized by XRD, BET and TEM.
- The effect of Cu loading on fused fly ash showed that Al: Cu > 1:2 caused a decrease in glycerol conversion by ~40% due to aggregation of Cu on the surface.
- A ratio Al: Cu of < 1:1 substantially decreased both the glycerol conversion and the 1,2-PDO selectivity indicating that a critical Cu loading is responsible for the hydrogenolysis activity.
- This study demonstrates that the reuse of a waste fly ash modified with an inexpensive metal such as Cu can make an economically viable process for 1,2-PDO.

6.5. REFERENCES

1. R. B. Mane, A. M. Hengne, A. A. Ghalwadkar, S. Vijayanand, P. H. Mohite, H. S. Potdar, C. V. Rode, *Catal. Lett.* **2010,** 135, 141-147.
2. R. B. Mane, C. V. Rode, *Org. Process Res. Dev.* **2012**, 16, 1043-1052.
3. R. B. Mane, S. E. Kondawar, P. S. Niphadkar, P. N. Joshi , K. R. Patil, C.V. Rode, *Catal. Today* **2012**,198,321-329.
4. D. Jain, C. Khatri, A. Rani, *Fuel Process. Technol.* **2010,** 91, 1015-1021.
5. R. J. Haynes, *J. Environ. Manage.* **2009,** 90, 43-53.
6. O. M. Dunens, K. J. Mackenzie, A.T. Harris, *Environ. Sci. Technol.* **2009,** 43, 7889-7894.
7. J. G. P. Born, P. Mulder, R. Louw, *Environ. Sci. Technol.* **1993,** 27, 1849-1863.
8. X. Xuan, C. Yue, S. Li, Q. Yao, *Fuel* **2003,** 82, 575-579.
9. C.V. Rode, R. B. Mane, A. S. Potdar, P. B. Patil , P. S. Niphadkar, P. N. Joshi, *Catal. Today* **2012,** 190, 31-37.
10. M. S. Kotwal, P. S. Niphadkar, S. S. Deshpande, V. V. Bokade , P. N. Joshi, *Fuel* **2009,** 88, 1773-1778.
11. S. B. Holmquist, *J. Am. Ceram. Soc.* **1961,** 44, 82-86.
12. T. J. Rockett, W. R. Foster, *Am. Mineralogist* **1967,** 52, 1234-1240.
13. Y. Shinohara, N. Kohyama, *Ind. Health* **2004,** 42, 277-285.
14. Z. Huang, F. Cui, H. Kang, J. Chen, X. Zhang, C. G. Xia, *Chem. Mater.* **2008,** 20, 5090-5099.
15. M. Morbidelli, A. Gavriilidis, A. Varma, *Catalyst design: Optimal distribution of catalyst in pellets, reactors and membranes*, Cambridge University, **2005,** p. 43.
16. E.P. Maris, W. C. Ketchie, M. Murayama, R.J. Davis, *J. Catal.* **2007,** 251, 281-294.
17. E.P. Maris, R. J. Davis, *J. Catal.* **2007,** 249, 328-337.

Chapter 7

Simultaneous glycerol dehydration and *in situ* hydrogenolysis over Cu-Al oxide under an inert atmosphere

Cheaper, safer, greener glycerol hydrogenolysis without external hydrogen was successfully accomplished over Cu-Al oxide catalyst under inert atmosphere due to its multifunctional ability of catalyzing dehydration, aqueous phase reforming, WGS and hydrogenation reactions simultaneously. Evidences of various active species such as Cu^{2+} in the form of CuO and $CuAl_2O_4$, along with Cu^0, Cu^{1+} were shown by the detailed catalyst characterization studies. Based on the activity and characterization results, a reaction pathway involving hydrogen generation through glycerol APR and its utilization for hydrogenation is also proposed. Our catalyst exhibited a consistent activity of 400 h for autogeneous hydrogenolysis of refined glycerol with 36% selectivity to 1,2-propanediol (1,2-PDO) which enhanced to 75% for an aqueous bio-glycerol feed.

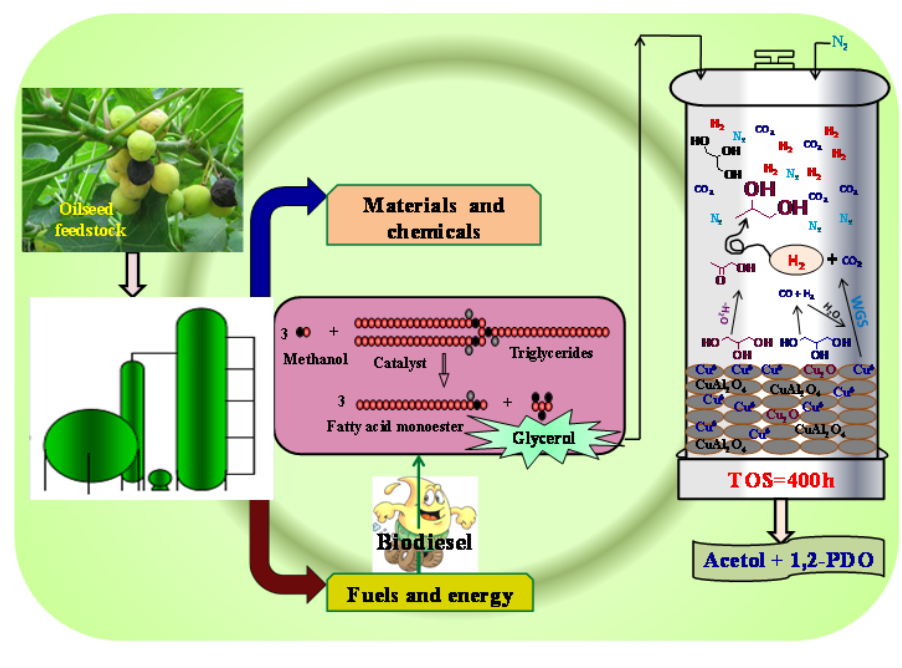

***Green Chem.* 2012, 14, 2780-2789**

7.1. INTRODUCTION

Hydrogen being a clean energy source, has been also attempted to be produced from biomass derived molecules containing C:O ratio of 1:1.[1-3] Glycerol, one of the simplest biomass derived molecule containing C:O = 1:1 is capable of generating hydrogen through its aqueous phase reforming (APR).[4] However, the latest economic assessment shows that the ratio of sale price to production cost for only hydrogen generation from glycerol is 1.05 which is much lower than that for 1,2-PDO production (1.57).[5]

Several types of catalyst systems have been reported for direct hydrogenolysis of glycerol to 1,2-PDO which have been already discussed in previous chapters.[6-12] In spite of few optimum catalyst systems being identified for glycerol hydrogenolysis to 1,2-PDO, the use of high pressure fossil derived hydrogen is one of the major limitation for the commercial prospective of such processes. In order to overcome this problem, D'Hondt *et al.* first reported platinum catalyzed glycerol hydrogenolysis using *in situ* hydrogen generated by aqueous phase reforming (APR) of glycerol.[13] This was followed by few other reports on supported Pt in combination with Ru and Sn, and RANEY® Ni catalysts for glycerol hydrogenolysis without using external hydrogen.[14-16] However, the prohibitive high cost, scarce availability of noble metals, their favored activity for alkane formation and relatively high selectivity to EG for nickel catalyst need to be overcome. Our Cu-Al catalyst, which showed excellent activity for glycerol dehydration and hydrogenolysis [17,18] is reported for the first time for *in situ* glycerol hydrogenolysis utilizing H_2 generated by glycerol APR under inert conditions and details of these results are discussed in this chapter.[19] Distinct spinel $CuAl_2O_4$ phase formation was identified even at low calcination temperature (400 ^oC) due to Cu-Al formulation prepared by the simultaneous co-precipitation and digestion technique. Multifunctional characteristics of this catalyst were found to be responsible for its uninterrupted *in situ* hydrogenolysis performance of 450 h using refined glycerol as well as bio-glycerol feed directly without any pretreatment.

7.2. EXPERIMENTAL

Cu-Al and 20% Cu/Al_2O_3 catalysts were prepared by simultaneous co-precipitation and

impregnation methods and the details of their preparation have been described in chapter 2 (sections 2.3.3 and 2.3.10). 3% Pt/C catalyst was purchased from Sigma-Aldrich, Bangalore, India. The catalysts were characterized by various techniques and a characterization procedures are described in chapter 2 (section 2.4). EDX of the activated catalyst confirmed the presence of Cu and Al (**Figure 7.1**). The activity testing of prepared catalysts for *in situ* glycerol hydrogenolysis to 1,2-PDO was carried out in both batch as well as continuous fixed bed reactors and its detailed experimental procedure is described in chapter 2 (sections 2.5.1 and 2.5.2).

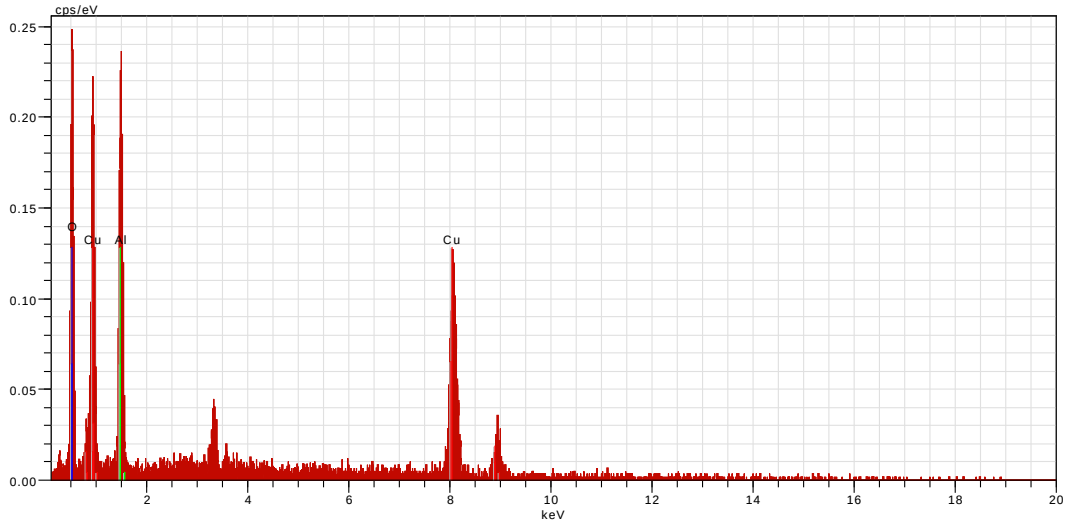

(a)

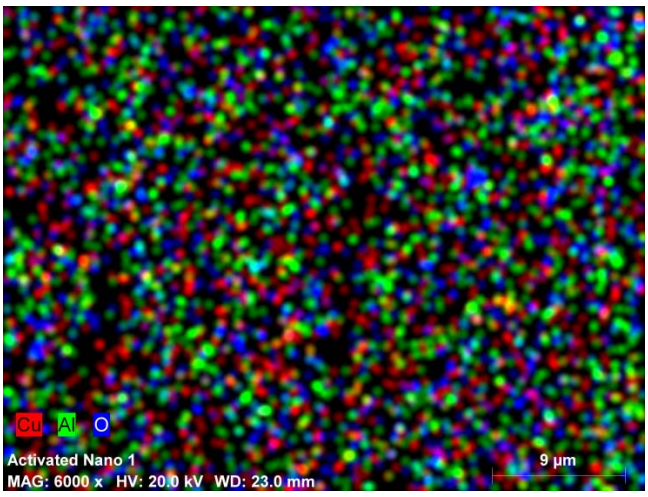

(b)

Figure 7.1. EDX of (a) Cu-Al catalyst (b) elemental map.

7.3. RESULTS AND DISCUSSION

7.3.1. Catalyst characterization

As our Cu-Al catalyst showed the excellent activity and selectivity for *in situ* hydrogenolysis of glycerol to 1,2-PDO under an inert atmosphere, its detailed characterization is discussed below.

Table 7.1 shows BET specific surface area and pore volume of calcined, reduced, used and pretreated used Cu-Al catalyst samples. Both the surface area and pore volume of the activated sample marginally decreased from 74 m^2g^{-1} (calcined) to 70 m^2 g^{-1} and from 0.60 to 0.55 m^3 g^{-1}, respectively. The mesoporous nature of the material was evidenced by a type IV, N_2 adsorption-desorption isotherm in which capillary

Table 7.1. Textural properties and ICP results of Cu-Al catalyst samples

Catalysts	BET surface area (m^2 g^{-1})	Pore volume (ml g^{-1})	Crystallite size from XRD (nm)	Wt% of Cu by ICP
Calcined	74	0.60	Amorphous nature	49.5
Reduced	70	0.55	15	52.8
Used and washed	23	0.064	40	52.4
Used, washed, recalcined and reactivated at 200 ^oC	56	0.245	27	-

condensation took place at higher pressures of adsorbate in addition to multilayer adsorption at lower pressures (**Figure 7.2**). The decrease in surface area of activated sample was due to the incorporation of Cu into the lattice of Al_2O_3 to form $CuAl_2O_4$ during the reduction process under H_2 at 200 ^oC for 12 h. This was further confirmed by XRD, XPS and other characterization techniques, the results of which are discussed below. About 70% decrease in surface area as well as 10-fold decrease in pore volume of

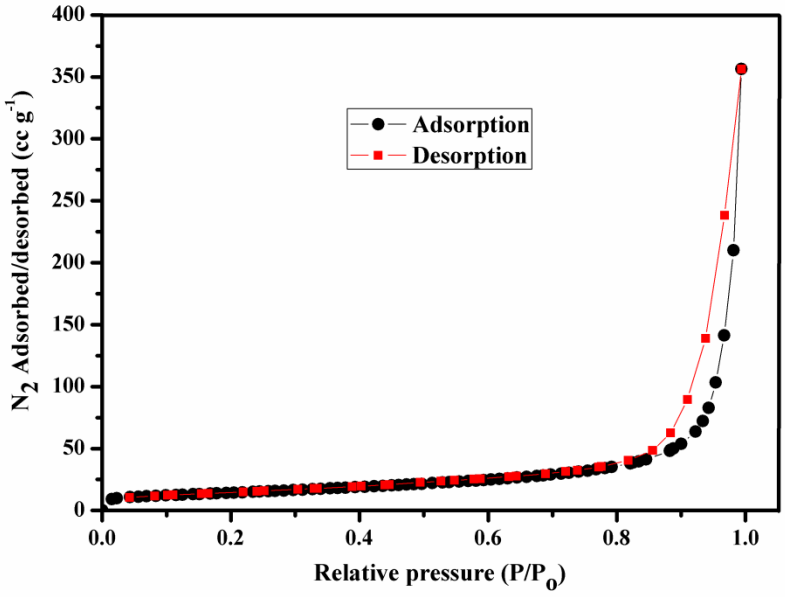

Figure 7.2. N_2 adsorption/desorption isotherm of reduced Cu-Al catalyst.

the used catalysts (after 450 h) was observed as compared to the fresh reduced sample. This was in accordance with the XRD results showing increase in crystallite size from 15 to 40 nm as a result of sintering of the Cu particles (**Table 7.1**) due to a long exposure of the catalyst to high temperature. The crystallite size of the used catalyst, after pretreatment of calcination and reduction, decreased substantially and was quite close to that of the fresh activated catalyst. This indicates that calcination followed by activation protocols caused the redispersion of Cu on the surface.[20] The weight percentage of Cu in the activated catalyst analyzed by ICP was 52.8%, close to the nominal percentage of 50%, used for the preparation. Copper content in the used sample was found to be almost same (52.4 %) as that in the fresh sample, confirming metal leaching did not occur under the reaction conditions.

Figure 7.3 shows the XRD patterns of calcined, reduced and used (after 450 h) samples of Cu-Al catalyst. The diffraction peaks at $2\theta = 35.7^o$ and 38.8^o confirmed the presence of CuO [(111) JCPDS file no. 80-1268] and $CuAl_2O_4$ [(222) JCPDS file no. 73-1958] phases respectively. The activated sample showed additional peaks at $2\theta = 43.5^0$ (111), 50.7^o (200) and 74.2^o (220) for metallic Cu (JCPDS file no. 85-1326) along with CuO, $CuAl_2O_4$ and Cu_2O [$2\theta = 36.6^o$, (101)] (JCPDS file no. 75-2357) phases with higher intensities, indicating higher crystallinity as compared to that of a calcined sample.

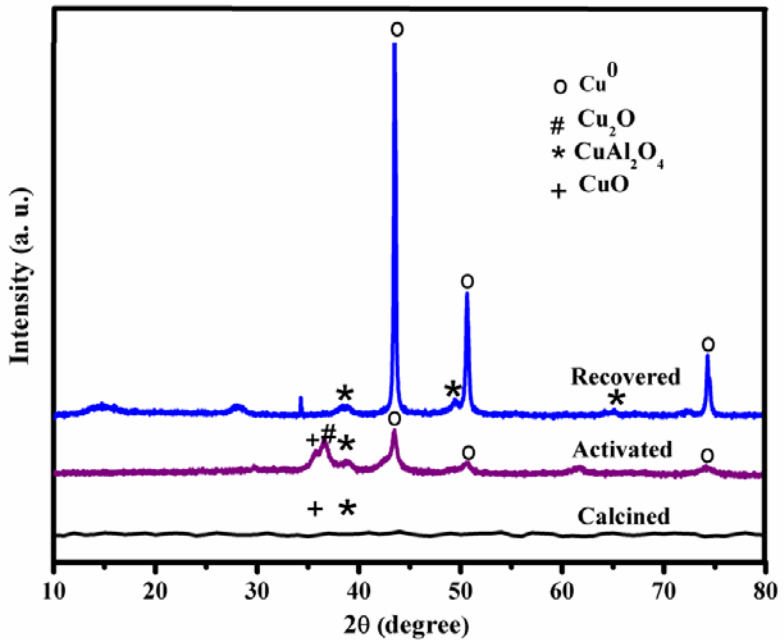

Figure 7.3. XRD patterns of Cu-Al catalyst samples.

This change in phase compositions was due to the sequential reduction of Cu^{2+} to Cu^0 *via* Cu^{1+} during activation protocol. The co-existence of Cu^0 and Cu^{1+} could be visualized either separately as a layer of Cu_2O on metallic Cu with oxygen vacancies exposing Cu^{1+}, or as Cu_2O/Cu^0 interfacial sites.[21] The complete disappearance of CuO and Cu_2O and appearance of metallic Cu phases in the recovered sample confirmed the reduction of Cu oxide species under reaction conditions.[22] This is also the evidence of atomic hydrogen being generated by glycerol APR. The higher peak intensity of metallic copper in the recovered sample could be attributed to the sintering of Cu causing increase in its crystallite size to 40 nm. The retention of $CuAl_2O_4$ phase in the recovered sample indicates the stability of this phase even after a prolonged exposure of the catalyst in presence of hydrogen.[22] These features of the Cu-Al catalyst have contributed to its excellent and longer TOS activity for *in situ* hydrogenolysis of glycerol to 1,2-PDO.

HR-TEM images of the activated Cu-Al catalyst in **Figure 7.4** (**a and b**) showed the spherical morphology of the particles having a diameter of 8-10 nm. The characteristic planes obtained from the '*d*' spacings of the fringe patterns (**Figure 7.4, c**) were found to be (111), (101) and (222) which matched with the XRD characterization, confirming the presence of Cu^0, Cu^{1+} and $CuAl_2O_4$ phases in the Cu-Al catalyst. The

same phases were also confirmed from the SAED image shown in **Figure 7.4 (d)**.

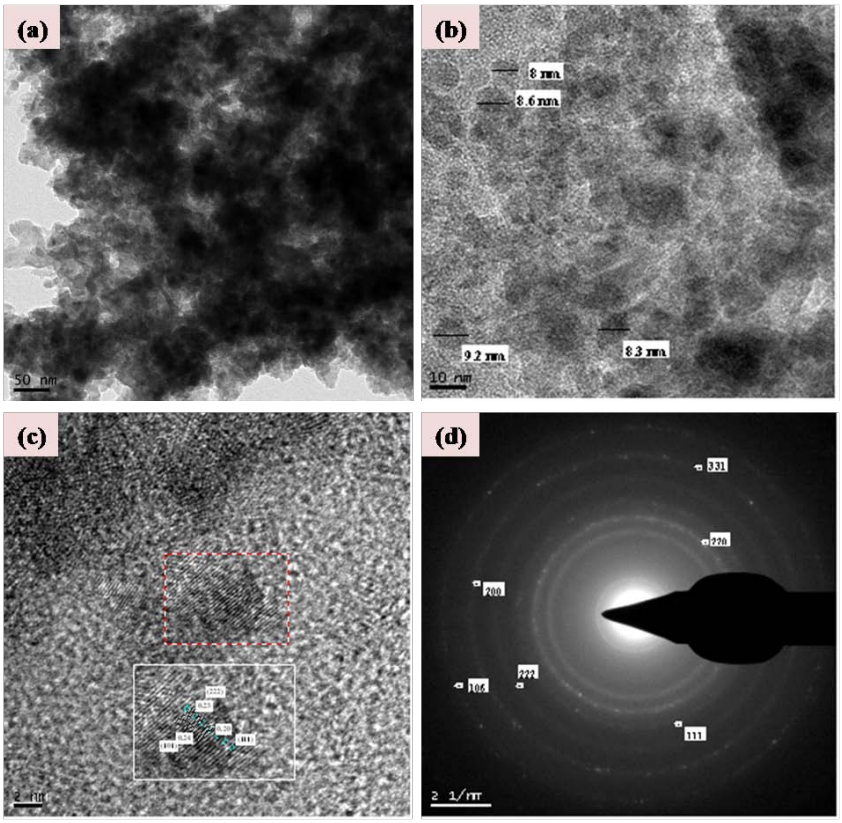

Figure 7.4. (a) HR-TEM image of Cu-Al catalyst (b) High magnification image showing 8-10 nm particles (c) High magnification image showing fringes (d) SAED image showing planes of Cu.

Cu 2*p* XPS of calcined and reduced Cu-Al catalyst samples are shown in **Figure 7.5 (a),** in which a broad peak observed in the range of 932-935 eV was due to the presence of various Cu species. A satellite peak at 940-946 eV was indicative of Cu^{2+} in the fully oxidized copper species such as CuO and $CuAl_2O_4$ in both the samples. The wide Cu $2p_{3/2}$ signals obtained for the calcined sample could be fitted satisfactorily to two principal peaks after deconvulation as shown in **Figure 7.5** (**b**). The predominant peak at 933.6 eV was assigned to Cu^{2+} of CuO, which is obviously due to its formation during calcination. Interestingly, another peak at 935 eV in **Figure 7.5** (**b**) was also due to Cu^{2+}, but from spinel $CuAl_2O_4$.[23] The same sample after activation in hydrogen at 200 ^oC for 12 h showed the presence of three peaks of different binding energies namely, 932.7 eV,

933.8 eV and 935 eV corresponding to metallic Cu and Cu^{2+} in CuO and $CuAl_2O_4$ respectively (**Figure 7.5, c**). This indicates the incomplete reduction of the catalyst under H_2 activation which was also supported by TPR studies, discussed later. At the same time, increase in the intensity of the peak at 935 eV, due to Cu^{2+} points out that the activation protocol enhances the $CuAl_2O_4$ formation. As the binding energies of Cu^0 and Cu^{1+} are indistinguishable, the presence of Cu^{1+} in the activated sample cannot be ruled out. This commensurates with the XRD pattern and is also expected from the step wise reduction of Cu^{2+} to Cu^0.

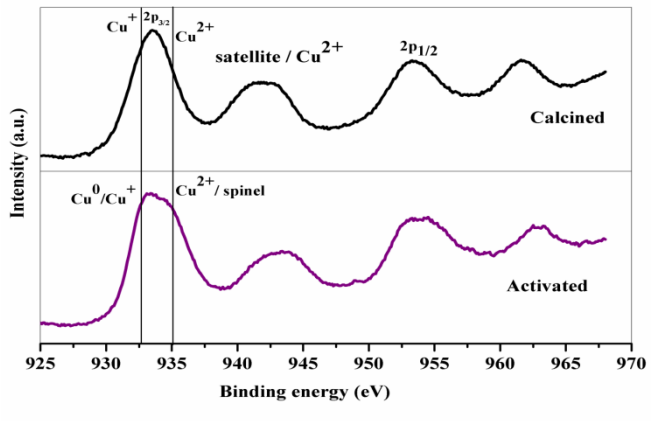

(a)

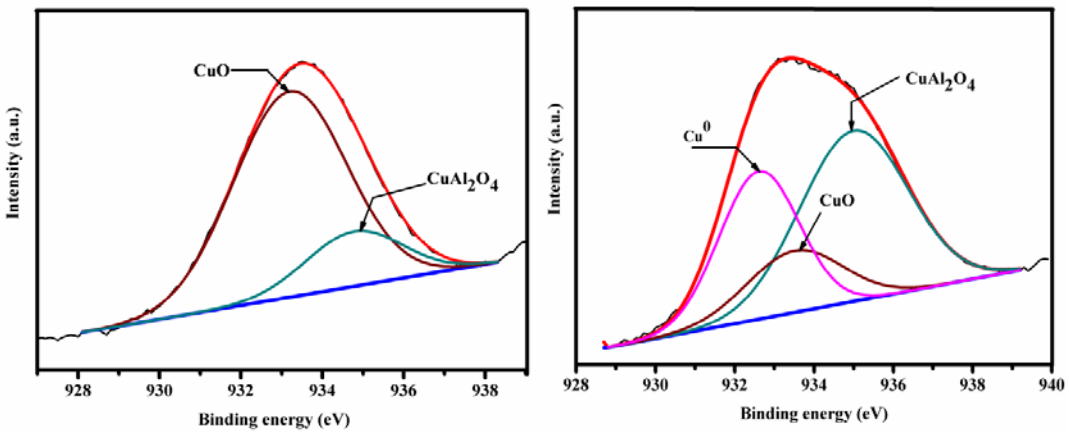

(b) **(c)**

Figure 7.5. XPS spectra of Cu-Al catalyst (a) calcined and activated samples (b) deconvulated Cu $2p_{3/2}$ spectra of calcined sample (c) deconvulated Cu $2p_{3/2}$ spectra of activated sample.

In order to distinguish between the type of Cu oxide being formed in calcination and activation protocols, the relative intensity ratios of Cu species from XPS spectra were calculated and are presented in **Table 7.2.** The higher intensity ratio of 4.36 of CuO indicates most of the Cu^{2+} is in the form of CuO in calcined sample. On the other hand, a ten times higher $CuAl_2O_4$ intensity ratio than that of CuO indicates that the majority of Cu is in the form of $CuAl_2O_4$ in the reduced catalyst. From these observations, it can be inferred that spinel $CuAl_2O_4$ is formed by the diffusion of Cu^{2+} into the lattice of Al and/or the strong interaction of Cu^{2+} with the Al hydroxide.[24] The intensity ratio of Cu^0 to Cu^{2+} in CuO was more than 3 times higher than that in $CuAl_2O_4$ which means that reduction of CuO was more facile than $CuAl_2O_4$.[25]

Table 7.2. XPS results of calcined and activated Cu-Al catalyst

	Relative intensity ratio			
Catalyst	**$CuAl_2O_4$ / CuO**	**CuO/ $CuAl_2O_4$**	**Cu^0/Cu^{2+} in $CuAl_2O_4$**	**Cu^0/Cu^{2+} in CuO**
Calcined	0.22	4.36	-	-
Reduced	3.1	0.31	0.64	2.1

This was also confirmed by TPR studies, discussed later. In accordance with the formation of $CuAl_2O_4$, the shift of O1*s* and Al 2*p* peaks was observed from 530.3 eV to 531.5 eV and from 73.6 eV to 74.7 eV respectively (**Figures 7.6, a and b**).[25] The XPS of Al was associated with a tailing due to the interference of Cu 3*p*.

FT-IR of reduced sample showed the absorption peak at 3471.58 cm^{-1} , which is due to longitudinal vibration of water, while the absorption peak at 1540.85 cm^{-1} belonged to bending vibration of H-O-H in the water (**Figure 7.7**). The peaks in the range of 850-500 cm^{-1} were ascribed to Cu-O-Al, Al-O-Al, longitudinal vibrations in $CuAl_2O_4$. [26,27]

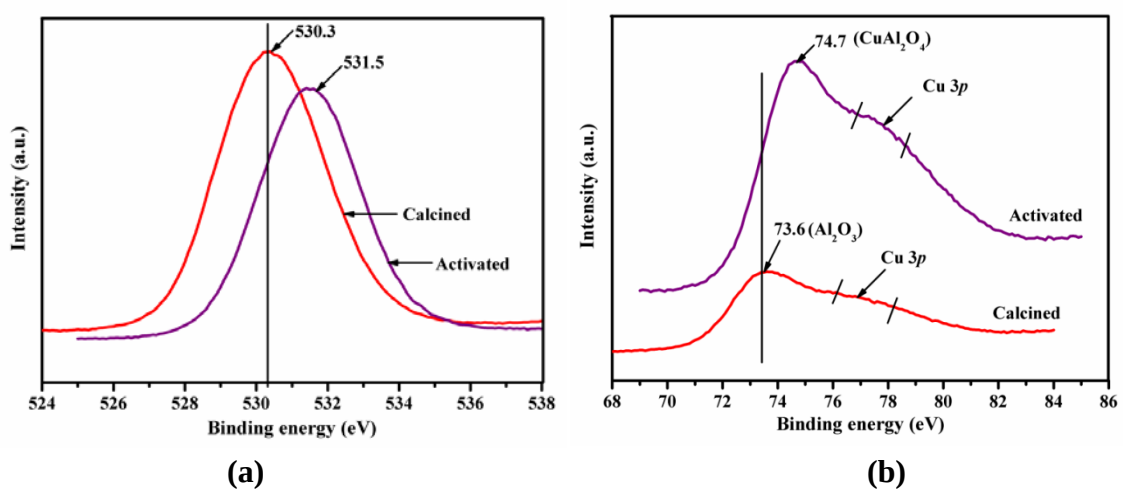

Figure 7.6. XPS spectra of the calcined and reduced Cu-Al catalyst (a) O 1*s* (b) Al 2*p*.

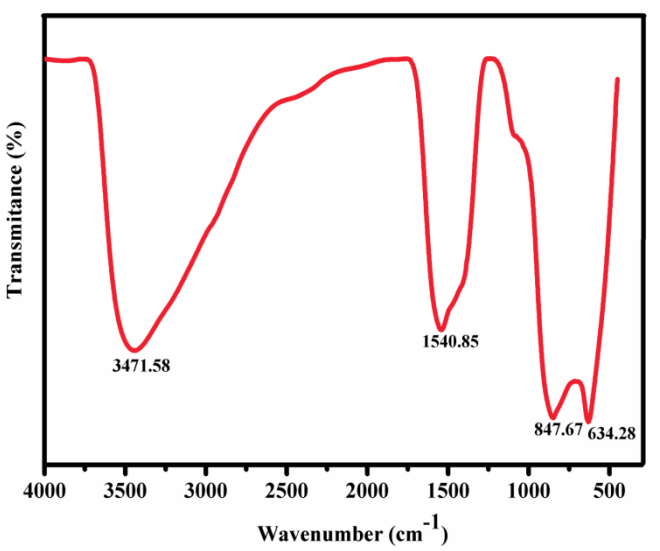

Figure 7.7. FT-IR spectra of Cu-Al catalyst.

The DTA thermogram of dry Cu-Al catalyst shown in **Figure 7.8**, reveals the first endothermic weak peak at 100 ^{o}C due to the loss of free water molecule. Another endothermic peak around 190 ^{o}C was due to the water/hydroxyl loss from the lattice. The broad exothermic peak between 200-700 ^{o}C represents the transformation of Cu hydroxide/nitrate to form CuO and $CuAl_2O_4$.[28,29] The thermogram (TG) was flat after 700 ^{o}C suggesting that the formation of stable oxides of Cu, such as CuO and spinel type

$CuAl_2O_4$. This result concurred with the findings of XRD and XPS which clearly showed the presence of CuO and $CuAl_2O_4$.

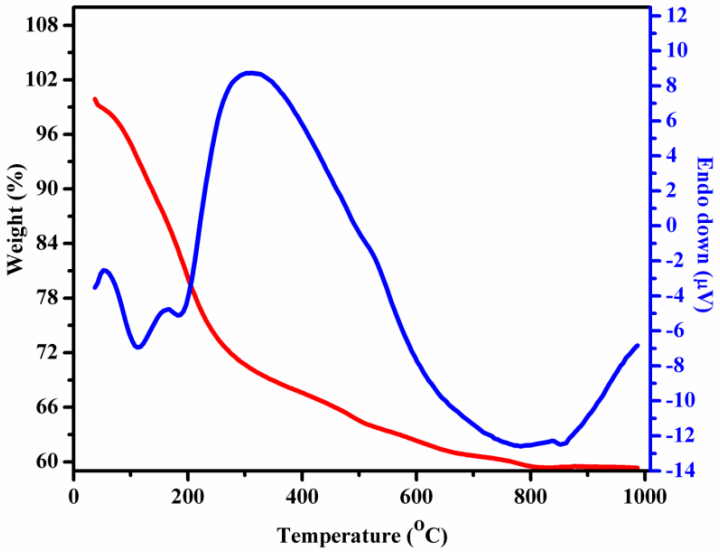

Figure 7.8. TG-DTA curves of Cu-Al catalyst.

The reduction behaviour of the calcined and activated Cu-Al catalyst was studied by H_2-TPR characterization and the respective profiles are shown in **Figure 7.9**. The calcined sample showed a single broad peak over the region of 180-200 ^oC due to the reduction of CuO. While in the reduced sample more intense reduction peaks were observed at temperatures higher than that from the calcined sample. The first reduction peak at about 230 ^oC, was assigned to the reduction of bulk CuO while another peak at a higher temperature of 352 ^oC comes from the reduction of Cu^{2+} in spinel $CuAl_2O_4$.[30] This also implies that the activated Cu-Al was not completely reduced to metallic Cu, even after reduction at 200 ^oC for 12 h. These results are in excellent agreement with the XRD and XPS studies.

Pyridine adsorption-desorption spectra of activated Cu-Al catalyst in the temperature range of 100-375 ^oC are shown in **Figure 7.10**. The spectra showed a single distinct peak at 1539 cm^{-1} that clearly confirms the presence of only BrØnsted acid sites. As the desorption temperature increased from 100-375 ^oC additional peaks at higher wave numbers were observed due to the ring vibrations of the pyridinium ion. After degassing at 375 ^oC, peak at 1539 cm^{-1} diminished while the peak appearing at 1552 cm^{-1}

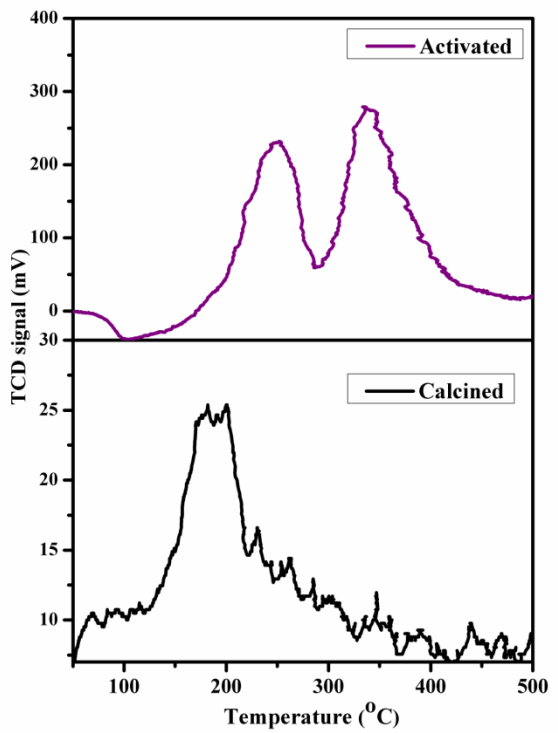

Figure 7.9. H_2-TPR profiles of calcined and activated Cu-Al catalyst.

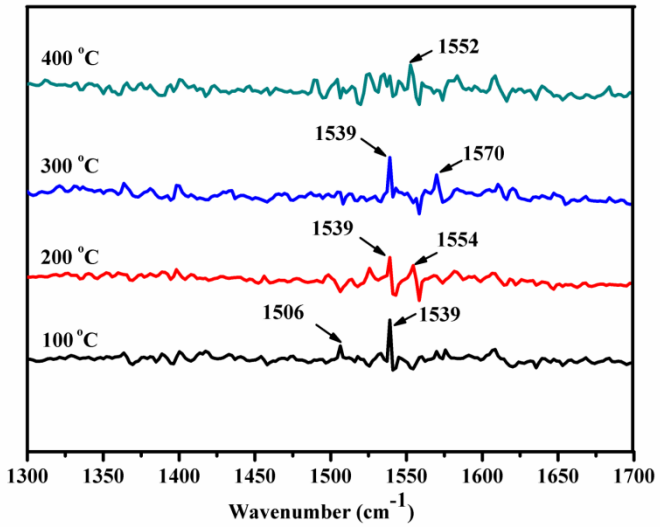

Figure 7.10. Py-IR of Cu-Al catalyst at various desorption temperatures.

Represents the residual pyridine on the BrØnsted acid sites.[31] The total concentration of acid sites was found to be 1.57 mmol g^{-1}, by NH_3-TPD measurements. CO_2- TPD of our catalyst showed two peaks at 190 °C and 280 °C indicating moderate basicity due to

surface hydroxyl groups **(Figure 7.11)**.[32]

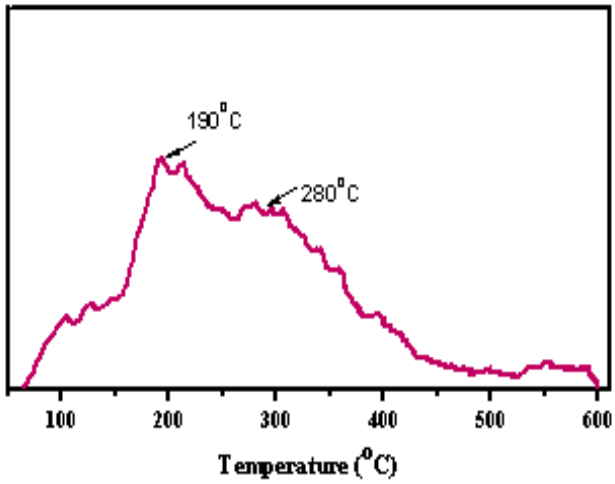

Figure 7.11. CO_2-TPD profile of the reduced Cu-Al catalyst.

7.3.2. Catalyst activity

The performance of Cu-Al catalyst along with other catalysts for glycerol dehydration under an inert atmosphere of nitrogen is shown in **Table 7.3**. The results are expressed in terms of carbon selectivity of liquid products, which was calculated as follows.

$$\text{C selectivity}\,(\%) = \frac{\text{Moles of individual product formed} \times \text{number of C atoms}}{\text{Moles of glycerol feed} \times \text{conversion} \times 3} \times 100$$

Cu-Al catalyst showed 24% conversion with 50% selectivity of total liquid products, indicating formation of gaseous products **(Table 7.4)**. Although acetol was the major liquid product (32%) as expected, however 1,2-PDO was also formed substantially with 18% selectivity. With increasing the catalyst loading to 3 g, a higher glycerol conversion of 51% and higher product selectivities of 36% and 24% to acetol and 1,2- PDO respectively, were obtained. On the other hand, much lower glycerol conversions of 10 and <2% were obtained for Cu/Al_2O_3 and Al_2O_3 alone, respectively, even at 230 ^oC. In both the cases, selective acetol formation was observed. Thus, the formation of 1,2-PDO under inert dehydration condition over Cu-Al indicated *in situ* hydrogen generation

Table 7.3. Catalyst screening for dehydration of glycerol under inert conditions

Catalysts	Catalyst wt (g)	Substrate	Temp. (^oC)	Conv. (mol %)	Selectivity (Carbon mole basis, %)		
					1,2-PDO	Acetol	Others
Cu-Al [a]	1	Glycerol	220	24	18	32	0.0
Cu-Al [a]	3	Glycerol	220	51	24	36	2
20% Cu/Al_2O_3 [a]	1	Glycerol	230	10	0.0	100	0.0
Al_2O_3 [a]	1	Glycerol	230	≤2	0.0	100	0.0
3%Pt/C [a]	0.5	Glycerol	220	59	9	2.3	<1
Cu-Al [b]	20	Glycerol	220	90	55	22	2.5
Cu-Al [b]	20	Glycerol	230	91	42	21	14
Cu-Al [a]	1	Acetol	220	73	0.0	0.0	100
Cu-Al [a]	1	1,2-PDO	220	40	0.0	17	16

Reaction conditions: [a] batch operation, reaction time, 3 h. [b] continuous operation at GHSV, 513 h^{-1}; LHSV, 1.53 h^{-1}.

Table 7.4. Gas phase analysis

Catalysts	Substrate	Temperature (^oC)	Gas phase composition (%)		
			H_2	CO_2	CH_4
Cu:Al (1:1)[a]	Glycerol	220	80	20	0.0
20% Cu/Al_2O_3 [a]	Glycerol	230	0.0	0.0	0.0
Al_2O_3 [a]	Glycerol	230	0.0	0.0	0.0
3%Pt/C [a]	Glycerol	220	86	8	6
Cu:Al (1:1)[b]	Glycerol	220	76	24	0.0
Cu:Al (1:1)[b]	Glycerol	230	80	20	0.0
Cu:Al (1:1) [a]	Acetol	220	0.0	0.0	0.0
Cu:Al (1:1) [a]	1,2-PDO	220	100	0.0	0.0

Reaction conditions: [a] batch operation, reaction time, 3 h. [b] continuous operation at GHSV,513 h^{-1}; LHSV, 1.53 h^{-1}.

followed by glycerol hydrogenolysis. As shown in **Scheme 7.1**, *in situ* H_2 generation is possible either by glycerol reforming or by dehydrogenation of glycerol to glyceraldehyde followed by its further dehydration to pyruvaldehyde.[33] Acetol was the only intermediate detected without observing any glyceraldehyde or pyruvaldehyde (the

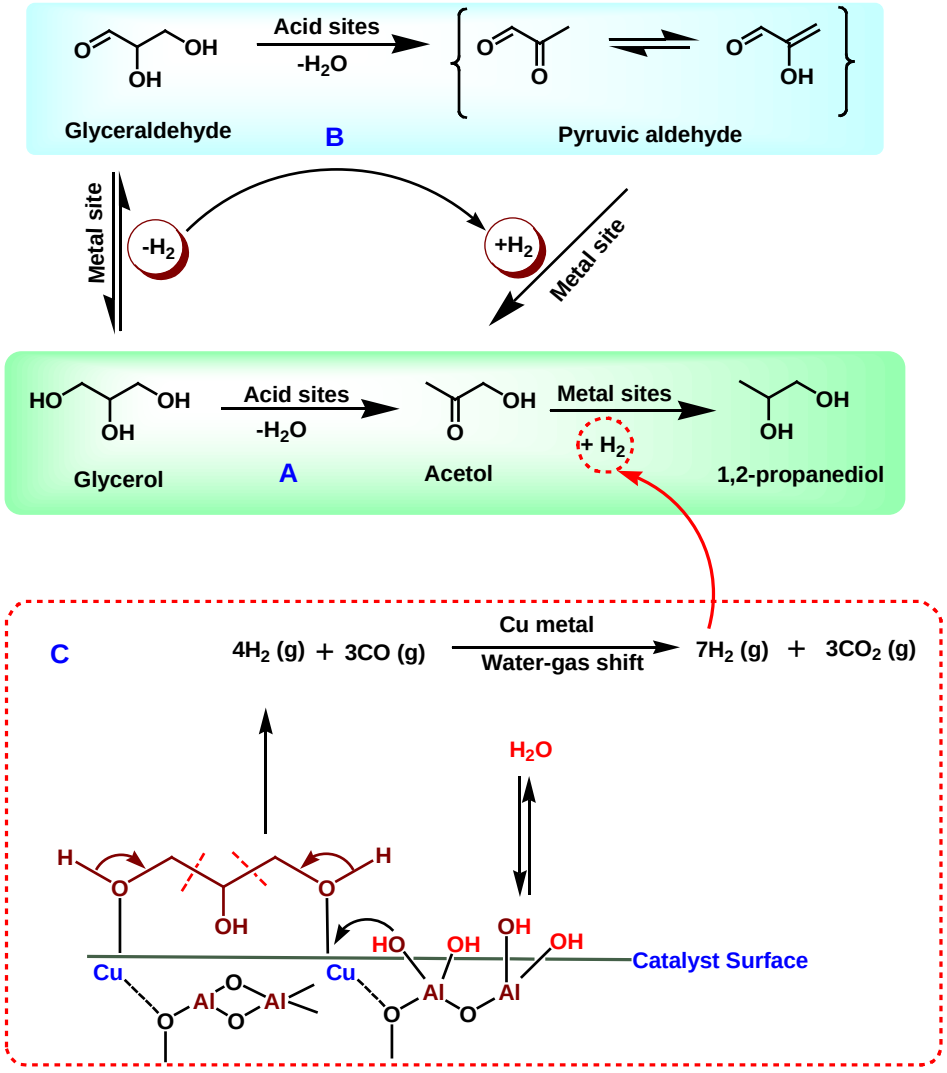

Scheme 7.1. Proposed reaction pathway for autogeneous hydrogenolysis of aqueous glycerol to 1, 2-propanediol over Cu-Al catalyst.

latter, if formed, underwent subsequent hydrogenation to acetol), thus giving the net hydrogen balance as zero (**route B**). Hence, the hydrogen utilized to give 1, 2-PDO from acetol under an inert atmosphere must be sourced from glycerol APR. In our proposed

mechanism, (**Scheme 7.1 C**), Cu and Al sites of the catalyst play distinct roles in glycerol reforming such that the water molecules are dissociatively adsorbed on Al sites, causing hydroxylation of the catalyst surface. This is followed by the transfer of hydroxyl groups to the adjacent Cu sites on which glycerol molecules are dissociatively adsorbed to give hydrogen and CO_2.[34] We propose here, formaldehyde as an intermediate (**Scheme 7.2**) [35] *via* Cu catalyzed dehydrogenation [36] and C-C cleavage of glycerol to give H_2 and CO, the latter is completely converted to CO_2 by WGS reaction on Cu sites under low temperature conditions (220 ^oC) of the present work.

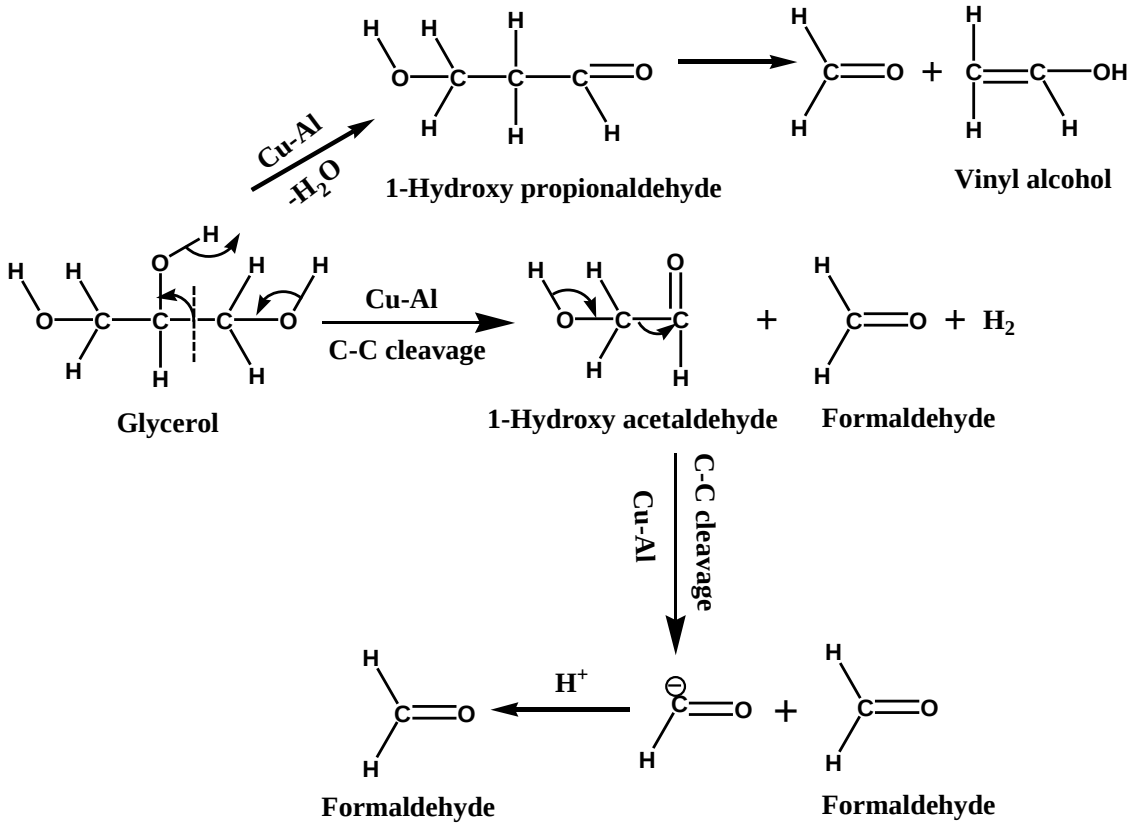

Scheme 7.2. Formaldehyde formation by C-C cleavage of glycerol under dehydration conditions.

Although Cu catalysts have not been directly reported for APR, since glycerol molecule has C-O ratio of 1:1, its APR is possible under lower temperature conditions, as observed

in our work.[37] *In situ* hydrogen generation *via* glycerol APR was confirmed by the gas phase analysis in which Cu-Al under various reaction conditions, gave only H_2 and CO_2 devoid of any CO and alkanes (**Figure 7.12**). The gas composition (**Table 7.4**) showed that the CO_2 obtained was lower than that from glycerol APR stoichiometry (70:30) due to its dissolution in water under reaction conditions to form carbonic acid, which was quantified by volumetric analysis, as shown in **Table 7.5.**

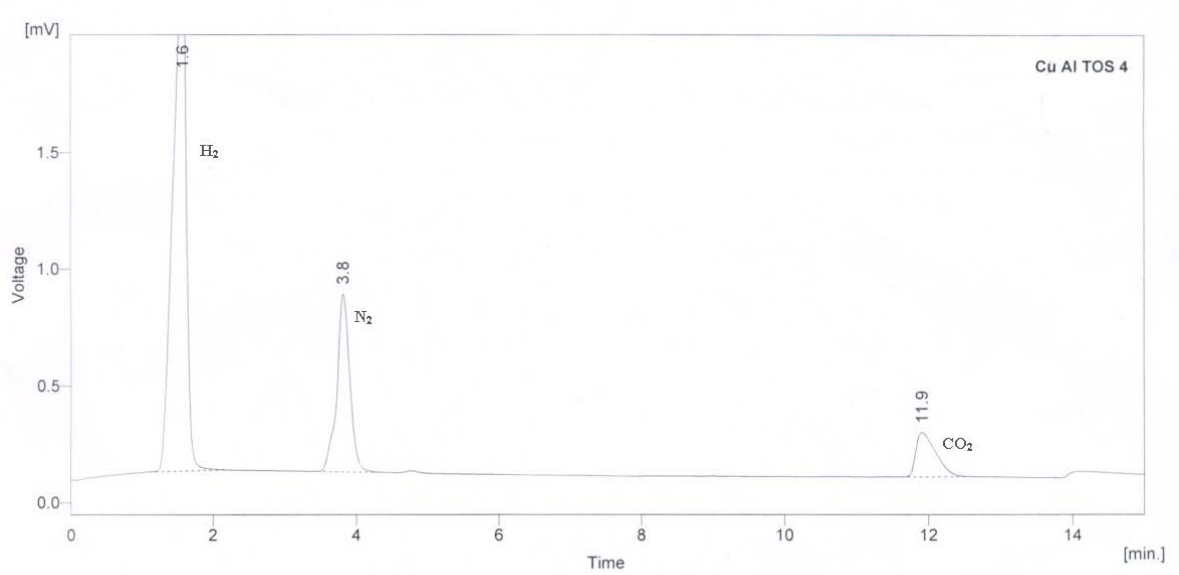

Result Table

	Reten. Time [min]	Area [mV.s]	Height [mV]	Area [%]	Height [%]	W05 [min]
1	1.583	575.781	45.897	68.4	70.7	0.20
2	3.820	192.816	15.253	22.9	23.5	0.18
3	11.907	73.018	3.807	8.7	5.9	0.31
	Total	841.615	64.957	100.0	100.0	

Figure 7.12. GC of gas phase composition (Cu-Al catalyst).

* N_2 was used as an inert in the reaction hence the compositions of other gases were calculated by excluding N_2.

Table 7.5. Carbonic acid formation as a function of reaction temperature

Temperature (^oC)	Normality (N)	Carbonic acid concentration (g)	CO_2 (%)
180	0.03	0.93	3.5
200	0.06	1.86	7
220	0.113	3.503	13.1
240	0.143	4.433	16.5

Glycerol reforming was also confirmed by considering the mole balance based on reducing equivalent of all the liquid products (acetol, 1,2-PDO and EG) formed, which showed that 0.1219 moles of glycerol were consumed in excess. This glycerol was converted to H_2 *via* APR and it was utilized for auto-hydrogenolysis to give 1,2-PDO.

Absence of any CO and CH_4 in the gas phase was due to the highly efficient $CuAl_2O_4$ phase formed (as confirmed by XRD and XPS discussed above), that is active towards water gas shift reaction at low temperature (220 ^oC).[38,39] In addition, WGS reaction is also more favorable and energetically faster as it involves a collision of two species rather than the collision of five species for CH_4 formation.[40] Unlike Ru and Pt catalysts, selective WGS reaction by suppressing CO reduction over Cu-Al catalyst results into higher availability of hydrogen for easy *in situ* hydrogenolysis of glycerol. In a separate experiment over 3% Pt/C catalyst, very low liquid product selectivity (~11 %) was observed and methane formation was also distinctly confirmed in the gaseous products (**Figure 7.13**).

Two additional dehydration experiments were carried out with acetol and 1,2-PDO as starting materials. 73% conversion of acetol was obtained with complete selectivity to isomerisation and C-C cleavage products (**Scheme 7.3**) *viz.* propionic and acetic acids without formation of 1,2-PDO indicating acetol did not undergo any reforming as its C-O ratio is <1. As shown in **Scheme 7.3**, pathway I is desirable for glycerol dehydration to give acetol followed by its further hydrogenation to 1,2-PDO and

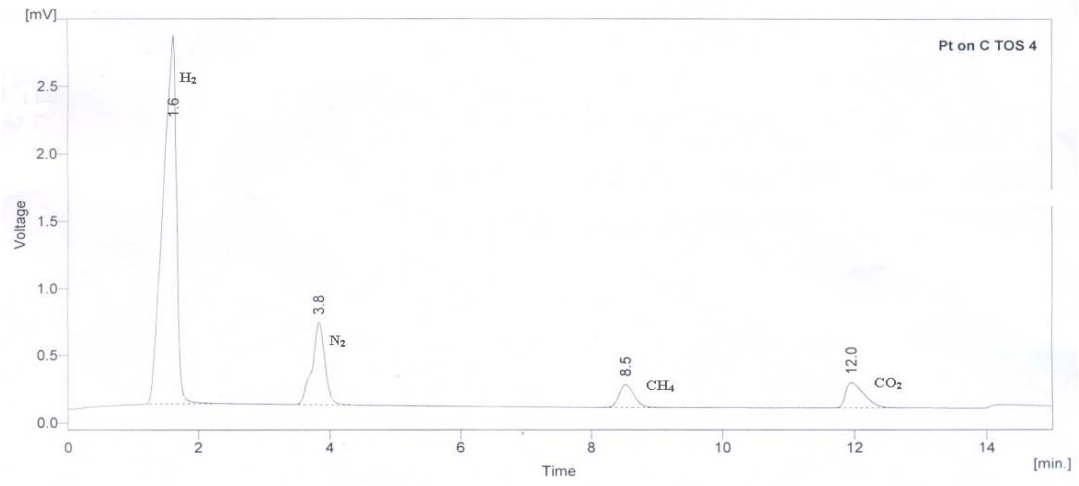

Result Table

	Reten. Time [min]	Area [mV.s]	Height [mV]	Area [%]	Height [%]	W05 [min]
1	1.623	787.095	54.745	72.9	73.8	0.24
2	3.833	166.526	12.223	15.4	16.5	0.19
3	8.520	54.057	3.410	5.0	4.6	0.25
4	11.950	72.082	3.757	6.7	5.1	0.31
	Total	1079.761	74.135	100.0	100.0	

Figure 7.13. GC of gas phase composition (3% Pt/C).

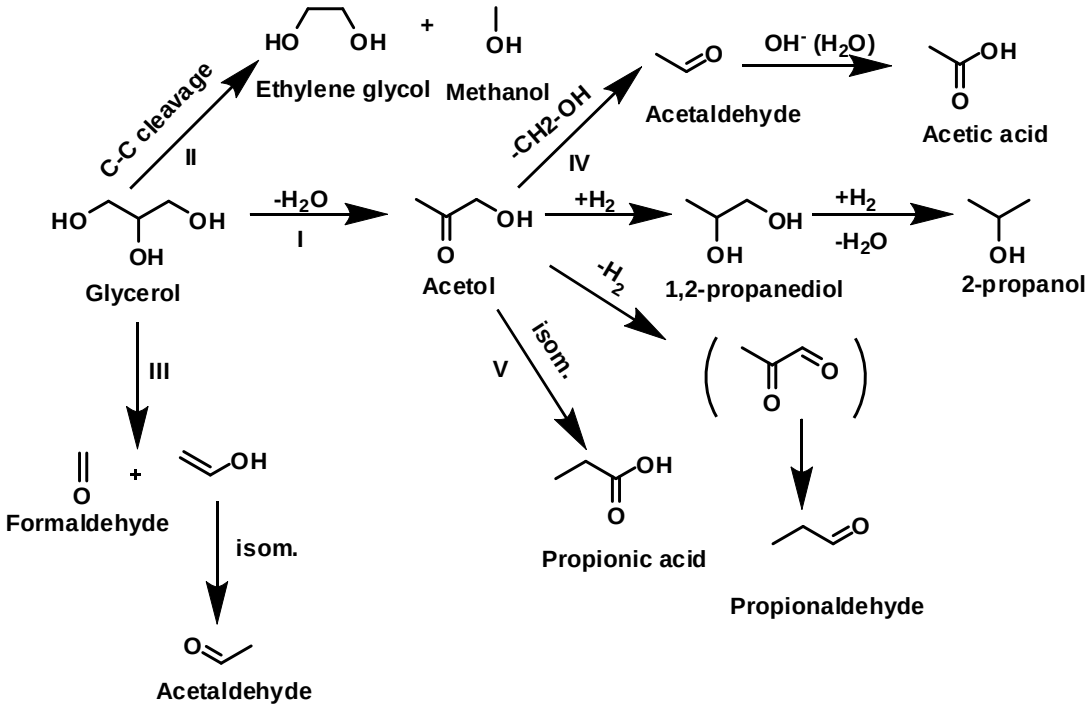

Scheme 7.3. Reaction pathways during autogeneous hydrogenolysis of aqueous glycerol under inert atmosphere.

its excess hydrogenation leads to undesirable 2-propanol formation. Pathways II, III, IV present the undesirable C-C cleavage leading to formation of ethylene glycol, formaldehyde, and acetaldehyde. Pathway V is the acetol isomerization giving propionic acid. 1, 2-PDO as a substrate gave 17% (**Table 7.3**) carbon selectivity to the dehydrogenation product acetol, which is evident from the complete H_2 selectivity (**Table 7.4**) and 2-propanol formation (16%) due to hydrogenation of remaining 1,2-PDO.

Cu-Al catalyst was also evaluated for continuous dehydration in a fixed bed reactor. It was observed that the carbon selectivity of total liquid products substantially increased (50 to 77%) from batch to continuous operation (**Table 7.3**). A three-fold enhancement of glycerol conversion in a continuous operation was achieved due to higher catalyst to substrate ratio (0.67) than that in a batch operation (0.05). Continuous operation also resulted in > two fold 1,2-PDO selectivity than that of acetol due to higher rates of both H_2 evolution by APR and hydrogenolysis of remaining glycerol at higher conversion levels. Other than 1,2-PDO and acetol, the commercially important major byproducts formed (< 2.5 %) were ethylene glycol and 1-propanol, while minor amounts of propionic acid, acetic acid, acetaldehyde, and propionaldehyde were also observed (**Scheme 7.3**). Byproduct formation was a strong function of temperature as indicated by their selectivity of 14% at 230 ^{o}C and none at 220 ^{o}C. These were formed due to C-C cleavage of glycerol, isomerisation of acetol and excessive hydrogenation of 1,2-PDO catalyzed by bifunctional Cu-Al catalyst arising from BrØnsted acidity and its hydrogenation ability.[41]

Figure 7.14 shows TOS of Cu-Al catalyst at 220 ^{o}C under inert atmosphere with an average glycerol conversion of 90% and a selectivity (C based) of 22-25% to 1, 2-PDO with remaining acetol (55 %) and others (2.5 %). Under an inert atmosphere only glycerol dehydration was expected, however, consistent formation of 1,2-PDO for 400 h confirms autogeneous glycerol hydrogenolysis over Cu-Al catalyst. The actual yield of 1,2-PDO achieved under our reaction conditions was 7 g while the theoretical yield would be 18 g with complete selectivity to 1,2-PDO under perfect reforming, indicating that minimizing the acetol formation would result in enhancement of the 1,2-PDO yield.

Another unique feature of autogeneous glycerol hydrogenolysis to 1,2-PDO was the maximum atom economy as demonstrated by calculations considering four different

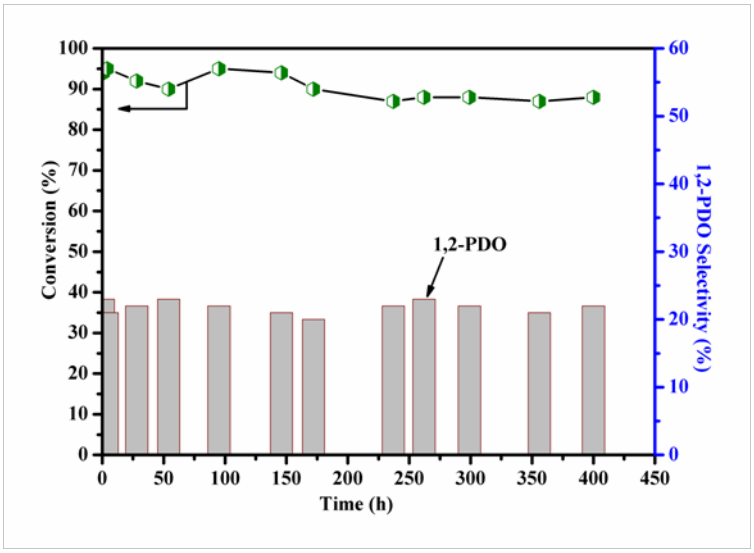

Figure 7.14. Time on stream activity of Cu-Al for dehydration of aqueous glycerol. **Reaction conditions:** Cu-Al catalyst, 20 g; glycerol, 20 wt%; N_2 pressure, 20 bar; GHSV, 513 h^{-1}; LHSV, 1.53 h^{-1}; temperature, 220 ^{o}C.

scenarios. In the first scenario of complete glycerol reforming to hydrogen, atom economy was only 9.6%, while it was 80 and 81% for acetol and 1,2-PDO individually. While for the fourth scenario of auto-hydrogenolysis considering the atom economy of both acetol and 1,2-PDO together highlights the profitability of this process.

Effect of various process parameters on glycerol conversion and product selectivities (C based) were also studied and the results are discussed below. The percentage conversion was calculated by using the following formula:

$$\text{Conversion}\,(\%) = \frac{\text{Initial conc. of glycerol} - \text{final conc. of glycerol}}{\text{Initial conc. of glycerol}} \times 100$$

Figure 7.15 shows two fold increase in glycerol conversion (35 to 70%) with the increase in temperature from 180 ^{o}C to 210 ^{o}C, and reached maximum of 90% at 220 ^{o}C at constant feed conditions. Although the glycerol conversion was only 35% at the lowest temperature of 180 ^{o}C, interestingly formation of acetol and 1,2-PDO was in equal amounts without any byproduct formation. The highest conversion at 220 ^{o}C was associated with lowering of 1,2-PDO selectivity due to byproducts being formed. 1,2-PDO selectivity picked up at the cost of acetol selectivity beyond 220 ^{o}C, indicating that

acetol hydrogenation to 1,2-PDO is kinetically faster than other reaction pathways. Carbonic acid formation also increased progressively, indicating a higher rate of glycerol reforming with increase in temperature **(Table 7.5)**.

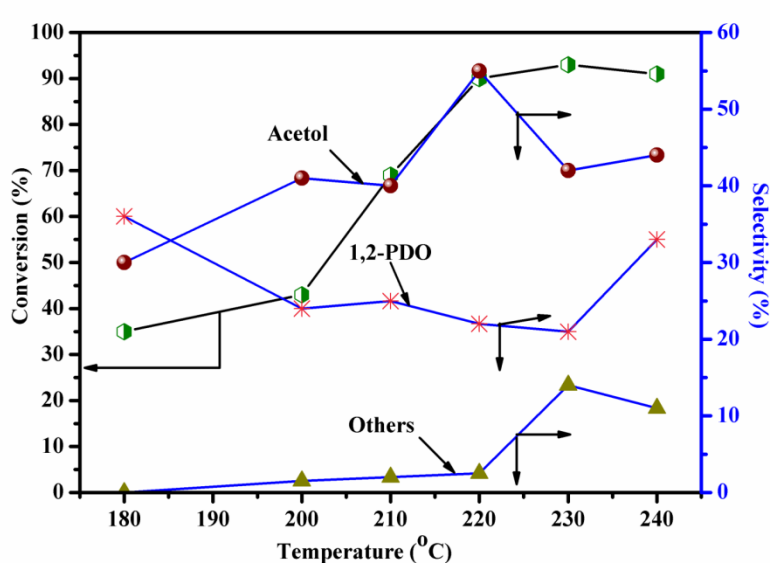

Figure 7.15. Effect of temperature on conversion and product selectivity.

Reaction conditions: Cu-Al catalyst, 20 g; glycerol, 20 wt%; N_2 pressure, 20 bar; GHSV, 513 h^{-1}; LHSV, 1.53 h^{-1}.

As seen from **Figure 7.16**, glycerol concentrations of 10 and 20% showed marginal changes in glycerol conversion and 1,2-PDO selectivity. However, a higher glycerol concentration of 40% resulted in drastic lowering of the glycerol conversion from 93 to 37%, which is due to competitive adsorption of glycerol on the catalyst active sites.

Figure 7.17 shows that the increase in feed flow rate gave higher acetol selectivity, sacrificing 1, 2-PDO and byproducts selectivity, while glycerol conversion decreased from 95% to 74 % with increase in flow rate from 18 to 54 mL h^{-1}. Thus, the dehydration and hydrogenolysis reactions can be manipulated by optimizing the feed flow rate.

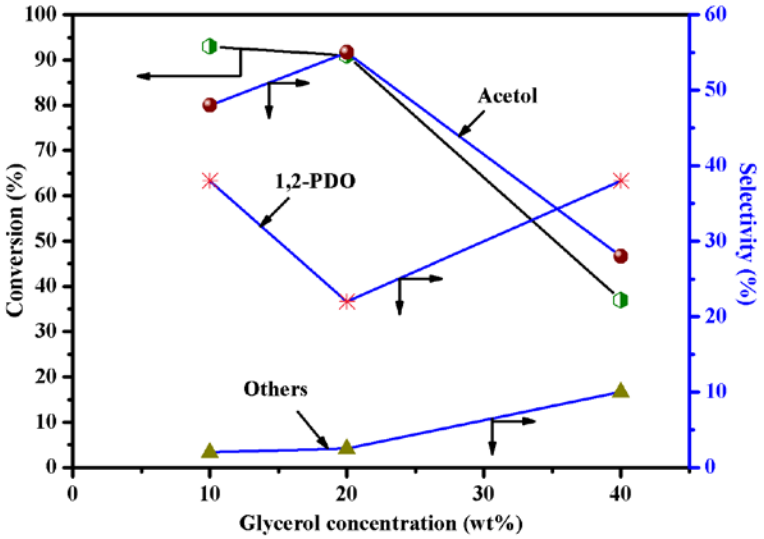

Figure 7.16. Effect of glycerol concentration on conversion and product selectivity. Reaction conditions: Cu-Al catalyst, 20 g; N_2 pressure, 20 bar; GHSV, 513 h^{-1}; LHSV, 1.53 h^{-1}; temperature, 220 ^oC.

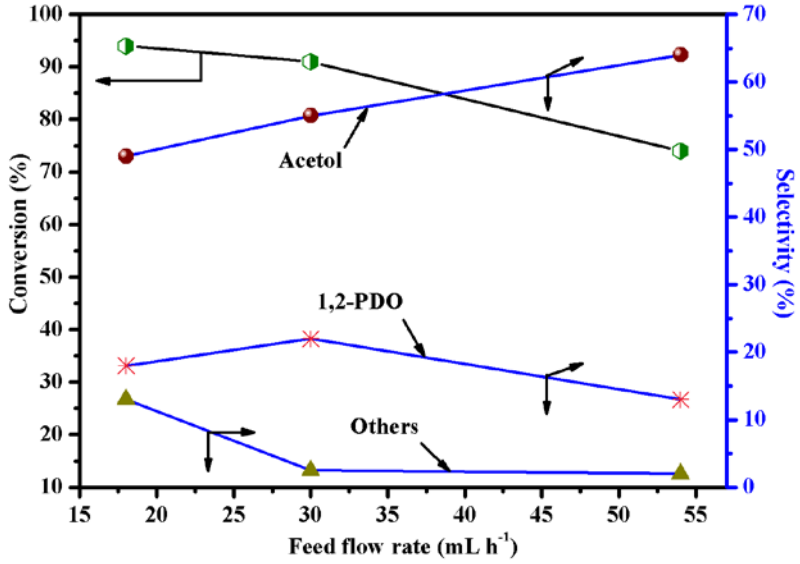

Figure 7.17. Effect of feed flow rate on conversion and product selectivity.

Reaction conditions: Cu-Al catalyst, 20 g; glycerol, 20 wt%; N_2 pressure, 20 bar; GHSV, 513 h^{-1}; temperature, 220 ^oC.

Encouraged by the TOS of 400 h of our catalyst, bio-glycerol feed, obtained from transesterification of vegetable oil, was also evaluated under the same conditions and the results are presented in **Figure 7.18**. The catalyst activity was stabilized at 65% conversion for 50 h on stream and very surprisingly, 1,2-PDO selectivity achieved was as high as 75% from the beginning of the continuous run. Since the bio-glycerol was used as obtained, the presence of trace alkali used during transesterification, could be responsible for higher activity towards hydrogenolysis of glycerol to 1,2-PDO. Similar observations on the positive effect of the alkali have been reported for glycerol hydrogenolysis.[42,43]

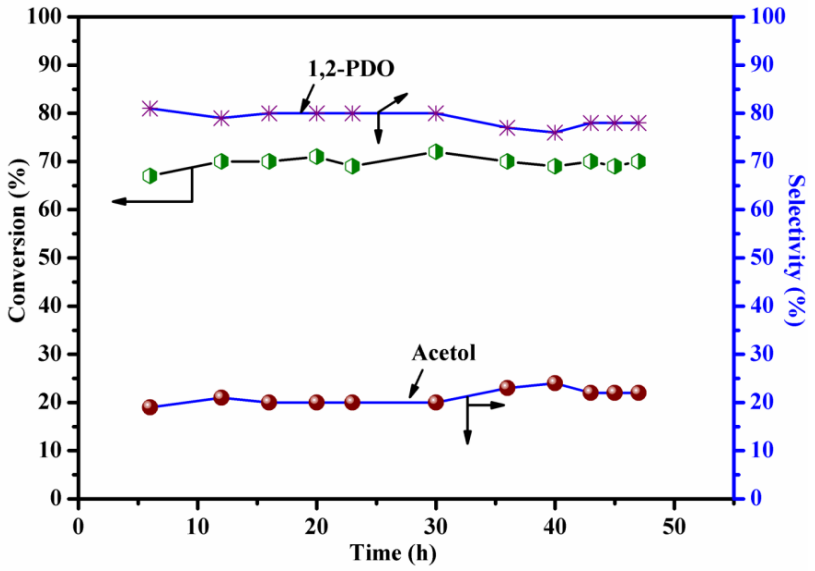

Figure 7.18. Bio-glycerol feed testing over Cu-Al catalyst: Time on stream activity.
Reaction conditions: Cu-Al catalyst, 20 g; bio-glycerol, 20 wt%; N_2 pressure, 20 bar; GHSV, 513 h^{-1}; LHSV, 1.53 h^{-1}; temperature, 220 ^{o}C.

After activation, Cu-Al catalyst showed the co-existence of stable Cu^0, Cu^{1+} and Cu^{2+} species, the latter due to formation of $CuAl_2O_4$. This feature undoubtedly contributes to the glycerol APR[44] followed by *in situ* hydrogenolysis of glycerol. In addition to this, the acidic characteristic of this catalyst was responsible for the dehydration of glycerol to acetol, which is an acid catalyzed reaction. The main advantage of glycerol APR is the atomic hydrogen formed on the active sites has immediate access for acetol hydrogenation.

7.4. CONCLUSIONS

- This is a first report of non-noble Cu-Al catalyst showing an excellent TOS activity for continuous autogeneous hydrogenolysis of aqueous glycerol under N_2 pressure with 1,2-PDO selectivity of 75% with bio-glycerol feed.
- Cu-Al catalyst prepared by simultaneous co-precipitation and digestion method, showed pre-dominantly $CuAl_2O_4$ formation during the activation under hydrogen at 200 ^oC for 12 h.
- The characteristic planes, (111), (101) and (222) obtained from HR-TEM matched with the XRD characterization, confirming the presence of Cu^0, Cu^{1+} and $CuAl_2O_4$ phases in the Cu-Al catalyst.
- The higher intensity ratio of $CuAl_2O_4$, evaluated from XPS, also proved that the majority of Cu^{2+} was in the form of $CuAl_2O_4$ in the activated catalyst.
- The coexistence of Cu^0, Cu^{1+} and Cu^{2+} species in the reduced Cu-Al catalyst was responsible for its multifunctional role, catalyzing C-C cleavage and glycerol dehydration to acetol, followed by its hydrogenation to 1,2-PDO, while completely suppressing the alkane formation.

7.5. REFERENCES

1. R. D. Cortright, R. R. Davda, J. A. Dumesic, *Nature* **2002**, 418, 964-967.
2. S. Adhikari , S. D. Fernando , A. Haryanto, *Energy Conversion and Management* **2009**, 50, 2600-2604.
3. G. Wen, Y. Xu, H. Ma, Z. Xu, Z. Tian, *Int. J. Hydrogen Energy* **2008**, 33, 6657-6666.
4. G. W. Huber, J. W. Shabaker, J. A. Dumesic, *Science* **2003**, 300, 2075-2078.
5. J. A. Posada, L. E. Rincon, A. A. Cardona, *Bioresour. Technol.* **2012**, 111, 282-293.
6. X. Wu, Z. Ma, Z. Ye, S. Qian, G. Zhaob, *Adv. Synth. Catal.* **2009**, 351, 158-162.
7. C. Montassier, J. C. Menezo, J. Naja, J. Barbier, J. M. Dominguez, P. Sarrazin, B. Didillon, *J. Mol. Catal*. **1994**, 91, 107-117.
8. D. Taher, M. E. Thibault, D. Di Mondo, M. Jennings, M. Schlaf, *Chem. Eur. J.* **2009,** 15, 10132–10143.
9. A. Bienholz, F. schwab, P. Claus, *Green Chem.* **2010**, 12, 290-295.
10. Z. Wu, Y. Mao, X. Wang, M. Zhang, *Green Chem.* **2011**, 13, 1311–1316.
11. J. Zhou, L. Guo, A. Guo, J. Mao, S. Zhang, *Green Chem.* **2010**, 12, 1835-1843.
12. M. A. Dasari, P. P. Kiatsimkul, W. R. Sutterlin, G. J. Suppes, *Appl. Catal. A* **2005**, 281, 225–231.
13. E. D'Hondt, S. Van de Vyver, B. F. Sels, P. A. Jacobs, *Chem. Commun.* **2008,** 6011-6012.
14. D. Roy, B. Subramaniam, R. V. Chaudhari, *Catal. Today* **2010**, 156, 31-37.
15. A. Y. Yin, X. Y. Guo, W. L. Dai, K. N. Fan, *Green Chem.* **2009**, 11, 1514-1516.
16. M. L. Barbelli, G. F. Santori, N. N. Nichio, *Bioresour. Technol.* **2012,** 111, 500-503.
17. R. B. Mane, A. M. Hengne, A. A. Ghalwadkar, S. Vijayanand, P. H. Mohite, H. S. Potdar, C. V. Rode, *Catal. Lett.* **2010**, 135, 141–147.
18. R. B. Mane, C. V. Rode, *Org. Proc. Res. Dev*. **2012**, 16, 1043-1052.
19. R. B. Mane, C. V. Rode, *Green Chem.* **2012**, 14, 2780-2789.
20. J. Zhou, J. Zhang, X. Guo, J. Mao, S. Zhang, *Green Chem.***2012**, 14, 156-163.

21. E. E. Miro, E. A. Lombardo, J. O. Petunchi, *J. Catal.* **1987**, 104, 176-185.
22. O. Ilinich, W. Ruettinger, X. Liu, R. Farrauto, *J. Catal.* **2007,** 247, 112-118.
23. P. A. Kumar, M. P. Reddy, L. K. Ju, B. Hyun-Sook, H. H. Phil, *J. Mol. Catal. A* **2008**, 291, 66-74.
24. R. Hierl, H. Knozinger, H. P. Urbach, *J. Catal.* **1981**, 69, 475-486.
25. B. R. Strohmeier, D. E. Levden, R. S. Field, D. M. Hercules, *J. Catal.* **1985**, 94, 514-530.
26. J. Yanyan, L. Jinggang, S. Xiaotao, N. Guiling, W. Chengyu, G. Xiumei, *J. Sol-Gel Sci. Technol.* **2007**, 42, 41-45.
27. R. T. Kumar, P. Suresh, N. C. S. Selvem, L. J. Kennedy, J. J. Judith Vijaya, *J. of Alloys and Compounds* **2012**, 522, 39-45.
28. E. D. Pierron, J. A. Rashkin, J. F. Roth, *J. Catal.* **1967**, 9, 38-44.
29. M. S-Niasari, F. Davar, M. Farhadi, *J. Sol-Gel Sci. Technol.* **2009**, 51, 48-52.
30. F. Severino, J. L. Brito, J. Laine, J. L. G. Fierro, A. L. Agudo, *J. Catal.* **1998**, 177, 82-95.
31. L. I. Darvell, K. Heiskanen, J. M. Jones, A. B. Ross, P. Simell, A. Williams, *Catal. Today* **2003**, 81, 681-692.
32. R. Shi, F. Wang, Tana, Y. Li, X. Huang, W. Shen, *Green Chem.* **2010**, 12, 108–113.
33. S. Wang, Y. Zhang, H. C. Liu, *Chem. Asian J.* **2010**, 5, 1100-1111.
34. P. D. Vaidya,A. E. Rodrigues, *Chem. Eng. Technol.* **2009**, 32, 1463-1469.
35. J. Deleplanque, J. –L. Dubois, J. –F. Devaux, W. Ueda, *Catal. Today* **2010**, 157, 351-358.
36. J. Schaferhans, S. Gomez-Quero, D. V. Andreeva, G. Rothenberg, *Chem. Eur. J.* **2011**, 17, 12254-12256.
37. R. R. Davda, J. W. Shabaker, G. W. Huber, R. D. Cortright, J. A. Dumesic, *Appl. Catal. B* **2005**, 56, 171-186.
38. B. L. Kniep, F. Girgsdies, T. Ressler, *J. Catal.* **2005**, 236, 34-44.
39. R. R. Soares, D. A. Simonetti, J. A. Dumesic, *Angew. Chem. Int. Ed.* **2006**, 45, 3982- 3985.

40. M. Slinn, K. Kendall, C. Mallon, J. Andrews, *Bioresour. Technol.* **2008**, 99, 5851-5858.
41. C. Monterra, S. Coluccia, A. Chiorino, F. Boccuzzi, *J. Catal.* **1978**, 54, 348-364.
42. E. P. Maris, W. C. Ketchie, M. Murayama, R. J. Davis, *J. Catal.* **2007**, 252, 281-294.
43. E. P. Maris, R. J. Davis, *J. Catal.* **2007**, 249, 328-337.
44. S. D. Jones, L. M. Neal, H. E. Hagelin-Weaver, *Appl. Catal. B* **2008**, 84, 631-642.

Chapter 8

Modified copper catalysts for selective liquid phase dehydration of aqueous glycerol to acetol

The influence of oxides of various metals *viz.* Ba, Mg, Zr, Zn, Al, and Cr in modified copper catalysts, on the formation of different copper species and acid sites responsible for dehydration of aqueous glycerol to acetol was studied in detail. The catalysts having higher acid strength and predominant BrØnsted acidity (Cu-Mg, Cu-Zr and Cu-Al) gave the highest acetol selectivity (76-92%) while, the catalysts with lower acidity such as Cu-Zn showed very poor (25%) selectivity to acetol inspite of the highest conversion of 68%. The presence of metallic Cu in highly active catalysts was confirmed by XRD and XANES-EXAFS characterization. Based on these results, two different catalytic pathways have been proposed highlighting the role of Lewis and BrØnsted acidity along with the metal sites in individual steps of glycerol dehydration reaction.

***RSC Adv.* 2013, 37, 16499-16508**

8.1. INTRODUCTION

In this chapter, we focused our attention on acetol which is a starting material for 1,2-propanediol (1,2-PDO) and an important commodity chemical.[1,2] Acetol is a non toxic and highly reactive molecule as it possesses both hydroxyl and carbonyl functional groups rendering its versatility in applications such as a green solvent, flavoring and tanning agent, in hydrogen production by catalytic steam reforming, in textile industry for fixation of a dye and an intermediate for fine chemicals and pharmaceutical manufacture.[3,4] Conventionally, acetol has been synthesized by several ways *e.g.* (i) reacting bromoacetone and sodium or potassium formate or acetate, followed by hydrolysis of the ester by methyl alcohol[5] (ii) by the direct oxidation of acetone with Bayer and Villiger's acetone-peroxide reagent (iii) palladium catalyzed dehydrogenation of aqueous propylene glycol in presence of hydrogen peroxide [6] (iv) biosynthetic route involving metabolically engineered micro-organisms using various substrates.[7,8] However, multistep synthesis, economical unviability due to use of expensive reagents in stoichiometric amounts, low yields and effluent disposal cost restrict the commercialization of any of these methods. The current production price of ~ USD 12.5 per kg of acetol can be substantially reduced by about 10 times (USD 1.25 per kg) using direct glycerol dehydration route.[9] The highly valuable acetol (hydroxyacetone) production from cheap bio-glycerol is not only beneficial to the environment protection but also boosts the process economics of biodiesel industries.[10,11]

Until now, catalytic dehydration of glycerol to acrolein is well reported in the literature, which is mainly focused on gas phase reaction over solid acid catalysts such as metal sulfates and phosphates, zeolites, supported mineral acids and heteropoly acids.[12] Acetol formation from glycerol follows a complex reaction pathway involving either direct dehydration of primary and/or secondary –hydroxyl group or dehydrogenation followed by dehydration depending on type and strength of acid sites present on the surface of the respective catalyst system (**Scheme 8.1**). Acetol formation was reported on both Lewis acid and metal sites while acrolein formation *via* 3-hydroxypropanal was favored in the presence of strong Brønsted acid sites.[13] There are very few reports on selective glycerol dehydration to acetol. Very recently, Sato *et al*. reported the vapour

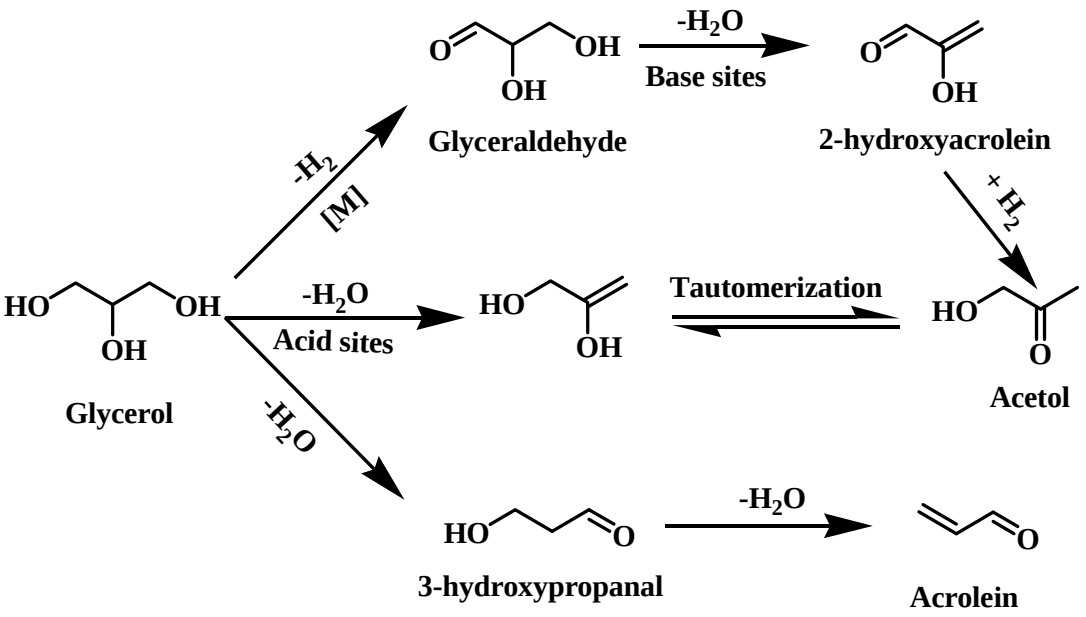

Scheme 8.1. Various glycerol dehydration pathways depending on acid and base sites of the catalysts.

phase glycerol dehydration to acetol over Ag supported catalysts among which Ag/SiO_2 showed higher glycerol conversion of 91% with 86% selectivity to acetol at 240 ^oC in H_2 flow.[14] Chiu *et al.* reported gas-phase conversion of glycerol to acetol in a semi-batch reactor at high pressure and temperature by reactive distillation over copper chromite catalyst with only 22% conversion of glycerol and 70% selectivity to acetol.[1,15] Role of various acidic and basic supports for vapor phase dehydration over copper catalysts also has been reported, in which acidic alumina supported copper (Cu/Al_2O_3) showed complete glycerol conversion and ~90% selectivity to acetol while basic support magnesia gave only 45% acetol selectivity.[16] Suprun *et al.* reported phosphate ion modified alumina, titania, SAPO-11, and SAPO-34 catalysts for gas–phase glycerol dehydration in which moderate acidity of SAPO-11 showed the highest selectivity to acetol (65%) as compared to that shown by catalysts having the strong acidity.[17] Use of high temperature (300 ^oC) liquid water and high pressure carbon dioxide was also reported for non-catalytic glycerol dehydration with low acetol yields (<2%).[18,19] The highest acetol selectivity of 69% was achieved with the optimum ratio of basic to acid

sites in case of sodium doped metal oxide catalysts for vapor phase glycerol dehydration.[20] Strong acid sites in sulfate and tungsten oxide modified zirconia catalysts showed higher selectivity to acrolein and other byproducts at the cost of acetol for gas –phase dehydration of glycerol.[21]

Thus, glycerol dehydration has been studied mainly under vapor phase conditions at higher temperature hence, the acetol selectivity was affected because of acrolein and other byproducts formation. Such processes are also accompanied by fast catalyst deactivation due to extensive coke deposition. Hence, liquid phase glycerol dehydration would be more preferred to achieve the highest selectivity to acetol. Our previous studies were mainly focused on process parameters effect for liquid phase glycerol dehydration and *in situ* glycerol hydrogenolysis respectively.[22,23] Whereas in this chapter, several catalysts were prepared by combining various chromium and non- chromium metal oxides with copper oxide which led to the formation of different copper species and acid sites required for low temperature dehydration of aqueous glycerol.[24] Our results revealed that the catalysts having both BrØnsted acidity and metallic copper showed better activity and acetol selectivity than those BrØnsted /Lewis acid and metal sites alone. Finally, two catalytic pathways have been proposed highlighting the role of Lewis and BrØnsted acid along with metal sites in individual steps of glycerol dehydration reaction.

8.2. EXPERIMENTAL

Copper catalysts with various metals such as Ba, Mg, Zr, Zn, Al and Cr were prepared by simultaneous co-precipitation and digestion method and detail experimental procedure is given in chapter 2 (section 2.3.3). The metallic copper was prepared by calcining $Cu(NO_3)_2.3H_2O$ at 400 ^oC for 3 h followed by its activation at 200 ^oC under H_2 flow for 12 h. The preparation procedure of sulfated zirconia ($S\text{-}ZrO_2$) was described in chapter 2 (section 2.3.11). The catalysts were characterized by various techniques *viz.* BET surface area, XRD, XPS, XANES, EXAFS, NH_3-TPD, CO_2-TPD and Py-IR, and detailed characterization procedures are described in chapter 2 (sections 2.4.2, 2.4.6, 2.4.7, 2.4.10, 2.4.12 and 2.4.11). All the batch dehydration reactions were carried out in a 300 mL

capacity stirred autoclave supplied by Parr Instruments Co. USA and continuous dehydration runs were carried out in a high-pressure, fixed-bed reactor set-up supplied by M/s Geomechanique, France, the details of which are given in chapter 2 (sections 2.5.1 and 2.5.2).

8.3. RESULTS AND DISCUSSION

8.3.1. Catalyst characterization

Among several copper based catalysts screened in this work, reduced Cu-Mg, Cu-Zr and Cu-Al showed the excellent activity and selectivity for liquid phase dehydration of glycerol to acetol under inert atmosphere. Hence identification of the active sites in these catalysts was attempted through their characterization and the results were also compared with other catalysts which showed very low activities.

XRD patterns (**Figure 8.1**) of reduced Cu-Al, Cu-Mg and Cu-Zr catalysts revealed the diffraction peaks at $2\theta = 43.5^{o}$ (111), 50.7^{o} (200) and 74.2^{o} (220) for metallic Cu [JCPDS file no. 85-1326] along with copper (I) oxide (Cu_2O) [$2\theta = 36.6^{o}$ (101); 29.5^{o} (110); 61.4^{o} (220)] (JCPDS file no. 78-2076) and copper (II) oxide (CuO) phases with $2\theta = 35.7^{o}$ ($\bar{1}11$) and 38.8^{o}(111) [JCPDS file no. 80-1268]. Cu-Mg and Cu-Zr samples showed more intense peaks for CuO phases compared to that observed in Cu-Al sample, while in the latter case, peaks for metallic copper were predominant, indicating that magnesium and zirconium suppressed the reduction of CuO during the catalyst activation protocol. The formation of metal-metal bond in the reduced Cu-Al sample was also evidenced by EXAFS analysis, which will be discussed below. The copper metal particle size in these catalysts was calculated from the diffraction peak at $2\theta = 43.5^{o}$ using the Scherrer equation and the order was found to be as follows, Cu-Zr (38.8 nm) > Cu-Al (14.4 nm) > Cu-Mg (5.5 nm) (**Table 8.1**).

The complete suppression of metallic copper phase formation was observed in case of reduced Cu-Ba and Cu-Zn catalysts. The distinct peaks at $2\theta = 23.9^{o}$ (111), 27.7^{o} (002), 33.7^{o} (200), 42.8^{o} (041), 44.9^{o} (132), and 46.8^{o} (113) [JCPDS file no. 71-2394] shown in the XRD pattern of Cu-Ba (**Figure 8.1**) were attributed to the formation of

barium carbonate ($BaCO_3$) phase. It is reported that barium carbonate is highly stable [25] affecting the glycerol dehydration activity as discussed later. The identified copper phases in reduced Cu-Ba catalyst were Cu_2O and CuO from the very low intensity peaks at $2\theta = 29.5^o$ (110) and $2\theta = 35.7^o$ ($\bar{1}11$) and 38.8^o (111) respectively. Similarly, for the reduced Cu-Zn catalyst, the Cu^0 phase was completely absent while only Cu_2O (major) and CuO phases were observed. Further ZnO phase was predominant as evidenced from the peaks at $2\theta = 31.7^o$ (100), 34.4^o (002), 47.4^o (111), 56.7^o (110), 62.8^o (103) and67.9^o (112) [JCPDS file no. 80-0075]. The absence of metallic Cu and the abundance of ZnO led to lower the selectivity to acetol, as discussed later. The XRD pattern of the Cu-Cr catalyst showed the metallic Cu (24.4 nm) as well as CuO phases while Cu_2O phase was completely absent and its dehydration activity was also lowest.

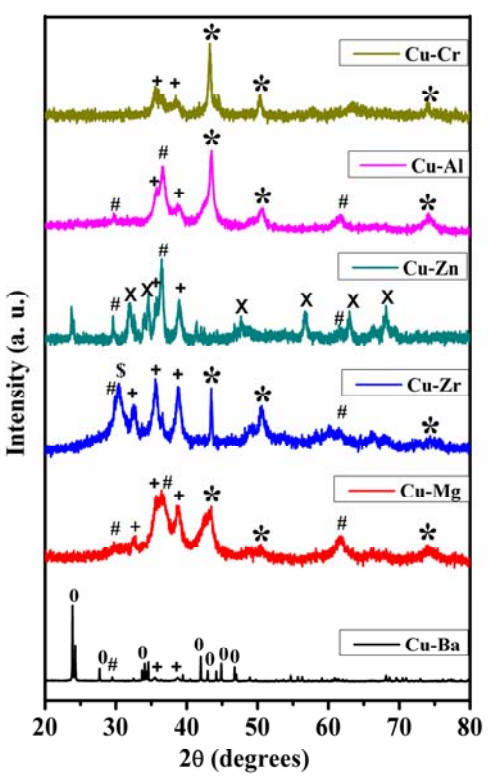

Figure 8.1. XRD patterns of different reduced copper catalysts. **(**$*$**)** Cu^0, (#) Cu_2O, (+) CuO, (0) $BaCO_3$, ($) t-$ZrO_2$, (X) ZnO.

Table 8.1. Crystallite sizes of different reduced (A) and recovered (R) copper catalysts

Catalyst	Crystallite size of Cu (nm)
ACu:Ba	-
ACu:Mg	5.5
ACu:Zr	38.8
ACu:Zn	-
ACu:Al	14.4
ANMT006	24.4
RCu:Ba	50.2
RCu:Mg	27.5
RCu:Zr	38.8
RCu:Zn	56.9
RCu:Al	35.6

The transformation of phases under reaction conditions was also studied by the XRD patterns of catalysts recovered after the dehydration reaction. Recovered Cu-Ba catalyst (**Figure 8.2**) showed only Cu^0 phase with higher crystallite size of 50.2 nm and complete disappearance of $BaCO_3$ phase indicating the aggregation and leaching respectively, under the dehydration conditions. Similarly, recovered Cu-Mg also showed only Cu^0 phase with complete disappearance of various Cu oxide phases due to its *in situ* reduction.[23] In case of recovered Cu-Zn and Cu- Zr samples, Cu^0 and Cu_2O phases were also observed in addition to the retention of oxide phases of the respective co-metals. The most salient feature of the recovered Cu-Al catalyst was coexistence of all the three phases of Cu *viz.* metallic and both Cu_2O and CuO phases. Particle sizes of metallic copper in all the recovered catalysts except for Cu-Zr were found to increase substantially, which indicates the aggregation of Cu particles under reaction conditions (**Table 8.1**).

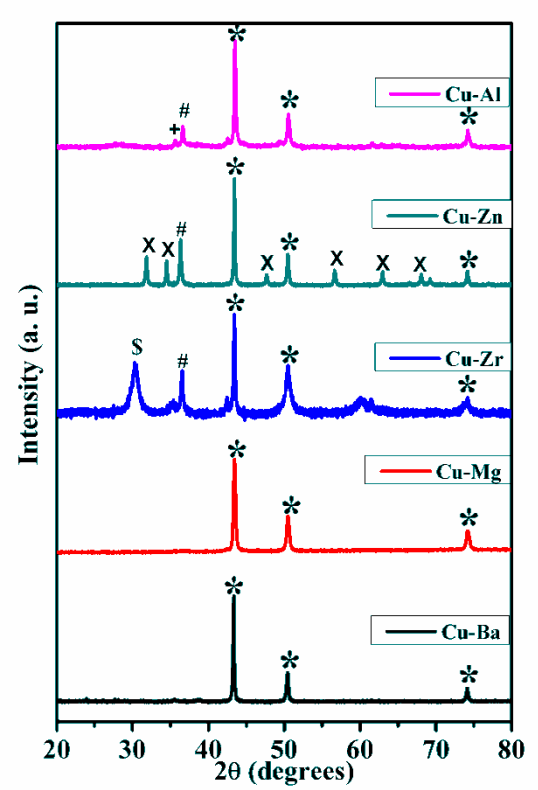

Figure 8.2. XRD patterns of different recovered copper catalysts. **(**$*$**)** Cu^0, (#) Cu_2O, (+) CuO, ($) t-$ZrO_2$, (X) ZnO.

Cu 2*p* XPS spectra of reduced copper catalysts are shown in **Figure 8.3** in which a broad peak of Cu $2p_{3/2}$ observed in the range of 932 to 935 eV was due to the presence of various Cu species. All the samples showed a peak at *ca.* 932 eV which could be attributed to either Cu^{1+} or Cu^0 species.[26] Other peaks at higher binding energies at *ca.* 933.5 and at *ca*. 935 eV were assigned to Cu^{2+} of CuO which was also supported by the satellite peak centered at 943 eV. As the XRD pattern of Cu-Zn did not show any metallic Cu phase, the peak at 932.3 eV could be assigned to only Cu^{1+} species. While in case of Cu-Al catalyst the peak at 935 eV assigned to Cu^{2+} could be due to the formation of CuO as well as of $CuAl_2O_4$ phases.[23]

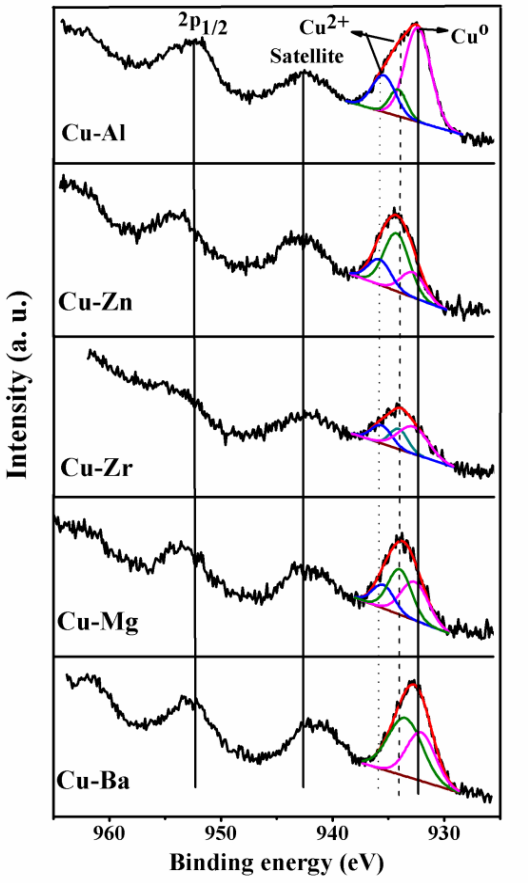

Figure 8.3. XPS spectra of different reduced copper catalysts.

EXAFS characterization of the Cu based catalysts were carried out in order to know the local environment *viz.* atomic identity, co-ordination number and bond distance of copper atoms while XANES revealed the oxidation state and electronic environment of copper atoms. **Figure 8.4** shows the Fourier transform of k^2-weighted Cu K-edge EXAFS spectra (FT range was 3-15 $Å^{-1}$) of the Cu-Al sample and curve-fitting results are summarized in **Table 8.2**. Only one peak was observed at 0.15 nm (phase shift uncorrected) in the Cu-Al sample after calcination at 400 ^oC (**Figure 8.4, a**), which is ascribed to Cu-O bond. After the activation of the Cu-Al sample with hydrogen for 12 h at 200 ^oC, the Cu-O peak intensity at 0.15 nm decreased and a new peak at 0.22 nm was formed (phase shift uncorrected) (**Figure 8.4, b**), which is ascribed to the Cu-Cu metal bond, indicating that the copper species in the Cu-Al sample were partially reduced from oxide to metal species. **Figure 8.4** (**c**) shows the FT-EXAFS of the Cu-Al sample after

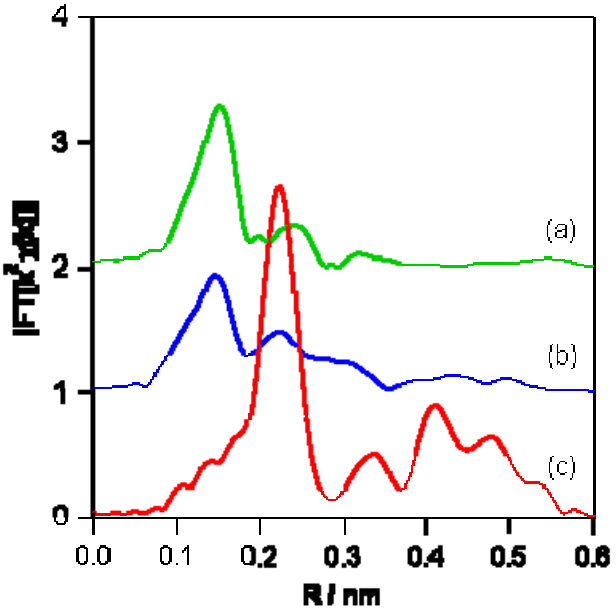

Figure 8.4. FT-EXAFS of Cu-Al catalyst (a) calcined (b) reduced (c) recovered.

Table 8.2. EXAFS curve fitting results of different copper catalysts

Sample	Cu-Cu				Cu-O			
	CN	R (nm)	s^2 / 10^{-4} (nm^2)	E_0 (eV)	CN	R (nm)	s^2 / 10^{-4} (nm^2)	E_0 (eV)
Cu foil	12.0	0.253	0.82	1.9	-	-	-	-
CuO	-	-	-	-	4.0	0.193	0.17	2.4
Cu_2O	-	-	-	-	2.1	0.186	0.17	7.0
Cu-Al (calcined)	-	-	-	-	3.8	0.195	0.41	-3.0
Cu-Al (reduced)	2.1	0.251	0.93	-2.0	2.1	0.186	0.36	1.7
Cu-Al (recovered)	8.9	0.253	0.81	1.6	-	-	-	-
Cu-Mg (calcined)	-	-	-	-	3.5	0.196	0.33	-2.7
Cu-Mg (reduced)	-	-	-	-	3.3	0.194	0.38	-1.7
Cu-Mg (recovered)	7.2	0.254	0.79	1.7	-	-	-	-
Cu-Zr (calcined)	-	-	-	-	3.5	0.194	0.059	-2.4
Cu-Zr (reduced)	3.1	0.252	0.96	0.2	1.6	0.195	0.12	8.2
Cu-Zr (recovered)	4.7	0.254	0.93	1.9	-	-	-	-

the glycerol dehydration. The peak intensity of Cu-Cu metal bond increased after dehydration indicating that reduction of copper species proceeded during the reaction.

Figure 8.5 shows the Fourier transform of k^2-weighted Cu K-edge EXAFS spectra (FT range was 3-15 $Å^{-1}$) of the Cu-Mg sample and curve-fitting results are summarized in **Table 8.2.** Similar to the Cu-Al sample, only Cu-O peak was observed at 0.15 nm (**Figure 8.5, a**) after the calcination. The peak intensity of Cu-O bond did not change and Cu-Cu metal peak did not appear after activation (**Figure 8.5, b**), indicating that copper cations were not reduced to metal species by hydrogen reduction in the Cu-Mg sample. After glycerol dehydration, the Cu-Cu metal peak was also formed in the Cu-Mg sample (**Figure 8.5, c**), indicating that copper cations were reduced to metal species during dehydration, however, the coordination number of Cu-Cu bond in the Cu-Mg sample was smaller than that of Cu-Al sample after dehydration, indicating that copper cation was not easily reduced to metal species in the Cu-Mg sample than that in Cu-Al sample.

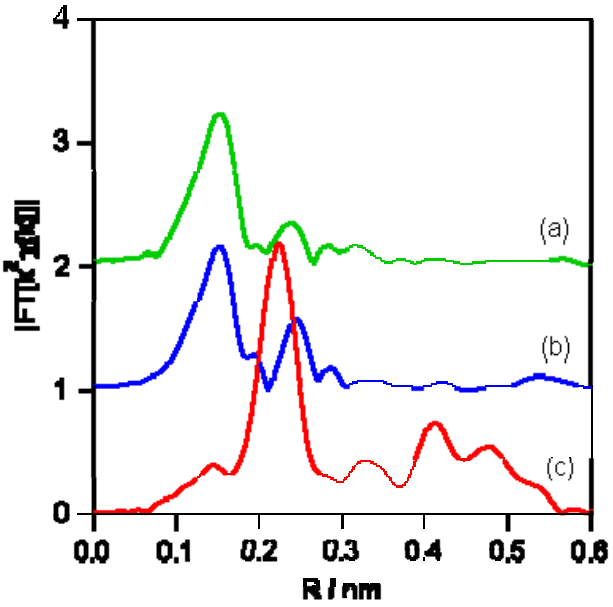

Figure 8.5. FT-EXAFS of Cu-Mg catalyst (a) calcined (b) reduced (c) recovered.

Figure 8.6 shows the FT-EXAFS of k^2-weighted Cu K-edge EXAFS spectra of Cu-Zr sample (FT range was 2-11 $Å^{-1}$) and curve-fitting results are summarized in **Table 8.2.** Similar to the Cu-Al and Cu- Mg samples, only Cu-O peak was observed at 0.15 nm

after calcination (**Figure 8.6, a**). In the reduced catalyst sample, the peak ascribed to Cu-Cu metal bonds was observed (**Figure 8.6, b**) and the peak intensity of Cu-Cu increased after dehydration (**Figure 8.6, c**). The comparison of the coordination numbers of the Cu-O and Cu-Cu bonds in the Cu-Al and Cu-Zr samples shows that copper in the Cu-Zr sample was more easily reduced to metal species than in the Cu-Al sample. On the other hand, the coordination number of Cu-Cu in the Cu-Al sample after dehydration was higher than that of the Cu-Zr sample after exposure to the same reaction conditions, indicating that the reduction of copper species in Cu-Zr was slow during dehydration as compared to that in Cu-Al sample.

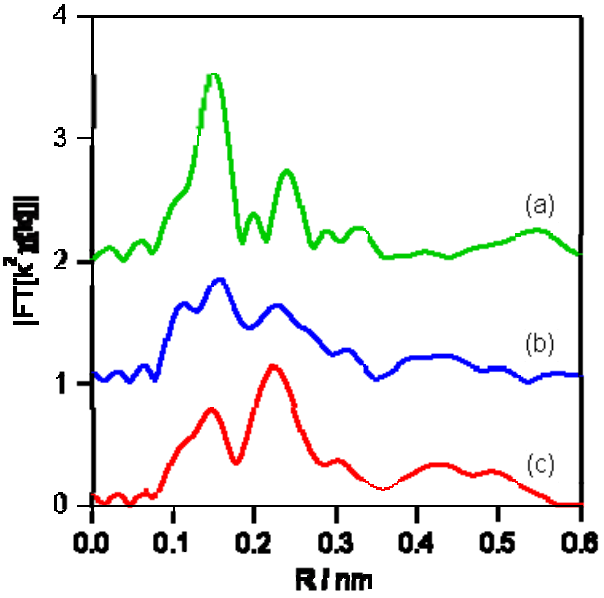

Figure 8.6. FT-EXAFS of Cu-Zr catalyst (a) calcined (b) reduced (c) recovered.

XANES measurements for all the samples including reference compounds CuO, Cu_2O and metallic Cu are shown in **Figure 8.7**, from which the oxidation states of Cu can be established. In all the calcined samples of Cu-Al, Cu-Mg and Cu-Zr, a shoulder peak of low intensity at 8988 eV was observed while a peak at 9000 eV with higher intensity could be attributed to the 1*s*- to 4*p* transition confirming the predominance of Cu in the 2+ state.[27] The coordination numbers of Cu-O in the calcined samples of Cu-Al, Cu-Mg and Cu-Zr were 3.8, 3.5 and 3.5, respectively, while Cu-Cu bonds were not observed (**Table 8.2**), which support that CuO phase was formed in these samples. In reduced

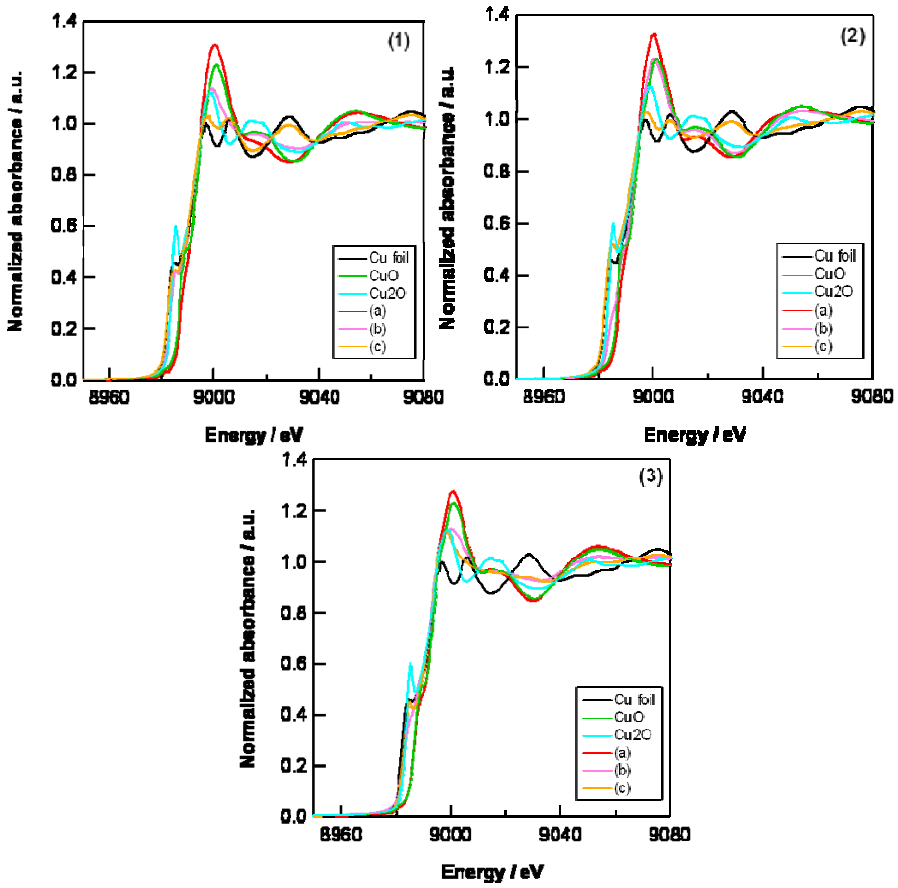

Figure 8.7. XANES of (1)Cu-Al (2)Cu-Mg (3)Cu-Zr catalysts (a) calcined (b) reduced (c) recovered.

Cu-Al and Cu-Zr samples, the presence of a peak at 8984 eV was mainly due to the reduction of Cu^{2+}cations to metallic Cu or Cu^{1+} however, a broad peak in the region of 8993- 9000 eV showed the evidence of copper in various oxidation states such as 1+, 2+ and 0. XRD, XPS patterns (**Figures 8.1, 8.3**) and both Cu-Cu and Cu-O bond formation (**Table 8.2**) also indicated that Cu^0, Cu_2O and CuO were formed in the reduced Cu-Al and Cu-Zr samples. These results confirm that the activation protocol resulted into the reduction of Cu^{2+} to Cu^{1+} and Cu^0 species. On the other hand, reduced Cu-Mg sample showed the peaks at 8985, 8988 and 9000 eV corresponding to Cu_2O and CuO only without any evidence of metallic copper. The Cu-Cu bond formation was not distinctly observed in the curve fitting analysis of FT-EXAFS (**Table 8.2**), in the reduced Cu-Mg sample unlike other samples. The XANES spectra of Cu catalysts with various co-metal oxides after the glycerol dehydration reaction had three absorption peaks at 8984, 8987

and 9005 eV which indicate the formation of metal species. The complete reduction of Cu species to metallic Cu in used sample is evidenced from the EXAFS also. The XRD and XPS studies support the XANES-EXAFS results on extent of formation of metallic Cu and its two oxide phases in various Cu based catalysts.

As the acid sites play an important role in glycerol dehydration reaction, the strength of acid sites was determined by NH_3 –TPD and the profiles for various reduced copper catalysts are shown in **Figure 8.8** while, the amount of NH_3 desorbed along with respective temperature maxima are given in **Table 8.3**. Among these catalysts, Cu-Mg showed a broad peak of NH_3 desorption in a temperature region of 200-360 ^oC, indicating the presence of moderate acid sites, while strong acid sites were evident from a small peak in the high temperature region of 400-500 ^oC.[28] TPD spectra of both Cu-Al and Cu-Zr catalysts, showed two peaks of high intensity in a temperature range of 500-700 ^oC, confirming the presence of strong acid sites. In case of Cu-Zn catalyst, a combination of weak and moderate acid sites was prevailing as observed by a broad peak in the range

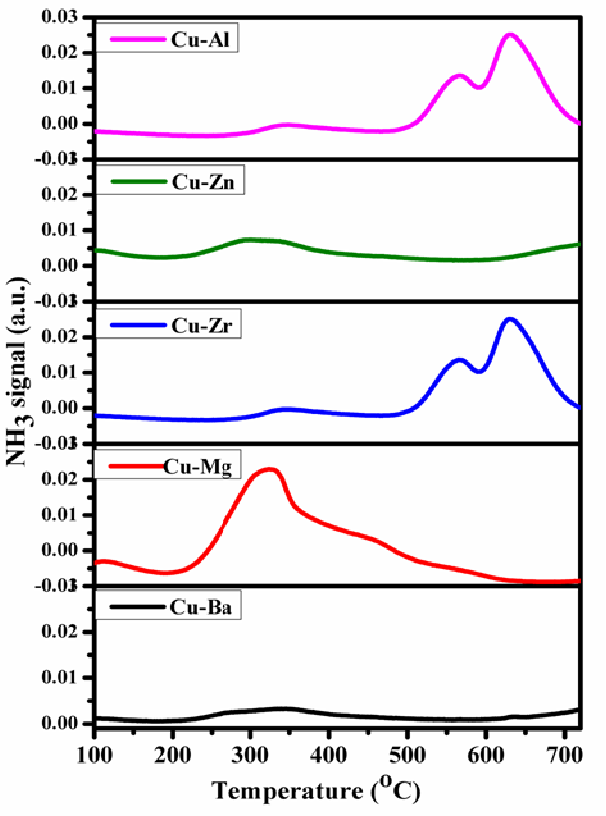

Figure 8.8. NH_3-TPD profiles of different reduced copper catalysts.

Table 8.3. NH_3-TPD results of different copper catalysts

Catalyst	Temperature at maximum (^oC)	NH_3 desorbed (mL g^{-1})
Cu-Ba	334	4.05
Cu-Mg	325	45.71
Cu-Zr	564	3.5
	630	5.9
Cu-Zn	302	7.52
Cu-Al	564	3.2
	630	6.31

240-400 ^oC. The low intensity of this peak (240- 400 ^oC) was indicative of lower acid strength as compared to that of Cu-Mg, Cu-Zr and Cu-Al catalysts. It should be noted that Cu-Ba did not show any NH_3 desorption peak, due to absence of any acid sites. From the NH_3-TPD results the acid strength appeared to follow the trend as Cu-Al>Cu-Zr>Cu-Mg>Cu-Zn>Cu-Ba. The observed variation in acid strength and/or even generation of new active sites was due to incorporation of second metal with Cu.[29] Although, similar dehydration activities of Cu-Al, Cu-Zr and Cu-Mg catalysts were observed, the acetol selectivity variation was in accordance with the acidity trend discussed above.

The distinction between Lewis and BrØnsted acid sites was also determined by py-IR studies. In **Figure 8.9**, Cu-Ba, Cu-Mg, Cu-Zn and Cu-Cr catalysts showed the characteristic bands for pyridine adsorbed on Lewis acid sites at 1507 cm^{-1}, 1458 cm^{-1}, 1436 cm^{-1} and 1445 cm^{-1} respectively.[30] In addition to Lewis acidity, all these catalysts except Cu-Cr also showed the pyridinium ion adsorption bands at 1533-1558 cm^{-1} assigned to BrØnsted acid sites.[31] In case of Cu-Zn, very low intensity of both Lewis and BrØnsted peaks indicate lower acidity which commensurate with the NH_3-TPD results discussed above. Accordingly, Cu-Zn catalyst showed very poor (25%) selectivity to acetol in spite of the highest glycerol conversion. Very interestingly, Cu-Zr and Cu-Al catalysts showed the bands only in the region of 1539-1559 cm^{-1} responsible

for BrØnsted acid sites. The role of Brønsted acid sites has directly reflected on the dehydration efficiency as evidenced by the highest acetol selectivity (87-92%) over Cu-Zr and Cu-Al catalysts.

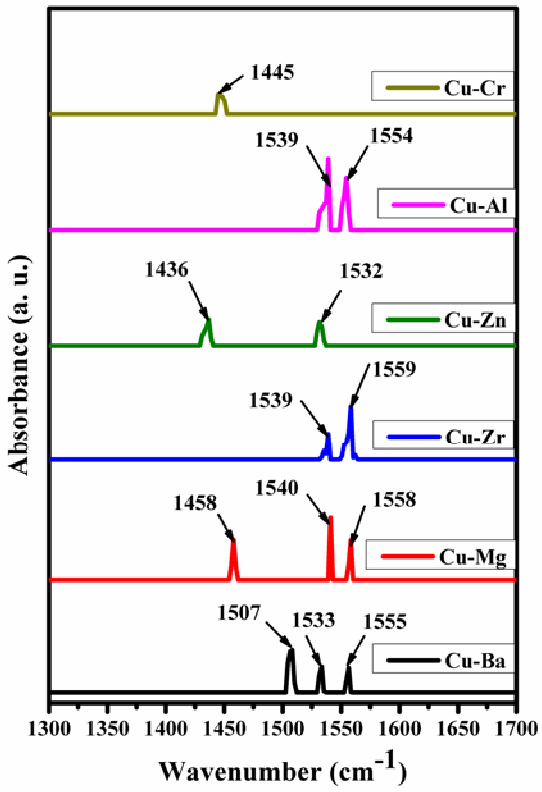

Figure 8.9. Py-IR of different reduced copper catalysts.

An attempt was made to correlate the variation in acid strengths with the basic sites of the catalysts measured by CO_2 TPD technique. All the catalysts except Cu-Mg showed a very mild basicity in the region of 135-280 ^oC (**Figure 8.10**).[32] In case of Cu-Ba catalyst, $BaCO_3$ formation is more facile as also confirmed by XRD, hence the peak observed at 146 ^oC may not be representative of its true basicity. CO_2 TPD profile of Cu-Mg catalyst showed a single small desorption peak at 123 ^oC, while two peaks of increased intensity at 322 and 387 ^oC indicated strong basicity of the catalyst. The dramatic increase in basicity of Cu-Mg was due to the incorporation of Cu metal with an ionic radius slightly larger than Mg^{2+} causing expansion of Mg-O bond length and the localization of the electron density on the oxygen atom.[33] However, the increased

basicity was observed at 322 and 387 °C, which is beyond the reaction temperature of 220 °C, hence might not participate in the reaction.[32]

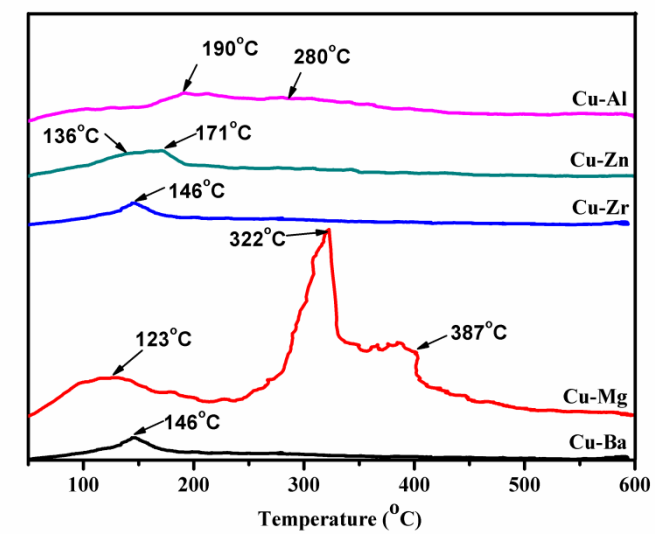

Figure 8.10. CO_2- TPD profiles of different reduced copper catalysts.

8.3.2. Catalyst activity

The surface areas and activity screening of Cu catalysts along with others for the glycerol dehydration in terms of glycerol conversion (%) and product selectivities (%) are shown in **Table 8.4**. Among the several catalysts prepared by modifying Cu with various metal oxides, Cu-Zn showed the highest conversion of 68% while Cu with Mg, Zr and Al showed almost similar activity with a conversion in the range of 21-24 %. The only Cr containing Cu-Cr catalyst though gave complete selectivity to acetol, glycerol conversion was < 5%. Interestingly, these observed activity results could not be explained simply on the basis of surface areas (**Table 8.4**). The acetol selectivity for these catalysts varied in the following order, Cu-Al>Cu-Zr>Cu-Mg. In spite of the highest activity of Cu-Zn catalyst, the selectivity to acetol was as low as 25 % with remaining selectivity to by products such as propionic acid, acetic acid, acetaldehyde and propionaldehyde along with minor amount of 1,2-PDO. Thus, the activity and selectivity patterns need to be explained based on active acid and metal sites rather than the surface area. The lowest acetol selectivity in case of Cu-Zn catalyst was due to its lowest acidity as well as

Table 8.4. Glycerol dehydration over different reduced catalysts

Catalyst	BET surface area ($m^2 g^{-1}$)	Conversion (%)	Selectivity (%)			
			Acetol	1,2-PDO	EG	Others[a]
Cu- Ba	5.4	9	98	2	-	-
Cu-Mg	46.2	24	79	20	1	-
Cu-Zr	22	21	87	13	-	-
Cu-Zn	22	68	25	2	-	73
Cu- Al	70	24	92	8	-	-
Cu-Al[b]	74	11	97	3	-	-
NMT006	31.7	<5	100	-	-	-
Cu-Al[c]	-	75	86	8		6
Cu-Al[d]	-	74	75	13		12
S-ZrO_2	100	-	-	-	-	-
CuO	ND	<1	45	-	-	55
Cu^0	ND	<1	96	-	-	4

Reaction conditions: 20 wt% glycerol aqueous solution, 100 mL; temperature, 220 ^oC; N_2 ambient pressure; catalyst, 1 g; reaction time, 3 h. [a]Propionic acid, acetic acid, acetaldehyde and propionaldehyde. [b]Calcined Cu-Al catalyst. [c]Continuous dehydration without N_2 pressure; GHSV, 500 h^{-1}; LHSV, 1.53 h^{-1}. [d] Continuous dehydration N_2 pressure, 20 bar; GHSV, 500 h^{-1}; LHSV, 2.82 h^{-1}.

absence of metallic Cu phase. A maximum acetol selectivity of 98% was achieved with Cu-Ba catalyst however; glycerol conversion was the lowest (9%) due to its low surface area (5.4 m^2g^{-1}), absence of metallic Cu and least acidity. Inspite of the similar activity performance of the non-chromium Cu based mixed metal oxides such as Cu-Mg, Cu-Zr and Cu-Al, only Cu-Al catalyst showed the highest acetol selectivity. Hence, it was further tested in a fixed bed reactor under continuous flow of N_2 at ambient pressure, which gave three times higher activity than that observed in batch dehydration due to

higher catalyst to substrate ratio (0.67) in the former case. The acetol selectivity of 86 % obtained, was marginally lower than that of batch dehydration (*ca.* 92%) as a result of *in situ* glycerol hydrogenation.[23] This performance was quite stable as evidenced by its on stream activity tested for 36 h (**Figure 8.11**). Under enhanced N_2 pressure conditions, although similar glycerol conversion (74%) was observed but acetol selectivity dropped down to 75%. This could be explained based on the fact that the external pressure of nitrogen would suppress desorption of acetol allowing its further reaction with *in situ* generated H_2 on the catalyst sites to give 1,2-PDO (chapter 7).

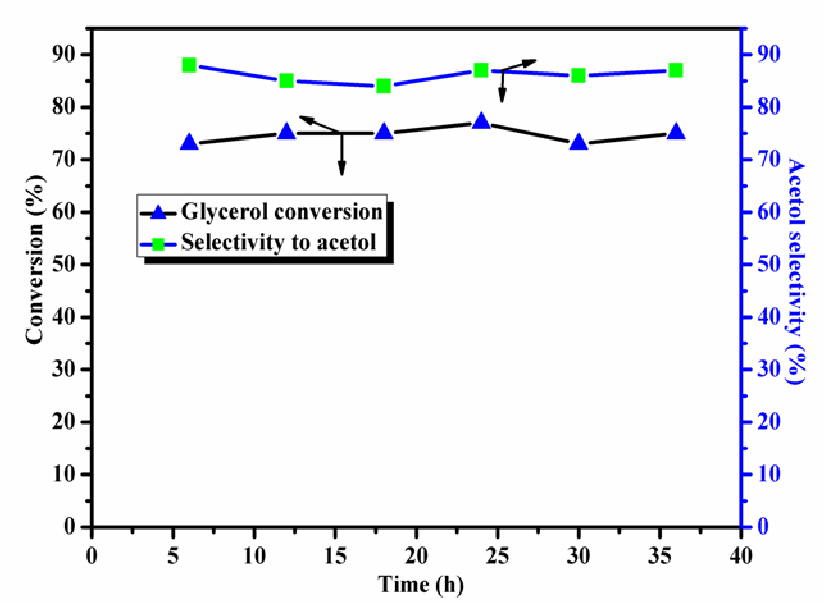

Figure 8.11. Time on stream activity of Cu-Al catalyst.

Reaction conditions: 20 wt% glycerol aqueous solution , without N_2 pressure; GHSV, 500 h^{-1}; LHSV, 1.53 h^{-1}.

A control dehydration experiment, using only calcined Cu-Al catalyst gave half (11%) the conversion than that of its reduced sample (24%), suggesting that the reduced metal sites also play a role in glycerol dehydration pathway to give acetol. The significance of individual sites such as acid, Cu oxide and metallic Cu in this reaction was also examined by the activity of Al_2O_3, [16] S-ZrO_2, CuO and metallic Cu respectively. As can be seen from **Table 8.4**, S-ZrO_2 did not show any activity as well as Al_2O_3 also gave <2 %

glycerol conversion. Similarly, individual CuO and metallic Cu showed poor glycerol conversion (< 4 %), confirming that various individual sites are not active but their appropriate combination is required to catalyze the glycerol dehydration reaction. As Cu-Cr, Al_2O_3 and S-ZrO_2 showed very poor to nil activity, these are not further discussed here.

Effect of glycerol concentration, temperature and catalyst loading on glycerol conversion and acetol selectivity were also studied over Cu-Al catalyst and the results are presented below.

Figure 8.12 shows about 50% decrease in glycerol conversion while acetol selectivity remaining constant at 92%, with three times increase in glycerol concentration (10-30%). This substantial lowering of glycerol conversion was due to substrate inhibited kinetics of the dehydration reaction.[34]

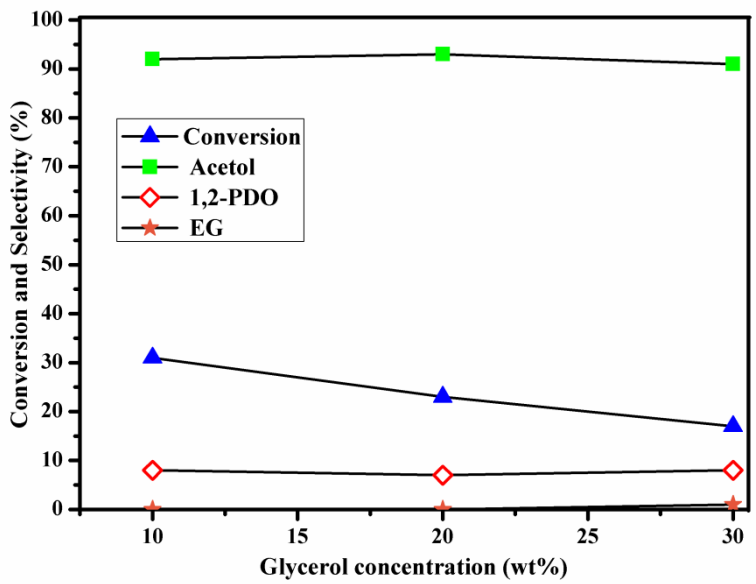

Figure 8.12. Effect of glycerol concentration on conversion and product selectivity. **Reaction conditions:** temperature, 220 ^oC; N_2 ambient pressure; catalyst, 1 g; reaction time, 3 h.

Glycerol conversion was found to be a mild function of temperature up to 220 ^oC while it increased sharply from 24 to 41% for further rise in temperature to 240 ^oC

(**Figure 8.13**). The acetol selectivity was also constant at 92% for an initial rise in temperature from 180 to 220 ^{o}C but decreased sharply to 80% at the highest temperature of 240 ^{o}C. As expected, the glycerol reforming favored at higher temperature resulted into enhanced selectivity to the *in situ* hydrogenation product 1,2-PDO.

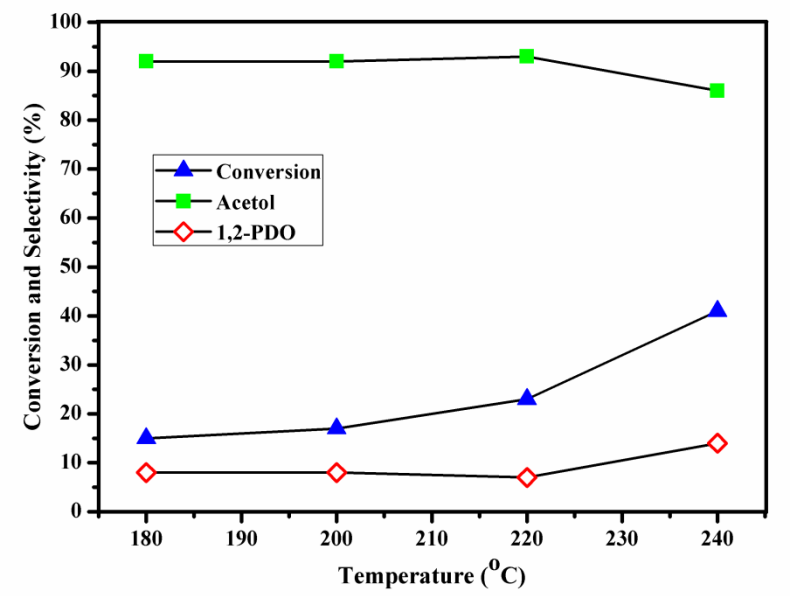

Figure 8.13. Effect of temperature on conversion and product selectivity.
Reaction conditions: 20 wt% glycerol aqueous solution , 100 mL; N_2 ambient pressure; catalyst, 1 g; reaction time, 3 h.

The effect of catalyst loading on the glycerol dehydration reaction was studied in the range of 0.8 to 3.0 g at 220 ^{o}C, and the results are presented in **Figure 8.14**. The glycerol conversion increased from 15 to 38% with marginal decrease in acetol selectivity from 92 to 84% for more than two fold increase in catalyst loading. With further increase in catalyst loading to 3 g, selectivity to acetol markedly decreased from 84 to 61%, while selectivity to the hydrogenation product 1, 2-PDO increased from 7 to 35% along with EG. This was due to the increased availability of active sites catalyzing the *in situ* hydrogenation of acetol as well as C-C cleavage of glycerol.

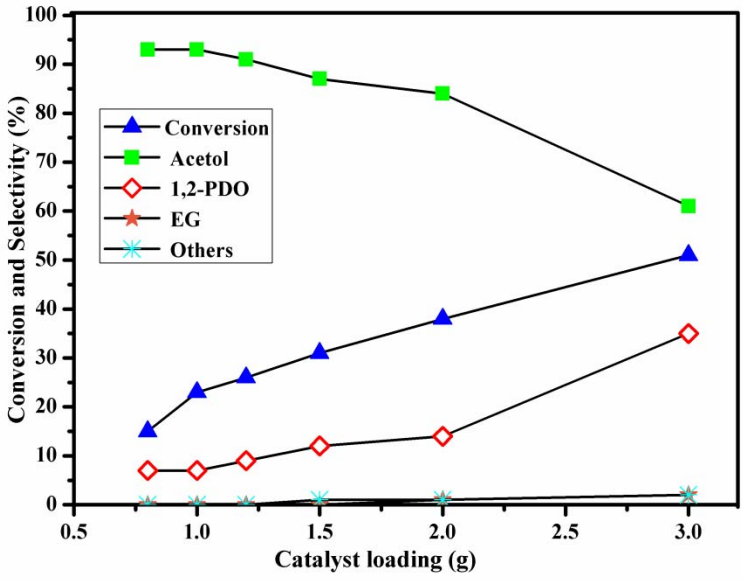

Figure 8.14. Effect of catalyst loading on glycerol conversion and product selectivity. **Reaction conditions :** 20 wt% glycerol aqueous solution, 100 mL; temperature, 220 ^{o}C; N_2 ambient pressure; reaction time, 3 h.

Table 8.5 shows the effect of solvents on dehydration of glycerol. In an aprotic and non-polar solvent like hexane, very low solubility of glycerol led to mainly the formation of oligomeric products of undissolved glycerol; affecting the acetol selectivity adversely (10%).[35]

Table 8.5. Effect of solvent on dehydration of glycerol

Solvent	Conversion (%)	Selectivity (%)			
		Acetol	1,2-PDO	EG	Others
Hexane	57	10	34	0	56
2-propanol	60	63	36	0	1
Dist. water	24	92	8	0	0

Reaction conditions : 20 wt% glycerol solution, 100 mL; temperature, 220 ^{o}C; N_2 ambient pressure; catalyst, 1 g; reaction time, 3 h.

Solubility of glycerol being higher in 2-propanol gave the highest glycerol conversion of 60% than that observed in water (24%). Nevertheless, due to the transfer hydrogenation of acetol to 1,2-PDO in 2-propanol the acetol selectivity drastically dropped down to 63% as compared to the dehydration reaction in water.[36]

The catalyst stability was established by its recycle studies in which the catalyst was filtered out after the first use followed by drying in an oven at 110 ^{o}C and then used for the subsequent glycerol dehydration. This procedure was followed for three subsequent dehydration reactions and the results are shown in **Figure 8.15.** Our Cu-Al catalyst showed consistent performance even after the second recycle. The marginal decrease in conversion from 24 to 22% after the second reuse could be due to the handling losses of the catalyst as well as metal sintering under reaction conditions of high temperature (220 ^{o}C). The stability of this catalyst was also demonstrated in a continuous dehydration run of 400 h as reported in our previous studies.[22]

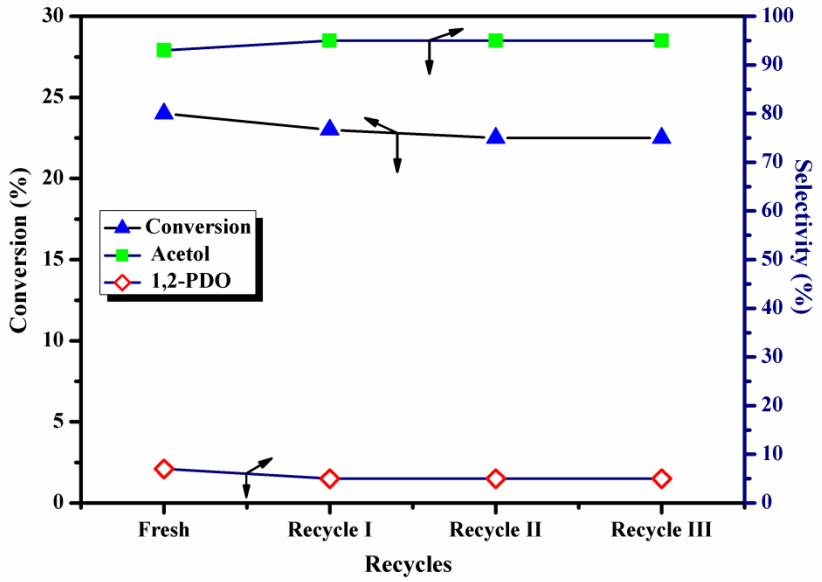

Figure 8.15. Cu-Al catalyst recycle results for glycerol dehydration to acetol.
Reaction conditions : 20 wt% glycerol aqueous solution, 100 mL; temperature, 220 ^{o}C; N_2 ambient pressure; catalyst, 1 g; reaction time, 3 h.

8.3.3. Reaction mechanism

From the characterization and activity results, it was observed that the catalysts (Cu-Mg, Cu-Al and Cu-Zr) having metallic copper along with BrØnsted or combination of BrØnsted and Lewis acidity showed higher selectivity to acetol. As the reaction is carried out in an aqueous medium, BrØnsted sites might be generated by interaction between Lewis sites and water. The concerted mechanism involving Lewis and BrØnsted acid sites is shown in **Scheme 8.2.**

Pathway A involves the abstraction of primary –OH of glycerol and simultaneous abstraction of proton of the adjacent carbon by bridging the O atom of the metal oxide to form enol i. e. 2-3-dihydroxy propene together with the hydrated active sites on the

.

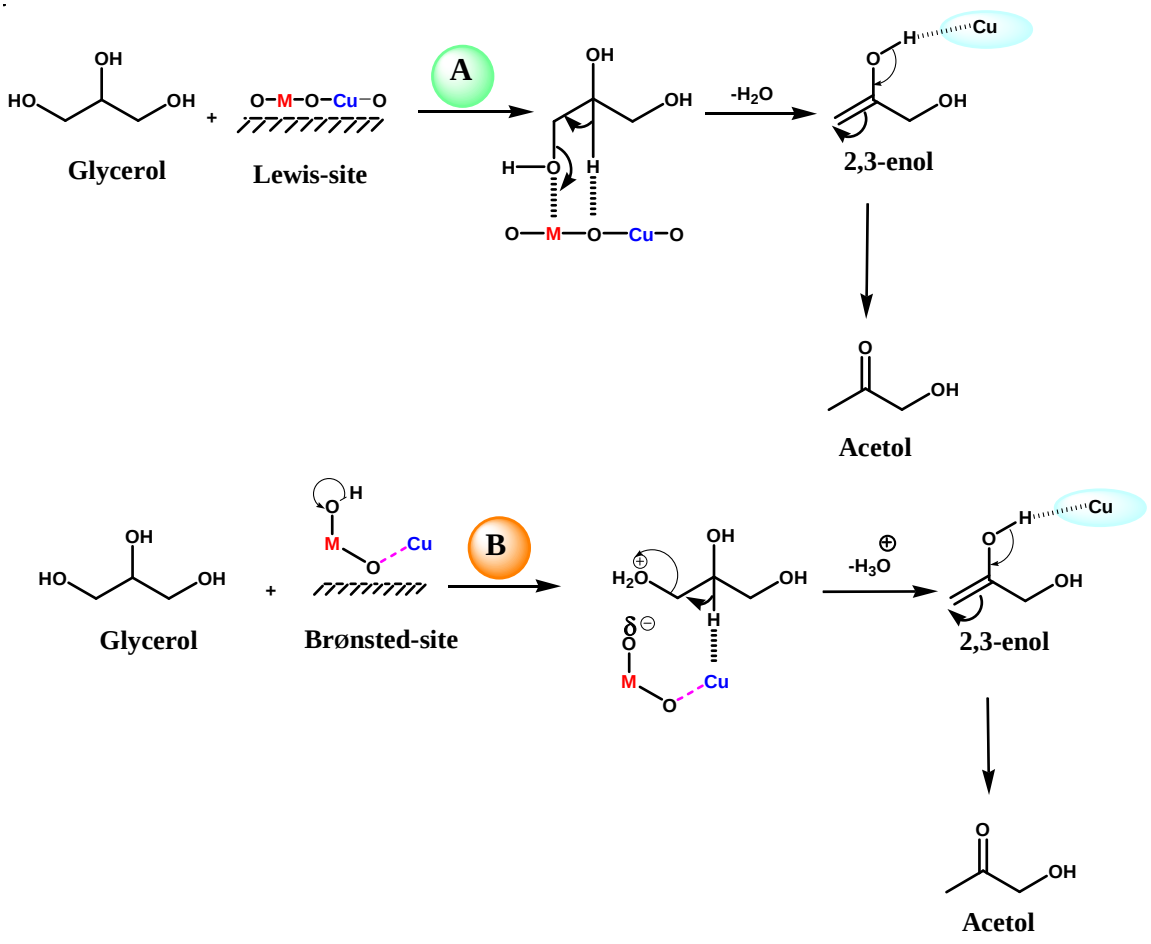

Scheme 8.2. Proposed reaction pathways for glycerol dehydration.

catalyst surface. Further tautomerization of the enol gives acetol through an abstraction of a proton by the metallic Cu and /or CuO with simultaneous protonation of the secondary carbon.[37] Thus, if the polarization power of the second metal cation is higher than Cu, it will abstract –OH *e.g.*, in case of Cu-Mg catalyst, Mg^{2+} having slightly higher polarizing power than that of the Cu^{2+}, will abstract the –OH from glycerol.

The protonation of the secondary –OH by BrØnsted acid sites being more facile because the intermediate secondary carbocation is more stable[38,39] to give a highly unstable aldehyde which on further dehydration forms acrolein (**Scheme 8.1**). However, in our case, the formation of only acetol (stable product) instead of an aldehyde and acrolein indicates the protonation of primary –OH of glycerol. The acetol formation is favored more than the acrolein because of: (i) steric constraints (ii) formation of acrolein is mainly catalyzed by strong BrØnsted acid sites (iii) acrolein formation is an endothermic reaction occurring under high temperature vapor phase conditions.[13]As all the active catalysts *viz.* Cu-Al, Cu-Zr and Cu-Mg showed the BrØnsted acidity, the alternate pathway B is proposed. The protonation of the primary –OH of glycerol followed by the subsequent proton abstraction of secondary carbon by Cu metal and/or oxygen of the metal oxide gives the enol form, 2-3-dihydroxy propene which on subsequent tautomerization gives acetol as discussed above. Most of the Cu in Cu-Zr and Cu-Al catalysts was in metallic form evidenced by XRD and EXAFS as discussed above. Hence, the proton abstraction during dehydration as well as tautomerization was proposed to be catalyzed by metallic copper rather than the metal oxide. This is also confirmed by very low activity and acetol selectivity of Cu-Ba and Cu-Zn respectively, in which metallic Cu was not distinctly observed. Our present studies reveal that catalysts having BrØnsted acidity and metallic Cu species showed the maximum acetol selectivity.

8.4. CONCLUSIONS

- The extent of different copper species formed and alteration in acid sites in various copper catalysts modified with Ba, Mg, Zr, Zn, Al, and Cr has been studied in detail to understand the role of active species in selective glycerol dehydration to acetol.

- The acetol selectivity for these catalysts varied as follows: Cu-Al > Cu-Zr > Cu-Mg. Among these, the most selective Cu-Al catalyst also gave a consistent performance even after the third use, confirming its stability under reaction conditions.
- Cu-Cu metal bond formation was observed distinctly by EXAFS of the Cu-Al and Cu-Zr catalysts.
- Similarly, both these catalysts exhibited moderate and/or strong acidity and presence of only BrØnsted sites responsible for enhancing their glycerol dehydration efficiency. Thus, glycerol dehydration to acetol was found to be catalyzed not only by BrØnsted acid sites but also by the metallic Cu.
- The role of BrØnsted acid sites and metallic copper was also assessed by a control dehydration experiment using only calcined Cu-Al, CuO, metallic Cu and acidic catalysts such as Al_2O_3 and S-ZrO_2.
- Based on these results, two catalytic pathways involving Lewis and BrØnsted acid sites are proposed for glycerol dehydration. In both the pathways, tautomerization of the enol gives acetol through an abstraction of a proton by the metallic Cu and /or CuO with simultaneous protonation of the secondary carbon.

8.5. REFERENCES

1. C. W. Chiu, M. A. Dasari, W. R. Sutterlin, G. J. Suppes, *AIChE J.* **2006,** 52, 3543–3548.
2. G. J. Suppes, W. R. Sutterlin, M. A. Dasari, US Patent 244312, **2005.**
3. X. Wu, Z. Ma, Z. Ye, S. Qian, G. Zhaob, *Adv. Synth. Catal.* **2009,** 351, 158-162.
4. M. H. Mohamad, R. Awang ,W. Md Z. W. Yunus, *Am. J. Appl. Sci.* **2011**, 8, 1135-1139.
5. P. Levene, A. Walti, *Org. Synth.* **1943,** 2, 5.
6. R. S. Disselkamp, B. D. Harris, T.R. Hart, *Catal. Commun.* **2008,** 9, 2250–2252.
7. P. Soucaille, F. Voelker, R. Figge, US Patent 20100279369, **2009.**
8. J. Ko, I. Kim, S. Yoo, B. Min, K. Kim, C. Park, *J. bacterial.* **2005,** 187, 5782–5789.
9. Special Report Chemical Processing, **2008.**
10. R. R. Soares, D. A. Simonetti, J. A. Dumesic, *Angew. Chem.* **2006,** 118, 4086 – 4089.
11. M. Pagliaro, R. Ciriminna, H. Kimura, M. Rossi, C. Della Pina, *Angew. Chem.* **2007,** 119, 4434 –4440.
12. B. Katryniok, S. Paul, M. Capron, F. Dumeignil, *ChemSusChem.* **2009,** 2, 719–730.
13. A. Alhanash, E. F. Kozhevnikova, I. V. Kozhevnikov, *Appl. Catal. A* **2010,** 378, 11–18.
14. S. Sato, D. Sakai, F. Sato, Y. Yamada, *Chem. Lett.* **2012,** 41, 965-966.
15. C. W. Chiu, A. Tekeei, W. R. Sutterlin, J. M. Ronco, G. J. Suppes, *AIChE J.* **2008,** 54, 2456-2463.
16. S. Sato, M. Akiyama, R. Takahashi , T. Hara , K. Inui, M. Yokota, *Appl. Catal. A* **2008,** 347, 186–191.
17. W. Suprun, M. Lutecki, T. Haber, H. Papp, *J. Mole. Catal. A* **2009,** 309, 71–78.
18. A. Yamaguchi, N. Hiyoshi, O. Sato, C. V. Rode, M. Shirai, *Chem. Lett.* **2008,** 37, 560-561.
19. A. Yamaguchi, N. Hiyoshi, O. Sato, M. Shirai, *Top. Catal.* **2010,** 53, 487–491.

20. A. K. Kinage, P. P. Upare, P. Kasinathan, Y. K. Hwang, J. S. Chang, *Catal. Commun.* **2010,** 11, 620-623.
21. G. Raju, P. S. Reddy, B. M. Reddy, *The Open Catal. J.* **2011,** 4, 83-87.
22. R. B. Mane, C. V. Rode, *Org. Process Res. Dev.* **2012,** 16, 1043−1052.
23. R. B. Mane, C. V. Rode, *Green. Chem.* **2012,** 14, 2780-2789.
24. R. B. Mane, A. Yamaguchi, A. Malawadkar, M. Shirai, C. V. Rode, *RSC Adv.* **2013,** 37, 16499-16508.
25. B. Sreedhar, Ch. SatyaVani, D. Keerthi Devi, M. V. B. Rao and C. Rambabu, *Am. J. Mater. Sci.* **2012,** 2, 5-13.
26. J. Agrell, H. Birgersson, M. Boutonnet, I. Melián-Cabrera, R. M. Navarro and J. L.G. Fierro, *J. Catal.* **2003,** 219, 389–403.
27. M. C. Hsio, H. P. Wang, Y. W. Yang, *Environ. Sci. Technol.* **2001,** 35, 2532-2535.
28. D. Mao , W. Yang, J. Xia, B. Zhang, Q. Song, Q. Chen, *J. Catal.* **2005,** 230, 140-149.
29. G. M. S. El Shafei, *J. Colloid and Inter. Sci.* **1996,** 182, 249-253.
30. Z. M. El-Bahy, R. Ohnishi, M. Ichikawa, *Appl. Catal. B* **2003,** 40, 81-91
31. T. Barzetti , E. Selli , D. Moscotti, L. Forni, *J. Chem. Soc. Faraday Trans.* **1996,** 92, 1401-1407.
32. J. Wang, C. Zeng, *J. Nat. Gas Chem.* **2005,** 14, 156-162
33. H. Kurokawa, T. Kato, T. Kuwabara, W. Ueda, Y. Morikawa, Y. Moro-Oka, T. Ikawa, *J. Catal.* **1990,** 126, 208-218.
34. M. M. Telkar, C. V. Rode, V. H. Rane, R. Jaganathan, R. V. Chaudhari, *Appl. Catal. A* **2001,** 216, 13–22.
35. A. Martin, M. Richter, *Eur. J. Lipid Sci. Technol.* **2011,** 113, 100–117.
36. M. G. Musolino, L. A. Scarpino, F. Mauriello, R. Pietropaolo, *Green. Chem.* **2009,** 11, 1511-1513.
37. K. Kongpatpanich, T. Nanok, B. Boekf, M. Probste, J. Limtrakul, *Phy. Chem. Chem. Phys.* **2011,** 13, 6462-6470.
38. J. ten Dam, U. Hanefeld, *ChemSusChem.* **2011,** 4, 1017-1034.

39. D. Coll, C. F. Delbecq, Y. Aray, P. Sautet, *Phys. Chem. Chem. Phys.* **2011,** 13, 1448–1456.

Chapter 9

Multifunctional Cu-Al catalysts for water gas shift reaction

Due to multifunctional nature of our Cu-Al catalyst, it was found to be highly active for glycerol hydrogenolysis, dehydration as well as autogeneous hydrogenolysis involving glycerol APR. Hence, we also explored it for water gas shift reaction (WGSR) and to our expectations it gave excellent activity for the same. The formation of various Cu species was achieved by systematically varying the Cu-Al composition and 70:30 ratio of Cu-Al was found to be the best for WGSR using reformate gas mixture. In addition, the Cu-Al (70:30) catalyst reduced under 100% H_2, showed a very stable time on stream of 100 h, at higher gas hourly space velocity (GHSV) of 36,201 h^{-1}. The presence of non-zero and metallic copper, lower extent of Cu aggregation along with particle size stabilization due to boehmite phase and Cu_2O, were the essential aspects for the observed WGSR activity.

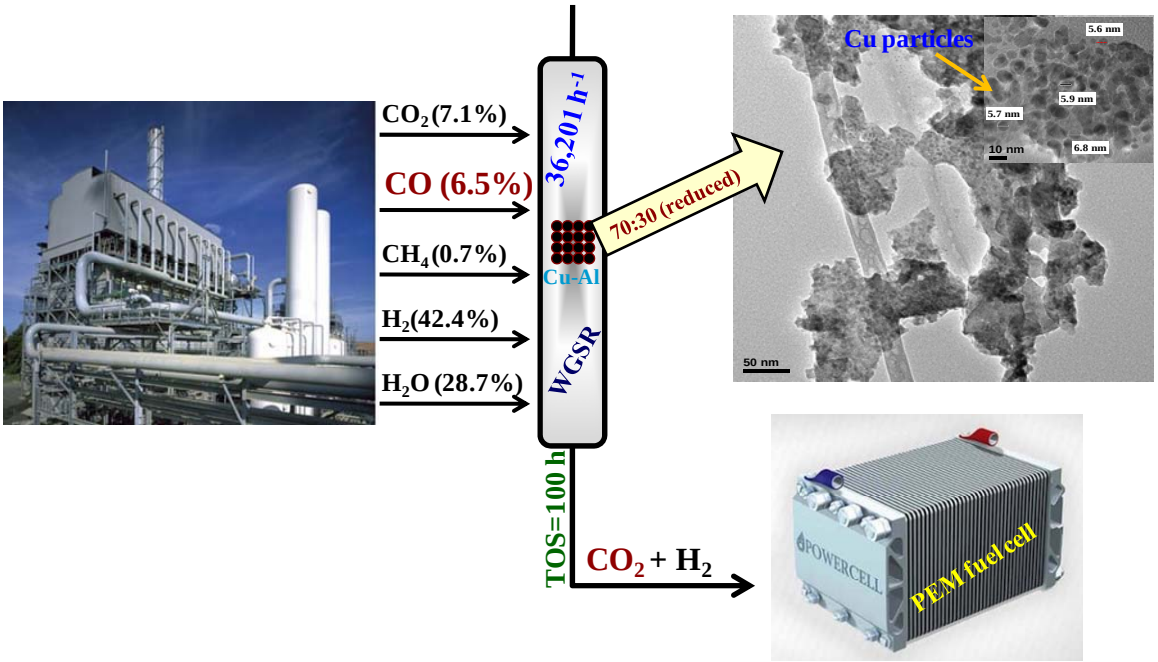

***ChemCatChem* (communicated, 2013)**

9.1. INTRODUCTION

As our multifunctional Cu-Al catalyst was found to be most active for selective aqueous phase hydrogenolysis of renewable glycerol to 1,2-PDO using external and *in situ* generated hydrogen as well as for dehydration of glycerol to acetol, its efficiency was also tested for the water gas shift reaction (WGSR) in order to generate hydrogen by utilizing CO and water from the reformate gas mixture. Increased concern towards the clean energy source proposed hydrogen as the ideal fuel having potential applications in various fields. Fuel cell is one of the primary technologies utilizing hydrogen and is considered as an attractive energy system because of its high power density, low-temperature operation, low emissions of NO_x and greenhouse gases.[1] Hydrogen obtained from hydrocarbons either by steam reforming or auto thermal reforming was used as a fuel for polymer electrolyte fuel cell (PEFCs).This reformed gas contains 1-10% CO, to which Pt electrode of PEFC is not tolerant.[2] So it is necessary to lower the CO level to <10-50 ppm for fuel cell application. The water gas shift reaction (WGSR, $CO+H_2O$) and preferential CO oxidation ($2CO+O_2$) not only reduce the CO content but also maximize H_2 yield.[3,4] The WGSR is mildly exothermic (ΔH = -40.6 kJ mol^{-1}) and thermodynamically favored at lower temperature but kinetically, the reactant gases are not active to reach the chemical equilibrium at lower temperature. Also, WGSR is not affected by the pressure as there is no change in volume from reactant to product. Industrially, WGSR is carried out using high (320-450 ^oC) and low (190-250 ^oC) temperature shift catalysts such as Fe_3O_4/Cr_2O_3 and $Cu/ZnO/A_2O_3$) respectively.[5] However, they are not viable for small scale operation due to long and tedious pretreatment procedure and are likely to be pyrophoric.[6] Therefore, there is a need to design highly efficient, air tolerant, cost effective and low temperature active catalysts for WGSR.

Ceria possessing high oxygen storage capacity (OSC) has been effectively used as a support for both noble (Au, Rh, Pt, Pd) as well as non noble metals (Cu, Ni) for low temperature WGSR.[7-10] Nevertheless, cost intensive factor restricts the application of noble metals hence, more focus is on development of non noble metal catalysts. Among these, Cu was the most attractive choice due to its higher activity for low temperature

WGSR. However, copper catalysts show lower stability to oxidant gases [11-13] hence, a challenge still exists to develop highly active and stable Cu-based catalysts. While studying the effect of different precipitants, Li *et al.* reported that CuO/CeO_2 catalyst using NH_3 rather than carbonates, gave much higher CO conversion (~ 90% at 200-250 ^oC) for WGSR for a feed of (10% CO, 60% H_2, 12% CO_2 and balance N_2) at much lower GHSV of 3000 h^{-1}.[14] Nanoclusters of noble metals as well as Cu individually encapsulated in mesoporous ceria prepared using expensive SBA-15 as a template were also evaluated for a feed composition (5.6% CO and 22.44% H_2O), different form that of a reformate gas.[15] Studies on bimetallic Cu-Ni on La-doped mesoporous ceria showed a synergetic effect of Cu in suppressing the methanation reaction and high WGS activity of Ni.[16] A major drawback associated with ceria is its irreversible reduction in presence of excess H_2 leading to the catalyst deactivation,[17,18] hence most of the studies using ceria were carried out under synthetic gaseous composition without H_2.

Besides CeO_2, commercially used support ZnO for Cu catalyst has been also studied by modifying it with alkali metals as well as by addition of Al_2O_3, SiO_2 and MnO.[19-23] The effect of catalyst calcination and reduction temperatures, Cu/Mn molar ratio and process parameters like CO and CO_2 concentration on the activity of spinel Cu/MnO were studied for WGSR under the realistic conditions of fuel cell.[24] Among various CuB_2O_4 spinel catalysts, only Cu-Zn-Al having easily reducible Cu gave higher activity for WGSR for H_2O/CO (= 4.4) and gas flow rate of 33 mL min^{-1}.[25] Under the conditions relevant to fuel cell application, the incorporation of CeO_2 and ZnO in Cu-Al_2O_3 did not show any promotional effect while Cu was the only active site for WGSR.[26] In another attempt to enhance the Cu activity recently, Lin *et al.* developed well dispersed Cu in a bimetallic Cu-Ni catalyst which inhibited methanation reaction leading to high catalyst activity in both medium and high temperature ranges (>350 ^oC).[27,28] Cu-Al-O_x catalysts prepared by various methods were reported to impart higher activity than commercial $Cu/ZnO/Al_2O_3$ catalyst even for DSS operation in WGSR, due to boehmite stabilized Cu particles.[29] While correlating the activity and basicity of Cu catalysts, it was shown that increase in weak basic sites on Cu-AlO_x and Cu-ZnO_x catalysts, increased the WGS activity per Cu^0 surface area.[30]

Although, several attempts were made to enhance stability and activity of copper catalysts for WGSR, most of these studies were at very low gas hourly space velocity (GHSV) and/or with non-reformate gas composition (with low CO concentration < 5%). Nevertheless, structural aspects of Cu-Al_2O_3 catalyst system seemed to be more promising hence in this work, we discussed various Cu species/phases formed by varying Cu-Al composition in the co-precipitated Cu-Al oxides. The screening of these catalysts showed that Cu-Al composition of 70:30 was the best for WGSR using reformate gas composition at higher GHSV (36,201 h^{-1}).[31] This composition was structurally investigated in detail for understanding its higher activity, complete CO_2 selectivity and stability.

9.2. EXPERIMENTAL

A series of Cu-Al catalysts were prepared by a co-precipitation method following the procedure given in chapter 2 (section 2.3.3). The catalysts with different at.% of Cu *viz.* 10, 30, 50, 70 and 80% were prepared and designated as Cu-Al-1, Cu-Al-3, Cu-Al-5, Cu-Al-7 and Cu-Al-8 repectively. All the prepared catalysts were calcined at 400 ^oC for 3 h. Prepared catalysts were characterized by various techniques and a detailed experimental procedure is given in chapter 2 (section 2.4). Activity tests were carried out from 200 to 400 ^oC under atmospheric pressure in a fixed-bed micro-tubular quartz reactor with an inner diameter of 4 mm and a detailed procedure is given in chapter 2 (section 2.5.3). The catalyst charged was 48 mg and a gas hourly space velocity (GHSV) of 36,201 h^{-1} was used to screen the catalysts in this study.

9.3. RESULTS AND DISCUSSION

9.3.1. Catalyst characterization

BET surface areas along with Cu metal area and its dispersion in Cu-Al catalysts with varied compositions are presented in **Table 9.1.** With increase in Cu loading from 10 to 30 at.%, BET surface area increased considerably however, it remained almost constant

in the range of 38-43 m^2 g^{-1} with further increase in Cu loading up to 80 at.%. Cu metal area as measured by N_2O adsorption method, increased by several folds with initial rise in Cu loading from 10 to 30 at.% while, further rise in Cu loading up to 70 at.% showed the decrease in Cu metal surface area from 4.22 to 1.69 m^2 g^{-1} and again increased to 5.66 m^2 g^{-1}. Similar trend was observed for the % Cu dispersion. The initial substantial enhancement in metal surface area was obviously due to the increased Cu content. While, decrease in surface area and Cu dispersion despite of a significant increase in the Cu loading up to 70 at.% was possibly due to the fact that all the Cu^0 sites on the surface could not be oxidized by N_2O because of metal aggregation.[32] However, further increase in Cu loading to 80 at.% resulted in much higher metal surface area but Cu dispersion did not increase proportionately because of much higher Cu loading than Al.

Table 9.1. Physico-chemical properties of Cu-Al catalysts

Catalyst	BET surface area (m^2g^{-1})	Cu metal surface area (m^2 g^{-1})	Cu dispersion (%)
Cu-Al -1	27.7	0.02	0.04
Cu-Al-3	39.0	4.22	2.18
Cu-Al -5	38.4	3.58	1.11
Cu-Al-7	32.4	1.69	0.37
Cu-Al -8	43.6	5.66	1.10

BET surface area of 70:30 Cu-Al samples after calcination and reduction under various conditions and that of used catalysts were measured and the results are given in **Table 9.2.** The sample reduced under 5 % H_2+N_2, showed slight increase in surface area than that of the calcined sample while the sample reduced under 100 % H_2 showed much lower surface area of 19 m^2 g^{-1}. This is due to the use of 100 % H_2 for reduction causing aggregation of Cu particles.[33] However, the activity results could not be explained based on only metal surface area and dispersion (discussed later).

Table 9.2. BET surface areas of calcined, reduced and used Cu-Al-7 catalyst.

Catalyst	BET surface area ($m^2 g^{-1}$)
Calcined	32.4
Reduced (5% H_2)	37.1
Reduced (100% H_2)	19.7
Used Cu-Al after 25 h	9.5
Used Cu-Al after 100 h	8.2

H_2-TPR profiles of various Cu-Al catalysts in **Figure 9.1** show very interesting features. The lowest Cu containing catalyst (10 at.%) showed two peaks, first prominent in the region of 350-400 ^oC and another small one at about 600 ^oC. Both the peaks observed at higher temperature than those in all the samples indicate that most of the loaded 10 at.% Cu diffused into Al lattice leading to the formation of $CuAl_2O_4$ which was rather difficult to reduce.[34] The shift of H_2 consumption peaks to lower temperature (<300 ^oC) for 30 and 50 at.% Cu loadings was due to surface enrichment with highly dispersed and hence easily reducible CuO species.[24] This result also corresponds with the Cu^0 surface area and metal dispersion (**Table 9.1**). The catalyst with 70 at.% Cu showed first, a small peak at ~ 250-300 ^oC and another broader peak at higher temperature of 350-400 ^oC. The presence of lower temperature peak represents the reduction of CuO species while the broader peak in the high temperature range indicates the aggregation and/or a high degree of interaction between the species. The strong interaction between mixed oxides with Al was also manifested by a broad reduction peak around 350 ^oC in case of TPR profile of the reduced sample of 70 at.% Cu loading. As the Cu loading was increased to 80 at.%, the interaction between Cu and Al decreased. This resulted in surface enrichment with the easily reducible CuO at lower temperature of 200 ^oC and bulky CuO and/or isolated Cu species reduced at higher temperature of 250 ^oC. From these results, 70:30 was found to be an optimum Cu-Al composition for maximum interaction between Cu and Al species giving the most efficient WGS catalyst.

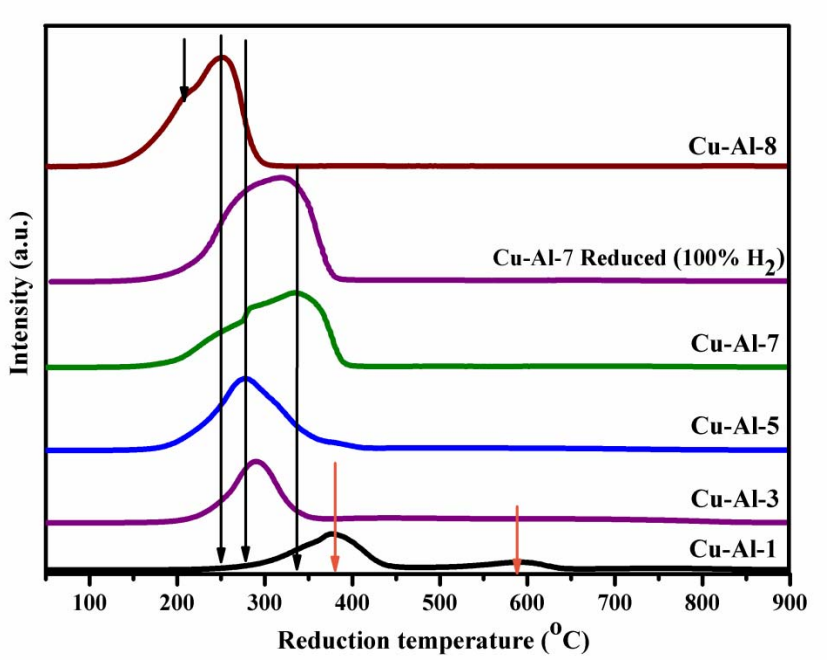

Figure 9.1. TPR of calcined Cu-Al catalysts of different compositions.

As the reduced Cu-Al catalysts were evaluated for WGS reaction, the XRD patterns of these samples are shown in **Figure 9.2.** The catalysts with the lower Cu loadings of 10 and 30 at.% did not show any distinct copper phases indicating fine dispersion of Cu. However, in the case of 10 at.% Cu loading, the peaks at 2θ = 23.8° (111), 27.6° (200), 39.6° (220) [JCPDS File no.s 77-2151, 77-2176] could be attributed to residual K_2O (precipitating agent used K_2CO_3). As Cu loading increased from 50-80 at.%, intensity as well as width of various peaks also increased indicating more crystalline nature of the catalysts. Sample with 50 at.% Cu showed two peaks at 2θ = 35.5° (002) and 38.8° (111) indicating the presence of only CuO [JCPDS file no. 80-1917] that remained unreduced even under 5 % H_2 at 200 °C conditions. Cu-Al-7 sample (Cu 70 at.%) showed peaks at 2θ = 35.5 ° (002), 38.8° (111), 48.8° (202), 58.5° (202), 66.1° (311), 68.1° (220) and less intensity peaks at 2θ = 36.4° (111), 61.7° (220) [JCPDS file no. 77-0199] attributed to CuO and Cu_2O phases, respectively. These results proved the stepwise reduction of CuO was started but complete reduction to Cu^0 was not observed. Further increase in Cu loading to 80 at.% showed the appearance of new peaks at 2θ = 43.2° (111), 50.4° (200), 74.1° (220) as a result of formation of metallic Cu phase [JCPDS file no. 85-1326].

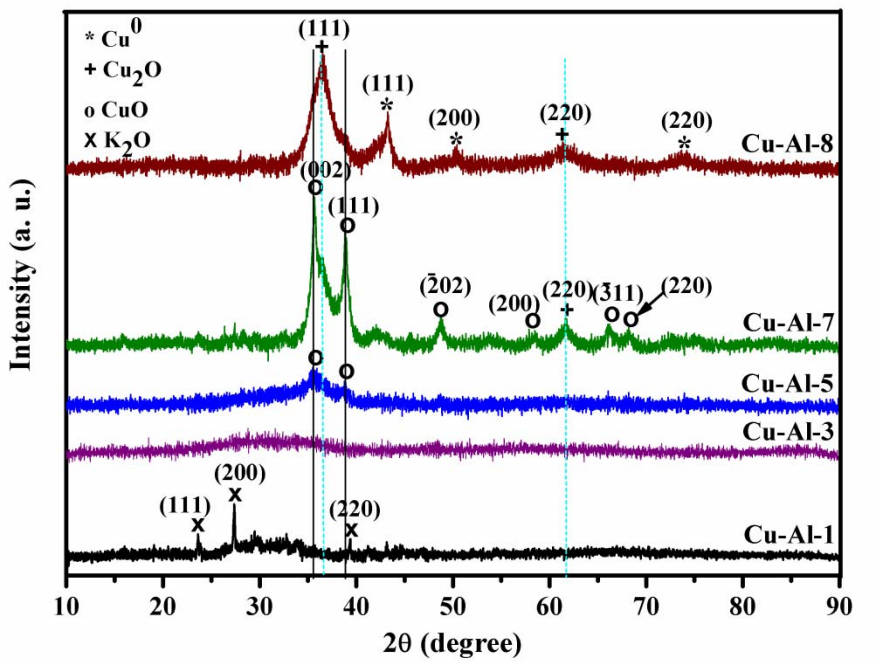

Figure 9.2. XRD of reduced (5% H_2+N_2) Cu-Al catalysts of different compositions.

Along with this, Cu_2O phase formation was also evident from a broad peak at $2\theta = 36.7^o$ (111) however, the presence of CuO could not be ruled out due to merging of the corresponding peaks at $2\theta = 35.5^o$ and a very small one at 38.8^o. Thus, the extent of reduction is higher although not complete, in the catalyst with higher Cu content as compared to other catalysts. These results also corroborate with the TPR characterization.

In order to understand the difference in activity of Cu-Al-7 catalyst reduced under two different conditions, their XRD characterization results were compared with each other as well as with those of calcined and used samples (**Figure 9.3**). As expected, the calcined sample showed the presence of only CuO phase evident from the reflections at $2\theta = 35.5^o$ (002), 38.8^o (111), 48.8^o (202), 66.2^o ($\bar{3}$11). XRD pattern of the catalyst reduced under pure hydrogen showed the peaks at $2\theta = 35.5^o$ (002), 38.8^o (111), 48.8^o (202) corresponding to CuO phase. Along with these, predominant peaks at $2\theta = 36.6^o$ (111), 42.1^o (200), 61.7^o (220) and less intensity peaks at $2\theta = 43.2^o$ (111), 74.1^o (220) attributable to Cu_2O and Cu^0, respectively, suggest the step-wise reduction of CuO. However under 5% H_2+N_2 conditions, the absence of Cu^0 phase and lower intensity peaks of Cu_2O confirmed the incomplete reduction of CuO. In case of used catalysts,

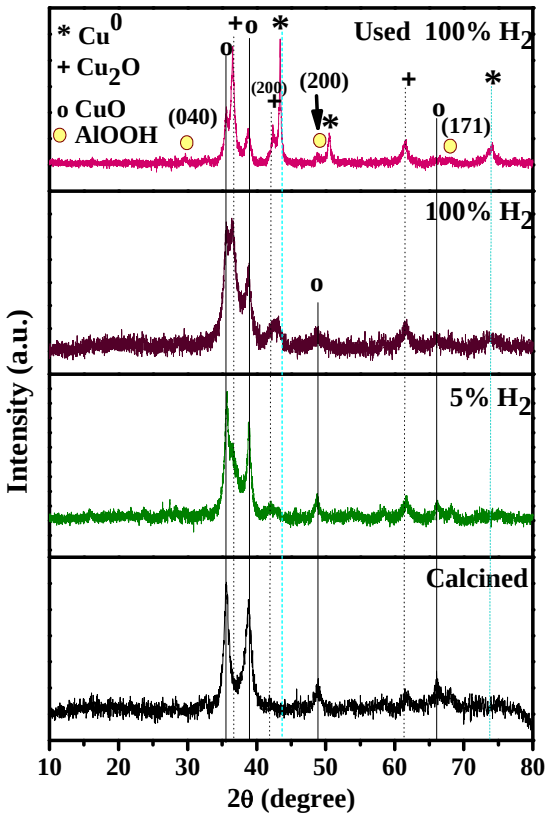

Figure 9.3. XRD of calcined, reduced and used (24 h) samples of Cu-Al-7 catalyst.

high intensity peaks at 2θ = 43.2° (111), 50.4° (200), 74.1° (220) and 36.6° (111), 61.7° (220), 29.4° (110) confirmed the progressive reduction of CuO to Cu^0 through Cu_2O under WGSR conditions. However, complete reduction of Cu_2O to Cu^0 is still not possible as water is known to oxidise Cu to Cu_2O but not the further oxidation to CuO.[35] The presence of stable CuO species (peaks at 2θ = 35.5° (002), 38.8° (111), 48.8° (202)) was due to its inaccessibility by surrounding Alx-Oy. Thus, co-existence of various reduced and oxidised Cu species contribute to the activity of the developed Cu-Al-7 catalyst (discussed later). Used Cu-Al-7 also showed the diffraction peaks at 2θ = 29.6° (040), 49.3° (200), 67.6° (171) [JCPDS file no. 72-0359] corresponding to boehmite (AlOOH) phase formed under WGS conditions where steam is one of the prevailing components.[36] Thus, not only Cu aggregation is prevented by the formation of boehmite but also Cu particle size gets stabilized due to presence of Cu_2O phase in 100 % H_2

reduced and used sample which was also evidenced from the HR-TEM images discussed later.[37]

The effect of different conditions on the particle size, morphology and fringe patterns of Cu-Al-7 catalyst was distinctly observed in HR-TEM images. **Figure 9.4** (**a**) showed bigger size (14-16 nm) particles of Cu-Al-7 catalyst reduced under 5 % H_2 than those of reduced under 100 % H_2 (5-7 nm, **Figure 9.4, b**). It is most likely that 100 % H_2 reduction led to the formation of smaller, partially and completely reduced Cu_2O and metallic Cu particles, respectively, as confirmed by XRD. Under 5 % H_2 reduction conditions, the catalyst mainly existed as CuO confirmed by the fringe pattern in **Figure 9.4** (**c**) that matched very well with the XRD analysis discussed above. Reduction under 100 % H_2 formed the catalyst with majority of smaller size Cu_2O and Cu^0 particles, as seen from the fringe pattern in **Figure 9.4** (**d**). In addition, needle-like typical morphology of boehmite was also observed (**Figure 9.5, a**).[38] Even after the reaction time of 24 and 100 h, particle size was stable in the range of 4-7 nm as shown in **Figure 9.6** (**a**). The fringe pattern in **Figure 9.6** (**b**) indicated that metallic Cu phase was formed during the reaction. In case of 100 h used sample, a number of small Cu metal particles (5 nm) were seen on the boehmite (**Figure 9.4, e**), the later helped to prevent the aggregation of metal particles. The fringe pattern of this sample shown in **Figure 9.4** (**f**) confirmed the existence of metallic Cu, Cu_2O and boehmite (AlO(OH)) phases.[29] The formation of boehmite phase was also clearly evident from the SEM images without any change in needle-like morphology in used samples of 24 and 100 h reaction time, as shown in **Figures 9.7** (**a**) **to** (**c**). The Cu metal aggregation was visible for the particles away from the boehmite phase. The inhibition of Cu metal particle aggregation by *in situ* formation of boehmite leads to high stability of the catalysts as discussed later.

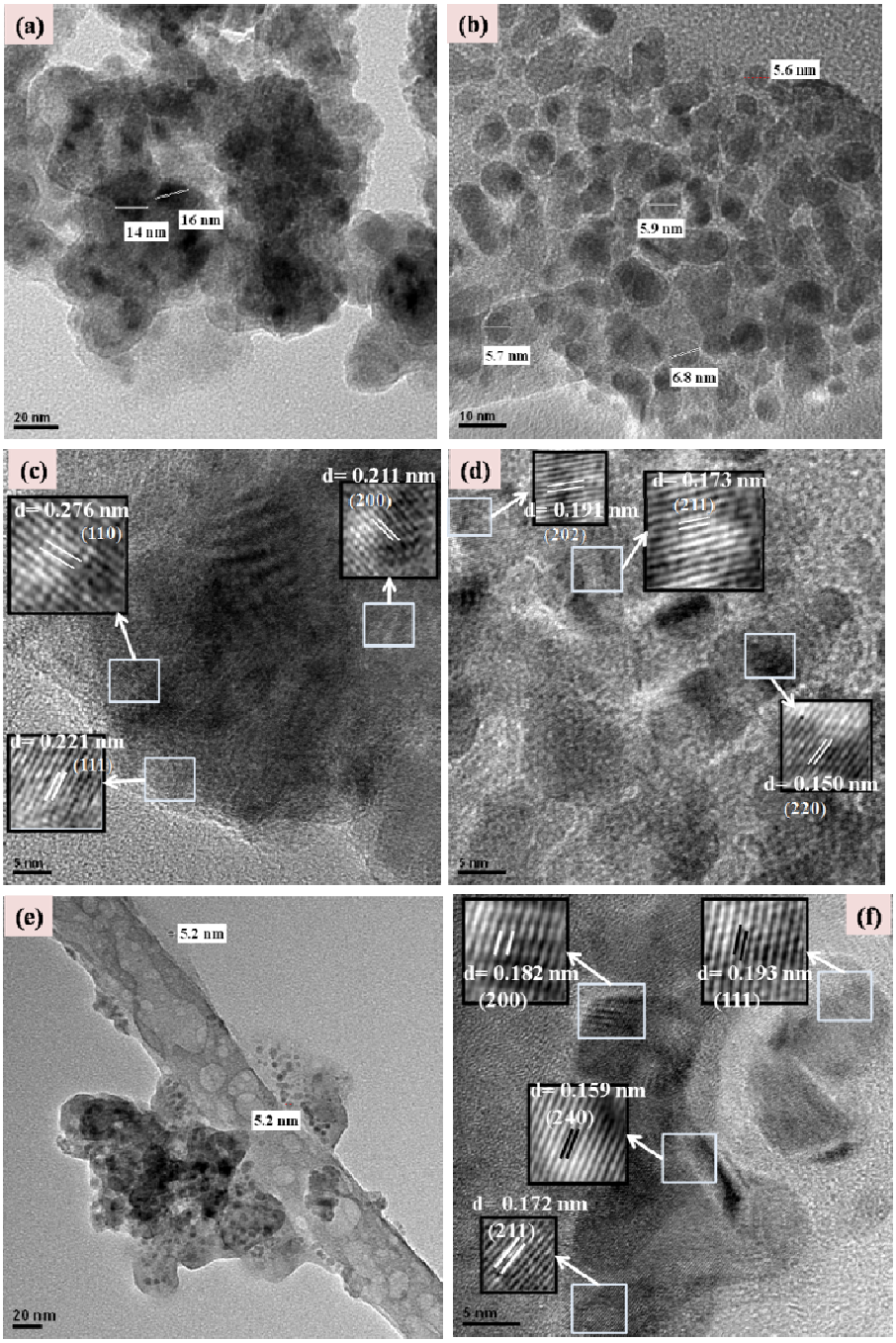

Figure 9.4. HR-TEM images of Cu-Al-7 catalysts (a) 5 % H_2 reduced- showing particle size of 14-16 nm (b) 100 % H_2 reduced-showing particle size of 5.6-6.8 nm (c) fringe pattern of 5 % H_2 reduced sample (d) fringe pattern of 100 % H_2 reduced sample (e) used 100 h sample (f) fringe pattern of used 100 h sample.

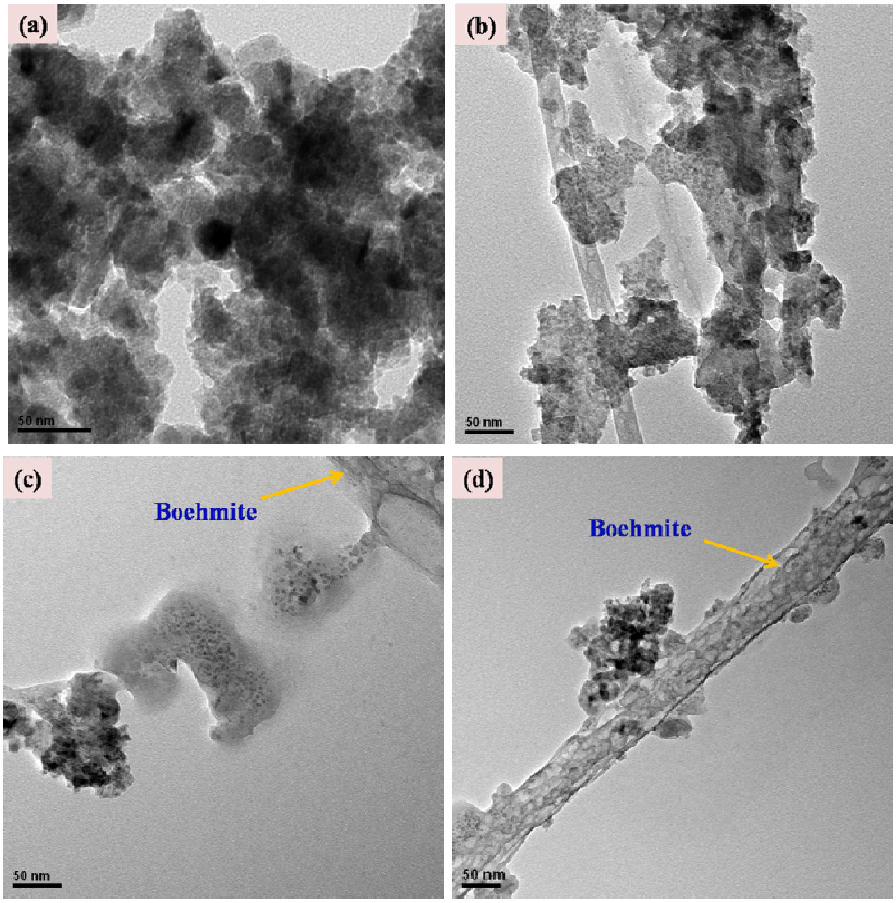

Figure 9.5. HR-TEM images of Cu-Al-7 (a) 5% H_2 reduced (b) 100% H_2 reduced (c) used 24 h (d) used 100 h.

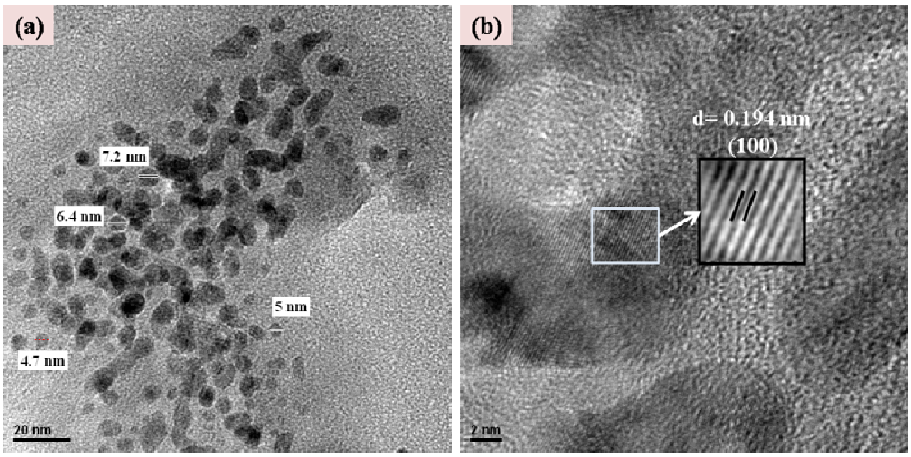

Figure 9.6. HR-TEM images of Cu-Al-7 (100 % H_2 reduced) used 24 h catalyst (a) showing particle size of 4-7 nm (b) fringe pattern with 'd' spacing.

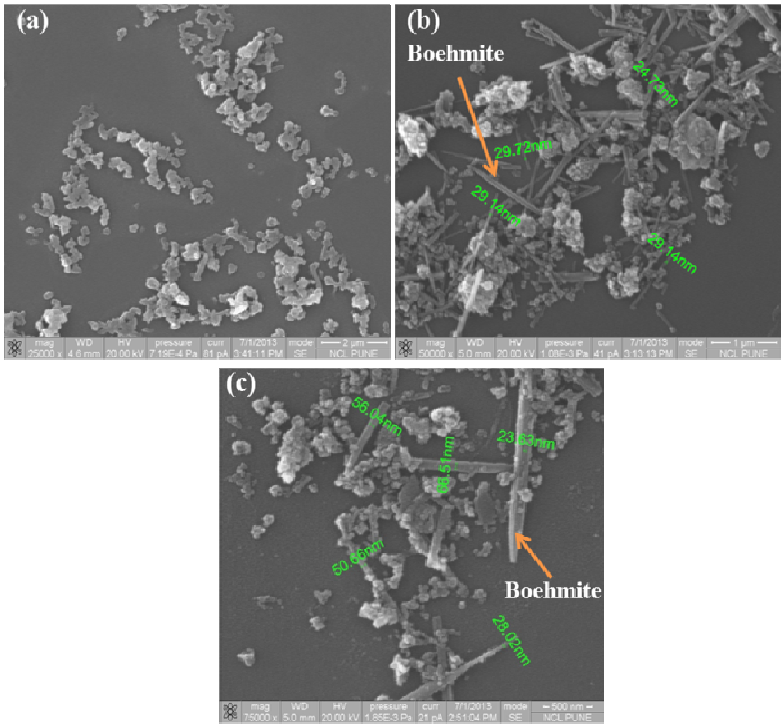

Figure 9.7. SEM images of Cu-Al-7 catalysts, 100% H_2 reduced samples (A) Reduced (B) used 24 h (C) used 100 h.

9.3.2. Catalyst activity

Figure 9.8 (**a)** shows the activity of Cu-Al catalysts with different compositions, for CO conversion at different temperatures. Cu- Al-1 catalyst with the lowest Cu loading of 10 at.% showed the least activity with CO conversion in the range of 5-30% for the rise in temperature from 200-400 ^{o}C. The CO conversion increased linearly from 30 to 69% with increase in Cu loading from 10-50%, at 400 ^{o}C. While for 70 at.% Cu loading, maximum conversion of 76% was observed at 360 ^{o}C than that at 400 ^{o}C (70%). Further increase in Cu loading to 80 at.% lowered the CO conversion dramatically to 60% at 400 ^{o}C which is even lower than that of Cu-Al-5 (Cu loading = 50 at.%). We strongly believe that although Cu is an active component in the catalyst, its appropriate concentration along with Al to form active species is necessary for the optimum activity. Similar observation was made in the case of Cu/MnO and other Cu-based catalysts in which it was concluded that the WGSR activity was not only dependent on Cu metal but also on

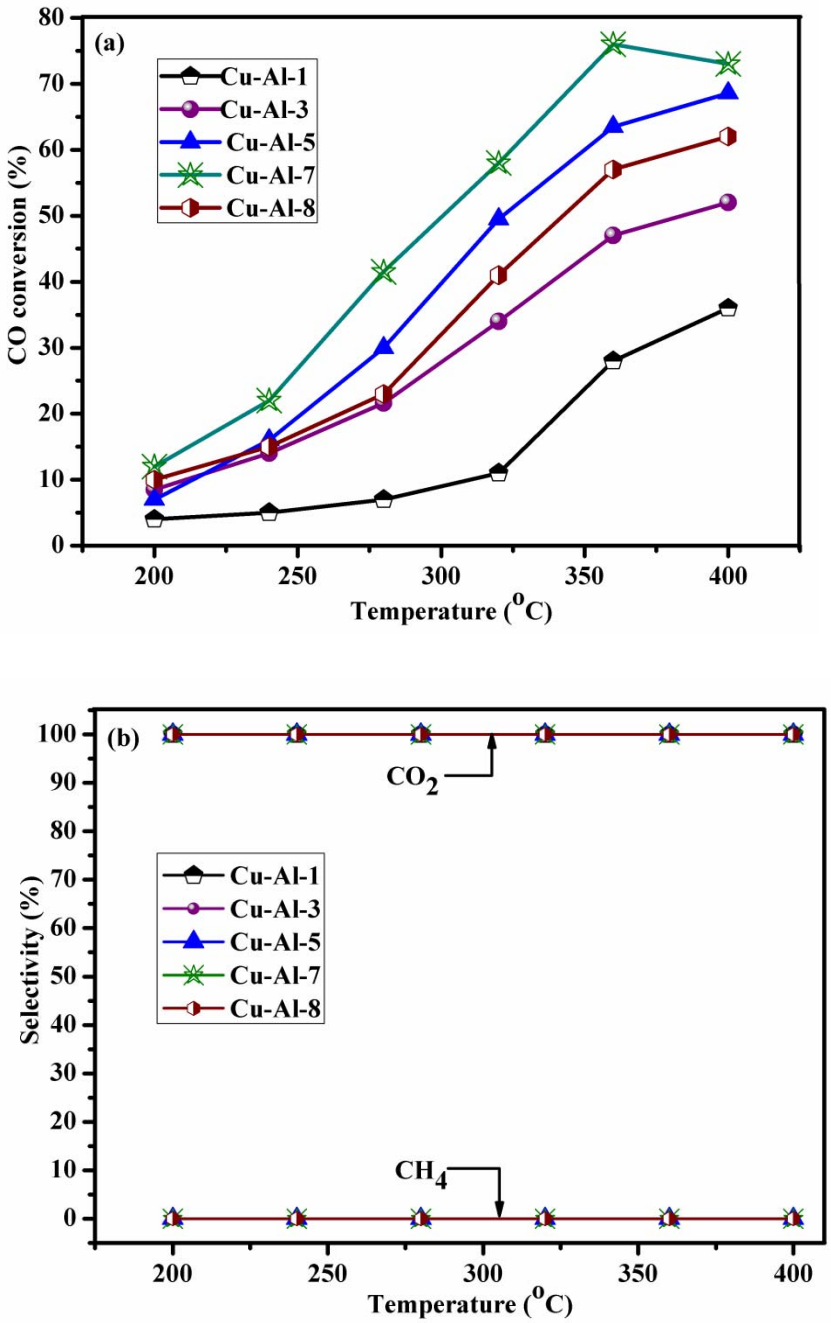

Figure 9.8. Activity of Cu-Al catalysts of different compositions (a) CO-conversion (b) CO_2 and CH_4 selectivity.

MnO and weak basicity of the support (ZnO_x, AlO_x).[24,30] Cu-Al-7 catalyst showed maximum conversion among all the catalysts, at all the temperatures. Generally, CO conversion is limited by temperature <350 °C, as expected from the thermodynamics.

Equally important is the higher surface coverage by CO_2 at lower temperatures retarding the catalyst activity predominantly.[24] Hence, achieving higher CO conversion is obvious at higher temperature. At the same time, another contributing feature of our catalyst was the higher extent of reduction of Cu species to metallic Cu at higher temperatures, as shown by TPR results. Interestingly, complete selectivity to CO_2 without formation of methane was achieved irrespective of Cu loading and reaction temperature (**Figure 9.8, b**).

From the catalyst screening studies, Cu-Al-7 catalyst was found to give the best performance hence further investigation on effect of catalyst pre-treatment parameters on WGSR activity was carried out over the same catalyst. **Figure 9.9** (**a**) shows a comparison of activities of calcined and reduced Cu-Al-7 catalysts using 5 % and 100 % H_2 conditions. Cu-Al-7 reduced under 5 % H_2 showed higher CO conversion than that observed for calcined and 100 % H_2 reduced sample, for the temperature range of 200-300 ^oC. With increase in temperature to 400 ^oC, CO conversion was the same at 73% for all the three catalysts. This observation and the fact that calcined sample showing similar or better performance than 100 % H_2 reduced sample at lower temperature indicate that active species formed may be similar under these reaction conditions. Whereas at 360 ^oC, Cu-Al-7 reduced at 5 % and 100 % H_2 showed higher CO conversion of 76 and 79% respectively, as compared to that of the calcined one. On the other hand, CO_2 selectivity was not influenced by the catalyst pre-treatment conditions (**Figure 9.9, b**).

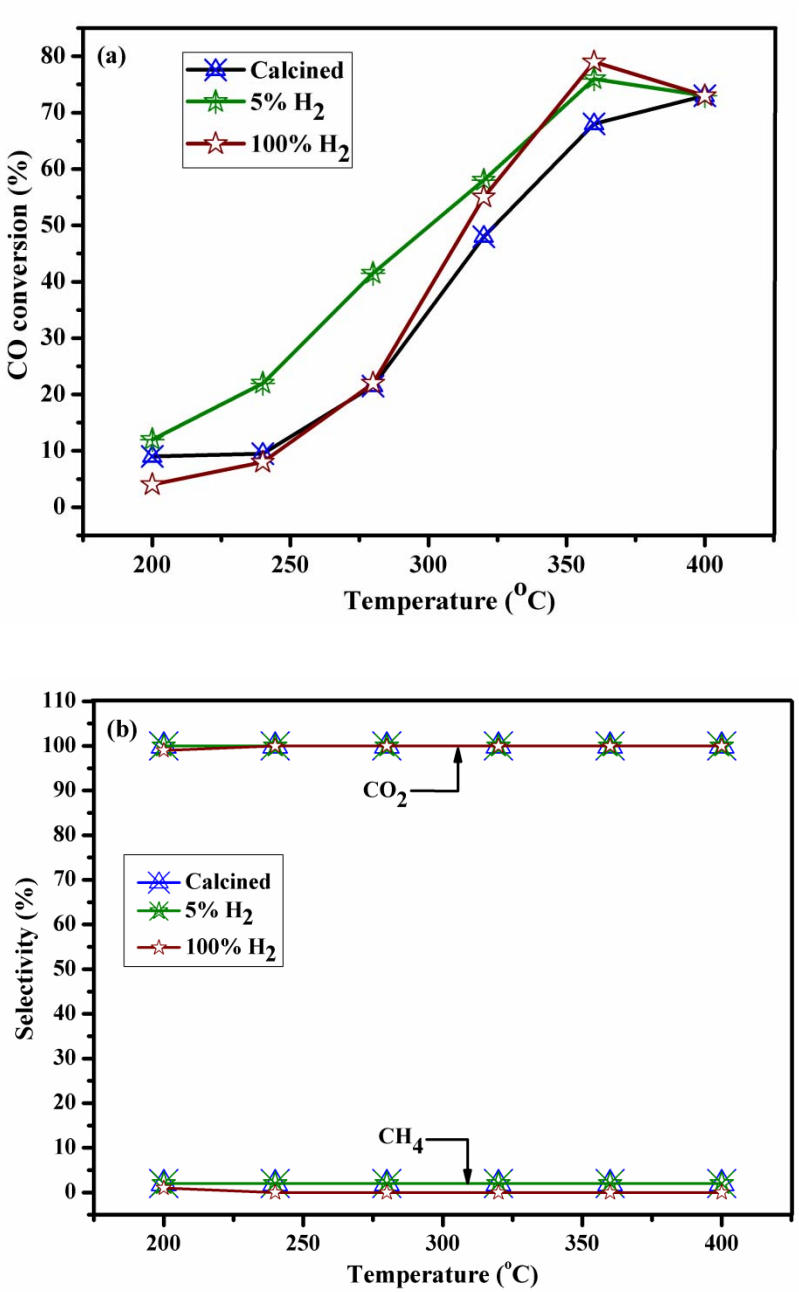

Figure 9.9. Effect of pretreatment conditions on activity of Cu-Al-7 catalysts (a) CO conversion with temperature over calcined, 5% and 100% H_2 reduced samples (b) CO_2 and CH_4 selectivity.

Therefore as discussed above, changes in reduction conditions affecting BET surface area, extent of reduction and Cu particle size, together do affect the WGSR activity of the same catalyst. The observed highest WGSR activity and selectivity of Cu-

Al-7 catalyst demonstrates the efficient redox mechanism operating as evident from the co-existence of different Cu species (Cu^{2+}, Cu^{1+} and Cu^{0}) in reduced and recovered samples.[39] Such non zero oxidation states of Cu are possible due to the presence of Al species, which in turn facilitate the electron acceptance ability of active copper. From the presence of CuO in the calcined and 5 % H_2 reduced sample; CuO and Cu_2O phases in 100 % H_2 reduced sample and Cu_2O and Cu^0 in the used (after 24 h at 360 °C) 100 % H_2 sample, **Scheme 9.1** is proposed below. Here, WGS reaction involving CO → CO_2 and H_2O → H_2 is also responsible for the inter-conversion among various Cu species.[32]

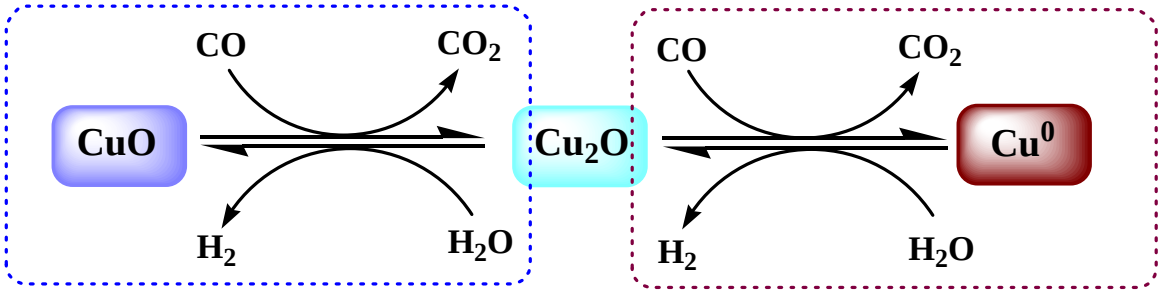

Scheme 9.1. Redox species of Cu in WGSR over Cu-Al catalyst.

As the samples of Cu-Al-7 reduced under 5 % and 100 % H_2 showed comparable WGSR activity at 360 °C, their stability was tested for continuous operation of 25 h and the results are shown in **Figure 9.10** (**a**). It was clearly observed that CO conversion deceased appreciably with time on stream for 5 % H_2 reduced sample as compared to that reduced with 100 % H_2. The 100 % H_2 reduced sample was further tested for an extended time of 100 h (**Figure 9.10, b**) which showed marginal decrease in activity from 79 to 73% for initial 24 h due to significant decrease in BET surface area from 19.7 to 9.5 $m^2 g^{-1}$ (**Table 9.2**). After 25 h, the activity was more or less constant as the surface area did not vary considerably (8.2 m^2g^{-1}).The consistent activity and stability of 100 % H_2 reduced sample was mainly due to the presence of various redox Cu species (mainly Cu_2O and Cu^0), particle stabilization due to Cu_2O phase, increased interaction between Cu-Al during activation protocol for 24 h and lower extent of Cu aggregation due to the formation of boehmite phase.

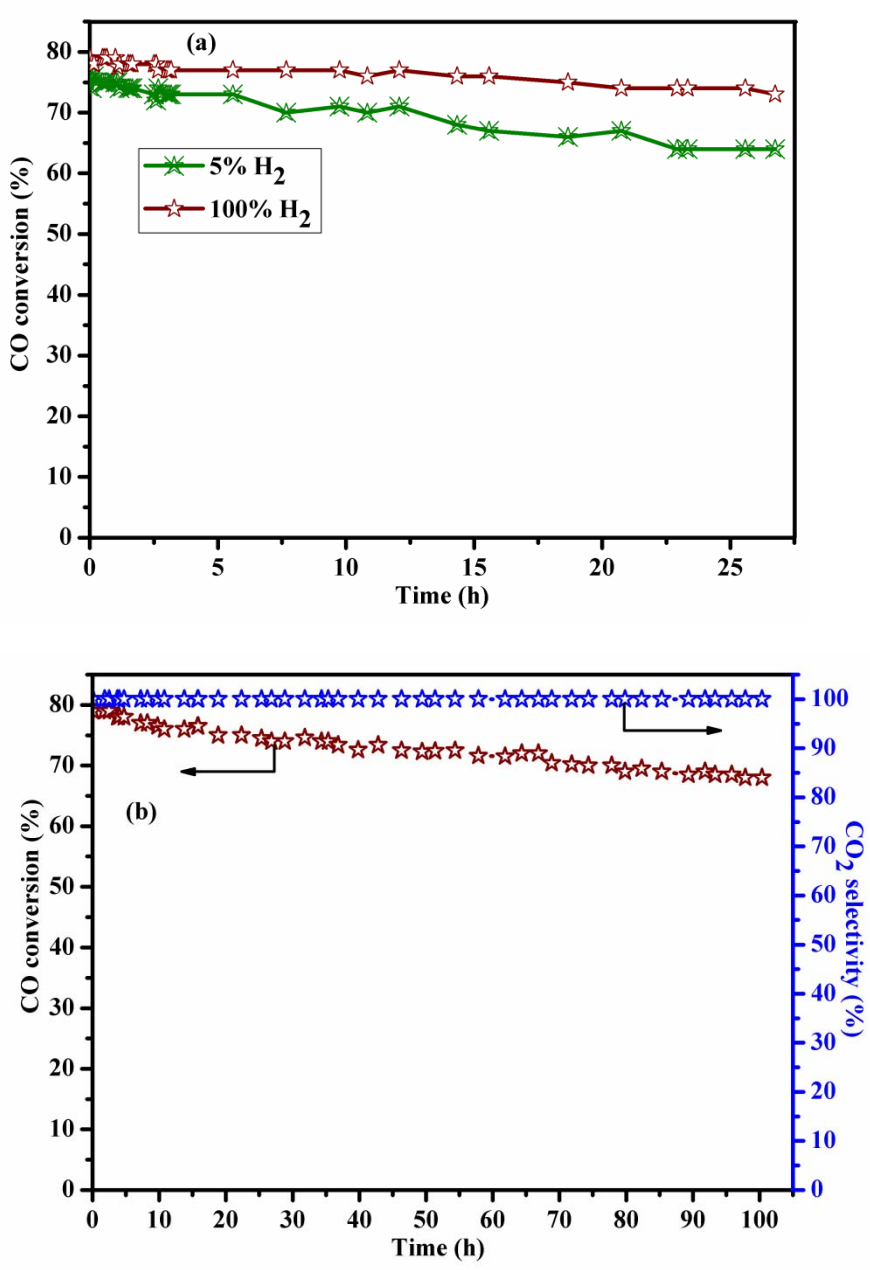

Figure 9.10. Time on stream activity of reduced Cu-Al-7 catalysts (a) comparison of 5% and 100 % H_2 reduced (b) 100 h stability of 100% reduced catalyst.

9.4. CONCLUSIONS

- Mixed Cu-Al oxides prepared by a co-precipitation method with varying Cu-Al compositions were found to efficiently catalyze the WGSR.
- Although all the catalysts studied in this work, were selective to CO_2 formation by suppressing methanation reaction, only Cu-Al-7 (Cu at.% = 70) catalyst showed the highest CO conversion within the temperature range from 200 to 400 ^{o}C at the GHSV of 36,201 h^{-1}.
- In addition, the Cu-Al-7 catalyst reduced under 100 % H_2 showed relatively stable activity with time on stream of 100 h.
- The co-existence of non-zero copper and metallic Cu in this catalyst, as proved by H_2-TPR, XRD and HR-TEM was an essential aspect for the observed WGSR activity.
- The change in reduction conditions played an important role for the variation in WGSR activity of the same catalyst.
- The contributing factors for the highest activity and stability of 100 % H_2 reduced Cu-Al-7 catalyst were: particle stabilization due to Cu_2O phase, increased interaction between Cu-Al during activation protocol for 24 h and lower extent of Cu aggregation due to boehmite phase.
- Complete CO_2 selectivity without methanation was observed for all the Cu-Al compositions irrespective of their pretreatment conditions.

9.5. REFERENCES

1. J. A. Rodriguez, P. Liu, J. Hrbek, J. Evans, M. Perez, *Angew. Chem. Int. Ed.* **2007,** 46, 1329-1332.
2. T. Shishido, M. Yamamoto, I. Atake , D. Li , Y. Tian, H. Morioka, M. Honda, T. Sano K. Takehira*, J. Mol. Catal. A* **2006,** 253, 270-278.
3. C. H. Kim, L.T. Thompson, *J. Catal.* **2005,** 230, 66-74.
4. P. Panagiotopoulou, D. I. Kondarides, *J. Catal.* **2004,** 225, 327-336.
5. C. Martos, J. Dufour, A. Ruiz, *Int. J. Hydrogen Energy* **2009,** 34, 4475-4481.
6. W. Ruettinger, O. Ilinich, R. J. Farrauto, *J. Power Sources* **2003,** 118, 61-65.
7. S. Hilaire, X. Wang, T. Luo, R. J. Gorte, J. Wagner, *Appl. Catal. A* **2001,** 215, 271-278.
8. R. Si, Y. W. Zhang, S. J. Li, B. X. Lin, C. H. Yan, *J. Phys. Chem.* B **2004,** 108, 12481-12488.
9. D. –W., Jeong, H. S. Potdar, H.-S., Roh, *Catal. Lett.* **2012,** 142, 439-444.
10. Q. Fu, W. Deng, H. Saltsburg, M. Flytzani-Stephanopoulos, *Appl. Catal. B* **2005,** 56, 57-68.
11. J. Wu, M. Saito, *J. Catal*. **2000,** 195, 420-422.
12. T. Shishido, M. Yamamoto, I. Atake, D. Li, Y. Tian, H. Morioka, M. Honda, T. Sano, K. Takehira, *J. Mol. Catal. A* **2006,** 253, 270-278.
13. Y. Tanaka, T. Takeguchi, R. Kikuchi, K. Eguchi, *Appl. Catal. A* **2005,** 279, 59-66.
14. L. Li, L. Song, H. Wang, C. Chen, Y. She, Y. Zhan , X. Lin, Q. Zheng*, Int. J. Hydrogen Energy* **2011,** 36, 8839-8849.
15. C. Wen, Y. Zhu, Y. Ye, S. Zhang, F. Cheng, Y. Liu, P. Wang, F. Tao, *ACS Nano* **2012,** 10, 9305-9313.
16. J. Lin, P. Biswas, V. V. Guliants, S. Misture, *Appl. Catal. A* **2010,** 387, 87-94.
17. S. Hilaire , X. Wang, T. Luo, R. J. Gorte , J. Wagner, *Appl. Catal. A* **2001,** 215, 271-278.
18. S. Takenaka, T. Shimizu, K. Otsuka, *Int. J. Hydrogen Energy* **2004,** 29, 1065-1073.

19. C. H. Bartholomew, R. J. Farrauto, *Fundamentals of Industrial Catalytic Processes*, John Wiley and Sons Ltd., Hoboken, NJ, **2006.**
20. T. Shishido, Y. Yamamoto, H. Morioka, K. Takai, K. Takehira, *Appl. Catal. A* 2004, 263, 249-253.
21. Y. Tanaka, T. Utaka, R. Kikuchi, K. Sasaki, K. Eguchi, *Appl.Catal. A* 2003, 238, 11-18.
22. H. Schaper, E. B. M. Doesburg, L.L.v. Reijen, *Appl. Catal. A* **1983,** 7, 211-220.
23. M.S. Spencer, *Top. Catal.* **1999,** 8, 259-266.
24. Y. Tanaka, T. Utaka, R. Kikuchi, T. Takeguchi, K. Sasaki, K. Eguchi, *J. Catal*. **2003,** 215, 271-278.
25. S. Boumaza, A. Auroux, S. Bennici, A. Boudjemaa, M. Trari, A. Bouguelia, R. Bouarab, *Reac. Kinet. Mech. Cat.* **2010,** 100, 145-151.
26. N. A. Koryabkina, A. A. Phatak, W. F. Ruettinger, R. J. Farrauto, F. H. Ribeiro, *J. Catal.* **2003,** 217, 233-239.
27. J. Lin, V. V. Guliants, *ChemCatChem* **2011,** 3, 1426-1430.
28. J. Lin, V.V. Guliants, *ChemCatChem* **2012,** 4, 1611-1621.
29. S. Nishimura, T. Shishido, K. Ebitani, K. Teramura, T. Tanaka, *Appl. Catal. A* **2010,** 387, 185-194.
30. K. Sagata, N. Imazu, H. Yahiro, *Catal. Today* **2013,** 201, 145-150.
31. R. B. Mane, D.-W. Jeong, A. Malawadkar, H.-S. Roh, C.V. Rode *ChemCatChem* (communicated, 2013).
32. J. B. Ko, C. M. Bae, Y. S. Jung, D. H. Kim, *Catal. Lett.* **2005,** 105,157-161.
33. C. Rhodes, G. J. Hutchings, A. M. Ward, *Catal. Today* **1995,** 23, 43-58.
34. F. Severino, J. L. Brito, J. Laine, J. L. G. Fierro, A. L. Agudo, *J. Catal.***1998,** 177, 82-95.
35. D. F. Shriver, P. W. Atkins, *Inorganic chemistry*, Oxford Uni. Press, 3rd edn., **1999.**
36. X. Y. Chen, S. W. Lee, *Chem. Phys. Lett.* **2007,** 438, 279-284.
37. R. B. Mane, A. M. Hengne, A. A. Ghalwadkar, V. Subramanian, P. H. Mohite, H. S. Potdar, C.V. Rode, *Catal. Lett*. **2010,** 135, 141-147.

38. H. Ivankovic, E. Tkalcec, R. Nass, H. Schmidt, *J. Eur. Ceram. Soc.* **2003,** 23, 283-292.

39. C. –S. Chen, T. –W. Lai, C. –C. Chen, *J. Catal.* **2010,** 273, 18-28.

Chapter 10

Summary and conclusions

The salient features of my research work and specific conclusions derived from these findings are summarized in this chapter.

10. SUMMARY AND CONCLUSIONS

In this thesis, a detailed study on preparation and characterization of several copper catalysts with and without chromium and promoters by several techniques has been carried out. These catalysts were evaluated for hydrogenolysis using external as well as *in situ* generated hydrogen and dehydration reactions of glycerol which is a co-product of biodiesel generation process. The significant achievement of this Ph.D. work was the development of a non-noble metal and non-chromium catalyst (Cu-Al) and a laboratory scale sustainable process for an industrially important commodity product such as 1,2-propanediol. In addition, the same multifunctional Cu-Al catalyst was also shown to successfully catalyze the water gas shift reaction (WGSR) which is again an important reaction in energy sector for fuel cell application. The knowledge of structure-activity correlation gained in this work helped to understand the multifunctional role of copper catalysts in all these reactions. The main conclusions of this work are summarized below.

- ✓ In the preliminary stage of this work, Cu-Cr catalysts reported for glycerol hydrogenolysis were investigated in more details. In this study, the effect of three promoters *viz*. Al, Zn and Ba was studied individually as well as in combination with each other for the hydrogenolysis of glycerol. Among these, Cu-Cr catalyst with Ba as a promoter showed the highest conversion of 34% with highest selectivity of 85% to 1, 2-PDO in a batch operation while in a continuous operation it gave still higher conversion of 65% with a higher (>7 fold) catalyst stability as compared to Cu-Cr catalyst without any promoter. Highest activity and selectivity with Ba was mainly due to its enhanced acidity catalyzing the first step of dehydration of glycerol to acetol and due to $BaCrO_4$ phase stabilizing the crystallite size of Cu^0 at a lower value of 69 nm than that compared to ~ 150 nm incase of bare Cu-Cr catalyst. In continuous operation, Cu-Cr -Ba catalyst gave time on stream (TOS) activity of 800 h for glycerol hydrogenolysis to 1,2-PDO without any deactivation-activation cycle. Study of effect of process conditions in a continuous operation revealed that glycerol conversion and selectivity to 1,2-PDO increased from 65 to 74% and from 82 to 91 % respectively, with increase in H_2 partial pressure from 20 to 60 bar, while the selectivity to acetol decreased from 10 to 3% indicating higher

hydrogenation rate at higher H_2 pressure.

- ✓ Encouraged by the initial results on Cu-Cr catalysts, the rational design of non-chromium Cu-Al nano catalyst was successfully achieved using simultaneous co-precipitation and digestion technique without any template or stabilizer. This novel catalyst showed three times higher activity than the bulk Cu-Cr catalyst for hydrogenolysis of glycerol in both 2-propanol and water solvents. Cu_2O phase formed after reduction was found to stabilize the particle size in a narrow range of 7-11 nm by inhibiting the sintering of copper particles under reaction conditions. The same catalyst was also found to catalyze the direct hydrogenolysis of glycerol to 1,2-PDO. TOS of this Cu-Al-5 catalyst for both continuous hydrogenolysis and dehydration of glycerol was found to be 400 h with an average glycerol conversion of 65% and 90% respectively. In glycerol dehydration, Cu-Al-5 catalyst showed the highest activity and acetol selectivity in water medium while, in 2-propanol as a reaction medium, transfer hydrogenation led to the formation of 1,2-PDO (10-38%). Effects of various reaction conditions on conversion, selectivity and global rates of the two processes were also investigated.

- ✓ Further, the effect of precipitating agents was systematically investigated in co-precipitation and solid state fusion followed by precipitation methods for Cu catalysts used in glycerol hydrogenolysis. The salient features of our study were that not only the surface area but also other physico-chemical properties such as reduced metal species, distribution and strength of acid sites, crystallite size, and morphology were important for the catalytic activity. CAP Na_2CO_3 catalyst prepared by using Na_2CO_3 showed predominantly metallic Cu with a crystallite size of 5 nm while, the one prepared with K_2CO_3 showed CuO phase along with Cu^0 having crystallite size of 12 nm. Due to the unique characteristics of CAP (Na_2CO_3), it showed the highest conversion of 62-63% with 1,2-PDO selectivity of 88%. The samples prepared by alkali fusion followed by precipitation (CAF NaOH and CAF KOH) showed different phases depending on the type of alkali metal used. *E.g.* CAF (NaOH) sample showed the presence of both Cu_2O and Cu^0 phases while CAF (KOH) sample showed the presence of CuO phase predominantly, indicating its

incomplete reduction. The samples prepared by fusion method invariably showed lower acid strengths than those of prepared by precipitation. Among all the catalysts, CAP (Na_2CO_3) catalyst showed the maximum acid sites (0.1483 mmol g^{-1}) in the temperature region used for hydrogenolysis. The change in cation from Na^+ to K^+ also lowered the acidity, fitting into the trend of alkali metals.

- ✓ In continuation of our work on a bi-functional Cu-Al nano catalyst for selective hydrogenolysis of glycerol to 1,2-propanediol, we thought of exploring the use of waste fly ash by incorporating Cu, as an efficient catalyst system for glycerol hydrogenolysis reported here for the first time. Cu impregnated non-pretreated fly ash was responsible for the accumulation of first step glycerol dehydration and C-C cleavage products acetol and EG, respectively. However, alkali pretreated fused fly ash with Cu (FA-2, Al:Cu=1:1) showed the highest activity and 1,2-PDO selectivity (>85%) in glycerol hydrogenolysis. The higher activity of FA-2 was mainly due to transformation of α-quartz to the tridymite phase of SiO_2 and very high dispersion of Cu on to its surface as characterized by XRD, BET and TEM. At higher Cu loading on fused fly ash (Al: Cu > 1:2) caused a decrease in glycerol conversion by ~40% due to aggregation of Cu on the surface. At the same time, a ratio Al: Cu of < 1:1 substantially decreased both the glycerol conversion and the 1,2-PDO selectivity indicating that a critical Cu loading is responsible for the hydrogenolysis activity. This study demonstrates that the reuse of a waste fly ash modified with an inexpensive metal such as Cu can make an economically viable process for 1,2-PDO.

- ✓ Another very unique achievement of this work was the same Cu-Al catalyst showing an excellent TOS activity for continuous autogeneous hydrogenolysis of aqueous glycerol under N_2 atmosphere with 1,2-PDO selectivity of 75% with bio-glycerol feed which is a first report of its kind. Evidences of various active species such as Cu^{2+} in the form of CuO and $CuAl_2O_4$, along with Cu^0, Cu^{1+} which led to formation of multifunctional sites catalyzing C-C cleavage and glycerol dehydration to acetol, followed by its hydrogenation to 1,2-PDO, while completely suppressing the alkane formation.

- ✓ Our previous studies showed an excellent activity of Cu-Al catalyst for glycerol hydrogenolysis as well as for its *in situ* hydrogenolysis. Both these reactions involve the first step dehydration to acetol hence, we also studied the liquid phase glycerol dehydration to acetol separately over several Cu catalysts by incorporating oxides of various metals *viz.* Ba, Mg, Zr, Zn, Al, and Cr. The catalysts having higher acid strength and predominant BrØnsted acidity (Cu-Mg, Cu-Zr and Cu-Al) gave the highest acetol selectivity (76-92%), while the catalysts with lower acidity such as Cu-Zn showed very poor (25%) selectivity to acetol inspite of the highest conversion of 68%. The presence of metallic Cu in highly active catalysts was confirmed by XRD and XANES-EXAFS characterization. Thus, glycerol dehydration to acetol was found to be catalyzed not only by BrØnsted acid sites but also by the metallic Cu.

- ✓ As Cu-Al catalyst was found to be highly active for autogeneous hydrogenolysis involving glycerol APR it was also explored for water gas shift reaction (WGSR) and to our expectations it gave excellent activity for the same. The formation of various Cu species was achieved by systematically varying the Cu-Al composition and 70:30 ratio of Cu-Al was found to be the best for WGSR using reformate gas mixture. In addition, the Cu-Al (70:30) catalyst reduced under 100% H_2, showed a very stable time on stream of 100 h, at higher gas hourly space velocity (GHSV) of 36,201 h^{-1}. The presence of non-zero and metallic copper, lower extent of Cu aggregation along with particle size stabilization due to boehmite phase and Cu_2O, were the essential aspects for the observed WGSR activity.

List of publications

Research papers in peer reviewed journals

Papers

1. **R. B. Mane**, A. M. Hengne, A. A. Ghalwadkar, S.Vijayanand, P. H. Mohite, H . S. Potdar, C. V. Rode, Cu:Al nano catalyst for selective hydrogenolysis of glycerol to 1, 2- propanediol, ***Catal. Lett.*** 2010, 135, 141-147.

2. C.V. Rode, A. A. Ghalwadkar, **R. B. Mane**, A. M. Hengne, S. T. Jadkar, N. S. Biradar, Selective hydrogenolysis of glycerol to 1, 2- propanediol: comparison of batch and continuous process operations, ***Org. Process Res. Dev.*** 2010, 14, 1385-1392.

3. **R. B. Mane**, A. A. Ghalwadkar, A. M. Hengne, Y. R. Suryawanshi, C. V. Rode, Role of promoters in copper chromite catalysts for hydrogenolysis of glycerol, ***Catal. Today*** 2011,164, 447-450.

4. **R. B. Mane**, C. V. Rode, Continuous dehydration and hydrogenolysis of glycerol over non-chromium copper catalyst: Laboratory scale process optimization, ***Org. Process Res. Dev.*** 2012, 16, 1043-1052.

5. C. V. Rode, **R. B. Mane**, A. S. Potdar, P. B. Patil, P. S. Niphadkar, P. N. Joshi, Copper modified waste fly ash as a promising catalyst for glycerol hydrogenolysis, ***Catal. Today*** 2012, 190, 31-37.

6. **R. B. Mane,** S. E. Kondawar, P. S. Niphadkar, P. N. Joshi, K. R. Patil, C. V. Rode, Effect of preparation parameters of Cu catalysts on their physico-chemical properties and activities for glycerol hydrogenolysis, ***Catal. Today*** 2012, 198, 321-329.

7. **R. B. Mane**, C. V. Rode, Simultaneous glycerol dehydration and *in situ* hydrogenolysis over Cu–Al oxide under an inert atmosphere, ***Green Chem.*** 2012, 14, 2780-2789.

8. **R. B. Mane**, A. Yamaguchi, A. Malawadkar, M. Shirai, C. V. Rode, Active sites in modified copper catalysts for selective liquid phase dehydration of aqueous glycerol to acetol, ***RSC Adv.*** 2013, 37, 16499-16508.

9. **R. B. Mane,** D.-W. Jeong, A. Malawadkar, H.-S. Roh, C.V. Rode Effect of Cu Composition on Activity and Stability of Cu-Al catalysts for Water Gas Shift Reaction, **submitted to *ChemCatChem***.

10. **R. B. Mane**, A. S. Potdar, J. M. Nadgeri, N. S. Biradar, C. V. Rode, Selectivity tuning options in hydrogenation of *m*-Chloronitrobenzene to *m*-Chloroaniline over mono- and bimetallic supported Pt catalysts, ***Ind. Eng. Chem. Res.*** 2012, 51, 15564-15572.

11. A. C. Garade, V. S. Kshirsagar, **R. B. Mane**, A. A. Ghalwadkar, U. D. Joshi, C. V. Rode, Acidity tuning of montmorillonite K10 by impregnation with dodecatungstophosphoric acid and hydroxyalkylation of phenol, ***Appl. Clay Sci.*** 2010, 48, 164-170.

12. V. S. Kshirsagar, A.C. Garade, **R. B. Mane**, K. R. Patil, A. Yamaguchi, M. Shirai, C. V. Rode, Characterization of clay intercalated cobalt-salen catalyst for the oxidation of *p*-Cresol, ***Appl. Catal. A*** 2009, 370, 16-23.

Book chapter

1. **R. B. Mane**, C. V. Rode, Catalytic recycling of glycerol formed in biodiesel production, *Recycling and Reuse of Materials and Their Products* (Ed.: S. Thomas) , Advances in Materials Science book series, Apple Academic Press, Inc, Vol. 3, Chapter 2, pp.9-26, 2013.

Patent

1. C. V. Rode, **R. B. Mane**, A. M. Hengne, A. A. Ghalwadkar, P. H. Mohite, H . S. Potdar, A process for preparation of hydroxyacetone or propylene glycol, WO Patent 2011/138643 A2.

Posters/Oral presentations in national/international symposia

Posters

1. **R. B. Mane,** A. M. Hengne, A. A. Ghalwadkar, P. H. Mohite**,** C. V. Rode, Downstream processing of bioglycerol to value added products,
   Catalysis Workshop, NCL Pune (India), 2008.

2. **R. B. Mane,** A. M. Hengne, A. A. Ghalwadkar, P. H. Mohite**,** C. V. Rode, Selective liquid phase dehydration of glycerol to hydroxyacetone,
   Indo-Russian Joint workshop on Catalysis for Bio-mass Conversion and Environmental engineering held at NCL, Pune, January 2009.

3. **R. B. Mane,** A. A. Ghalwadkar**,** P. H. Mohite, A. M. Hengne, C. V. Rode, Performance of NCL catalysts for selective hydrogenolysis of glycerol to 1, 2 propylene glycol,
   Indo-Russian Joint workshop on Catalysis for Bio-mass Conversion and Environmental engineering held at NCL, Pune, January 2009. **Best Poster award.**

4. **R. B. Mane,** A. M. Hengne, P. H. Mohite, A. A. Ghalwadkar, C. V. Rode, Liquid phase dehydration of glycerol to hydroxyacetone,
   Science Day NCL, Pune, India, February 2009. **Best poster award.**

5. **R. B. Mane**, A. A. Ghalwadkar, P. H. Mohite, A. M. Hengne, C. V. Rode, Non chromium copper catalyst for selective liquid phase hydrogenolysis of glycerol to 1, 2 propylene glycol,
   ACEPT 09**,** NCL, Pune, India, June 2009.

6. **R. B. Mane,** A. M. Hengne, A. A. Ghalwadkar, S.Vijayanand, P. H. Mohite, H . S. Potdar, C. V. Rode, Selective hydrogenolysis of aqueous glycerol to 1,2-propanediol over nano copper based catalyst,
   Science Day NCL, Pune, India, February 2010.

7. **R. B. Mane**, C. V. Rode, A. A. Ghalwadkar, A. M. Hengne, P. H. Mohite, Dehydration *vs.* hydrogenolysis of aqueous glycerol over non chromium Cu catalysts,
   Sixth Tokyo Conference on Advanced Catalytic Science and Technology (TOCAT6) and The Fifth Asia Pacific Congress on Catalysis (APCAT5), Sapporo, Japan, 18-25th July 2010.

8. **R. B. Mane**, C. V. Rode, V. R. Mate, V. S. Kshirsagar, Nanostructured Co_3O_4 catalyst for selectivity tuning in liquid phase oxidation of phenol derivatives, Novel Nanostructures and Catalysis, Lake Toya, Japan, 24-25th July 2010.

9. **R. B. Mane**, J. M. Nadgeri, C. V. Rode, Nano structured supported Pd catalyst for selective hydrogenation of 2-butyne-1,4-diol,
   Novel Nanostructures and Catalysis, Lake Toya, Japan, 24-25th July 2010.

10. **R. B. Mane**, P. Patil, C. V. Rode, Catalyst screening and process optimization for selective dehydration of glycerol to acetol,
    Science Day, NCL, Pune, India, February 2011.

11. **R. B. Mane,** Chandrashekhar V. Rode and Hyun-Seog Roh, Cu-Al catalyzed water gas shift reaction for H_2 production,
    2nd Asia-Pacific Forum on Renewable Energy (AFORE) 2012, Nov. 26-29, Jeju, Korea.

12. **R. B. Mane,** C. V. Rode, Aqueous phase reforming of glycerol for *in situ* hydrogenolysis to 1,2-propanediol,
    AFORE Nov. 26-29, 2012, Jeju, Korea.

13. **R. B. Mane,** C. V. Rode, A. Yamaguchi, M. Shirai, Dehydration of aqueous glycerol to acetol mediated by acid sites of Cu:Al catalyst,
    The 12th Asia-Pacific Conference, Doshisha University, Kyoto, Japan, March-2013.

14. U. D. Joshi, **R. B. Mane**, A. Yamaguchi, M. Shirai, C. V. Rode,

Synthesis of MCM-41 using flyash without hydrothermal method,
ZMPC 2012: International Symposium on Zeolites and Microporous Crystals, Hiroshima, Japan, 28th July -1st Aug., 2012.

Oral presentations

1. **R. B. Mane**, A. A. Ghalwadkar, A. M. Hengne, C. V. Rode, Role of promoters in copper chromite catalysts for hydrogenolysis of glycerol, Sixth Tokyo Conference on Advanced Catalytic Science and Technology (TOCAT6) and The Fifth Asia Pacific Congress on Catalysis (APCAT5), Sapporo, Japan, 18-25th July 2010

2. **R.B. Mane**, C.V. Rode Green process for 1,2-propanediol by catalytic conversion of renewable feedstock,
   National Conference on Recent Trends in Chemistry, Satara, India, Oct. 2010.

3. **R. B. Mane** , C. V. Rode, M. Shirai , Influence of co-metal with Cu, on activity and selectivity in hydrogenolysis of glycerol to 1,2-propanediol, 3rd International Congress on Green Process Engineering (GPE), Kuala-Lumpur, Malaysia, 6-8th Dec. 2011.

4. **R. B. Mane** , C. V. Rode, Time on stream activity of non chromium catalyst for hydrogenolysis of glycerol,
   3rd International Congress on Green Process Engineering (GPE), Kuala-Lumpur, Malaysia, 6-8th Dec. 2011.

5. C. V. Rode, **R. B. Mane**, M. Shirai, Catalytic downstream processing of glycerol byproduct generated in bio-diesel manufacture,
   International Conference on Recycle and Reuse of Materials (ICRM), Kottayam, India, 5-7th Aug. 2011.

6. **R. B. Mane,** C. V. Rode, Towards CO_2 neutral commodity chemicals through biomass utilization,
   Third international conference on natural polymers, bio-polymers, bio-materials, their composites, blends, IPNs, polyelectrolytes and gels:Micro to nano scales (ICNP-2012), Kottayam, India, 26-28th, Oct. 2012.

7. **R. B. Mane,** C. V. Rode, Emerging Second Generation Biofuels,
   Third international conference on natural polymers, bio-polymers, bio-materials, their composites, blends, IPNs, polyelectrolytes and gels: Micro to nano scales (ICNP-2012), Kottayam, India, 26-28th, Oct. 2012,